

Geometric Integration of a Constrained Cosserat Beam Model

Dissertation

zur Erlangung des Doktorgrades der Naturwissenschaften (Dr. rer. nat.)

der

Naturwissenschaftlichen Fakultät II
Chemie, Physik und Mathematik

der Martin-Luther-Universität Halle-Wittenberg,

vorgelegt von

Herrn Stefan Hante
geb. am 26. März 1990 in Eisenach

Gutachter: Prof. Dr. M. Arnold
Prof. Dr. O. Brüls

Tag der Verteidigung: 16. Juni 2022

Contents

List of Algorithms	4
List of Figures	5
1. Introduction	7
2. Elements of Lie Group Theory	10
2.1. Differential Geometric Aspects	10
2.2. The Concept of Derivative Vectors	17
2.3. The Lie Group $\mathbb{S}^3 \times \mathbb{R}^3$	23
2.4. Isomorphies and Matrix Lie Groups	28
2.5. Mechanical Systems with Lie Group Structured Configuration Spaces . . .	32
2.6. Lie Groups as Riemannian Manifolds and Metric Spaces	38
3. RATTLie	46
3.1. Derivation	47
3.1.1. Conservative Systems	47
3.1.2. External Forces	51
3.1.3. SHAKELie	52
3.1.4. Extension to Nonholonomic Constraints	52
3.2. Convergence Analysis	53
3.2.1. The Local Error	54
3.2.2. The Global Error	58
3.2.3. The Lagrange Multipliers	60
3.3. Implementation Details	62
4. A Flexible Cosserat Beam Model and Its Discretization in Space	67
4.1. Rigid Bodies	68
4.2. The Cosserat Beam	70
4.2.1. The Continuous Cosserat Beam Model	70
4.2.2. Discretizing the Cosserat Beam Model in Space	76
5. Numerical Experiments	83
5.1. Examples and Benchmarks	83
5.2. Implementation	88
5.3. Results and Interpretation	90
6. Conclusion	106
7. References	108
A. Lie Group Functions	115
A.1. Linear Lie Groups \mathbb{R}^n	115

A.2. Lie Group of Rotation Matrices $SO(3)$	115
A.3. The Special Euclidean Group $SE(3)$	116
A.4. The Lie Group of Unit Quaternions \mathbb{S}^3	117
A.5. The Semi-Direct Product $\mathbb{S}^3 \ltimes \mathbb{R}^3$	118
A.6. The Lie Group of Unit Dual Quaternions UDQ	119
B. Functions with Isolated Singularity	120
C. The Heavy Top in Several Lie Group Formulations	121
C.1. Unconstrained in $SO(3)$	122
C.2. Unconstrained in \mathbb{S}^3	122
C.3. Constrained in the Direct Product $SO(3) \times \mathbb{R}^3$	122
C.4. Constrained in the Direct Product $\mathbb{S}^3 \times \mathbb{R}^3$	123
C.5. Constrained in $SE(3)$	123
C.6. Constrained in the Semi-Direct Product $\mathbb{S}^3 \ltimes \mathbb{R}^3$	123
C.7. Constrained in Unit Dual Quaternions UDQ	124
D. Generalizing the Cosserat Beam Model: A Micropolar Shell Model	124
D.1. The Continuous Cosserat Shell	125
D.2. Discretizing the Cosserat Shell Model in Space	127

List of Algorithms

1.	One time step of RATTLie $t_0 \rightarrow t_1$	64
2.	Calculation of Lagrange multipliers for the (nonholonomic) RATTLie by using the λ^\pm quantities obtained by two subsequent steps of the (nonholonomic) RATTLie	65
3.	Separately calculated Lagrange multipliers and acceleration using two subsequent time steps	65
4.	Separately calculated Lagrange multipliers and acceleration for nonholonomic systems using two subsequent time steps	65
5.	One time step of nonholonomic RATTLie $t_0 \rightarrow t_1$	66

List of Figures

1.	Rolling disk: Top view: Trajectory of the midpoint of the disk (blue), trajectory of a point on the edge of the disk (green) as well as the initial configuration of the disk (red).	97
2.	Description of the flying spaghetti benchmark [73]: Initial position as well as applied forces and moments on the left and the magnitude of the forces and moments on the right.	97
3.	Flying spaghetti: Snapshots of the configuration with $M = 16$ beam segments at $t = 0, 2, 3, 4, \dots, 15$ and the trajectory of the end points in blue. The reader should cross their eyes in order to perceive a three-dimensional image.	98
4.	Roll-up: Snapshots of the configuration with $M = 8$ beam segments at $t = 0, 0.5, 1, 1.5, 2, 3, 30$ and the trajectory of the right end point in blue.	98
5.	Fast heavy top: Maximum of the absolute discretized L^2 error in the configuration variable q expressed in $SO(3) \times \mathbb{R}^3$. Results were calculated with RATTLie, the reference solution with the generalized- α method ($\rho_\infty = 0.9$) in the Lie group $SO(3)$ and $h = 2^{-21} \approx 4.8 \times 10^{-7}$. The data for $SO(3) \times \mathbb{R}^3$ and $\mathbb{S}^3 \times \mathbb{R}^3$ closely coincide as well as the data for $SE(3)$, $\mathbb{S}^3 \times \mathbb{R}^3$, and UDQ	99
6.	Slow heavy top: Maximum of the absolute discretized L^2 error in the configuration variable q expressed in $SO(3) \times \mathbb{R}^3$. Results were calculated with RATTLie, the reference solution with the generalized- α method ($\rho_\infty = 0.9$) in the Lie group $SO(3)$ and $h = 2^{-21} \approx 4.8 \times 10^{-7}$. The data for $SO(3) \times \mathbb{R}^3$ and $\mathbb{S}^3 \times \mathbb{R}^3$ closely coincide as well as the data for $SE(3)$, $\mathbb{S}^3 \times \mathbb{R}^3$, and UDQ	99
7.	Kirchhoff beam model: Flying spaghetti: Maximum of the absolute discretized L^2 error in the configuration variables q with different integration schemes. The reference solution was calculated with RATTLie and $h = 2^{-20} \approx 9.5 \times 10^{-7}$	100
8.	Kirchhoff beam model: Flying spaghetti: Maximum of the absolute discretized L^2 error in the derivative vectors \mathbf{v} with different integration schemes. The reference solution was calculated with RATTLie and $h = 2^{-20} \approx 9.5 \times 10^{-7}$	100
9.	Kirchhoff beam model: Flying spaghetti: Maximum of the absolute discretized L^2 error in the Lagrange multiplier $\boldsymbol{\lambda}$ with different integration schemes. The reference solution was calculated with RATTLie (separately calculated $\boldsymbol{\lambda}$) and $h = 2^{-20} \approx 9.5 \times 10^{-7}$	101
10.	Fast heavy top: Average computation time compared to the computation time with Lie group $SE(3)$. Results were calculated with RATTLie. The relative computation times have been averaged over 100 runs.	101

11.	Rolling disk: Maximum of the absolute discretized L^2 error in the configuration variables q , the derivative vectors \mathbf{v} , the Lagrange multipliers corresponding to the holonomic constraints $\boldsymbol{\lambda}$ and the Lagrange multipliers corresponding to the nonholonomic constraints $\boldsymbol{\eta}$. Results were calculated with the nonholonomic RATTLie; the reference solution with $h = 2^{-21} \approx 4.7684 \times 10^{-7}$	102
12.	Kirchhoff beam model: Flying spaghetti: Maximum of the absolute discretized L^2 error in the different approximations to the Lagrange multiplier $\boldsymbol{\lambda}$. The reference solution was calculated with RATTLie (separately calculated $\boldsymbol{\lambda}$) and $h = 2^{-20} \approx 9.5 \times 10^{-7}$	102
13.	Kirchhoff beam model: Flying spaghetti: Maximum of the absolute discretized L^2 error in q , \mathbf{v} and $\boldsymbol{\lambda}$ with RATTLie and variable step sizes that were chosen pseudo-randomly between h_{\max} and $h_{\max}/4$. The reference solution was calculated with RATTLie and $h = 2^{-18} \approx 3.8 \times 10^{-6}$	103
14.	Fast heavy top: Change of mechanical energy over time. Results were calculated in the Lie group $\mathbb{S}^3 \times \mathbb{R}^3$, with step size $h = 2^{-16} \approx 1.5 \times 10^{-5}$ with different integration schemes.	103
15.	Kirchhoff beam model: Flying spaghetti: Maximum of the absolute discretized L^2 error in the configuration variables q , the derivative vectors \mathbf{v} and the Lagrange multipliers $\boldsymbol{\lambda}$. Results were calculated with RATTLie with time step size $h = 2^{-15} \approx 3.05 \times 10^{-5}$ and the reference solution used $M = 256$ spatial discretization intervals.	104
16.	Cosserat beam model: Roll-up: Distance $\ \mathbf{x}_0(t) - \mathbf{x}_M(t)\ _2 + \ -p_0(t) - p_M(t)\ _2$ between the end points of the beam over time t . Note that due to the 360° rotation of the right end, the orientation $p_M(t)$ approaches the antipode $-p_0(t)$. Both curves closely coincide.	104
17.	Cosserat beam model: Roll-up: Velocity $\ [\boldsymbol{\Omega}_M^\top(t), \mathbf{U}_M^\top(t)]^\top\ _2$ of the right end of the beam over time t . Both curves closely coincide.	105

1. Introduction

In order to fathom real-world problems, differential equations have to be solved. Specifically, for simulating a mechanical system, these differential equations often come in the form of differential-algebraic equations of differentiation index three, see e. g. [37]. The reason being that these systems are often large and have to be written in coordinates which are not minimal, leading to algebraic constraints. Moreover, nonlinearities in the configuration space naturally arise, e. g. when large three-dimensional rotations are present in the model and linear descriptions of orientation like Euler angles are infeasible due to the singularities they entail. This has led to the analysis of geometric integration methods that evolve on manifolds, specifically on Lie groups, spanning from one-step methods [27, 46] such as Runge-Kutta methods over the generalized- α method [7, 8, 16, 18, 76] up to multi-step methods such as BDF [84, 85], as well as variational integrators [24, 44, 56]. Often, notation from abstract geometry has been used to formulate them. However, Brüls et al. [8, 16] have coined a language which was geared more towards the mechanical interpretation of these abstract formulations and closer to the actual implementation of the methods. In this thesis, we call this the language of derivative vectors.

An especially challenging instance of mechanical systems is the simulation of thin and highly flexible beams, e. g. by Cosserat beam models [32, 71]. There have been different approaches to finding a numerical solution to the equations of motion of the beam model: full discretization, see e. g. [23, 45] or, following a method of lines approach [81], a semi-discretization in space. For this semi-discretization in space, which will also be used in this thesis, there are several possibilities: Finite differences, see e. g. [9, 53], finite Elements, see e. g. [33, 76], or a variational approach [24, 56] are feasible. However, for low discretization orders, these methods may lead to the same discretizations. In this thesis, we are going to use the toolbox of variational integrators for the spatial discretization, although it was inspired by the finite differences approach by Lang and Linn [51, 52].

It is clear that the bending and twisting of an ordinary beam are soft degrees of freedom compared to shearing and extension, which are usually a lot stiffer. In order to avoid numerical problems with very stiff problems, one can neglect the stiff degrees of freedom by working with a Kirchhoff beam model instead. In this thesis, we are going to consider the Kirchhoff beam model as a constrained Cosserat beam model [51, 53, 60], enabling us to easily switch between Cosserat and Kirchhoff models and allowing us to omit the stiff degrees of freedom if desired.

Concerning the time integration method, we are not only going to apply readily available Lie group integration methods for second order DAEs like the generalized- α method [8] and the BLieDF method [85]. In contrast, we will consider a new integration method called RATTLie, which we already published in [44]. It is a generalization of the well-known RATTLE method to Lie group structured configuration spaces. In order to derive RATTLie, we interpret RATTLE as a variational integrator and follow its construction [63] in a Lie group using the language of derivative vectors. Furthermore, we will analyze the integration method RATTLie, but not from the viewpoint of variational

integrators, but as a general one-step method. From this technical analysis, it follows that RATTLie is convergent of second order and moreover that it is not restricted to constant time step sizes, see also [10]. Also, we give an interpretation for the two Lagrange multipliers that arise in RATTLE and RATTLie. Moreover, two different ways of calculating an approximation to the Lagrange multipliers will be shown. The Lagrange multiplier becomes especially important when constraint forces have to be accurately evaluated.

The remainder of this thesis is structured in the following way: In section 2 we will present all the necessary tools from Lie group theory and mechanics on Lie group structured configuration spaces that will be used in the following sections. Specifically, section 2.1 will cover the differential geometric aspects which are not specially tailored to numerical algorithms or mechanics. They constitute the base of all forthcoming investigations. In contrast, section 2.2 is concerned with the way Lie groups can be used in the context of numerical algorithms and gives an in-depth introduction to the language of derivative vectors and how it relates to the standard notation of Lie groups. Section 2.3 introduces a special kind of Lie group with semi-direct product structure $\mathbb{S}^3 \ltimes \mathbb{R}^3$, which we will later use to describe rigid bodies as well as the Cosserat beam model. This Lie group will be related to other well-known Lie groups and especially matrix Lie groups in section 2.4. Then, in section 2.5, we are considering constrained mechanical systems on Lie group structured configuration spaces, their equations of motion and their derivation from variational principles. The last subsection 2.6 considers Lie groups as Riemannian manifolds, giving rise to a notion of distance on the Lie group arising from its geometric structure and irrespective of how it can be embedded in a higher-dimensional linear space. These considerations are a building block in the proof of convergence of the Lie group time integration method RATTLie, which is the subject of section 3.

Specifically, in section 3.1, we will show how the RATTLie method can be derived from the variational principles which are used to derive the continuous equations of motion of mechanical systems. First, we start with conservative systems in section 3.1.1, then add external forces in section 3.1.2. Additionally, we consider a related method called SHAKELie in section 3.1.3 and also generalize RATTLie to systems with nonholonomic constraints in section 3.1.4. Section 3.2 gives a proof of convergence of the RATTLie method. In order to do so, we first analyze the local errors in section 3.2.1 and then apply a generalization of the standard proof of convergence for one-step methods on Lie groups to RATTLie in section 3.2.2. However, this proof only shows convergence of the configuration and the derivative vectors. The convergence of the Lagrange multipliers and how to calculate them accurately is considered in section 3.2.3. Finally, section 3.3 gives some implementation details of RATTLie as well as algorithms in high-level pseudocode.

In section 4, we are considering flexible Cosserat models. In order to do so, we first have to introduce rigid bodies in section 4.1. The main part of Cosserat beam models is presented in section 4.2. In section 4.2.1, we give a derivation of the continuous equations of motion of the Cosserat beam and in section 4.2.2 we explain our spatial discretization.

All of the above comes together in section 5, where numerical experiments are considered. First, we describe our test problems in section 5.1, then present the actual implementation

of the numerical algorithms as well as test problems in section 5.2, and finally show the results as well as give interpretations in section 5.3.

The last section 6 concludes the thesis. Moreover, the appendices give some in-depth information about Lie group functions and the equations of the heavy top example for different Lie groups as well as how to implement them with a special attention to the implementation of functions with removable singularities, which arise in this context.

Notations

We have aimed to be very clear with our notation by, e. g., not omitting arguments, matrix multiplication signs, etc. This also ties into the language of derivative vectors, which is very explicit in its notation. The goal was to be as close to the implementation as possible and to avoid any ambiguities, even for people who are not very familiar with the language of Lie groups. Sometimes we have to deviate from this stipulation for reasons of readability, but we indicate when we do so. As usual, scalar variables are printed in roman italics, but as visual aid, we have set vectors in bold italics and matrices in upright bold. Often, when considering three-dimensional vectors, lowercase usually denotes that the vector is measured with respect to the inertial frame and uppercase denotes that it is measured with respect to the body-fixed frame. Furthermore, elements of abstract mathematical structures such as Lie groups, Lie algebras, or tangent spaces are also written in roman italics. The same style applies to functions that map to the aforementioned quantities. Moreover, we use the notation df for the differential (or pushforward) of a function f . This means that for $f: X \rightarrow Y$ with manifolds X, Y , the differential $df(x): T_x X \rightarrow T_{f(x)} Y$ is for each $x \in X$ a linear function mapping from the tangent spaces $T_x X$ to $T_{f(x)} Y$. Applying a linear function to an element of a linear space is, as it is often done, denoted without parentheses, such that $df(x) a$ is the application of the linear function $df(x)$ to a . Furthermore, we will sometimes write a superscript operation of a function value directly after the function in order to remove visual clutter, e. g. $\mathbf{T}^{-1}(\mathbf{v}) = (\mathbf{T}(\mathbf{v}))^{-1}$ and $\mathbf{D}\boldsymbol{\Phi}^\top(q) = (\mathbf{D}\boldsymbol{\Phi}(q))^\top$. Additionally, the transpose of the inverse of a matrix \mathbf{A} is written as $\mathbf{A}^{-\top}$. If a function is infinitely differentiable, we will call it a smooth function. Finally, note that the variable n is usually the dimension of a general Lie group, but is also used as the index for time discretization.

2. Elements of Lie Group Theory

Lie groups are a well-researched topic that has, as a special application, gained importance in the research of numerical simulation of mechanical systems, see e. g. [15, 18, 27, 44, 46, 54, 65, 66, 84]. In section 2.1, we will at first briefly introduce Lie groups and their differential geometric aspects. Then, we will show the concept of derivative vectors in section 2.2 which will be used to treat velocities of curves that evolve in a Lie group. Furthermore, in section 2.3, we will introduce the semi-direct product Lie group $\mathbb{S}^3 \ltimes \mathbb{R}^3$ which will be used to describe rigid body configuration in this thesis. In order to do so, we consider the Lie group of unit quaternions \mathbb{S}^3 . Section 2.4 deals with Lie group isomorphisms, direct Lie group products, matrix Lie groups as well as unit dual quaternions and how they relate to $\mathbb{S}^3 \ltimes \mathbb{R}^3$. The next section 2.5 considers mechanical systems that are formulated in such a way that the configuration space has Lie group structure. The last section 2.6 considers Lie groups as metric spaces by constructing a metric from a scalar product on the tangent space. We also investigate the relation between the Lie group operation and the metric distance function. These are the tools needed for the convergence analysis in section 3.

2.1. Differential Geometric Aspects

This section is devoted to the purely theoretical part of Lie groups which will be needed in the numerical algorithms presented in this thesis. Most of the following statements can be found in books from the context of pure mathematics [1, 38, 77, 80], more numerically oriented paper by Iserles et al. [46] or the famous textbook by Hairer, Lubich and Wanner on geometrical numerical integration [35]. A lot of this theoretical matter, especially on matrix Lie groups, is also reproduced by works in numerical analysis and mechanical engineering, see e. g. [16, 20, 23, 54, 56, 64, 84].

First, we will need some notion of smooth manifolds. Since all the examples we are going to deal with in this thesis are regular surfaces, we will merely define what a regular surface is and avoid the technicalities of abstract manifolds:

Definition 2.1: *Regular surface in \mathbb{R}^N , see [19, Chapter 0, Example 4.2].*

A subset $M \subseteq \mathbb{R}^N$ is called a regular surface of dimension $n \leq N$ if for every $p \in M$ there exists a neighborhood $V_p \subseteq \mathbb{R}^N$ and a mapping $\chi_p: U_p \subseteq \mathbb{R}^n \rightarrow M \cap V_p$ of an open set $U_p \subseteq \mathbb{R}^n$ onto $M \cap V_p$ such that

- χ_p is a smooth homeomorphism and
- the linear map $d\chi_p(q): \mathbb{R}^n \rightarrow \mathbb{R}^N$ is injective for all $q \in U_p$. Since $n \leq N$ this is equivalent to the requirement that the Jacobian $\chi_p'(q) \in \mathbb{R}^{N \times n}$ has full rank.

In do Carmo's book [19], this is given as an example for smooth manifolds.

This definition is still rather technical, but the following lemma already covers a lot of the manifolds that will be considered in this thesis:

Lemma 2.2: *Inverse image of a regular value [19, Chapter 0, Example 4.3].*

A set $M \subseteq \mathbb{R}^N$ is a regular surface of dimension $n \leq N$, if it can be written as

$$M = \mathbf{F}^{-1}(\mathbf{a}) = \{p \in \mathbb{R}^N : \mathbf{F}(p) = \mathbf{a}\},$$

where $\mathbf{F}: U \subseteq \mathbb{R}^N \rightarrow \mathbb{R}^{N-n}$ is a smooth map of an open set U and $\mathbf{a} \in \mathbb{R}^{N-n}$ is a regular value of \mathbf{F} , meaning that the differential $d\mathbf{F}(p): \mathbb{R}^N \rightarrow \mathbb{R}^{N-n}$ is surjective for all $p \in \mathbf{F}^{-1}(\mathbf{a})$. Since $n \leq N$ this is equivalent to the requirement that the Jacobian $\mathbf{F}'(p) \in \mathbb{R}^{(N-n) \times N}$ has full rank.

This means that such a set $M \subseteq \mathbb{R}^N$ is also a smooth manifold according to [19]. Next, we need the notion of a group:

Definition 2.3: *Groups.*

A tuple (G, \circ) of a set G and a mapping $\circ: G \times G \rightarrow G$ is called a group if

- there exists an identity element $e \in G$ such that

$$e \circ g = g, \quad g \in G,$$

- for each element $g \in G$ there is an inverse element $g^{-1} \in G$ such that

$$g \circ g^{-1} = e,$$

- and the mapping \circ is associative:

$$(a \circ b) \circ c = a \circ (b \circ c), \quad a, b, c \in G.$$

Due to the associativity, we can omit parentheses. We call the mapping \circ the group operation and by abuse of notation, we say that G is a group, if the group operation can be concluded from the context.

Now we can define Lie groups:

Definition 2.4: *Lie groups.*

A tuple (G, \circ) is called a Lie group if G is a regular surface (or more generally a smooth manifold), (G, \circ) is a group and the mapping

$$G \times G \rightarrow G, \quad (a, b) \mapsto a^{-1} \circ b$$

is smooth.

Often, in introductory work to Lie groups like [38] and in work on numerical algorithms on Lie groups like [16] only a special kind of Lie group is considered:

Definition 2.5: *Matrix Lie groups.*

A Lie group (G, \circ) is called a matrix Lie group, if $G \leq GL(\aleph)$ for some $\aleph \in \mathbb{N}$. Here, $GL(\aleph) \subseteq \mathbb{R}^{\aleph \times \aleph}$ is the group of real invertible $\aleph \times \aleph$ matrices and $A \leq B$ denotes that A is a subgroup of B for two groups A and B .

Sometimes, matrix Lie groups are defined to be closed subgroups of $GL(\aleph)$ without having to rely on the notion of a general Lie group [38].

In this thesis, however, we will encounter Lie groups that are not matrix Lie groups themselves, but are still isomorphic to matrix Lie groups, meaning they have essentially the same structure as their matrix Lie group counterpart. Algorithms that are designed for matrix Lie groups can thus in principle be applied to those Lie groups as well; for an example see [9].

Remark 2.6: *Lie group isomorphisms.*

It can be shown that a continuous homomorphism $\psi: G \rightarrow H$ between two Lie groups G and H must always be smooth [38, Corollary 3.50]. From group theory it is known that the image $\psi(G)$ must always be a subgroup of H . If ψ is injective, then the inverse map $\psi^{-1}: \psi(G) \rightarrow G$ must be a group isomorphism between $\psi(G)$ and G . If ψ is bicontinuous, meaning that ψ^{-1} is continuous as well, then, applying the same argument as before, ψ^{-1} is also smooth. This makes any injective bicontinuous group homomorphism $\psi: G \rightarrow H$ a diffeomorphism between G and $\psi(G)$. This means that G and $\psi(G)$ are not only isomorphic as groups, but also diffeomorphic as regular surfaces and thus isomorphic as Lie groups.

From now on in this section, let (G, \circ) always be an n -dimensional Lie group with $n \in \mathbb{N}$.

Lie groups provide a lot more structure than manifolds or even regular surfaces do because all tangent spaces are isomorphic. In order to construct the tangent space isomorphism, we can use the derivative of the left or right translation.

Definition 2.7: *Left and right translation.*

We define for $p \in G$ the left translation

$$L_p: G \rightarrow G, \quad q \mapsto L_p(q) = p \circ q \quad (2.1)$$

as well as the right translation

$$R_p: G \rightarrow G, \quad q \mapsto R_p(q) = q \circ p. \quad (2.2)$$

Their derivatives

$$dL_p(q): T_q G \rightarrow T_{L_p(q)} G = T_{p \circ q} G$$

and

$$dR_p(q): T_q G \rightarrow T_{R_p(q)} G = T_{q \circ p} G$$

are isomorphisms between the vector spaces $T_q G$ and $T_{p \circ q} G$ or $T_{q \circ p} G$, respectively. By deriving the trivial identity $L_a(L_b(c)) = L_{a \circ b}(c)$, we get the following useful equation:

$$dL_a(b \circ c) \, dL_b(c) = dL_{a \circ b}(c), \quad a, b, c \in G. \quad (2.3)$$

In the case that $G \leq GL(\mathbb{N})$ is a matrix Lie group, it is clear that

$$dL_{\mathbf{A}}(\mathbf{B}) \, \mathbf{C} = \mathbf{A} \cdot \mathbf{C}, \quad \mathbf{A}, \mathbf{B} \in G \subseteq GL(\mathbb{N}), \, \mathbf{C} \in T_{\mathbf{B}} G \subseteq GL(\mathbb{N}). \quad (2.4)$$

In this thesis, we will usually use the derivative of the left translation in order to represent all derivatives in the tangent space $T_e G$ of the identity element $e \in G$.

Now, we will consider automorphisms Ψ_h of the Lie group G that can be expressed by conjugation

$$\Psi_h: G \rightarrow G, \quad g \mapsto h \circ g \circ h^{-1},$$

where $h \in G$. Differentiating this automorphism at the origin leads us to the adjoint representation of G , see [46, Definition 2.12]:

$$\text{Ad}_h: T_e G \rightarrow T_e G, \quad a \mapsto d\Psi_h(e) \, a$$

for $h \in G$. Now, we want to differentiate the Ad_h with respect to its subscript. In order to do so, we define

$$\alpha_a: G \rightarrow T_e G, \quad g \mapsto \text{Ad}_g(a)$$

for $a \in T_e G$.

Definition 2.8: *The adjoint operator.*

We define the adjoint operator ad_a for all $a \in T_e G$ by

$$\text{ad}_a: T_e G \rightarrow T_e G, \quad b \mapsto d\alpha_b(e) \, a. \quad (2.5)$$

It can be shown that

$$\text{ad}_a(b) = \left. \frac{d^2}{ds \, dt} \rho(s) \circ \sigma(t) \circ \rho(-s) \right|_{s=t=0}, \quad (2.6)$$

where $\rho, \sigma: (-\varepsilon, \varepsilon) \rightarrow G$ are smooth curves with $\rho(0) = \sigma(0) = e$, $\rho'(0) = a$ and $\sigma'(0) = b$, see [46]. Furthermore, we can pull apart the differentiation with respect to s in the following way

$$\left. \frac{d^2}{ds \, dt} \rho(s) \circ \sigma(t) \circ \rho(-s) \right|_{s=t=0} = \left. \frac{d^2}{ds \, dt} \rho(s) \circ \sigma(t) \circ \rho(0) \right|_{s=t=0} + \left. \frac{d^2}{ds \, dt} \rho(0) \circ \sigma(t) \circ \rho(-s) \right|_{s=t=0},$$

which then gives us the following formula for the adjoint operator:

$$\text{ad}_a(b) = \left. \frac{d}{ds} dL_{\rho(s)}(e) \, b \right|_{s=0} - \left. \frac{d}{dt} dL_{\sigma(t)}(e) \, a \right|_{t=0}. \quad (2.7)$$

The tangent space $T_e G$ is called $\mathfrak{g} = T_e G$, the Lie algebra of G , because \mathfrak{g} is a linear space and the adjoint operator fulfills the definition of a Lie bracket on \mathfrak{g} since it is bilinear, antisymmetric and fulfills the Jacobi identity

$$\text{ad}_a(\text{ad}_b(c)) + \text{ad}_c(\text{ad}_a(b)) + \text{ad}_b(\text{ad}_c(a)) = 0, \quad a, b, c \in T_e G.$$

In the case that $G \leq GL(\mathbb{N})$ is actually a matrix Lie group we can see from (2.7) that it holds

$$\text{ad}_{\mathbf{A}}(\mathbf{B}) = \mathbf{A} \cdot \mathbf{B} - \mathbf{B} \cdot \mathbf{A}, \quad \mathbf{A}, \mathbf{B} \in T_{\mathbf{I}} G \subseteq GL(\mathbb{N}).$$

Lemma 2.9: *Bivariate functions, see e. g. [17].*

Let us consider a differentiable function

$$q: (-\varepsilon, \varepsilon) \times (-\varepsilon, \varepsilon) \rightarrow G, \quad (s, t) \mapsto q(s, t)$$

with $q(0, 0) = e$ and functions a, b with

$$q'(s, t) = \text{d}L_{q(s,t)}(e) a(s, t) \quad \text{and} \quad \dot{q}(s, t) = \text{d}L_{q(s,t)}(e) b(s, t),$$

where the dot denotes the derivative with respect to t and the prime denotes the derivative with respect to s :

$$\dot{\bullet} = \frac{\text{d}}{\text{d}t} \bullet \quad \text{and} \quad \bullet' = \frac{\text{d}}{\text{d}s} \bullet.$$

Then it holds

$$\text{ad}_{a(0,0)}(b(0, 0)) = \dot{a}(0, 0) - b'(0, 0).$$

Proof. First let us derive $q'(0, t)$ with respect to t at $t = 0$ and $\dot{q}(s, 0)$ with respect to s at $s = 0$:

$$\begin{aligned} \dot{q}'(0, 0) &= \frac{\text{d}}{\text{d}t} \text{d}L_{q(0,t)}(e) a(0, 0) \Big|_{t=0} + \text{d}L_{q(0,0)}(e) \dot{a}(0, 0), \\ \dot{q}'(0, 0) &= \frac{\text{d}}{\text{d}s} \text{d}L_{q(s,0)}(e) b(0, 0) \Big|_{s=0} + \text{d}L_{q(0,0)}(e) b'(0, 0). \end{aligned}$$

This can be used in (2.7) with $\rho(s) = q(s, 0)$, $\sigma(t) = q(0, t)$, $a = a(0, 0)$ and $b = b(0, 0)$ in order to obtain

$$\text{ad}_{a(0,0)}(b(0, 0)) = \dot{q}'(0, 0) - \text{d}L_{q(0,0)}(e) b'(0, 0) - (\dot{q}'(0, 0) - \text{d}L_{q(0,0)}(e) \dot{a}(0, 0)),$$

from which the assertion follows since $q(0, 0) = e$ and $\text{d}L_e(e)$ is the identity. \square

Let us now consider the following initial value problem on G :

$$\dot{q}_a(t) = \text{d}L_{q_a(t)}(e) a, \quad q(0) = e \tag{2.8}$$

with a constant $a \in T_e G$. It is clear that an analytic solution q must always fulfill $q_a(t) \in G$, since $\text{d}L_{q(t)}(e) a \in T_{q(t)} G$.

Definition 2.10: *The exponential map, see e. g. [80].*

We call $a \mapsto q_a(1)$ the exponential map of the constant $a \in T_e G$:

$$\exp: T_e G \rightarrow G, \quad a \mapsto \exp(a) = q_a(1),$$

where $q_a(1)$ is the solution of (2.8) at $t = 1$.

The exponential map thus gives us a relation between the tangent spaces and the Lie group itself as well as the possibility to solve initial value problems with a right-hand side that is constant when mapped to $T_e G$ by the left translation. It is easy to show that the initial value problem

$$\dot{q}(t) = dL_{q(t)}(e) a, \quad q(t_0) = q_0 \in G \quad (2.9a)$$

has the solution

$$q(t) = q_0 \circ \exp((t - t_0)a). \quad (2.9b)$$

In the case that $G \leq GL(\mathbb{N})$ is a matrix Lie group, it is well-known that the exponential map coincides with the matrix exponential

$$\exp(\mathbf{A}) = \text{expm}(\mathbf{A}) = \sum_{k=0}^{\infty} \frac{1}{k!} \mathbf{A}^k, \quad (2.10)$$

for $\mathbf{A} \in G$, see e. g. [38].

Lemma 2.11: *Properties of the exponential map, [80, Theorem 2.10.1].*

The exponential map is smooth. Furthermore, there is an open neighborhood $U \subset T_e G$ of $0 \in T_e G$ such that $\exp|_U: U \rightarrow \exp(U) \subseteq G$ is a smooth diffeomorphism.

Lemma 2.11 allows us to define the inverse of the exponential map, which is called the logarithm.

Definition 2.12: *Logarithm.*

The logarithm

$$\log: \exp(U) \subseteq G \rightarrow U \subseteq T_e G, \quad g \mapsto \log(g) = \exp^{-1}(g)$$

is the inverse of the exponential map on the open neighborhood $U \subseteq T_e G$ from lemma 2.11. Often, we will call an element of $\exp(U)$ “sufficiently close” to the identity $e \in G$.

By definition it holds

$$\exp(\log(g)) = g, \quad \log(\exp(a)) = a$$

for $g \in \exp(U)$ and $a \in U$. Notice that $\log(g)$ is well-defined if $g \in G$ is sufficiently close to the identity.

When we look at the flow of the initial value problem (2.8) which defines the exponential map, it can be seen that $q_a(1 + \tau) = \exp((1 + \tau)a)$ for $a \in T_e G$ and $\tau \in \mathbb{R}$. On the other hand, we could solve (2.8) up to $t = 1$ and then start solving (2.9) with $t_0 = 1$ and $q_0 = q_a(1)$, which gives us $q_a(1 + \tau) = q_a(1) \circ \exp(\tau a)$. This implies that

$$\exp(a + b) = \exp(a) \circ \exp(b), \quad \text{if } b = \tau a \text{ for some } \tau \in \mathbb{R}. \quad (2.11)$$

It directly follows that

$$(\exp(a))^{-1} = \exp(-a). \quad (2.12)$$

Unfortunately, (2.11) does not hold in general when b is not a multiple of a . The Baker-Campbell-Hausdorff formula, see e.g. [80], gives us the possibility to express the Lie product of two values of the exponential map as only one value of the exponential map $\exp(a) \circ \exp(b) = \exp(c)$ and a formula for determining $c \in T_e G$ from a and b . In this thesis, however, we will only need a qualitative result of the following form:

Lemma 2.13: *Qualitative Baker-Campbell-Hausdorff formula [35, 46].*

For $a, b \in T_e G$ and $h \rightarrow 0$ it holds

$$\exp(ha) \circ \exp(hb) = \exp\left(ha + hb + \frac{h^2}{2} \text{ad}_a(b) + \mathcal{O}(h^3)\right). \quad (2.13)$$

Similar to the equation (2.11), we can now find $\text{ad}_a(\tau a)$ for $a \in T_e G$ and $\tau \in \mathbb{R}$ by applying (2.6) with $\rho(s) = \exp(sa)$ and $\sigma(t) = \exp(t\tau a)$. We can easily see that $\rho(0) = \sigma(0) = e$, $\rho'(0) = \text{d}L_e(e) a = a$ and $\sigma'(t) = \text{d}L_e(e) \tau a = \tau a$ since both ρ and σ are the solutions to (2.8) with different constants. Now, it can be seen that

$$\rho(s) \circ \sigma(t) \circ \rho(-s) = \exp(sa) \circ \exp(t\tau a) \circ \exp(-sa) = \exp(sa + t\tau a - sa) = \exp(t\tau a),$$

where we have used (2.11). Obviously, $\exp(t\tau a)$ is constant with respect to s , so according to (2.6) it follows

$$\text{ad}_a(\tau a) = 0 \in T_e G. \quad (2.14)$$

Now, let us consider the derivative

$$\text{dexp}(a): T_e G \rightarrow T_{\exp(a)} G$$

of the exponential map for $a \in T_e G$. We will again use the identification of all tangent spaces with $T_e G$ but this time via the derivative of the right translation and write

$$\text{dexp}(a) b = \text{d}R_{\exp(a)}(e) \text{d}xp_a(b).$$

for $a, b \in T_e G$ and where $\text{d}xp_a: T_e G \rightarrow T_e G$ is a linear function, which is the right trivialized tangent of the exponential map.

Lemma 2.14: *A formula for dxp , [80].*

For the right trivialized tangent dxp_a of the exponential map it holds

$$\text{dxp}_a(b) = \sum_{k=0}^{\infty} \frac{1}{(k+1)!} \text{ad}_a^k(b),$$

for all $a, b \in T_e G$, where $\text{ad}_a^0(b) = b$ and $\text{ad}_a^k(b) = \text{ad}_a^{k-1}(\text{ad}_a(b))$ for $k \in \mathbb{N}$.

Note that in research concerned with Lie groups in numerical applications and especially in this thesis, we will use the left translation instead:

$$\text{dexp}(a) b = \text{d}L_{\text{exp}(a)}(e) \text{dxp}_{-a}(b). \quad (2.15)$$

Note that usually, the right trivialized tangent is written as dexp , but due to the danger of confusion with the derivative of exp , we have used the symbol dxp instead.

2.2. The Concept of Derivative Vectors

Lie groups have been widely used in numerical contexts [15, 18, 27, 44, 46, 54, 65, 66, 84]. Often in this field, especially in recent times, the tangent space $T_e G$ of the identity element has been identified with \mathbb{R}^n through an isomorphism, giving rise to the concept of derivative vectors [8, 16]. The tangent space $T_e G$ is of course an n -dimensional vector space and said vector space isomorphism is called the tilde operator [16]

$$\tilde{\bullet}: \mathbb{R}^n \rightarrow T_e G, \quad \mathbf{a} \mapsto \tilde{\mathbf{a}}. \quad (2.16)$$

We use derivative vectors to describe derivatives of Lie group valued functions:

Definition 2.15: *Derivative vectors [16].*

Consider a differentiable G -valued function q . We call $\mathbf{v}(t) \in \mathbb{R}^n$ the derivative vector of $q(t)$ if it holds

$$\dot{q}(t) = \text{d}L_{q(t)}(e) \widetilde{\mathbf{v}(t)}. \quad (2.17)$$

Note that the tilde operator $\tilde{\bullet}$ could be chosen arbitrarily but is always chosen in such a way that the derivative vectors measure physical quantities, e. g. angular velocity.

Often, we will encounter functions $\boldsymbol{\xi}: G \rightarrow \mathbb{R}^k$ that map from the Lie group G to some real vector space \mathbb{R}^k . The derivative $\text{d}\boldsymbol{\xi}(g): T_g G \rightarrow \mathbb{R}^k$ takes arguments from the tangent space $T_g G$. We want to relate this derivative to the space \mathbb{R}^n in which the derivative vectors reside. Thus, we introduce the following differential operator:

Definition 2.16: *Derivative with respect to a Lie group element.*

For a differentiable function $\boldsymbol{\xi}: G \rightarrow \mathbb{R}^k$ with $k \in \mathbb{N}$, we define $\mathbf{D}\boldsymbol{\xi}(g) \in \mathbb{R}^{k \times n}$ as the $k \times n$ matrix that fulfills

$$\mathbf{D}\boldsymbol{\xi}(g) \cdot \mathbf{y} = \text{d}\boldsymbol{\xi}(g) \text{d}L_g(e) \tilde{\mathbf{y}} \quad (2.18)$$

for all $\mathbf{y} \in \mathbb{R}^n$.

This differential operator has not yet been widely used in Lie group methods, but helps to facilitate notation: Often, for each function ξ , a new matrix valued function $\Xi = \mathbf{D}\xi$ was introduced, see e. g. [8].

Now, we will take some more concepts from section 2.1 and adopt them to our concept of derivative vectors:

Definition 2.17: *The hat operator [17].*

In order to describe the adjoint operator ad in terms of derivative vectors, we define the hat operator

$$\widehat{\bullet}: \mathbb{R}^n \rightarrow \mathbb{R}^{n \times n}, \quad \mathbf{a} \mapsto \widehat{\mathbf{a}}$$

as the unique linear function with the property

$$\widehat{\widehat{\mathbf{a}}} \cdot \mathbf{b} = \text{ad}_{\widehat{\mathbf{a}}}(\widetilde{\mathbf{b}}).$$

Definition 2.18: *The exponential map of derivative vectors.*

We introduce the abbreviation

$$\widetilde{\text{exp}}: \mathbb{R}^n \rightarrow G, \quad \mathbf{a} \mapsto \widetilde{\text{exp}}(\mathbf{a}) = \text{exp}(\widetilde{\mathbf{a}})$$

which is a concatenation of the exponential map exp and the tilde operator $\widetilde{\bullet}$.

Definition 2.19: *The logarithm of derivative vectors.*

We introduce the function

$$\widetilde{\text{log}}: \text{exp}(U) \rightarrow \mathbb{R}^n, \quad g \mapsto \widetilde{\text{log}}(g),$$

with U from lemma 2.11 such that

$$\widetilde{\widetilde{\text{log}}(g)} = \text{log}(g).$$

Essentially, $\widetilde{\text{log}}$ is just the concatenation of the inverse of the tilde operator $\widetilde{\bullet}$ and log .

Definition 2.20: *The tangent operator [16].*

The tangent operator

$$\mathbf{T}: \mathbb{R}^n \rightarrow \mathbb{R}^{n \times n}, \quad \mathbf{a} \mapsto \mathbf{T}(\mathbf{a})$$

describes the left trivialized tangent, see (2.15), of the exponential map in terms of the derivative vectors via the relation

$$\mathbf{T}(\widetilde{\mathbf{a}}) \cdot \mathbf{b} = \text{dexp}_{-\widetilde{\mathbf{a}}}(\widetilde{\mathbf{b}}).$$

We collect a couple of properties of the tangent operator:

Remark 2.21: *Properties of the tangent operator.*

If we use definition 2.20 together with equation (2.15), we get

$$\frac{d}{dt} \widetilde{\exp}(\mathbf{a}(t)) = \frac{d}{dt} \exp(\widetilde{\mathbf{a}}(t)) = dL_{\widetilde{\exp}(\mathbf{a}(t))}(e) \tau(\mathbf{T}(\mathbf{a}(t)) \cdot \dot{\mathbf{a}}(t)), \quad (2.19)$$

with the tilde operator written as $\tau(\bullet) = \widetilde{\bullet}$ and where \mathbf{a} is a differentiable function.

From lemma 2.14 we can deduce [17, 46]

$$\mathbf{T}(\mathbf{a}) = \sum_{k=0}^{\infty} \frac{(-1)^k}{(k+1)!} \widehat{\mathbf{a}}^k, \quad \mathbf{a} \in \mathbb{R}^n. \quad (2.20)$$

For the matrix inverse of the tangent operator it holds

$$\mathbf{T}^{-1}(\mathbf{y}) = \sum_{i=0}^{\infty} \frac{(-1)^i B_i}{i!} \widehat{\mathbf{y}}^i, \quad \mathbf{y} \in \mathbb{R}^n, \quad (2.21)$$

where $(B_i)_{i \in \mathbb{N}_0} = (1, -\frac{1}{2}, \frac{1}{6}, 0, \dots)$ are the Bernoulli numbers, see [35, Lemma III.4.2] or [64], where this expansion is written in terms of dexp .

From

$$\mathbf{a} = \widetilde{\log}(\widetilde{\exp}(\mathbf{a}))$$

for all $\mathbf{a} \in \mathbb{R}^n$ close enough to the origin it follows by differentiation with respect to \mathbf{a} in the direction \mathbf{b} that

$$\begin{aligned} \mathbf{b} &= d\widetilde{\log}(\widetilde{\exp}(\mathbf{a})) \, d\widetilde{\exp}(\mathbf{a}) \, \mathbf{b} \\ &= d\widetilde{\log}(\widetilde{\exp}(\mathbf{a})) \, dL_{\widetilde{\exp}(\mathbf{a})}(e) \, \mathbf{T}(\mathbf{a}) \cdot \mathbf{b} \\ &= \mathbf{D}\widetilde{\log}(\widetilde{\exp}(\mathbf{a})) \cdot \mathbf{T}(\mathbf{a}) \cdot \mathbf{b} \end{aligned}$$

Since this has to hold for all directions $\mathbf{b} \in \mathbb{R}^n$, we get the helpful formula

$$\mathbf{D}\widetilde{\log}(q) = \mathbf{T}^{-1}(\widetilde{\log}(q)), \quad q \in \exp(U) \subseteq G, \quad (2.22)$$

where we have set $q = \widetilde{\exp}(\mathbf{a})$ and U is the open set from lemma 2.11.

Now, we will prove a qualitative Taylor's theorem for G -valued functions:

Lemma 2.22: *Qualitative Taylor's theorem for Lie group valued functions.*

Let q be a three times continuously differentiable G -valued function with derivative vectors $\mathbf{v}(t)$ according to (2.17). Then it holds

$$q(t+h) = q(t) \circ \widetilde{\exp}(h\mathbf{v}(t) + \frac{h^2}{2}\dot{\mathbf{v}}(t) + \mathcal{O}(h^3)) \quad (2.23)$$

for $h \rightarrow 0$. A formula of this kind can be found in [64], where even more terms are provided. It is based on the idea of the Magnus expansion [62].

Proof. Let $|h|$ be small enough such that

$$\psi(h) = \widetilde{\log}(q^{-1}(t) \circ q(t+h))$$

is well-defined. It is clear that $\psi(0) = \mathbf{0}$. Now, we will find the first two derivatives of $\psi(h)$ by differentiating both sides of

$$\widetilde{\exp}(\psi(h)) = q^{-1}(t) \circ q(t+h)$$

with respect to h , where we have omitted the argument h of ψ :

$$\begin{aligned} dL_{\widetilde{\exp}(\psi)}(e) \mathbf{T}(\widetilde{\psi}) \cdot \psi' &= dL_{q^{-1}(t)}(q(t+h)) \dot{q}(t+h) \\ &= dL_{q^{-1}(t) \circ q(t+h)}(e) \widetilde{\mathbf{v}(t+h)} = dL_{\widetilde{\exp}(\psi)}(e) \widetilde{\mathbf{v}(t+h)}, \end{aligned}$$

using (2.19) and (2.3). It follows

$$\mathbf{T}(\psi(h)) \cdot \psi'(h) = \mathbf{v}(t+h).$$

We can see that it holds $\psi'(0) = \mathbf{v}(t)$, because $\psi(0) = \mathbf{0}$ and $\mathbf{T}(\mathbf{0}) = \mathbf{I}$. Differentiating once more at $h = 0$, we get, keeping $\psi(0) = \mathbf{0}$, $\widehat{\mathbf{0}} = \mathbf{0}$ and the expansion (2.20) in mind:

$$\mathbf{T}(\mathbf{0}) \cdot \psi''(0) + \left(\mathbf{0} + \frac{(-1)^1}{(1+1)!} \widehat{\psi'(0)} + \mathbf{0} \right) \cdot \psi'(0) = \dot{\mathbf{v}}(t).$$

This means that $\psi''(0) = \dot{\mathbf{v}}(t)$, because of (2.14). Now, we apply the standard qualitative Taylor's theorem to ψ around $h = 0$ with order two and get

$$q(t+h) = q(t) \circ \widetilde{\exp}(\psi(h)) = q(t) \circ \widetilde{\exp}(\psi(0) + h\psi'(0) + \frac{h^2}{2}\psi''(0) + \mathcal{O}(h^3))$$

for $h \rightarrow 0$ which implies the assertion. \square

Lemma 2.23: *Bivariate functions, see e. g. [17].*

Let us consider a continuously differentiable function with $q(s, t) \in G$ and derivative vectors $\mathbf{a}(s, t)$ and $\mathbf{b}(s, t)$ corresponding to the derivative with respect to s and t respectively:

$$q'(s, t) = dL_{q(s,t)}(e) \widetilde{\mathbf{a}(s,t)} \quad \text{and} \quad \dot{q}(s, t) = dL_{q(s,t)}(e) \widetilde{\mathbf{b}(s,t)}.$$

Then it holds

$$\widehat{\mathbf{a}(s,t)} \cdot \mathbf{b}(s, t) = \dot{\mathbf{a}}(s, t) - \mathbf{b}'(s, t).$$

Proof. We will apply lemma 2.9 to $p(\sigma, \tau) = (q(s, t))^{-1} \circ q(s + \sigma, t + \tau)$. Its derivative vectors are given by

$$\begin{aligned} p'(\sigma, \tau) &= dL_{(q(s,t))^{-1}}(q(s + \sigma, t + \tau)) dL_{q(s+\sigma, t+\tau)}(e) \widetilde{\mathbf{a}}(s + \sigma, t + \tau) \\ &= dL_{p(\sigma, \tau)} \widetilde{\mathbf{a}}(s + \sigma, t + \tau), \end{aligned}$$

$$\begin{aligned} \text{and} \quad \dot{p}(\sigma, \tau) &= dL_{(q(s,t))^{-1}}(q(s + \sigma, t + \tau)) dL_{q(s+\sigma, t+\tau)}(e) \widetilde{\mathbf{b}}(s + \sigma, t + \tau) \\ &= dL_{p(\sigma, \tau)} \widetilde{\mathbf{b}}(s + \sigma, t + \tau), \end{aligned}$$

where we have used (2.3). Thus, from lemma 2.9 it follows

$$\text{ad}_{\widetilde{\mathbf{a}(s,t)}}(\widetilde{\mathbf{b}(s,t)}) = \widetilde{\dot{\mathbf{a}}(s,t)} - \widetilde{\mathbf{b}'(s,t)},$$

from which the assertion follows by applying the inverse of the tilde operator and definition 2.17 of the hat operator. \square

In the following, we will consider a nonlinear generalization $\Delta(q_0, q_1; h) \in \mathbb{R}^n$ of difference quotients of $q_0, q_1 \in G$ and $h > 0$ on Lie groups. The next Lemma shows that it has similar properties to the regular difference quotient $(\mathbf{q}_1 - \mathbf{q}_0)/h$ for $\mathbf{q}_0, \mathbf{q}_1 \in \mathbb{R}^n$ in that it can be used to approximate derivatives of functions of scalar arguments up to second order:

Lemma 2.24: *Nonlinear generalization of difference quotients.*

Define the nonlinear difference quotient

$$\Delta(q_0, q_1; h) = \frac{1}{h} \widetilde{\log}(q_0^{-1} \circ q_1)$$

for $q_0, q_1 \in G$ and $h > 0$. For a three times continuously differentiable function $q: I \subseteq \mathbb{R} \rightarrow G$, with derivative vectors $\mathbf{v}(t)$ and points $t_0, t_1 \in I$ it holds

$$\Delta(q(t_0), q(t_1); t_1 - t_0) = \mathbf{v}\left(\frac{t_0 + t_1}{2}\right) + \mathcal{O}((t_1 - t_0)^2)$$

and furthermore

$$\Delta(q(t_0), q(t_1); t_1 - t_0) = \mathbf{v}(\tau) + \mathcal{O}(t_1 - t_0)$$

for any $\tau \in [t_0, t_1]$ and $t_1 - t_0 \rightarrow 0$.

Proof. Let $h = (t_1 - t_0)/2$ and $t_{1/2} = t_0 + h = t_1 - h$. We can use the qualitative Taylor's theorem from lemma 2.22 in order to obtain

$$\begin{aligned} q(t_1) &= q(t_{1/2} + h) = q(t_{1/2}) \circ \widetilde{\exp}(h\mathbf{v}(t_{1/2}) + \frac{h^2}{2}\dot{\mathbf{v}}(t_{1/2}) + \mathcal{O}(h^3)), \\ q(t_0) &= q(t_{1/2} - h) = q(t_{1/2}) \circ \widetilde{\exp}(-h\mathbf{v}(t_{1/2}) + \frac{h^2}{2}\dot{\mathbf{v}}(t_{1/2}) + \mathcal{O}(h^3)). \end{aligned}$$

Now, it follows by applying the qualitative Baker-Campbell-Hausdorff formula from lemma 2.13

$$(q(t_0))^{-1} \circ q(t_1) = \widetilde{\exp}(2h\mathbf{v}(t_{1/2}) + \frac{h^2}{2}\dot{\mathbf{v}}(t_{1/2}) - \frac{h^2}{2}\dot{\mathbf{v}}(t_{1/2}) + \frac{h^2}{2}\widehat{\mathbf{v}(t_{1/2})} \cdot \mathbf{v}(t_{1/2}) + \mathcal{O}(h^3)),$$

because of (2.12) and (2.14). Now, the first result follows by taking the logarithm $\widetilde{\log}$ on both sides and dividing by $t_1 - t_0$.

The second result follows analogously by expanding q around τ with $h = t_1 - \tau$ and $h = t_0 + \tau$. \square

An alternative proof can be found in [44].

Lemma 2.25: *Derivatives of Δ .*

For the derivatives $\Delta(q_0, q_1; h)$ with respect to the first and second argument it holds

$$\begin{aligned}\mathbf{D}_1\Delta(q_0, q_1; h) &= -\frac{1}{h}\mathbf{T}^{-1}(-h\Delta(q_0, q_1; h)), \\ \mathbf{D}_2\Delta(q_0, q_1; h) &= \frac{1}{h}\mathbf{T}^{-1}(h\Delta(q_0, q_1; h)),\end{aligned}$$

if $q_0, q_1 \in G$ are sufficiently close to each other.

Proof. Let $\mathbf{w} \in \mathbb{R}^n$ be arbitrary but fixed. We consider

$$\begin{aligned}\mathbf{D}_2\Delta(q_0, q_1; h) \cdot \mathbf{w} &= \frac{1}{h} d_{q_1} \widetilde{\log}(L_{q_0^{-1}}(q_1)) dL_{q_1}(e) \widetilde{\mathbf{w}} \\ &= \frac{1}{h} d\widetilde{\log}(q_0^{-1} \circ q_1) dL_{q_0^{-1}}(q_1) dL_{q_1}(e) \widetilde{\mathbf{w}} = \frac{1}{h} d\widetilde{\log}(q_0^{-1} \circ q_1) dL_{q_0^{-1} \circ q_1}(e) \widetilde{\mathbf{w}} \\ &= \frac{1}{h} \mathbf{D}\widetilde{\log}(q_0^{-1} \circ q_1) \cdot \mathbf{w} = \frac{1}{h} \mathbf{T}^{-1}(\widetilde{\log}(q_0^{-1} \circ q_1)) \cdot \mathbf{w},\end{aligned}$$

where we have used definition 2.16, as well as (2.3) and (2.22). The second identity follows since \mathbf{w} was arbitrary. Furthermore, it holds

$$\Delta(q_0, q_1; h) = \frac{1}{h} \widetilde{\log}((q_1^{-1} \circ q_0)^{-1}) = -\frac{1}{h} \widetilde{\log}(q_1^{-1} \circ q_0) = -\Delta(q_1, q_0; h)$$

by using (2.12). Therefore, the first identity follows by

$$\begin{aligned}\mathbf{D}_1\Delta(q_0, q_1; h) &= -\mathbf{D}_2\Delta(q_1, q_0; h) \\ &= -\frac{1}{h}\mathbf{T}^{-1}(h\Delta(q_1, q_0; h)) = -\frac{1}{h}\mathbf{T}^{-1}(-h\Delta(q_0, q_1; h)). \quad \square\end{aligned}$$

Now we introduce an interpolation function $\text{Ip}(\tau, q_0, q_1)$ for $\tau \in [0, 1]$ and $q_0, q_1 \in G$, which is supposed to be a function q with $q(0) = q_0$, $q(1) = q_1$ and a constant derivative vector \mathbf{v} . If q_0 and q_1 are close enough to each other, we define $\text{Ip}(\tau, q_0, q_1)$ by

$$\text{Ip}(\tau, q_0, q_1) = q_0 \circ \widetilde{\exp}(\tau \widetilde{\log}(q_0^{-1} \circ q_1)). \quad (2.24)$$

This interpolation generalizes the ordinary linear interpolation as well as the spherical linear interpolation SLERP, see e. g. [40]. In order to see that Ip has similar approximation properties, we will prove the following:

Lemma 2.26: *Interpolation Ip approximates with second order.*

Let $q: (-h_0, h_0) \rightarrow G$ be twice continuously differentiable with $h_0 > 0$. Then it holds

$$\text{Ip}(\tau, q(0), q(h)) = q(\tau h) \circ \widetilde{\exp}(\mathcal{O}(h^2))$$

for $\tau \in [0, 1]$ and $h \rightarrow 0$.

Proof. On the one hand, lemma 2.24 implies

$$\text{Ip}(\tau, q(0), q(h)) = q(0) \circ \widetilde{\text{exp}}\left(\tau h \Delta(q(0), q(h); h)\right) = q(0) \circ \widetilde{\text{exp}}\left(\tau h(\mathbf{v}(0) + \boldsymbol{\xi}_1)\right) \quad (2.25)$$

with $\boldsymbol{\xi}_1 \in \mathcal{O}(h)$ and on the other hand the qualitative Taylor's formula from lemma 2.22 gives us

$$q(\tau h) = q(0) \circ \widetilde{\text{exp}}(\tau h \mathbf{v}(0) + h \boldsymbol{\xi}_2)$$

with $\boldsymbol{\xi}_2 \in \mathcal{O}(h)$. Rearranging this equation using (2.12) yields

$$q(0) = q(\tau h) \circ \widetilde{\text{exp}}(-\tau h \mathbf{v}(0) - h \boldsymbol{\xi}_2)$$

and by inserting it in (2.25) as well as applying the qualitative Baker-Campbell-Hausdorff formula from lemma 2.13 the assertion follows:

$$\begin{aligned} \text{Ip}(\tau, q(0), q(h)) &= q(\tau h) \circ \widetilde{\text{exp}}(-\tau h \mathbf{v}(0) - h \boldsymbol{\xi}_2) \circ \widetilde{\text{exp}}\left(\tau h(\mathbf{v}(0) + \boldsymbol{\xi}_1)\right) \\ &= q(\tau h) \circ \widetilde{\text{exp}}(\tau h \mathbf{v}(0) - \tau h \mathbf{v}(0) + h(\boldsymbol{\xi}_1 - \boldsymbol{\xi}_2)), \end{aligned}$$

where $h(\boldsymbol{\xi}_1 - \boldsymbol{\xi}_2) \in \mathcal{O}(h^2)$. □

Remark 2.27: *Piecewise interpolation.*

Let $t_0 < t_1 < \dots < t_N$ be a grid and $q_0, q_1, \dots, q_N \in G$. Then we define the interpolation

$$\text{pIp}(\tau, (t_n)_{n=0, \dots, N}, (q_n)_{n=0, \dots, N}) = \text{Ip}\left(\frac{\tau - t_n}{t_{n+1} - t_n}, q_n, q_{n+1}\right), \quad \text{if } \tau \in [t_n, t_{n+1})$$

and $\text{pIp}(t_N, (t_n)_{n=0, \dots, N}, (q_n)_{n=0, \dots, N}) = q_N$.

Consider now a function $q: [t_0, t_e] \rightarrow G$ with $t_0 < t_e$ and a grid $t_0 < t_1 < \dots < t_N = t_e$. Then the piecewise interpolation on the data $(t_n, q(t_n))$ approximates the original function q with second order if q is smooth enough:

$$\text{pIp}(\tau, (t_n)_{n=0, \dots, N}, (q_n)_{n=0, \dots, N}) = q(\tau) \circ \widetilde{\text{exp}}(\mathcal{O}(h_{\max}^2)),$$

where $h_{\max} = \max_{n=1, \dots, N}(t_n - t_{n-1})$ for $h_{\max} \rightarrow 0$. This is a direct consequence of lemma 2.26.

2.3. The Lie Group $\mathbb{S}^3 \ltimes \mathbb{R}^3$

In this section, we will consider the Lie group $\mathbb{S}^3 \ltimes \mathbb{R}^3$, which is a semi-direct product of the Lie group of unit quaternions $\mathbb{S}^3 \subseteq \mathbb{R}^4$ and the real vector space \mathbb{R}^3 . We will later see that it is closely related to the Lie group of rigid body motions $SE(3)$.

Note that in the following, we will identify the orientation of a rigid body with its rotation from some reference orientation, the position with the translation from some reference position and likewise the combination of orientation and position with the rigid

transformation from some reference orientation and position. This allows us to sensibly talk about concatenation of these transformations which define the Lie group operation of $\mathbb{S}^3 \times \mathbb{R}^3$.

First, we will consider quaternions. For an introduction to this topic refer to e. g. [26, 40]. In this thesis, we will identify the space of quaternions with the four-dimensional vector space \mathbb{R}^4 . Typically, we would number the components of a quaternion $\mathbf{p} \in \mathbb{R}^4$ starting by zero:

$$\mathbf{p} = \begin{bmatrix} p_0 \\ p_1 \\ p_2 \\ p_3 \end{bmatrix},$$

where we call $\text{Re } \mathbf{p} = p_0 \in \mathbb{R}$ the real or scalar part and $\text{Im } \mathbf{p} = [p_1, p_2, p_3]^\top \in \mathbb{R}^3$ the imaginary or vector part of the quaternion $\mathbf{p} \in \mathbb{R}^4$. We define the quaternion multiplication $*$: $\mathbb{R}^4 \rightarrow \mathbb{R}^4$ by

$$\mathbf{p} * \mathbf{q} = \begin{bmatrix} (\text{Re } \mathbf{p})(\text{Re } \mathbf{q}) - (\text{Im } \mathbf{p})^\top \cdot (\text{Im } \mathbf{q}) \\ (\text{Re } \mathbf{p})(\text{Im } \mathbf{q}) + (\text{Re } \mathbf{q})(\text{Im } \mathbf{p}) + (\text{Im } \mathbf{p}) \times (\text{Im } \mathbf{q}) \end{bmatrix},$$

where $\times: \mathbb{R}^3 \times \mathbb{R}^3 \rightarrow \mathbb{R}^3$ is the cross product. We can see that the quaternion multiplication is not commutative, since $\mathbf{p} \times \mathbf{q} = -\mathbf{q} \times \mathbf{p}$. The quaternions form a division algebra (skew field) with quaternion multiplication $*$, regular addition $+$, zero $\mathbf{0} \in \mathbb{R}^4$ and one $[1, 0, 0, 0]^\top$, see e. g. [26]. The inverse element with respect to $*$ of a quaternion $\mathbf{p} \in \mathbb{R}^4 \setminus \{\mathbf{0}\}$ can be expressed by the conjugate

$$\bar{\mathbf{p}} = \begin{bmatrix} \text{Re } \mathbf{p} \\ -\text{Im } \mathbf{p} \end{bmatrix}$$

and the Euclidean norm $\|\bullet\|_2$:

$$\mathbf{p}^{-1} = \frac{\bar{\mathbf{p}}}{\|\mathbf{p}\|_2^2}. \quad (2.26)$$

Furthermore, for the norm of a quaternion product it holds

$$\|\mathbf{p} * \mathbf{q}\|_2 = \|\mathbf{p}\|_2 \|\mathbf{q}\|_2. \quad (2.27)$$

Let us now focus on the set \mathbb{S}^3 of unit quaternions

$$\mathbb{S}^3 = \{\mathbf{p} \in \mathbb{R}^4: \|\mathbf{p}\|_2^2 = 1\},$$

which is a regular surface of dimension three, since $\mathbf{p} \mapsto \|\mathbf{p}\|_2^2 - 1$ is a quadratic polynomial whose differential only vanishes at the origin, see lemma 2.2. Due to (2.26) and (2.27), it follows that \mathbb{S}^3 must be a subgroup of $(\mathbb{R}^4 \setminus \{\mathbf{0}\}, *)$. Since the quaternion multiplication and its inversion are clearly smooth mappings, unit quaternions $(\mathbb{S}^3, *)$ form a Lie group with the identity element $e = [1, 0, 0, 0]^\top$. It is well-known in the literature, see e. g. [40],

that unit quaternions can be used to describe rotations of rigid bodies. The result of the rotation of a vector $\mathbf{w} \in \mathbb{R}^3$ that is encoded in a unit quaternion $p \in \mathbb{S}^3$ is given by

$$p \triangleright \mathbf{w} = \text{Im} \left(p * \begin{bmatrix} 0 \\ \mathbf{w} \end{bmatrix} * \bar{p} \right).$$

Rotating a vector is actually a left action from \mathbb{S}^3 on \mathbb{R}^3 since it holds

$$(p * q) \triangleright \mathbf{w} = p \triangleright (q \triangleright \mathbf{w})$$

for $p, q \in \mathbb{S}^3$ and $\mathbf{w} \in \mathbb{R}^3$. Note that the two unit quaternions $p \in \mathbb{S}^3$ and $-p \in \mathbb{S}^3$ describe the same rotation. It can be shown that there is a smooth two-to-one mapping between unit quaternions \mathbb{S}^3 and the Lie group of rotation matrices $SO(3)$, see e. g. [40]. We can consider $p \in \mathbb{S}^3$ to describe the rotation of a rigid body from a reference orientation. The Lie algebra $\mathfrak{s}^3 = T_e \mathbb{S}^3$ is given by all quaternions with vanishing real part

$$T_e \mathbb{S}^3 = \{\mathbf{p} \in \mathbb{R}^4 : \text{Re } \mathbf{p} = 0\},$$

because for every $p \in \mathbb{S}^3$, p must be normal to $T_p \mathbb{S}^3$ which can be seen by differentiating the unity constraint for any differentiable curve in \mathbb{S}^3 passing through p . Since the quaternion multiplication is linear in \mathbb{R}^4 , we can immediately see that for $p, q \in \mathbb{S}^3$ and $a \in T_q G \subseteq \mathbb{R}^4$

$$dL_p(q) a = p * a.$$

In order to identify the elements of $T_e \mathbb{S}^3$ with angular velocities, we choose the tilde operator as follows:

$$\tilde{\boldsymbol{\Omega}} = \begin{bmatrix} 0 \\ \frac{1}{2} \boldsymbol{\Omega} \end{bmatrix} \in T_e \mathbb{S}^3, \quad \boldsymbol{\Omega} \in \mathbb{R}^3,$$

see e. g. [53]. Note that if a differentiable curve $p(t) \in \mathbb{S}^3$ describing the time-dependent orientation of a rigid body and that has derivative vectors $\boldsymbol{\Omega}(t)$, then the components of $\boldsymbol{\Omega}(t)$ describe the angular velocities around the body-fixed frame ($p \triangleright \mathbf{e}_1, p \triangleright \mathbf{e}_2, p \triangleright \mathbf{e}_3$), where \mathbf{e}_i for $i = 1, 2, 3$ are the canonical base vectors of \mathbb{R}^3 . Furthermore it holds

$$\frac{d}{dt} (p(t) \triangleright \mathbf{w}) = p(t) \triangleright (\boldsymbol{\Omega} \times \mathbf{w}) \tag{2.28}$$

for every $\mathbf{w} \in \mathbb{R}^3$. The exponential map is given by

$$\widetilde{\text{exp}}(\boldsymbol{\Omega}) = \begin{bmatrix} \cos(\|\boldsymbol{\Omega}\|_2/2) \\ \frac{\boldsymbol{\Omega}}{\|\boldsymbol{\Omega}\|_2} \sin(\|\boldsymbol{\Omega}\|_2/2) \end{bmatrix}$$

for $\boldsymbol{\Omega} \in \mathbb{R}^3 \setminus \{\mathbf{0}\}$, because by differentiating $\widetilde{\text{exp}}(t\boldsymbol{\Omega})$ with respect to t , we get

$$\frac{d}{dt} \widetilde{\text{exp}}(t\boldsymbol{\Omega}) = \begin{bmatrix} -\|\boldsymbol{\Omega}\|_2 \sin(t\|\boldsymbol{\Omega}\|_2/2)/2 \\ \boldsymbol{\Omega} \cos(t\|\boldsymbol{\Omega}\|_2/2)/2 \end{bmatrix} = \widetilde{\text{exp}}(t\boldsymbol{\Omega}) * \begin{bmatrix} 0 \\ \boldsymbol{\Omega}/2 \end{bmatrix} = dL_{\widetilde{\text{exp}}(t\boldsymbol{\Omega})}(e) \tilde{\boldsymbol{\Omega}}.$$

Of course, $\widetilde{\exp}(\mathbf{0}) = e$. The exponential $\widetilde{\exp}$ is injective on the open ball around the origin of \mathbb{R}^3 with radius 2π and its inverse, the logarithm $\widetilde{\log}$ is given by

$$\widetilde{\log}(p) = 2 \arccos(\operatorname{Re} p) \frac{\operatorname{Im} p}{\|\operatorname{Im} p\|_2}$$

for $\|\operatorname{Im} p\|_2 \neq 0$. Furthermore it holds $\widetilde{\log}(e) = \mathbf{0}$, which can be easily verified by calculating $\widetilde{\exp}(\widetilde{\log}(p)) = p$ for $|\operatorname{Re} p| \neq -1$. We can calculate the adjoint operator by using (2.7) for $a, b \in T_e \mathbb{S}^3$:

$$\operatorname{ad}_a(b) = a * b - b * a,$$

leading to

$$\widehat{\boldsymbol{\Omega}} = \operatorname{skw}(\boldsymbol{\Omega}),$$

where $\operatorname{skw}: \mathbb{R}^3 \rightarrow \mathbb{R}^{3 \times 3}$ transforms a 3D vector into the skew-symmetric matrix

$$\operatorname{skw} \left(\begin{bmatrix} \Omega_1 \\ \Omega_2 \\ \Omega_3 \end{bmatrix} \right) = \begin{bmatrix} 0 & -\Omega_3 & \Omega_2 \\ \Omega_3 & 0 & -\Omega_1 \\ -\Omega_2 & \Omega_1 & 0 \end{bmatrix} \quad (2.29)$$

with the property $\operatorname{skw}(\mathbf{a}) \cdot \mathbf{b} = \mathbf{a} \times \mathbf{b}$. Since the hat operator is equal to the hat operator of the Lie algebra of $SO(3)$, the tangent operator and its inverse are the same as in the case of $SO(3)$, see [17]. Note that in order to implement these functions, we need to be careful in a small neighborhood of the origin of $T_e \mathbb{S}^3$, because a dramatic loss of significance can occur. The functions related to $(\mathbb{S}^3, *)$ and notes on how to implement them properly can be found in appendix A.4.

In the same way that $(\mathbb{S}^3, *)$ describes rotations of a rigid body from a reference orientation, we can describe the translation of a rigid body from a reference position by the linear Lie group $(\mathbb{R}^3, +)$. Now, we are interested in rigid body motions (p, \mathbf{x}) that rotate and translate the body; thus take the form

$$\mathbf{w} \mapsto p \triangleright \mathbf{w} + \mathbf{x}$$

for some rotation $p \in \mathbb{S}^3$ and translation $\mathbf{x} \in \mathbb{R}^3$. The concatenation of two such rigid body motions (p_1, \mathbf{x}_1) and (p_2, \mathbf{x}_2) would then be

$$\mathbf{w} \mapsto p_1 \triangleright (p_2 \triangleright \mathbf{w} + \mathbf{x}_2) + \mathbf{x}_1 = (p_1 * p_2) \triangleright \mathbf{w} + (\mathbf{x}_1 + p_1 \triangleright \mathbf{x}_2).$$

Let us thus define a function

$$\begin{aligned} \circ: (\mathbb{S}^3 \times \mathbb{R}^3) \times (\mathbb{S}^3 \times \mathbb{R}^3) &\rightarrow \mathbb{S}^3 \times \mathbb{R}^3, \\ ((p_1, \mathbf{x}_1), (p_2, \mathbf{x}_2)) &\mapsto (p_1, \mathbf{x}_1) \circ (p_2, \mathbf{x}_2) = (p_1 * p_2, \mathbf{x}_1 + p_1 \triangleright \mathbf{x}_2). \end{aligned}$$

It is easy to see that \circ is associative, that $e = ([1, 0, 0, 0]^\top, \mathbf{0}) \in \mathbb{S}^3 \times \mathbb{R}^3$ is the identity element and to every element $(p, \mathbf{x}) \in \mathbb{S}^3 \times \mathbb{R}^3$ there is an inverse element

$$(p, \mathbf{x})^{-1} = (\bar{p}, -\bar{p} \triangleright \mathbf{x}).$$

Thus, $\mathbb{S}^3 \times \mathbb{R}^3$ together with \circ is a group, which we will call $(\mathbb{S}^3 \times \mathbb{R}^3, \circ)$ or, by abuse of notation $\mathbb{S}^3 \times \mathbb{R}^3$. More specifically, $\mathbb{S}^3 \times \mathbb{R}^3$ is an (outer) semi-direct product of the two groups \mathbb{S}^3 and \mathbb{R}^3 . Since \circ and the inversion are obviously smooth and $\mathbb{S}^3 \times \mathbb{R}^3 \subseteq \mathbb{R}^4 \times \mathbb{R}^3$ is a regular surface as the direct product of two regular surfaces, $\mathbb{S}^3 \times \mathbb{R}^3$ forms a Lie group of dimension $3 + 3 = 6$. The tangent space at the identity element is given by

$$T_e(\mathbb{S}^3 \times \mathbb{R}^3) = T_e(\mathbb{S}^3 \times \mathbb{R}^3) = \{(a, \mathbf{y}) \in \mathbb{R}^4 \times \mathbb{R}^3 : a \in T_{[1,0,0,0]^\top} \mathbb{S}^3\},$$

since, as a manifold, $\mathbb{S}^3 \times \mathbb{R}^3$ is a direct product. Now, we can calculate

$$dL_{(p,\mathbf{x})}(e)(a, \mathbf{w}) = (p * a, p \triangleright \mathbf{w})$$

with $(p, \mathbf{x}) \in \mathbb{S}^3 \times \mathbb{R}^3$ and $(a, \mathbf{w}) \in T_e(\mathbb{S}^3 \times \mathbb{R}^3)$ by taking a differentiable curve $(q(t), \mathbf{y}(t)) \in \mathbb{S}^3 \times \mathbb{R}^3$ with the property $(q(0), \mathbf{y}(0)) = e$ and $d/dt(q(t), \mathbf{y}(t))|_{t=0} = (\dot{q}(0), \dot{\mathbf{y}}(0)) = (a, \mathbf{w})$ and differentiating $L_{(p,\mathbf{x})}(q(t), \mathbf{y}(t))$ at $t = 0$. We will identify the elements of $T_e(\mathbb{S}^3 \times \mathbb{R}^3)$ by the following tilde operator:

$$\widetilde{\begin{bmatrix} \boldsymbol{\Omega} \\ \mathbf{U} \end{bmatrix}} = \left(\begin{bmatrix} 0 \\ \frac{1}{2} \boldsymbol{\Omega} \end{bmatrix}, \mathbf{U} \right).$$

Note that if a differentiable curve $(p(t), \mathbf{x}(t))$ describing the motion of a rigid body and that has derivative vectors $[\boldsymbol{\Omega}^\top(t), \mathbf{U}^\top(t)]^\top$, then the components of $\boldsymbol{\Omega}(t)$ and $\mathbf{U}(t)$ describe the angular velocities around and velocities along the body-fixed frame $(p(t) \triangleright \mathbf{e}_1, p(t) \triangleright \mathbf{e}_2, p(t) \triangleright \mathbf{e}_3)$, respectively. The exponential map $\widetilde{\text{exp}}$ is given by

$$\widetilde{\text{exp}}\left(\begin{bmatrix} \boldsymbol{\Omega} \\ \mathbf{U} \end{bmatrix}\right) = (\widetilde{\text{exp}}_{\mathbb{S}^3}(\boldsymbol{\Omega}), \mathbf{T}_{\mathbb{S}^3}^\top(\boldsymbol{\Omega}) \cdot \mathbf{U}), \quad (2.30)$$

where $\widetilde{\text{exp}}_{\mathbb{S}^3}$ and $\mathbf{T}_{\mathbb{S}^3}$ are the exponential map and tangent operator from the Lie group of unit quaternions \mathbb{S}^3 . We can prove this by showing that $d/dt \widetilde{\text{exp}}(t\mathbf{v}) = dL_{\widetilde{\text{exp}}(t\mathbf{v})}(e) \tilde{\mathbf{v}}$ for any $\mathbf{v} \in \mathbb{R}^6$ and $\widetilde{\text{exp}}(\mathbf{0}) = e$, which is obvious. Let $\mathbf{v} = [\boldsymbol{\Omega}^\top, \mathbf{U}^\top]^\top$:

$$\frac{d}{dt} \widetilde{\text{exp}}(t\mathbf{v}) = \left(\frac{1}{2} \widetilde{\text{exp}}_{\mathbb{S}^3}(t\boldsymbol{\Omega}) * \begin{bmatrix} 0 \\ \boldsymbol{\Omega} \end{bmatrix}, \sum_{k=0}^{\infty} \frac{\text{skw}(t\boldsymbol{\Omega})^k}{k!} \cdot \mathbf{U} \right),$$

where the equality in the first component is known from the definition of $\widetilde{\text{exp}}_{\mathbb{S}^3}$ and in the second component, we have used the series definition of the tangent operator, that the hat operator in \mathbb{S}^3 is skw , and that $\text{skw}(\boldsymbol{\Omega})^\top = -\text{skw}(\boldsymbol{\Omega})$. Furthermore, it can be seen that $\sum_{k=0}^{\infty} \frac{\text{skw}(t\boldsymbol{\Omega})^k}{k!} \cdot \mathbf{U} = \widetilde{\text{exp}}_{\mathbb{S}^3}(\boldsymbol{\Omega}) \triangleright \mathbf{U}$ by using Rodrigues' rotation formula, see e. g. [46]. In the end, we get

$$\frac{d}{dt} \widetilde{\text{exp}}(t\mathbf{v}) = \left(\frac{1}{2} \widetilde{\text{exp}}_{\mathbb{S}^3}(t\boldsymbol{\Omega}) * \begin{bmatrix} 0 \\ \boldsymbol{\Omega} \end{bmatrix}, \widetilde{\text{exp}}_{\mathbb{S}^3}(t\boldsymbol{\Omega}) \triangleright \mathbf{U} \right) = dL_{\widetilde{\text{exp}}(t\mathbf{v})}(e) \tilde{\mathbf{v}}$$

and therefore, the right-hand side of (2.30) really is the exponential function concatenated with the tilde operator. Similar to the case of \mathbb{S}^3 , the exponential $\widetilde{\exp}$ is injective for all $[\boldsymbol{\Omega}^\top, \mathbf{U}^\top]^\top \in \mathbb{R}^6$ with $\|\boldsymbol{\Omega}\|_2 < 2\pi$ and its inverse $\widetilde{\log}$ is then given by

$$\widetilde{\log}((p, \mathbf{x})) = \begin{bmatrix} \widetilde{\log}_{\mathbb{S}^3}(p) \\ \mathbf{T}_{\mathbb{S}^3}^{-\top}(\widetilde{\log}_{\mathbb{S}^3}(p)) \cdot \mathbf{x} \end{bmatrix}$$

for $(p, \mathbf{x}) \in \mathbb{S}^3 \times \mathbb{R}^3$ with $\operatorname{Re} p \neq -1$. Now, we will focus on deriving the adjoint operator by using (2.7) with $\rho(s) = (p_1(s), \mathbf{x}_1(s))$, $\sigma(t) = (p_2(t), \mathbf{x}_2(t))$, where $\rho(0) = \sigma(0) = e$ and

$$\rho'(0) = \widetilde{\mathbf{w}}_1 = \begin{bmatrix} \widetilde{\boldsymbol{\Omega}}_1 \\ \widetilde{\mathbf{U}}_1 \end{bmatrix}, \quad \dot{\sigma}(0) = \widetilde{\mathbf{w}}_2 = \begin{bmatrix} \widetilde{\boldsymbol{\Omega}}_2 \\ \widetilde{\mathbf{U}}_2 \end{bmatrix}.$$

It follows

$$\begin{aligned} \operatorname{ad}_{\widetilde{\mathbf{w}}_1}(\widetilde{\mathbf{w}}_2) &= \left. \frac{d}{ds} \left(p_1(s) * \begin{bmatrix} 0 \\ \frac{1}{2} \boldsymbol{\Omega}_2 \end{bmatrix}, p_1(s) \triangleright \mathbf{U}_2 \right) \right|_{s=0} - \left. \frac{d}{dt} \left(p_2(t) * \begin{bmatrix} 0 \\ \frac{1}{2} \boldsymbol{\Omega}_1 \end{bmatrix}, p_2(t) \triangleright \mathbf{U}_1 \right) \right|_{t=0} \\ &= \left(\begin{bmatrix} 0 \\ \frac{1}{2} \boldsymbol{\Omega}_1 \end{bmatrix} * \begin{bmatrix} 0 \\ \frac{1}{2} \boldsymbol{\Omega}_2 \end{bmatrix}, \boldsymbol{\Omega}_1 \times \mathbf{U}_2 \right) - \left(\begin{bmatrix} 0 \\ \frac{1}{2} \boldsymbol{\Omega}_2 \end{bmatrix} * \begin{bmatrix} 0 \\ \frac{1}{2} \boldsymbol{\Omega}_1 \end{bmatrix}, \boldsymbol{\Omega}_2 \times \mathbf{U}_1 \right) \\ &= \begin{bmatrix} 0 \\ \frac{1}{2}(\boldsymbol{\Omega}_1 \times \boldsymbol{\Omega}_2) \end{bmatrix}, \boldsymbol{\Omega}_1 \times \mathbf{U}_2 - \boldsymbol{\Omega}_2 \times \mathbf{U}_1, \end{aligned}$$

where we have used (2.28) and the fact that the cross product is anticommutative. It immediately follows that for the hat operator it holds

$$\begin{bmatrix} \widehat{\boldsymbol{\Omega}}_1 \\ \widehat{\mathbf{U}}_1 \end{bmatrix} \cdot \begin{bmatrix} \widehat{\boldsymbol{\Omega}}_2 \\ \widehat{\mathbf{U}}_2 \end{bmatrix} = \begin{bmatrix} \boldsymbol{\Omega}_1 \times \boldsymbol{\Omega}_2 \\ \boldsymbol{\Omega}_1 \times \mathbf{U}_2 - \boldsymbol{\Omega}_2 \times \mathbf{U}_1 \end{bmatrix}, \quad \begin{bmatrix} \widehat{\boldsymbol{\Omega}} \\ \widehat{\mathbf{U}} \end{bmatrix} = \begin{bmatrix} \operatorname{skw}(\boldsymbol{\Omega}) & \mathbf{0} \\ \operatorname{skw}(\mathbf{U}) & \operatorname{skw}(\boldsymbol{\Omega}) \end{bmatrix}.$$

It can be seen that the hat operator of $\mathbb{S}^3 \times \mathbb{R}^3$ coincides with the hat operator of $SE(3)$ and therefore, the tangent operator and its inverse are the same, [17]. The functions related to $(\mathbb{S}^3 \times \mathbb{R}^3, \circ)$ and notes on how to implement them properly can be found in appendix A.5.

2.4. Isomorphies and Matrix Lie Groups

Now, we will see that the Lie groups $(\mathbb{R}^3, +)$, $(\mathbb{S}^3, *)$ are in fact isomorphic to matrix Lie groups, which is well-known, and show that this holds true for their semi-direct product $(\mathbb{S}^3 \times \mathbb{R}^3, \circ)$ and the Lie group of unit dual quaternions as well. Moreover, direct products of Lie groups which are isomorphic to matrix Lie groups are shown to be isomorphic to matrix Lie groups as well [38]. This gives us the possibility to apply time integration methods designed for matrix Lie groups to the aforementioned Lie groups as well as their direct products, for an example see e. g. [9].

Furthermore, finding explicit expressions for the exponential map for a Lie group can often be easier by first considering its isomorphic matrix Lie group, where the exponential map is given by the exponential series (2.10).

Remark 2.28: *Linear Lie groups are isomorphic to matrix Lie groups, see e. g. [38].*

We consider the mapping

$$\psi: \mathbb{R}^3 \rightarrow GL(4), \quad \mathbf{x} \mapsto \psi(\mathbf{x}) = \begin{bmatrix} \mathbf{I}_3 & \mathbf{x} \\ \mathbf{0} & 1 \end{bmatrix}.$$

It is clear that ψ is smooth and injective. The inverse map ψ^{-1} is just a projection and therefore smooth as well. Furthermore, it can be seen that

$$\psi(\mathbf{x}) \cdot \psi(\mathbf{y}) = \begin{bmatrix} \mathbf{I} & \mathbf{x} + \mathbf{y} \\ \mathbf{0} & 1 \end{bmatrix} = \psi(\mathbf{x} + \mathbf{y})$$

for $\mathbf{x}, \mathbf{y} \in \mathbb{R}^3$. Thus, ψ is also a homomorphism and therefore, $(\mathbb{R}^3, +)$ is isomorphic to a matrix Lie group.

Remark 2.29: *Unit quaternions are isomorphic to a matrix Lie group.*

The quaternion multiplication can also be written with a matrix vector product and a matrix-valued mapping $\mathbf{Q}: \mathbb{R}^4 \rightarrow \mathbb{R}^{4 \times 4}$, see e. g. [35, 53]:

$$\mathbf{p} * \mathbf{q} = \mathbf{Q}(\mathbf{p}) \cdot \mathbf{q},$$

where

$$\mathbf{Q}(\mathbf{p}) = \begin{bmatrix} p_0 & -p_1 & -p_2 & -p_3 \\ p_1 & p_0 & -p_3 & p_2 \\ p_2 & p_3 & p_0 & -p_1 \\ p_3 & -p_2 & p_1 & p_0 \end{bmatrix} = \begin{bmatrix} \operatorname{Re} \mathbf{p} & -\operatorname{Im} \mathbf{p}^\top \\ \operatorname{Im} \mathbf{p} & \mathbf{I}_3 \operatorname{Re} \mathbf{p} + \operatorname{skw}(\operatorname{Im} \mathbf{p}) \end{bmatrix},$$

where $\mathbf{p} = [p_0, p_1, p_2, p_3]^\top$. Moreover, it holds

$$\mathbf{Q}(\mathbf{p} * \mathbf{q}) = \mathbf{Q}(\mathbf{p}) \cdot \mathbf{Q}(\mathbf{q})$$

for $\mathbf{p}, \mathbf{q} \in \mathbb{R}^4$. This means that \mathbf{Q} is a homomorphism from $(\mathbb{R}^4, *)$ to a subgroup of $GL(4)$. The mapping \mathbf{Q} is obviously smooth as well invertible, since its inverse function is again a projection. Therefore, the Lie group $(\mathbb{R}^4, *)$ is isomorphic to a matrix Lie group. With the same argument and restricting \mathbf{Q} to \mathbb{S}^3 , we get that the Lie group of unit quaternions $(\mathbb{S}^3, *)$ is isomorphic to a matrix Lie group.

Remark 2.30: *Direct product Lie groups, see e. g. [38].*

Let us consider two Lie groups (G_1, \circ_1) and (G_2, \circ_2) that are isomorphic to matrix Lie groups. Then there are injective bicontinuous homomorphisms $\psi_k: G_k \rightarrow GL(\mathfrak{N}_k)$ for $k = 1, 2$. We consider the direct product $(G_1 \times G_2, \bullet)$ with the group operation defined component-wise:

$$(g_1, g_2) \bullet (h_1, h_2) = (g_1 \circ_1 h_1, g_2 \circ_2 h_2).$$

Then we can easily construct

$$\psi: G_1 \times G_2 \rightarrow GL(\mathfrak{N}_1 + \mathfrak{N}_2), \quad (g_1, g_2) \mapsto \psi((g_1, g_2)) = \begin{bmatrix} \psi_1(g_1) & \mathbf{0} \\ \mathbf{0} & \psi_2(g_2) \end{bmatrix},$$

which is obviously injective, bicontinuous and a homomorphism. Therefore, the direct product $(G_1 \times G_2, \bullet)$ is isomorphic to a matrix Lie group as well.

Remark 2.31: *The semi-direct product $(\mathbb{S}^3 \times \mathbb{R}^3, \circ)$ is isomorphic to a matrix Lie group.*

Let us first consider the mapping $\mathbf{w} \mapsto p \triangleright \mathbf{w}$ of rotating a vector \mathbf{w} around the origin by a unit quaternion $p \in \mathbb{S}^3$. This mapping is linear in \mathbf{w} and therefore there must be a matrix $\mathbf{R}(p) \in \mathbb{R}^{3 \times 3}$ with the same properties, namely

$$\mathbf{R}(p) = [p \triangleright \mathbf{e}_1, p \triangleright \mathbf{e}_2, p \triangleright \mathbf{e}_3] = \frac{\partial}{\partial \mathbf{w}}(p \triangleright \mathbf{w}).$$

The map \mathbf{R} is known as the Euler map that maps the unit quaternions to rotation matrices $SO(3)$, [40]. We can see that \mathbf{R} is actually smooth and also fulfills the requirements of a homomorphism [40]. It is, however, not injective, since antipodal unit quaternions $p \in \mathbb{S}^3$ and $-p \in \mathbb{S}^3$ encode the same rotation. Let us now construct the mapping

$$\psi: \mathbb{S}^3 \times \mathbb{R}^3 \rightarrow GL(8), \quad (p, \mathbf{x}) \mapsto \psi((p, \mathbf{x})) = \begin{bmatrix} \mathbf{Q}(p) & \mathbf{0} & \mathbf{0} \\ \mathbf{0} & \mathbf{R}(p) & \mathbf{x} \\ \mathbf{0} & \mathbf{0} & 1 \end{bmatrix}.$$

Here, we can actually see a matrix resembling an element from $SE(3)$ in the lower right block. Now, we show that ψ is actually a homomorphism:

$$\begin{aligned} \psi((p_1, \mathbf{x}_1)) \cdot \psi((p_2, \mathbf{x}_2)) &= \begin{bmatrix} \mathbf{Q}(p_1) \cdot \mathbf{Q}(p_2) & \mathbf{0} & \mathbf{0} \\ \mathbf{0} & \mathbf{R}(p_1) \cdot \mathbf{R}(p_2) & \mathbf{x}_1 + \mathbf{R}(p_1) \cdot \mathbf{x}_2 \\ \mathbf{0} & \mathbf{0} & 1 \end{bmatrix} \\ &= \begin{bmatrix} \mathbf{Q}(p_1 * p_2) & \mathbf{0} & \mathbf{0} \\ \mathbf{0} & \mathbf{R}(p_1 * p_2) & \mathbf{x}_1 + p_1 \triangleright \mathbf{x}_2 \\ \mathbf{0} & \mathbf{0} & 1 \end{bmatrix} \\ &= \psi((p_1, \mathbf{x}_1) \circ (p_2, \mathbf{x}_2)). \end{aligned}$$

Furthermore, ψ is smooth, since \mathbf{Q} and \mathbf{R} are smooth. Its inverse map ψ^{-1} is again given by a projection, which is smooth as well. Therefore, $(\mathbb{S}^3 \times \mathbb{R}^3, \circ)$ is isomorphic to a matrix Lie group, too.

Remark 2.32: *Relation between $\mathbb{S}^3 \times \mathbb{R}^3$ and $SE(3)$.*

The Euler map $\mathbf{R}: \mathbb{S}^3 \rightarrow SO(3)$ is a smooth two-to-one homomorphism. Let us consider the equivalence relation \sim with

$$p_1 \sim p_2 \quad \text{if and only if} \quad p_1 \in \{p_2, -p_2\}.$$

Then it can be seen that the set $\mathbb{S}^3 / \sim = \{[p]_{\sim} : p \in \mathbb{S}^3\}$ of equivalence classes of \mathbb{S}^3 forms a group with

$$[p_1]_{\sim} * [p_2]_{\sim} = [p_1 * p_2]_{\sim},$$

because $(-p_1) * p_2 = -(p_1 * p_2)$ etc. This group is then isomorphic to $SO(3)$ with the homomorphism

$$\mathbf{R}_\sim : \mathbb{S}^3 / \sim \rightarrow SO(3), \quad [p]_\sim \mapsto \mathbf{R}_\sim([p]_\sim) = \mathbf{R}(p) = \mathbf{R}(-p),$$

which is surjective [40]. Using quaternions in a numerical algorithm, however, can be more efficient than using rotation matrices, see [42]. Moreover, \mathbb{S}^3 is simply connected, where $SO(3)$ is not [39, Proposition 1.17].

We can make the same argument for $\mathbb{S}^3 \times \mathbb{R}^3$: We consider an equivalence relation that identifies antipodal quaternions

$$(p_1, \mathbf{x}_1) \sim (p_2, \mathbf{x}_2) \quad \text{if and only if} \quad p_1 \in \{p_2, -p_2\} \text{ and } \mathbf{x}_1 = \mathbf{x}_2.$$

Similar to before, $\mathbb{S}^3 \times \mathbb{R}^3 / \sim = \{[(p, \mathbf{x})]_\sim : (p, \mathbf{x}) \in \mathbb{S}^3 \times \mathbb{R}^3\}$ becomes a group. Now, we can define a mapping $\psi : \mathbb{S}^3 \times \mathbb{R}^3 / \sim \rightarrow SE(3)$ by

$$\psi([(p, \mathbf{x})]_\sim) = \begin{bmatrix} \mathbf{R}(p) & \mathbf{x} \\ \mathbf{0} & 1 \end{bmatrix} = \begin{bmatrix} \mathbf{R}(-p) & \mathbf{x} \\ \mathbf{0} & 1 \end{bmatrix}.$$

Similar to remark 2.31, we can now see that ψ is actually a homomorphism. Since the Euler map \mathbf{R} is surjective, ψ is surjective as well. Therefore, the group $\mathbb{S}^3 \times \mathbb{R}^3 / \sim$ is isomorphic to $SE(3)$.

Remark 2.33: *Dual quaternions.*

Often, especially in mechanics, unit dual quaternions are used to describe the position and orientation of a rigid body [48, 49, 55]. The set of unit dual quaternions can be defined as

$$UDQ = \{\mathbf{p} + \epsilon \mathbf{r} : \mathbf{p}, \mathbf{r} \in \mathbb{R}^4, \|\mathbf{p}\|_2^2 = 1, \mathbf{p}^\top \cdot \mathbf{r} = 0\},$$

where ϵ is the dual unit with $\epsilon^2 = 0$ but $\epsilon \neq 0$. By introducing the operation

$$(\mathbf{p}_1 + \epsilon \mathbf{r}_1) * (\mathbf{p}_2 + \epsilon \mathbf{r}_2) = \mathbf{p}_1 * \mathbf{p}_2 + \epsilon(\mathbf{r}_1 * \mathbf{p}_2 + \mathbf{p}_1 * \mathbf{r}_2),$$

the tuple $(UDQ, *)$ becomes a group with identity element $e = [1, 0, 0, 0]^\top + \epsilon \mathbf{0}$ and inverse elements

$$(\mathbf{p} + \epsilon \mathbf{r}) * (\mathbf{p}^{-1} - \epsilon \mathbf{p}^{-1} * \mathbf{r} * \mathbf{p}^{-1}) = \mathbf{p} * \mathbf{p}^{-1} + \epsilon(\mathbf{r} * \mathbf{p}^{-1} - \mathbf{p} * \mathbf{p}^{-1} * \mathbf{r} * \mathbf{p}^{-1}) = e.$$

The term “unit” dual quaternions comes from the fact that for $\mathbf{p} + \epsilon \mathbf{r} \in UDQ$ it holds

$$(\mathbf{p} + \epsilon \mathbf{r}) * (\bar{\mathbf{p}} + \epsilon \bar{\mathbf{r}}) = e.$$

We can think of dual quaternions as elements of \mathbb{R}^{4+4} and write $UDQ = \mathbf{F}^{-1}(\mathbf{0})$ with

$$\mathbf{F}(\mathbf{p} + \epsilon \mathbf{r}) = \begin{bmatrix} \mathbf{p}^\top \cdot \mathbf{p} - 1 \\ \mathbf{p}^\top \cdot \mathbf{r} \end{bmatrix}.$$

By applying lemma 2.2, we can see that UDQ is a manifold, because

$$\mathbf{F}'\left(\begin{bmatrix} \mathbf{p} \\ \mathbf{r} \end{bmatrix}\right) = \begin{bmatrix} \mathbf{p}^\top & \mathbf{0}^\top \\ \mathbf{r}^\top & \mathbf{p}^\top \end{bmatrix}$$

has full rank for $\mathbf{p} \neq 0$. Therefore, $(UDQ, *)$ is a Lie group.

Furthermore, UDQ is isomorphic to $\mathbb{S}^3 \times \mathbb{R}^3$. This can be seen by constructing a bicontinuous bijective homomorphism

$$\psi: UDQ \rightarrow \mathbb{S}^3 \times \mathbb{R}^3,$$

see remark 2.6. This map can be chosen to be

$$\psi(\mathbf{p} + \epsilon \mathbf{r}) = (\mathbf{p}, 2 \operatorname{Im}(\mathbf{r} * \mathbf{p}^{-1})),$$

which is obviously continuous. Its inverse is a continuous function given by

$$\psi^{-1}((p, \mathbf{x})) = p + \frac{1}{2} \epsilon \begin{bmatrix} 0 \\ \mathbf{x} \end{bmatrix} * p,$$

because we can see that $\psi(\psi^{-1}((p, \mathbf{x}))) = (p, \mathbf{x})$ for all $(p, \mathbf{x}) \in \mathbb{S}^3 \times \mathbb{R}^3$ and $\psi^{-1}(\psi(\mathbf{p} + \epsilon \mathbf{r})) = \mathbf{p} + \epsilon \mathbf{r}$ for all $\mathbf{p} + \epsilon \mathbf{r} \in UDQ$ by using that $\operatorname{Re}(\mathbf{r} * \mathbf{p}^{-1}) = \mathbf{r}^\top \cdot \mathbf{p} = 0$. This means that ψ must be bijective as well. Furthermore, we can see that ψ is a homomorphism:

$$\begin{aligned} & \psi(\mathbf{p}_1 + \epsilon \mathbf{r}_1) \circ \psi(\mathbf{p}_2 + \epsilon \mathbf{r}_2) \\ &= (\mathbf{p}_1 * \mathbf{p}_2, 2 \operatorname{Im}(\mathbf{r}_1 * \mathbf{p}_1^{-1}) + \mathbf{p}_1 \triangleright 2 \operatorname{Im}(\mathbf{r}_2 * \mathbf{p}_2^{-1})) \\ &= (\mathbf{p}_1 * \mathbf{p}_2, 2 \operatorname{Im}(\mathbf{r}_1 * \mathbf{p}_1^{-1}) + 2 \operatorname{Im}(\mathbf{p}_1 * \mathbf{r}_2 * \mathbf{p}_2^{-1} * \mathbf{p}_1^{-1})) \\ &= (\mathbf{p}_1 * \mathbf{p}_2, 2 \operatorname{Im}(\mathbf{r}_1 * \mathbf{p}_2 * \mathbf{p}_2^{-1} * \mathbf{p}_1^{-1}) + 2 \operatorname{Im}(\mathbf{p}_1 * \mathbf{r}_2 * \mathbf{p}_2^{-1} * \mathbf{p}_1^{-1})) \\ &= (\mathbf{p}_1 * \mathbf{p}_2, 2 \operatorname{Im}((\mathbf{r}_1 * \mathbf{p}_2 + \mathbf{p}_1 * \mathbf{r}_2) * (\mathbf{p}_1 * \mathbf{p}_2)^{-1})) \\ &= \psi((\mathbf{p}_1 + \epsilon \mathbf{r}_1) * (\mathbf{p}_2 + \epsilon \mathbf{r}_2)) \end{aligned}$$

for $\mathbf{p}_1 + \epsilon \mathbf{r}_1, \mathbf{p}_2 + \epsilon \mathbf{r}_2 \in UDQ$, where we used $\operatorname{Re}(\mathbf{r}_2 * \mathbf{p}_2^{-1}) = \mathbf{r}_2^\top \cdot \mathbf{p}_2 = 0$ again.

The Lie group of unit dual quaternions is therefore isomorphic to the Lie group of $\mathbb{S}^3 \times \mathbb{R}^3$ and is an interesting way to represent the semi-direct product structure. In comparison to $\mathbb{S}^3 \times \mathbb{R}^3$ however, UDQ is computationally inferior [42] since an additional parameter has to be stored per rigid body configuration, the concatenation and exponential map require more floating-point operations, and the position vector is not readily available but has to be computed from the dual part.

2.5. Mechanical Systems with Lie Group Structured Configuration Spaces

If we consider a mechanical system, we need to find a way to describe the configuration of the system by some parameters. We call the set of the descriptions of all possible

configurations the configuration space G . In this section, we will briefly discuss constrained mechanical systems where the configuration space G is also a Lie group (G, \circ) . The equations of motion of such a system with holonomic constraints can be written in the form of the following differential-algebraic equations (DAE), see e. g. [17]:

$$\dot{q}(t) = dL_{q(t)} \widetilde{\mathbf{v}}(t), \quad (2.31a)$$

$$\mathbf{M} \cdot \dot{\mathbf{v}}(t) = \widetilde{\mathbf{v}}(t)^\top \cdot \mathbf{M} \cdot \mathbf{v}(t) + \mathbf{f}(t, q(t), \mathbf{v}(t)) - \mathbf{D}\Phi^\top(q(t)) \cdot \boldsymbol{\lambda}(t), \quad (2.31b)$$

$$\mathbf{0} = \Phi(q(t)), \quad (2.31c)$$

where $q(t) \in G$ is the configuration of the system at a time instant t , $\mathbf{v}(t) \in \mathbb{R}^n$ is the associated derivative vector, $\mathbf{M} \in \mathbb{R}^{n \times n}$ is a constant, positive definite and symmetric mass matrix, $\mathbf{f}(t, q(t), \mathbf{v}(t)) \in \mathbb{R}^n$ is the vector of internal and external forces formulated in the language of derivative vectors, $\Phi: G \rightarrow \mathbb{R}^k$ is the differentiable submersion with $k \leq n$ that we call constraint function and $\boldsymbol{\lambda}(t) \in \mathbb{R}^k$ is a Lagrange multiplier. The term $\widetilde{\mathbf{v}}(t)^\top \cdot \mathbf{M} \cdot \mathbf{v}(t)$ represents the Coriolis forces. It appears due to the fact that the derivative vectors are not measured with respect to the inertial frame. In earlier works about Lie group time integration, see e. g. [8, 16], the Coriolis force would not be considered separately as it is here, but only as part of the forces \mathbf{f} . The term $-\mathbf{D}^\top\Phi(q(t)) \cdot \boldsymbol{\lambda}(t)$ is the constraint force which ensures that the constraints (2.31c) are fulfilled.

Since the system is constrained, the configuration $q(t)$ does not only have to be an element of G , but $q(t)$ has to be an element of the regular surface $\mathfrak{M} = \{p \in G: \Phi(p) = \mathbf{0}\} \subseteq G$. We call \mathfrak{M} the constraint manifold. Unfortunately, \mathfrak{M} generally does not need to have a Lie group structure, so we rely on representing the configurations in a larger space G that does have a Lie group structure and require the constraint equation (2.31c).

We do not consider state-dependent mass matrices, because for mechanical systems consisting only of rigid bodies, we can always choose a configuration space G such that the mass matrix \mathbf{M} is constant, see section 4.1.

We assume that the constraint function Φ is a submersion, meaning that the rank of its differential, which is equal to the rank of $\mathbf{D}\Phi(q) \in \mathbb{R}^{k \times n}$, is constant and equal to k . We will see that this makes (2.31) a DAE of differentiation index of (at most) three. First, we differentiate the constraint equation twice, giving us the so-called hidden constraints

$$\mathbf{0} = \mathbf{D}\Phi(q(t)) \cdot \mathbf{v}(t), \quad (2.32a)$$

$$\mathbf{0} = \mathbf{D}^2\Phi(q(t)) (\mathbf{v}(t), \mathbf{v}(t)) + \mathbf{D}\Phi(q(t)) \cdot \dot{\mathbf{v}}(t), \quad (2.32b)$$

on velocity and acceleration level, respectively. Here $\mathbf{D}^2\Phi(p) (\mathbf{a}, \mathbf{b})$ is an abbreviation for

$$\mathbf{D}^2\Phi(p) (\mathbf{a}, \mathbf{b}) = \mathbf{D}_p(\mathbf{D}\Phi(p) \cdot \mathbf{a}) \cdot \mathbf{b}. \quad (2.33)$$

Now, we can replace the constraint equation (2.31c) by the hidden constraint on acceleration level (2.32b), which is analytically equivalent. By bringing the constraint forces to the left-hand side, combining both equations to one equation of vectors in \mathbb{R}^{n+k} , we

arrive at the following formulation

$$\dot{q}(t) = dL_{q(t)}(e) \widetilde{\mathbf{v}}(t), \quad (2.34a)$$

$$\begin{bmatrix} \mathbf{M} & \mathbf{D}\Phi^\top(q(t)) \\ \mathbf{D}\Phi(q(t)) & \mathbf{0} \end{bmatrix} \cdot \begin{bmatrix} \dot{\mathbf{v}}(t) \\ \boldsymbol{\lambda}(t) \end{bmatrix} = \begin{bmatrix} \widetilde{\mathbf{v}}(t)^\top \cdot \mathbf{M} \cdot \mathbf{v}(t) + \mathbf{f}(t, q(t), \mathbf{v}(t)) \\ -\mathbf{D}^2\Phi(q(t))(\mathbf{v}(t), \mathbf{v}(t)) \end{bmatrix}. \quad (2.34b)$$

We can see that the matrix on the left-hand side of (2.34b) is invertible, because it is obviously symmetric and both \mathbf{M} as well as $\mathbf{D}\Phi(q(t))$ have full rank by requirement. Its inverse is given by

$$\begin{bmatrix} \mathbf{M} & \mathbf{D}\Phi^\top \\ \mathbf{D}\Phi & \mathbf{0} \end{bmatrix}^{-1} = \begin{bmatrix} \mathbf{M}^{-1} + \mathbf{M}^{-1} \cdot \mathbf{D}\Phi^\top \cdot \mathbf{S}^{-1} \cdot \mathbf{D}\Phi \cdot \mathbf{M}^{-1} & -\mathbf{M}^{-1} \cdot \mathbf{D}\Phi^\top \cdot \mathbf{S}^{-1} \\ -\mathbf{S}^{-1} \cdot \mathbf{D}\Phi \cdot \mathbf{M}^{-1} & \mathbf{S}^{-1} \end{bmatrix}, \quad (2.35)$$

where we have omitted the argument $q(t)$ and used the Schur complement [82, 86]

$$\mathbf{S} = \mathbf{0} - \mathbf{D}\Phi(q(t)) \cdot \mathbf{M}^{-1} \cdot \mathbf{D}\Phi^\top(q(t)).$$

By multiplying (2.34b) from the left with the matrix from (2.35) and subsequently differentiating the equation for $\boldsymbol{\lambda}(t)$, we get an ordinary differential equation in $q(t)$, $\mathbf{v}(t)$ and $\boldsymbol{\lambda}(t)$ which is equivalent to both (2.31) as well as (2.34). Since we had to differentiate three times counting from (2.31) and once counting from (2.34) in order to arrive at an ODE, we have shown that their differentiation index is in fact (at most) 3 and 1, respectively. This also justifies the names “index-3 formulation” for (2.31) and “index-1 formulation” for (2.34).

In the following, we want to derive the equations of motion (2.31) from variational principles. In order to do that, we will use variations:

Remark 2.34: *Variations.*

Let us first consider a continuous curve \mathbf{x} in a real vector space \mathbb{R}^n . Now, we can consider a family of slightly perturbed curves \mathbf{x}^ϵ such that for $\epsilon = 0$ we have $\mathbf{x}^0 = \mathbf{x}$. Furthermore, we consider the mapping $\epsilon \mapsto \mathbf{x}^\epsilon$ to be differentiable. Then, we define the derivative of \mathbf{x}^ϵ with respect to ϵ at $\epsilon = 0$ to be the variation $\delta\mathbf{x}$ of \mathbf{x} :

$$\delta\mathbf{x}(t) = \left. \frac{d}{d\epsilon} \mathbf{x}^\epsilon(t) \right|_{\epsilon=0}.$$

The quantity $\delta\mathbf{x}(t)$ can be thought of as an infinitesimal motion [69].

The same can be done for curves q in a Lie group G , see [54]:

$$\delta q(t) = \left. \frac{d}{d\epsilon} q^\epsilon(t) \right|_{\epsilon=0} \in T_{q(t)}G$$

with a family of perturbed curves q^ϵ in G that are differentiable in ϵ . We will use the concept of derivative vectors and introduce the derivative vector $\delta\mathbf{q}(t)$ corresponding to $q(t)$ via the relation

$$\delta q(t) = dL_{q(t)}(e) \widetilde{\delta\mathbf{q}}(t). \quad (2.36)$$

Note that the derivative vector $\delta\mathbf{q}(t) \in \mathbb{R}^n$ with respect to the variation has a bold variation symbol, whereas the variation $\delta q(t) \in T_{q(t)}G$ has a non-bold variation symbol.

Of course, we can apply the variation to the derivative vector $\mathbf{v}(t)$ of $q(t)$ with respect to the derivative d/dt

$$\delta\mathbf{v}(t) = \delta\dot{\mathbf{q}}(t) + \widehat{\mathbf{v}(t)} \cdot \delta\mathbf{q}(t), \quad (2.37)$$

see e. g. [17], where

$$\delta\dot{\mathbf{q}}(t) = \frac{d}{dt}\delta\mathbf{q}(t).$$

This can be easily proved through lemma 2.23.

Remark 2.35: *Conservative mechanical systems.*

We consider a conservative mechanical system with kinetic energy

$$\mathcal{T}(\mathbf{v}(t)) = \frac{1}{2}\mathbf{v}^\top(t) \cdot \mathbf{M} \cdot \mathbf{v}(t)$$

and some potential energy $\mathcal{U}(q(t))$. We consider the action integral with an augmented Lagrangian [63] on the time span $[t_0, t_e]$:

$$\mathcal{S}(q, \boldsymbol{\lambda}) = \int_{t_0}^{t_e} \mathcal{T}(\mathbf{v}(t)) - \mathcal{U}(q(t)) - \boldsymbol{\Phi}^\top(q(t)) \cdot \boldsymbol{\lambda}(t) dt. \quad (2.38)$$

Now, we can use Hamilton's principle of stationary action

$$0 = \delta\mathcal{S}(q, \boldsymbol{\lambda}) \quad (2.39a)$$

where we describe the variation of $q(t)$ with derivative vectors

$$\delta q(t) = dL_{q(t)}(e) \widehat{\delta\mathbf{q}(t)} \quad (2.39b)$$

and the boundary conditions

$$\mathbf{0} = \delta\mathbf{q}(t_0) = \delta\mathbf{q}(t_e). \quad (2.39c)$$

Carrying out the details, we get, omitting the argument t :

$$\begin{aligned} 0 &= \delta\mathcal{S}(q, \boldsymbol{\lambda}) \\ &= \int_{t_0}^{t_e} \delta\mathcal{T}(\mathbf{v}) - \delta\mathcal{U}(q) - \delta(\boldsymbol{\Phi}^\top(q) \cdot \boldsymbol{\lambda}) dt \\ &= \int_{t_0}^{t_e} \mathbf{v}^\top \cdot \mathbf{M} \cdot \delta\mathbf{v} - (\mathbf{D}\mathcal{U}(q) + \boldsymbol{\lambda}^\top \cdot \mathbf{D}\boldsymbol{\Phi}(q)) \cdot \delta\mathbf{q} - \boldsymbol{\Phi}^\top(q) \cdot \delta\boldsymbol{\lambda} dt \\ &= \int_{t_0}^{t_e} \mathbf{v}^\top \cdot \mathbf{M} \cdot \delta\dot{\mathbf{q}} + (\mathbf{v}^\top \cdot \mathbf{M} \cdot \widehat{\mathbf{v}} - \mathbf{D}\mathcal{U}(q) - \boldsymbol{\lambda}^\top \cdot \mathbf{D}\boldsymbol{\Phi}(q)) \cdot \delta\mathbf{q} - \boldsymbol{\Phi}^\top(q) \cdot \delta\boldsymbol{\lambda} dt \\ &= \int_{t_0}^{t_e} (-\dot{\mathbf{v}}^\top \cdot \mathbf{M} + \mathbf{v}^\top \cdot \mathbf{M} \cdot \widehat{\mathbf{v}} - \mathbf{D}\mathcal{U}(q) - \boldsymbol{\lambda}^\top \cdot \mathbf{D}\boldsymbol{\Phi}(q)) \cdot \delta\mathbf{q} - \boldsymbol{\Phi}^\top(q) \cdot \delta\boldsymbol{\lambda} dt \end{aligned}$$

where we have used the relationship (2.37) and partial integration where the boundary values $\mathbf{v}^\top(t) \cdot \mathbf{M} \cdot \delta \mathbf{q}(t) \Big|_{t_0}^{t_e}$ vanish due to the boundary conditions (2.39c). Since this has to hold for all variations $\delta \mathbf{q}(t)$ and $\delta \boldsymbol{\lambda}(t)$, equations (2.31b) and (2.31c) follow by transposing with

$$\mathbf{f}(t, q(t), \mathbf{v}(t)) = -\mathbf{D}\mathcal{U}^\top(q(t)).$$

Remark 2.36: *Forced mechanical systems.*

We consider a mechanical system as in remark 2.35 but this time with some external forces $\mathcal{F}^\top(t, q(t), \mathbf{v}(t)) \in \mathbb{R}^n$ acting on it. Of course, these external forces are formulated in the language of derivative vectors. This time, we use the Lagrange-d'Alembert principle instead of Hamilton's principle of stationary action (2.39):

$$0 = \delta \mathcal{S}(q, \boldsymbol{\lambda}) + \int_{t_0}^{t_e} \mathcal{F}(t, q(t), \mathbf{v}(t)) \cdot \delta \mathbf{q}(t) dt, \quad (2.40a)$$

$$\delta q(t) = dL_{q(t)}(e) \widetilde{\delta \mathbf{q}(t)}, \quad (2.40b)$$

$$\mathbf{0} = \delta \mathbf{q}(t_0) = \delta \mathbf{q}(t_e). \quad (2.40c)$$

Since we already know from remark 2.35 how to treat $\delta \mathcal{S}(q, \boldsymbol{\lambda})$, we can immediately conclude from (2.40)

$$0 = \int_{t_0}^{t_e} \left(-\dot{\mathbf{v}}^\top \cdot \mathbf{M} + \mathbf{v}^\top \cdot \mathbf{M} \cdot \hat{\mathbf{v}} - \mathbf{D}\mathcal{U}(q) \right. \\ \left. + \mathcal{F}(t, q, \mathbf{v}) - \boldsymbol{\lambda}^\top \cdot \mathbf{D}\Phi(q) \right) \cdot \delta \mathbf{q} - \Phi^\top(q) \cdot \delta \boldsymbol{\lambda} dt,$$

where we have omitted the argument t again. As before, this has to hold for all variations, thus (2.31) follows with

$$\mathbf{f}(t, q(t), \mathbf{v}(t)) = -\mathbf{D}\mathcal{U}^\top(q(t)) + \mathcal{F}^\top(t, q(t), \mathbf{v}(t)).$$

Remark 2.37: *Mechanical systems with nonholonomic constraints.*

This time, we consider a mechanical system as in remark 2.35, but the system is subjected to nonholonomic constraints in Pfaffian form

$$\mathbf{0} = \mathbf{B}(q(t)) \cdot \mathbf{v}(t), \quad (2.41)$$

where $\mathbf{B}(q(t)) \in \mathbb{R}^{k_{\text{nonhol}} \times n}$, where $k + k_{\text{nonhol}} \leq n$. This kind of nonholonomic constraint can appear when there is sliding or rolling without slip in the system [69].

The variational principle we use to derive the equations of motion is similar to Hamilton's principle of stationary action (2.39), but we have to require that the nonholonomic constraint is also fulfilled for the variations $\delta \mathbf{q}(t)$. This can be explained by the fact that each perturbed trajectory $q^\epsilon(t)$ which is the solution of (2.39b), see remark 2.34,

has to fulfill the nonholonomic constraints as well. Thus, the variational principle for conservative systems reads

$$0 = \delta\mathcal{S}(q, \boldsymbol{\lambda}), \quad (2.42a)$$

$$\delta q(t) = dL_{q(t)}(e) \widetilde{\delta q}(t), \quad (2.42b)$$

$$\boldsymbol{0} = \boldsymbol{\delta q}(t_0) = \boldsymbol{\delta q}(t_e), \quad (2.42c)$$

$$\boldsymbol{0} = \mathbf{B}(q(t)) \cdot \boldsymbol{\delta q}(t). \quad (2.42d)$$

Just as in remark 2.35, it follows

$$0 = \int_{t_0}^{t_e} (-\dot{\boldsymbol{v}}^\top \cdot \mathbf{M} + \boldsymbol{v}^\top \cdot \mathbf{M} \cdot \widehat{\boldsymbol{v}} - \mathbf{D}\mathcal{U}(q) - \boldsymbol{\lambda}^\top \cdot \mathbf{D}\boldsymbol{\Phi}(q)) \cdot \boldsymbol{\delta q} - \boldsymbol{\Phi}^\top(q) \cdot \delta \boldsymbol{\lambda} dt,$$

but this time, this has to hold for all variations $\boldsymbol{\delta q}(t)$ that fulfill (2.42d) and all variations $\delta \boldsymbol{\lambda}(t)$. Here, the factor in front of $\boldsymbol{\delta q}(t)$ does not have to vanish, but its transpose still has to be an element of the image of $\mathbf{B}^\top(q(t))$ for each $t \in [t_0, t_e]$. We will represent this element as $\mathbf{B}^\top(q(t)) \cdot \boldsymbol{\mu}(t)$, where $\boldsymbol{\mu}(t) \in \mathbb{R}^{k_{\text{nonhol}}}$. Combining the above statements, we get the equations of motion

$$\dot{q}(t) = dL_{q(t)} \widetilde{\boldsymbol{v}}(t), \quad (2.43a)$$

$$\mathbf{M} \cdot \boldsymbol{v}(t) = \widehat{\boldsymbol{v}}(t)^\top \cdot \mathbf{M} \cdot \boldsymbol{v}(t) + \boldsymbol{f}(t, q(t), \boldsymbol{v}(t)) - \mathbf{D}\boldsymbol{\Phi}^\top(q(t)) \cdot \boldsymbol{\lambda}(t) - \mathbf{B}^\top(q(t)) \cdot \boldsymbol{\mu}(t), \quad (2.43b)$$

$$\boldsymbol{0} = \boldsymbol{\Phi}(q(t)), \quad (2.43c)$$

$$\boldsymbol{0} = \mathbf{B}(q(t)) \cdot \boldsymbol{v}(t). \quad (2.43d)$$

This way of deriving the equations of motion is well-known for the case that $G = \mathbb{R}^n$, see [33].

Remark 2.38: *Unconstrained mechanical systems.*

If we considered a mechanical system without constraints, the equations of motion take the form

$$\dot{q}(t) = dL_{q(t)} \widetilde{\boldsymbol{v}}(t), \quad (2.44a)$$

$$\mathbf{M} \cdot \dot{\boldsymbol{v}}(t) = \widehat{\boldsymbol{v}}(t)^\top \cdot \mathbf{M} \cdot \boldsymbol{v}(t) + \boldsymbol{f}(t, q(t), \boldsymbol{v}(t)). \quad (2.44b)$$

We could think of them as the same equations of motion (2.31) with $\boldsymbol{\Phi}(q(t)) \in \mathbb{R}^0$ and $\boldsymbol{\lambda}(t) \in \mathbb{R}^0$ being vectors in the zero-dimensional vector space $\mathbb{R}^0 = \{0\}$. This interpretation means that we simply omit all occurrences of $\boldsymbol{\Phi}$ and $\boldsymbol{\lambda}$. Here, $\boldsymbol{a}^\top \cdot \boldsymbol{b} = 0$ for all $\boldsymbol{a}, \boldsymbol{b} \in \mathbb{R}^0$. Mathematically, however, (2.44) is an ordinary differential equation, whereas (2.31) is a DAE. Treating an ODE as a special case of a DAE is unusual, but all results for these semi-explicit DAEs hold as long as they do not explicitly require the number of constraints to be nonzero. A DAE, however, cannot be treated as if it was an ODE [37, 78].

2.6. Lie Groups as Riemannian Manifolds and Metric Spaces

In this subsection, we will construct a metric tensor on a smooth, n -dimensional Lie group G with certain properties. From this, we can construct a notion of distance between arbitrary points of the Lie group, thus constructing a metric space which inherits the properties of the metric tensor.

Consider a scalar product

$$\langle \bullet, \bullet \rangle_e : T_e G \times T_e G \rightarrow \mathbb{R} \quad (2.45)$$

on the Lie algebra $T_e G$. Such a scalar product exists, since $T_e G$ is a finite-dimensional linear space. It is most convenient in the context of this thesis to apply the concept of derivative vectors and therefore, use a tilde operator (2.16) to construct $\langle \bullet, \bullet \rangle_e$ from the Euclidean scalar product on \mathbb{R}^n :

$$\langle \tilde{\mathbf{a}}, \tilde{\mathbf{b}} \rangle_e = \widetilde{\mathbf{a}^\top \cdot \mathbf{b}}. \quad (2.46)$$

The Lie group operation relates all tangent spaces among each other, thus we can immediately define

$$\langle \bullet, \bullet \rangle_q : T_q G \times T_q G \rightarrow [0, \infty), \quad (a, b) \mapsto \langle a, b \rangle_q = \langle dL_{q^{-1}}(q) a, dL_{q^{-1}}(q) b \rangle_e \quad (2.47)$$

for $q \in T \setminus \{e\}$. It is obvious that $\langle \bullet, \bullet \rangle_q$ is a scalar product on the tangent space $T_q G$ for any $q \in G$. Since the left multiplication is smooth, the mapping $q \mapsto \langle X(q), Y(q) \rangle_q$ is smooth for all smooth vector fields X, Y on G . That means we can use $\langle \bullet, \bullet \rangle_q$ as a positive-definite metric tensor and the Lie group G equipped with $\langle \bullet, \bullet \rangle_q$ becomes a Riemannian manifold.

Lemma 2.39: *Left invariance of $\langle \bullet, \bullet \rangle_q$.*

The metric tensor $\langle \bullet, \bullet \rangle_q$ is left invariant:

$$\langle dL_r(q) a, dL_r(q) b \rangle_{L_r(q)} = \langle a, b \rangle_q, \quad \text{for all } q, r \in G \text{ and } a, b \in T_q G. \quad (2.48)$$

Proof. Let $r, q \in G$, $a, b \in T_q G$ and consider

$$\begin{aligned} \langle dL_r(q) a, dL_r(q) b \rangle_{L_r(q)} &= \langle dL_{L_r(q)^{-1}}(L_r(q)) dL_r(q) a, dL_{L_r(q)^{-1}}(L_r(q)) dL_r(q) b \rangle_e \\ &= \langle dL_{q^{-1} \circ r^{-1}}(r \circ q) dL_r(q) a, dL_{q^{-1} \circ r^{-1}}(r \circ q) dL_r(q) b \rangle_e \\ &= \langle dL_{q^{-1} \circ r^{-1} \circ r}(q) a, dL_{q^{-1} \circ r^{-1} \circ r}(q) b \rangle_e = \langle a, b \rangle_q, \end{aligned}$$

where we have used (2.3). □

A right invariant metric tensor $\langle \bullet, \bullet \rangle_{*,q}$ has the property

$$\langle dR_r(q) a, dR_r(q) b \rangle_{*,R_r(q)} = \langle a, b \rangle_{*,q}, \quad \text{for all } q, r \in G \text{ and } a, b \in T_q G, \quad (2.49)$$

where

$$R_r : G \rightarrow G, \quad q \mapsto R_r(q) = q \circ r$$

is the right multiplication for all $r \in G$. Metric tensors that are left and right invariant are called bi-invariant. Compact Lie groups, as well as Abelian Lie groups have bi-invariant metric tensors [2]. In the case of simply connected Lie groups, bi-invariant metric tensors exist if and only if the Lie group G is a direct product of compact Lie groups and Abelian Lie groups [2, Section 2.4]. The Lie group $SE(3)$ is a classical example of a Lie group, where one-parameter subgroups $\tau \mapsto \exp(\tau V)$ with constant $V \in \mathfrak{se}(3)$ cannot be geodesics [34, Chapter 2.2], which is equivalent to the fact that no bi-invariant Riemannian metric tensor can exist. Unfortunately, the metric tensor $\langle \bullet, \bullet \rangle_q$ from (2.47) is not generally right invariant.

Now, we will use the metric tensor in order to define a distance function on G , see e. g. [29]. In order to do so, we define a norm on each tangent space by

$$\| \bullet \|_q: T_q G \rightarrow [0, \infty), \quad a \mapsto \|a\|_q = \sqrt{\langle a, a \rangle_q}. \quad (2.50)$$

Due to the definition (2.47) of $\langle \bullet, \bullet \rangle_q$, we immediately receive

$$\|a\|_q = \|dL_{q^{-1}}(q) a\|_e \quad (2.51)$$

and due to the left invariance (2.48) it follows

$$\|dL_r(q) a\|_{L_r(q)} = \|a\|_q \quad (2.52)$$

for all $r \in G$. Now, we define the set of all differentiable curves from $p \in G$ to $q \in G$ by

$$\Gamma(p, q) = \{\gamma \in C^1([0, 1] \rightarrow G) : \gamma(0) = p, \gamma(1) = q\},$$

the length of a curve $\gamma \in \Gamma(p, q)$ by

$$\mathbf{L}(\gamma) = \int_0^1 \|\gamma'(s)\|_{\gamma(s)} ds,$$

and finally the distance between p and q by

$$d: G \times G \rightarrow [0, \infty), \quad (p, q) \mapsto d(p, q) = \inf_{\gamma \in \Gamma(p, q)} \mathbf{L}(\gamma). \quad (2.53)$$

Lemma 2.40: G is a metric space.

The tuple (G, d) is a metric space.

Proof. We need to show positive definiteness, symmetry and the triangle inequality. Let $p, q \in G$:

Positive definiteness: It is trivial that $d(p, q) \geq 0$. For $\gamma(s) \equiv p$, we have $\gamma \in \Gamma(p, p)$ and from $\gamma'(s) \equiv 0$ it follows $d(p, p) = 0$.

Symmetry: For every $\gamma \in \Gamma(p, q)$ there is a $\sigma \in \Gamma(q, p)$ defined by $\sigma(s) = \gamma(1 - s)$. Both curves have the same length since

$$\begin{aligned} \mathbf{L}(\sigma) &= \int_0^1 \|\sigma'(s)\|_{\sigma(s)} \, ds = \int_0^1 \|-\gamma'(1 - s)\|_{\gamma(1-s)} \, ds \\ &= \int_1^0 -\|\gamma'(s)\|_{\gamma(s)} \, ds = \int_0^1 \|\gamma'(s)\|_{\gamma(s)} \, ds = \mathbf{L}(\gamma). \end{aligned}$$

Obviously, the mapping

$$\Gamma(p, q) \rightarrow \Gamma(q, p), \quad \gamma(s) \mapsto \gamma(1 - s)$$

is a bijection that keeps the length invariant. Therefore

$$d(p, q) = \inf_{\gamma \in \Gamma(p, q)} \mathbf{L}(\gamma) = \inf_{\sigma \in \Gamma(q, p)} \mathbf{L}(\sigma) = d(q, p).$$

Triangle inequality: Let $r \in G$ and $\sigma_1 \in \Gamma(p, r)$, $\sigma_2 \in \Gamma(r, q)$. Define the following piece-wise differentiable curve from p to q :

$$\gamma(s) = \begin{cases} \sigma_1(2s), & s \in [0, 1/2] \\ \sigma_2(2s - 1), & s \in [1/2, 1]. \end{cases}$$

This curve γ is not an element of $\Gamma(p, q)$, because it may be not differentiable at $s = 1/2$. Nevertheless, we can calculate its length:

$$\begin{aligned} \mathbf{L}(\gamma) &= \int_0^1 \|\gamma'(s)\|_{\gamma(s)} \, ds = \int_0^{1/2} \|2\sigma_1'(2s)\|_{\sigma_1(2s)} \, ds + \int_{1/2}^1 \|2\sigma_2'(2s - 1)\|_{\sigma_2(2s-1)} \, ds \\ &= \frac{1}{2} \int_0^1 \|2\sigma_1'(s)\|_{\sigma_1(s)} \, ds + \frac{1}{2} \int_0^1 \|2\sigma_2'(s)\|_{\sigma_2(s)} \, ds = \mathbf{L}(\sigma_1) + \mathbf{L}(\sigma_2). \end{aligned}$$

Let $\gamma_m \in \Gamma(p, q)$ be a sequence with $\mathbf{L}(\gamma_m - \gamma) \rightarrow 0$. The length is continuous, so we have $\mathbf{L}(\gamma) = \lim_{m \rightarrow \infty} \mathbf{L}(\gamma_m)$. Now, we know that for each $m \in \mathbb{N}$ it holds

$$d(p, q) = \inf_{\sigma \in \Gamma(p, q)} \mathbf{L}(\sigma) \leq \mathbf{L}(\gamma_m),$$

by letting $m \rightarrow \infty$ follows

$$d(p, q) \leq \mathbf{L}(\gamma) = \mathbf{L}(\sigma_1) + \mathbf{L}(\sigma_2)$$

and finally by taking the infimum over all $\sigma_1 \in \Gamma(p, r)$ and all $\sigma_2 \in \Gamma(r, q)$:

$$d(p, q) \leq \inf_{\sigma_1 \in \Gamma(p, r)} \mathbf{L}(\sigma_1) + \inf_{\sigma_2 \in \Gamma(r, q)} \mathbf{L}(\sigma_2) = d(p, r) + d(r, q). \quad \square$$

Lemma 2.41: *Logarithm and distance.*

Let $p, q \in G$ be sufficiently close to each other such that $p^{-1} \circ q \in \exp(T_e G)$. Then it holds

$$d(p, q) \leq \|\widetilde{\log}(p^{-1} \circ q)\|_2 = \|\widetilde{\log}(q^{-1} \circ p)\|_2, \quad (2.54)$$

if the metric tensor was constructed using (2.46).

Proof. For $p, q \in G$ and $\gamma(s) = p \circ \widetilde{\exp}(s \widetilde{\log}(p^{-1} \circ q))$ it holds $\gamma \in \Gamma(p, q)$. The derivative of γ is given by

$$\gamma'(s) = dL_{\gamma(s)}(e) \log(p^{-1} \circ q),$$

see (2.9). Then we have

$$\mathbf{L}(\gamma) = \int_0^1 \|dL_{\gamma(s)}(e) \log(p^{-1} \circ q)\|_{\gamma(s)} ds = \int_0^1 \|\log(p^{-1} \circ q)\|_e ds = \|\widetilde{\log}(p^{-1} \circ q)\|_2,$$

where we have used the left invariance, see (2.48), the definition of the scalar product, see (2.46), and the fact that the norm induced by the Euclidean scalar product of \mathbb{R}^n is the Euclidean norm $\|\bullet\|_2$. The last equality follows from (2.12), which implies

$$\widetilde{\log}(p^{-1} \circ q) = -\widetilde{\log}((p^{-1} \circ q)^{-1}) = -\widetilde{\log}(q^{-1} \circ p). \quad \square$$

Lemma 2.42: *A Lipschitz condition for differentiable functions on G .*

Consider a differentiable function $\varphi: G \rightarrow G$ and a bounded and connected set $U \subset G$. Then there is a constant $\varkappa > 0$ such that

$$d(\varphi(p), \varphi(q)) \leq \varkappa d(p, q) \quad \text{for all } p, q \in U.$$

To be more precise, the function φ only has to be differentiable on the set

$$K(U) = \{p \in G: 2d(p, u) \leq \sup_{a, b \in U} d(a, b) \text{ for all } u \in U\}.$$

Proof. Let $p, q \in G$. We consider the derivative $d\varphi(q): T_q G \rightarrow T_{\varphi(q)} G$ and its operator norm

$$\|d\varphi(q)\|_{\varphi(q), q} = \sup_{0 \neq a \in T_q G} \frac{\|d\varphi(q) a\|_{\varphi(q)}}{\|a\|_q}.$$

The operator norm of linear operators of finite-dimensional linear spaces is always finite and it follows

$$\|d\varphi(q) a\|_{\varphi(q)} \leq \|d\varphi(q)\|_{\varphi(q), q} \|a\|_q \quad \text{for all } a \in T_q G.$$

Now, let $\gamma \in \Gamma(p, q)$ with $\gamma(s) \in K(U)$ for all $s \in [0, 1]$ and consider the length of the image of γ under φ :

$$\begin{aligned} \mathbf{L}(\varphi \circ \gamma) &= \int_0^1 \|(\varphi \circ \gamma)'(s)\|_{(\varphi \circ \gamma)(s)} ds = \int_0^1 \|d\varphi(\gamma(s)) \gamma'(s)\|_{\varphi(\gamma(s))} ds \\ &\leq \int_0^1 \|d\varphi(\gamma(s))\|_{\varphi(\gamma(s)), \gamma(s)} \|\gamma'(s)\|_{\gamma(s)} ds \leq \varkappa \mathbf{L}(\gamma) \end{aligned} \quad (2.55)$$

with

$$\varkappa = \sup_{g \in K(U)} \|d\varphi(g)\|_{\varphi(g), g}.$$

Since φ is differentiable on the closed and bounded set $K(U) \subseteq G$, its derivative has to be continuous on $K(U)$ and therefore, the supremum exists and is finite due to the extreme value theorem.

Now, consider a sequence $(\gamma_m)_{m \in \mathbb{N}} \subseteq \Gamma(p, q)$ with $L(\gamma_m) \rightarrow d(p, q)$ for $m \rightarrow \infty$. We can assume that $\gamma_m([0, 1]) \subset K(U)$ due to the triangle inequality and the definition of $K(U)$. By putting γ_m in (2.55) and taking the limit $m \rightarrow \infty$, the claim follows. \square

Lemma 2.43: *A qualitative Lipschitz condition.*

Consider a continuously differentiable function $\mathbf{F}: G \rightarrow \mathbb{R}^w$ for $w \in \mathbb{N}$ and $a(h), b(h) \in G$ such that $d(a(h), b(h)) \rightarrow 0$ for $h \rightarrow 0$. Then it holds

$$\mathbf{F}(a(h)) - \mathbf{F}(b(h)) \in \mathcal{O}\left(d(a(h), b(h))\right).$$

Proof. Let $h \in \mathbb{R}$ be fixed and $\gamma: [0, 1] \rightarrow G$ be a differentiable curve from $a(h)$ to $b(h)$. Then we use the fundamental theorem of calculus to see that

$$\mathbf{F}(\gamma(1)) - \mathbf{F}(\gamma(0)) = \int_0^1 d\mathbf{F}(\gamma(s)) \gamma'(s) ds.$$

Now, we can use the generalized triangle inequality to obtain

$$\|\mathbf{F}(a(h)) - \mathbf{F}(b(h))\|_2 \leq \int_0^1 \|d\mathbf{F}(\gamma(s)) \gamma'(s)\|_2 ds.$$

Similar to the proof of lemma 2.42, we conclude

$$\|d\mathbf{F}(\gamma(s)) \gamma'(s)\|_2 \leq \|d\mathbf{F}(\gamma(s))\|_{2, \gamma(s)} \|\gamma'(s)\|_{\gamma(s)}$$

from the fact that linear operators of finite-dimensional linear spaces always have a finite operator norm. It follows

$$\|\mathbf{F}(a(h)) - \mathbf{F}(b(h))\|_2 \leq \int_0^1 \|d\mathbf{F}(\gamma(s))\|_{2, \gamma(s)} \|\gamma'(s)\|_{\gamma(s)} ds.$$

Then, we can take the maximum of the norm $\|d\mathbf{F}(\gamma(s))\|_{2, \gamma(s)}$ over a compact set and take the infimum over all curves γ . The compact set could be, e.g. the closure of $\{g \in G: d(a, g) + d(g, b) \leq d(a, b) + \varepsilon\}$ for an $\varepsilon > 0$. The argument holds since all sufficiently short curves from a to b have to belong to that set. We can conclude that there exists a $K > 0$ such that

$$\|\mathbf{F}(a(h)) - \mathbf{F}(b(h))\|_2 \leq Kd(a(h), b(h)).$$

Now, the assertion follows. \square

Lemma 2.44: *Left invariance.*

The distance function d is left invariant in the sense that

$$d(r \circ p, r \circ q) = d(p, q)$$

for all $r, p, q \in G$.

Proof. The assertion follows directly from lemma 2.39 and the definition of d in (2.53). \square

Lemma 2.45: *Almost right invariance.*

The distance function d is almost right invariant in the sense that

$$d(p \circ r, q \circ r) \leq \varrho(r)d(p, q)$$

for all $r, p, q \in G$, where $\varrho: G \rightarrow [0, \infty)$ is continuous.

Proof. Two versions of a proof can be found in [70]. Let $p, q, r \in G$ and $a \in T_q G$. Since right-multiplication and left-multiplication commute

$$L_p(R_r(q)) = p \circ q \circ r = R_r(L_p(q)),$$

we have

$$dL_p(R_r(q)) \, dR_r(q) = dR_r(L_p(q)) \, dL_p(q). \quad (2.56)$$

Consider now

$$\begin{aligned} \|dR_r(q) a\|_{R_r(q)} &= \|dL_{(q \circ r)^{-1}}(q \circ r) \, dR_r(q) a\|_e \\ &= \|dR_r(L_{(q \circ r)^{-1}}(q \circ r)) \, dL_{(q \circ r)^{-1}}(q) a\|_e \\ &= \|dR_r(e) \, dL_{r^{-1}}(e) \, dL_{q^{-1}}(q) a\|_e \\ &\leq \|dR_r(e) \, dL_{r^{-1}}(e)\|_{e,e} \|dL_{q^{-1}}(q) a\|_e = \varrho(r) \|a\|_q, \end{aligned}$$

where we have used (2.3) and defined $\varrho(r) = \|dR_r(e) \, dL_{r^{-1}}(e)\|_{e,e}$. Since Lie group multiplication and inversion are differentiable, ϱ must at least be continuous.

For the set of differentiable curves from $p \circ r$ to $q \circ r$ it holds

$$\Gamma(p \circ r, q \circ r) = \{R_r \circ \gamma : \gamma \in \Gamma(p, q)\},$$

so we can write each element $\sigma \in \Gamma(p \circ r, q \circ r)$ as $\sigma(s) = \gamma(s) \circ r = (R_r \circ \gamma)(s)$ for a $\gamma \in \Gamma(p, q)$. For the length it holds

$$\begin{aligned} \mathbf{L}(\sigma) &= \int_0^1 \|\sigma'(s)\|_{\sigma(s)} \, ds = \int_0^1 \|dR_r(\gamma(s)) \, \gamma'(s)\|_{R_r(\gamma(s))} \, ds \\ &\leq \int_0^1 \varrho(r) \|\gamma'(s)\|_{\gamma(s)} \, ds = \varrho(r) \mathbf{L}(\gamma). \end{aligned}$$

Now, it follows

$$\begin{aligned} d(p \circ r, q \circ r) &= \inf_{\sigma \in \Gamma(p \circ r, q \circ r)} \mathbf{L}(\sigma) = \inf_{\gamma \in \Gamma(p, q)} \mathbf{L}(R_r \circ \gamma) \\ &\leq \varrho(r) \inf_{\gamma \in \Gamma(p, q)} \mathbf{L}(\gamma) = \varrho(r) d(p, q). \end{aligned} \quad \square$$

The following lemma can be used in the error analysis of Lie group methods for solving differential equations on Lie groups, as has been done in e. g. [29, 70]. It replaces the triangle inequality for norms in vector spaces in the form of

$$\|(\mathbf{a}_1 + \mathbf{b}_1) - (\mathbf{a}_2 + \mathbf{b}_2)\| \leq \|\mathbf{a}_1 - \mathbf{a}_2\| + \|\mathbf{b}_1 - \mathbf{b}_2\|$$

for vectors $\mathbf{a}_1, \mathbf{a}_2, \mathbf{b}_1, \mathbf{b}_2$.

Lemma 2.46: *Error translation.*

For a left invariant and almost right invariant distance d on G it holds

$$d(a_1 \circ b_1, a_2 \circ b_2) \leq \varrho(b_k)d(a_1, a_2) + d(b_1, b_2), \quad k = 1, 2$$

for $a_1, a_2, b_1, b_2 \in G$.

Proof. A similar proof can be found in [70]. We use the triangle inequality, left invariance, and almost right invariance:

$$\begin{aligned} d(a_1 \circ b_1, a_2 \circ b_2) &\leq d(a_1 \circ b_1, a_1 \circ b_2) + d(a_1 \circ b_2, a_2 \circ b_2) \\ &\leq d(b_1, b_2) + \varrho(b_2)d(a_1, a_2). \end{aligned}$$

The result for $k = 1$ follows in the same way. □

Remark 2.47: *Right invariant, almost left invariant metric.*

We could also, instead of using the left translation in (2.47), use the right translation. This would yield a distance function d that is right invariant, see lemma 2.44,

$$d(p \circ r, q \circ r) = d(p, q)$$

and only almost left invariant, see lemma 2.45,

$$d(r \circ p, r \circ q) \leq \rho(r)d(p, q)$$

for all $r, p, q \in G$ with a continuous $\rho: G \rightarrow [0, \infty)$. Lemmas 2.40, 2.41, 2.42 and 2.43 still hold for this left invariant metric. The error translation from lemma 2.46 becomes

$$d(a_1 \circ b_1, a_2 \circ b_2) \leq d(a_1, a_2) + \rho(a_k)d(b_1, b_2), \quad k = 1, 2$$

for $a_1, a_2, b_1, b_2 \in G$.

Remark 2.48: *Bi-invariant metric.*

Consider a connected and simply connected Lie group G . If there exists a bi-invariant metric on G then G must be isomorphic to a direct product of a compact Lie group and an Abelian Lie group, see [2, Section 2.4].

Let $G = K \times \mathbb{R}^n$ be connected and simply connected, where K is a compact Lie group and $n \in \mathbb{N} \cup \{0\}$. Let the identity element of G be $(e, \mathbf{0}) \in G$. Then we can choose the following scalar product (2.45):

$$\left\langle \begin{bmatrix} k_1 \\ \mathbf{v}_1 \end{bmatrix}, \begin{bmatrix} k_2 \\ \mathbf{v}_2 \end{bmatrix} \right\rangle_e = -B(k_1, k_2) + \langle \mathbf{v}_1, \mathbf{v}_2 \rangle_{\mathbb{R}^n},$$

where $k_1, k_2 \in T_e K$ and $\mathbf{v}_1, \mathbf{v}_2 \in T_{\mathbf{0}} \mathbb{R}^n = \mathbb{R}^n$, $\langle \bullet, \bullet \rangle_{\mathbb{R}^n}$ is a scalar product on \mathbb{R}^n , B is the Cartan-Killing-Form of K defined by

$$B(\widehat{\mathbf{k}}_1, \widetilde{\mathbf{k}}_2) = \text{trace}(\widehat{\mathbf{k}}_1 \cdot \widetilde{\mathbf{k}}_2),$$

where $\widehat{\bullet}$ and $\widetilde{\bullet}$ are the hat operator and the tilde operator of K , see [2, Theorem 2.35]. This leads to a bi-invariant metric and distance function, which is unique up to a constant and up to the choice of $\langle \bullet, \bullet \rangle_{\mathbb{R}^n}$, [2, Proposition 2.48].

For any Lie group G with a bi-invariant metric, the exponential map \exp is surjective and the shortest curve (geodesic) from $p \in G$ to $q \in G$ with respect to this metric is given by

$$[0, 1] \rightarrow G, \quad s \mapsto p \circ \exp(s \log(p^{-1} \circ q)),$$

see [2, Theorem 2.27]. This means that the interpolation I_p from (2.24) is a geodesic interpolation for the Lie groups \mathbb{R}^3 , \mathbb{S}^3 , $SO(3)$ and their direct products, but is not generally geodesic for $SE(3)$, see [34, Chapter 2.2], and therefore the same holds for $\mathbb{S}^3 \times \mathbb{R}^3$ and UDQ .

3. RATTLie

In order to simulate a mechanical system, a suitable time integration method has to be applied for finding an approximate solution to the equations of motion of the system. In this thesis, we are focusing on constrained mechanical systems whose equations of motion take the form (2.31a) of a DAE on a (finite-dimensional, real) Lie group G . There are already some numerical integrators designed to solve this kind of equation such as the Lie group generalized- α method [18] or the BLieDF-method [84].

In this section, we will discuss such a time integration method – RATTLie [44]:

$$q_{n+1} = q_n \circ \widetilde{\exp}(h_n \mathbf{v}_{n+1/2}) \quad (3.1a)$$

$$\mathbf{M} \cdot \mathbf{v}_n = \mathbf{T}^{-\top}(-h_n \mathbf{v}_{n+1/2}) \cdot \mathbf{M} \cdot \mathbf{v}_{n+1/2} - \frac{h_n}{2} \mathbf{f}(t_n, q_n, \mathbf{v}_n) + \frac{h_n}{2} \mathbf{D}\Phi^\top(q_n) \cdot \boldsymbol{\lambda}_n^+ \quad (3.1b)$$

$$\mathbf{0} = \Phi(q_{n+1}) \quad (3.1c)$$

$$\begin{aligned} \mathbf{M} \cdot \mathbf{v}_{n+1} &= \mathbf{T}^{-\top}(h_n \mathbf{v}_{n+1/2}) \cdot \mathbf{M} \cdot \mathbf{v}_{n+1/2} \\ &\quad + \frac{h_n}{2} \mathbf{f}(t_{n+1}, q_{n+1}, \mathbf{v}_{n+1}) - \frac{h_n}{2} \mathbf{D}\Phi^\top(q_{n+1}) \cdot \boldsymbol{\lambda}_{n+1}^- \end{aligned} \quad (3.1d)$$

$$\mathbf{0} = \mathbf{D}\Phi(q_{n+1}) \cdot \mathbf{v}_{n+1}. \quad (3.1e)$$

It approximates the solution $q(t)$ and $\mathbf{v}(t)$ of (2.31) on a time grid $\{t_0, t_1, \dots, t_N\}$ with variable time step sizes $h_n = t_{n+1} - t_n$ and consistent initial conditions

$$q_0 = q(t_0), \quad \mathbf{v}_0 = \mathbf{v}(t_0). \quad (3.1f)$$

RATTLie was inspired by the well-known integration scheme RATTLE, which was first developed by Andersen [5], where it was applied in the field of molecular dynamics. Later, RATTLE was analyzed numerically as a symplectic integration scheme with order of convergence of two [35]. It can be considered an extension of the symplectic Euler scheme to constrained systems [35], but it can also be seen as a variational integrator [63]. In this thesis, we use the approach of variational integrators together with the toolkit of Lie groups in order to derive RATTLie [44], a generalization of RATTLE to Lie group structured configuration spaces. Variational Lie group integrators have been considered before, see e. g. [24, 54], but here, we work with the concept of derivative vectors [8, 16], where the unknowns are from a linear space which parametrizes the corresponding Lie algebra and therefore the tangent spaces. While RATTLE is usually only considered with constant step sizes, we allow an arbitrary time grid. There has been research on RATTLE with variable time step sizes in [10], but here we do not need any time reparametrization. First, conservative systems are considered and subsequently external forces are added to the system.

Apart from RATTLie itself, we will derive two close relatives: Firstly, the integration scheme SHAKELie, which can be considered a generalization of SHAKE. Unfortunately, it ultimately suffers from the same problems as SHAKE, namely an accumulation of round-off errors [35, Section VII.1.4], see also [6]. Secondly, we extend RATTLie to nonholonomic constraints, which we had already published in the conference proceedings [41]. This

follows along the lines of the work of Ferraro et al. [30], but uses the approach of variational integrators as well as Lie group structured configuration spaces.

Then we analyze the convergence behavior of RATTLie. Here, we do not rely on the symplecticity of RATTLie or the fact that we derived it as a variational integrator. Instead, we construct a special metric on the Lie group which is the configuration space, similar to the work of Faltinsen [29], see also [70], and follow along the lines of the convergence analysis of one-step methods [36, 78]. This comprises the analysis of the local error, which can be done by applying Taylor's theorem and the BCH formula, as well as the analysis of the global error, where the error propagation has to be considered. Subsequently, we analyze how to calculate the Lagrange multipliers, which is not straightforward, since the λ_n^+ and λ_n^- do not approximate the Lagrange multiplier $\lambda(t)$ in a desirable manner.

Lastly, we will give some implementation details for RATTLie as well as for the nonholonomic RATTLie, including algorithms in pseudocode.

3.1. Derivation

In this section, we will show how to derive RATTLie using tools from variational integrators. A major part of the following derivation has already been published in [44].

3.1.1. Conservative Systems

First, we will consider constrained conservative systems with a potential energy $\mathcal{U}(q(t))$, a kinetic energy $\mathcal{T}(\mathbf{v}(t)) = \frac{1}{2}\mathbf{v}^\top(t) \cdot \mathbf{M} \cdot \mathbf{v}(t)$ and the constraints $\mathbf{0} = \Phi(q(t))$. The continuous equations of motion can be derived using the variational principle (2.39), where the Lagrange multiplier $\lambda(t)$ is introduced. We consider a time grid $t_0 < t_1 < \dots < t_N = t_e$ with time step sizes $h_n = t_{n+1} - t_n$ for $n = 0, \dots, N-1$. Now, we will restrict the admissible functions q to continuous functions q^d with piecewise constant derivative vectors. Specifically,

$$q^d(t) = q_n \circ \widetilde{\exp}((t - t_n)\mathbf{v}_{n+1/2}), \quad t \in [t_n, t_{n+1}] \quad (3.2)$$

where

$$\mathbf{v}_{n+1/2} = \frac{1}{h_n} \widetilde{\log}(q_n^{-1} \circ q_{n+1}) \quad (3.3)$$

for $n = 0, \dots, N-1$. This means that $q^d(t) = \text{pIp}(t, (t_n)_{n=0, \dots, N}, (q_n)_{n=0, \dots, N})$ with the piecewise interpolation from remark 2.27. We can see that $\mathbf{v}_{n+1/2}$ actually coincides with the derivative vector for $t \in (t_n, t_{n+1})$. In the following short proof we will write the tilde operator as $\tau(\bullet) = \widetilde{\bullet}$ and use the differential dexp of the exponential map, see (2.15):

$$\begin{aligned} \dot{q}^d(t) &= \text{d}L_{q_n} \left(\widetilde{\exp}((t - t_n)\mathbf{v}_{n+1/2}) \right) \text{dexp}((t - t_n)\mathbf{v}_{n+1/2}) \tau \left(\frac{\text{d}}{\text{d}t} (t - t_n)\mathbf{v}_{n+1/2} \right) \\ &= \text{d}L_{q_n} \left(\widetilde{\exp}((t - t_n)\mathbf{v}_{n+1/2}) \right) \text{d}L_{\exp((t-t_n)\mathbf{v}_{n+1/2})}(e) \tau \left(\mathbf{T}((t - t_n)\mathbf{v}_{n+1/2}) \cdot \mathbf{v}_{n+1/2} \right) \\ &= \text{d}L_{q_n \circ \widetilde{\exp}((t-t_n)\mathbf{v}_{n+1/2})}(e) \widetilde{\mathbf{v}_{n+1/2}} = \text{d}L_{q^d(t)}(e) \widetilde{\mathbf{v}_{n+1/2}}. \end{aligned} \quad (3.4)$$

Here we have used (2.19), (2.3), and that $(t - t_n)\mathbf{v}_{n+1/2}$ commutes with $\mathbf{v}_{n+1/2}$. Thus, we can define the derivative vectors \mathbf{v}^d by

$$\dot{q}^d(t) = dL_{q^d(t)}(e) \widetilde{\mathbf{v}^d(t)}, \quad t \neq t_n, \quad n = 0, \dots, N, \quad (3.5)$$

$$\mathbf{v}^d(t) = \mathbf{v}_{n+1/2}, \quad t \in (t_n, t_{n+1}), \quad n = 0, \dots, N-1. \quad (3.6)$$

We also allow $\boldsymbol{\lambda}^d$, the Lagrange multiplier associated with q^d , to be discontinuous at t_0, \dots, t_N and define the one-sided limits

$$\boldsymbol{\lambda}_n^+ = \lim_{\delta \rightarrow 0^+} \boldsymbol{\lambda}^d(t_n + \delta), \quad n = 0, \dots, N-1,$$

$$\boldsymbol{\lambda}_n^- = \lim_{\delta \rightarrow 0^-} \boldsymbol{\lambda}^d(t_n + \delta), \quad n = 1, \dots, N.$$

Now, we will put the q^d and $\boldsymbol{\lambda}^d$ in the action functional (2.38), split up the integration interval and approximate the remaining integral with the trapezoidal rule:

$$\begin{aligned} \mathcal{S}(q^d, \boldsymbol{\lambda}^d) &= \int_{t_0}^{t_e} \mathcal{T}(\mathbf{v}^d(t)) - \mathcal{U}(q^d(t)) - \boldsymbol{\Phi}^\top(q^d(t)) \cdot \boldsymbol{\lambda}^d(t) dt \\ &= \sum_{n=0}^{N-1} \left(\int_{t_n}^{t_{n+1}} \mathcal{T}(\mathbf{v}^d(t)) dt - \int_{t_n}^{t_{n+1}} \mathcal{U}(q^d(t)) + \boldsymbol{\Phi}^\top(q^d(t)) \cdot \boldsymbol{\lambda}^d(t) dt \right) \\ &= \sum_{n=0}^{N-1} \left(\frac{h_n}{2} \mathbf{v}_{n+1/2}^\top \cdot \mathbf{M} \cdot \mathbf{v}_{n+1/2} - \int_{t_n}^{t_{n+1}} \mathcal{U}(q^d(t)) + \boldsymbol{\Phi}^\top(q^d(t)) \cdot \boldsymbol{\lambda}^d(t) dt \right) \\ &\approx \sum_{n=0}^{N-1} \left(\frac{h_n}{2} \mathbf{v}_{n+1/2}^\top \cdot \mathbf{M} \cdot \mathbf{v}_{n+1/2} - \frac{h_n}{2} \left(\mathcal{U}(q^d(t_n)) + \boldsymbol{\Phi}^\top(q^d(t_n)) \cdot \boldsymbol{\lambda}_n^+ \right) \right. \\ &\quad \left. - \frac{h_n}{2} \left(\mathcal{U}(q^d(t_{n+1})) + \boldsymbol{\Phi}^\top(q^d(t_{n+1})) \cdot \boldsymbol{\lambda}_{n+1}^- \right) \right) \\ &= \sum_{n=0}^{N-1} \frac{h_n}{2} \left(\mathbf{v}_{n+1/2}^\top \cdot \mathbf{M} \cdot \mathbf{v}_{n+1/2} - \mathcal{U}(q_n) - \boldsymbol{\Phi}^\top(q_n) \cdot \boldsymbol{\lambda}_n^+ - \mathcal{U}(q_{n+1}) - \boldsymbol{\Phi}^\top(q_{n+1}) \cdot \boldsymbol{\lambda}_{n+1}^- \right) \\ &=: \mathcal{S}^d((q_n)_{n=0}^N, (\boldsymbol{\lambda}_n^+)_{n=0}^{N-1}, (\boldsymbol{\lambda}_n^-)_{n=1}^N), \end{aligned}$$

where we define the discrete action functional \mathcal{S}^d in terms of the discrete configurations q_n for $n = 0, \dots, N$ and the one-sided limits of the Lagrange multiplier $\boldsymbol{\lambda}_n^+$ for $n = 0, \dots, N-1$ and $\boldsymbol{\lambda}_n^-$ for $n = 1, \dots, N$. We introduce the discrete augmented Lagrange function

$$\mathcal{L}^d(q_n, q_{n+1}, \boldsymbol{\lambda}_n^+, \boldsymbol{\lambda}_{n+1}^-) = \frac{h_n}{2} \left(\mathbf{v}_{n+1/2}^\top \cdot \mathbf{M} \cdot \mathbf{v}_{n+1/2} - \mathcal{U}(q_n) - \boldsymbol{\Phi}^\top(q_n) \cdot \boldsymbol{\lambda}_n^+ \right. \left. - \mathcal{U}(q_{n+1}) - \boldsymbol{\Phi}^\top(q_{n+1}) \cdot \boldsymbol{\lambda}_{n+1}^- \right), \quad (3.7)$$

which allows us to write

$$\mathcal{S}^d((q_n)_{n=0}^N, (\boldsymbol{\lambda}_n^+)_{n=0}^{N-1}, (\boldsymbol{\lambda}_n^-)_{n=1}^N) = \sum_{n=0}^{N-1} \mathcal{L}^d(q_n, q_{n+1}, \boldsymbol{\lambda}_n^+, \boldsymbol{\lambda}_{n+1}^-).$$

Now, we use a discrete analogue of the variational principle (2.39) in order to derive the discrete equations of motion:

$$0 = \delta \mathcal{S}^d((q_n)_{n=0}^N, (\boldsymbol{\lambda}_n^+)_{n=0}^{N-1}, (\boldsymbol{\lambda}_n^-)_{n=1}^N), \quad (3.8a)$$

$$\boldsymbol{\delta q}_0 = \boldsymbol{\delta q}_N = \boldsymbol{0}, \quad (3.8b)$$

where $\boldsymbol{\delta q}_n$ are the derivative vectors of q_n with respect to the variation, see (2.39b). Then, we interchange variation and summation in (3.8) and shift indices, keeping (2.18) and (3.8b) in mind:

$$\begin{aligned} 0 &= \sum_{n=0}^{N-1} \left(\mathbf{D}_1 \mathcal{L}^d(q_n, q_{n+1}, \boldsymbol{\lambda}_n^+, \boldsymbol{\lambda}_{n+1}^-) \cdot \boldsymbol{\delta q}_n + \mathbf{D}_2 \mathcal{L}^d(q_n, q_{n+1}, \boldsymbol{\lambda}_n^+, \boldsymbol{\lambda}_{n+1}^-) \cdot \boldsymbol{\delta q}_{n+1} \right. \\ &\quad \left. + d_3 \mathcal{L}^d(q_n, q_{n+1}, \boldsymbol{\lambda}_n^+, \boldsymbol{\lambda}_{n+1}^-) \cdot \delta \boldsymbol{\lambda}_n^+ + d_4 \mathcal{L}^d(q_n, q_{n+1}, \boldsymbol{\lambda}_n^+, \boldsymbol{\lambda}_{n+1}^-) \cdot \delta \boldsymbol{\lambda}_{n+1}^- \right) \\ 0 &= \sum_{n=1}^{N-1} \mathbf{D}_1 \mathcal{L}^d(q_n, q_{n+1}, \boldsymbol{\lambda}_n^+, \boldsymbol{\lambda}_{n+1}^-) \cdot \boldsymbol{\delta q}_n + \sum_{n=1}^N \mathbf{D}_2 \mathcal{L}^d(q_{n-1}, q_n, \boldsymbol{\lambda}_{n-1}^+, \boldsymbol{\lambda}_n^-) \cdot \boldsymbol{\delta q}_n \\ &\quad + \sum_{n=0}^{N-1} d_3 \mathcal{L}^d(q_n, q_{n+1}, \boldsymbol{\lambda}_n^+, \boldsymbol{\lambda}_{n+1}^-) \cdot \delta \boldsymbol{\lambda}_n^+ + \sum_{n=1}^N d_4 \mathcal{L}^d(q_{n-1}, q_n, \boldsymbol{\lambda}_{n-1}^+, \boldsymbol{\lambda}_n^-) \cdot \delta \boldsymbol{\lambda}_n^- \\ &= \sum_{n=1}^{N-1} \left(\mathbf{D}_1 \mathcal{L}^d(q_n, q_{n+1}, \boldsymbol{\lambda}_n^+, \boldsymbol{\lambda}_{n+1}^-) + \mathbf{D}_2 \mathcal{L}^d(q_{n-1}, q_n, \boldsymbol{\lambda}_{n-1}^+, \boldsymbol{\lambda}_n^-) \right) \cdot \boldsymbol{\delta q}_n \\ &\quad + \sum_{n=0}^{N-1} d_3 \mathcal{L}^d(q_n, q_{n+1}, \boldsymbol{\lambda}_n^+, \boldsymbol{\lambda}_{n+1}^-) \cdot \delta \boldsymbol{\lambda}_n^+ + \sum_{n=1}^N d_4 \mathcal{L}^d(q_{n-1}, q_n, \boldsymbol{\lambda}_{n-1}^+, \boldsymbol{\lambda}_n^-) \cdot \delta \boldsymbol{\lambda}_n^-. \end{aligned}$$

Since this has to hold for all variations $(\boldsymbol{\delta q}_n)_{n=1}^{N-1}, (\delta \boldsymbol{\lambda}_n^+)_{n=0}^{N-1}, (\delta \boldsymbol{\lambda}_n^-)_{n=1}^N$, we get the discrete equations of motion

$$\mathbf{D}_1 \mathcal{L}^d(q_n, q_{n+1}, \boldsymbol{\lambda}_n^+, \boldsymbol{\lambda}_{n+1}^-) + \mathbf{D}_2 \mathcal{L}^d(q_{n-1}, q_n, \boldsymbol{\lambda}_{n-1}^+, \boldsymbol{\lambda}_n^-) = \boldsymbol{0}, \quad n = 1, \dots, N-1, \quad (3.9a)$$

$$d_3 \mathcal{L}^d(q_n, q_{n+1}, \boldsymbol{\lambda}_n^+, \boldsymbol{\lambda}_{n+1}^-) = \boldsymbol{0}, \quad n = 0, \dots, N-1, \quad (3.9b)$$

$$d_4 \mathcal{L}^d(q_{n-1}, q_n, \boldsymbol{\lambda}_{n-1}^+, \boldsymbol{\lambda}_n^-) = \boldsymbol{0}, \quad n = 1, \dots, N. \quad (3.9c)$$

Now, we rearrange (3.9a):

$$-\mathbf{D}_1 \mathcal{L}^d(q_n, q_{n+1}, \boldsymbol{\lambda}_n^+, \boldsymbol{\lambda}_{n+1}^-) = \mathbf{D}_2 \mathcal{L}^d(q_{n-1}, q_n, \boldsymbol{\lambda}_{n-1}^+, \boldsymbol{\lambda}_n^-), \quad n = 1, \dots, N-1.$$

The left-hand side and the right-hand side define two matching canonical momenta \mathbf{p}_n^+ and \mathbf{p}_n^- , respectively. This approach is called the discrete Legendre transformation [63]. Applying the inverse of the continuous Legendre transform, we write the momenta in terms of velocities:

$$\mathbf{p}_n^+ = \mathbf{p}_n^- = (\mathbf{M} \cdot \mathbf{v}_n)^\top,$$

which are associated with the configurations q_n for $n = 1, \dots, N - 1$. Then, we can write (3.9a) in the form

$$(\mathbf{M} \cdot \mathbf{v}_n)^\top = -\mathbf{D}_1 \mathcal{L}^d(q_n, q_{n+1}, \boldsymbol{\lambda}_n^+, \boldsymbol{\lambda}_{n+1}^-), \quad n = 1, \dots, N - 1, \quad (3.10a)$$

$$(\mathbf{M} \cdot \mathbf{v}_{n+1})^\top = \mathbf{D}_2 \mathcal{L}^d(q_n, q_{n+1}, \boldsymbol{\lambda}_n^+, \boldsymbol{\lambda}_{n+1}^-), \quad n = 0, \dots, N - 2. \quad (3.10b)$$

We can easily see that (3.10) is equivalent to (3.9) and the back-transformation from momenta to velocities justifies that \mathbf{v}_n is an approximation to $\mathbf{v}(t_n)$.

If we look at (3.9b) and (3.9c), we notice that they are the same for $n = 1, \dots, N - 1$ since

$$d_3 \mathcal{L}^d(q_n, q_{n+1}, \boldsymbol{\lambda}_n^+, \boldsymbol{\lambda}_{n+1}^-) = d_4 \mathcal{L}^d(q_{n-1}, q_n, \boldsymbol{\lambda}_{n-1}^+, \boldsymbol{\lambda}_n^-) = \mathbf{D} \boldsymbol{\Phi}^\top(q_n).$$

Thus for $n = 1, \dots, N - 1$, we replace one of them by

$$\boldsymbol{\theta} = \mathbf{D} \boldsymbol{\Phi}(q_n) \cdot \mathbf{v}_n, \quad (3.11)$$

which is similar to the hidden constraint (2.32a), since we want the approximations (q_n, \mathbf{v}_n) to belong to the set $\{(q, \mathbf{v}) \in G \times \mathbb{R}^n : \boldsymbol{\theta} = \boldsymbol{\Phi}(q) = \mathbf{D} \boldsymbol{\Phi}(q) \cdot \mathbf{v}\}$.

Now, we need to calculate the derivatives of \mathcal{L}^d with respect to the first and second argument $\mathbf{D}_1 \mathcal{L}^d(q_n, q_{n+1}, \boldsymbol{\lambda}_n^+, \boldsymbol{\lambda}_{n+1}^-)$ and $\mathbf{D}_2 \mathcal{L}^d(q_n, q_{n+1}, \boldsymbol{\lambda}_n^+, \boldsymbol{\lambda}_{n+1}^-)$. We keep in mind that (3.3) is equivalent to $\mathbf{v}_{n+1/2} = \boldsymbol{\Delta}(q_n, q_{n+1}; h_n)$, see lemma 2.24. Its derivatives are thus given by

$$\mathbf{D}_{q_n} \mathbf{v}_{n+1/2} = \mathbf{D}_1 \boldsymbol{\Delta}(q_n, q_{n+1}; h_n) = -\frac{1}{h_n} \mathbf{T}^{-1}(-h_n \mathbf{v}_{n+1/2}), \quad (3.12a)$$

$$\mathbf{D}_{q_{n+1}} \mathbf{v}_{n+1/2} = \mathbf{D}_2 \boldsymbol{\Delta}(q_n, q_{n+1}; h_n) = \frac{1}{h_n} \mathbf{T}^{-1}(h_n \mathbf{v}_{n+1/2}), \quad (3.12b)$$

see lemma 2.25. Then, we can calculate the derivatives of the discrete Lagrangian by applying (2.18) and (3.12) to (3.7) for $n = 0, \dots, N - 1$:

$$\left. \begin{aligned} & \mathbf{D}_1 \mathcal{L}^d(q_n, q_{n+1}, \boldsymbol{\lambda}_n^+, \boldsymbol{\lambda}_{n+1}^-) \\ & = -\mathbf{v}_{n+1/2}^\top \cdot \mathbf{M} \cdot \mathbf{T}^{-1}(-h_n \mathbf{v}_{n+1/2}) - \frac{h_n}{2} \mathbf{D} \mathcal{U}(q_n) - \frac{h_n}{2} (\boldsymbol{\lambda}_n^+)^\top \cdot \mathbf{D} \boldsymbol{\Phi}(q_n) \end{aligned} \right\} \quad (3.13a)$$

$$\left. \begin{aligned} & \mathbf{D}_2 \mathcal{L}^d(q_n, q_{n+1}, \boldsymbol{\lambda}_n^+, \boldsymbol{\lambda}_{n+1}^-) \\ & = \mathbf{v}_{n+1/2}^\top \cdot \mathbf{M} \cdot \mathbf{T}^{-1}(h_n \mathbf{v}_{n+1/2}) - \frac{h_n}{2} \mathbf{D} \mathcal{U}(q_{n+1}) - \frac{h_n}{2} (\boldsymbol{\lambda}_{n+1}^-)^\top \cdot \mathbf{D} \boldsymbol{\Phi}(q_{n+1}) \end{aligned} \right\} \quad (3.13b)$$

Now, by rearranging (3.3), using (3.13) in (3.10) together with (3.9b) and (3.11), the equation take the form (3.1) for $n = 0, \dots, N - 1$ with

$$\mathbf{f}(t_n, q_n, \mathbf{v}_n) = -\mathbf{D} \mathcal{U}^\top(q_n), \quad n = 0, \dots, N.$$

We have extended the index range in which the equations should hold to $n = 0, \dots, N - 1$ in order to obtain an integrator which can calculate approximations to $q(t_n)$ and $\mathbf{v}(t_n)$ for $n = 1, \dots, N$ from consistent initial values q_0 and \mathbf{v}_0 . We can justify this by using $q_{-1} = q_0$ and $q_{N+1} = q_N$ as the boundaries with $h_{-1} = h_N = 0$.

3.1.2. External Forces

In this section, we consider the same constrained mechanical system as before, but now subjected to external forces $\mathcal{F}(t, q, \mathbf{v})$ depending on the time t , the configuration q , and the derivative vector \mathbf{v} . We derived the equations of motion for such a system by using the variational principle (2.40). In order to derive a forced version of RATTLie, we restrict the space of admissible functions q to continuous functions q^d with piecewise constant derivative vectors as in the previous section 3.1.1. The principle then reads

$$0 = \delta \int_{t_0}^{t_e} \mathcal{T}(\mathbf{v}^d(t)) - \mathcal{U}(q^d(t)) dt + \int_{t_0}^{t_e} \mathcal{F}^\top(t, q^d(t), \mathbf{v}^d(t)) \cdot \delta \mathbf{q}^d(t) dt, \quad (3.14)$$

where

$$\delta q^d(t) = dL_{q^d(t)}(e) \widetilde{\delta \mathbf{q}^d(t)}, \quad t \in [t_0, t_e].$$

The first integral is treated in the same way as in section 3.1.1. For the second integral, we use a similar method of splitting the integration interval, applying the trapezoidal rule, and shifting the summation index:

$$\begin{aligned} & \int_{t_0}^{t_e} \mathcal{F}^\top(t, q^d(t), \mathbf{v}^d(t)) \cdot \delta \mathbf{q}^d(t) dt \\ &= \sum_{n=0}^{N-1} \int_{t_n}^{t_{n+1}} \mathcal{F}^\top(t, q^d(t), \mathbf{v}_{n+1/2}) \cdot \delta \mathbf{q}^d(t) dt \\ &\approx \sum_{n=0}^{N-1} \frac{h_n}{2} (\mathcal{F}^\top(t_n, q_n, \mathbf{v}_{n+1/2}) \cdot \delta \mathbf{q}_n + \mathcal{F}^\top(t_{n+1}, q_{n+1}, \mathbf{v}_{n+1/2}) \cdot \delta \mathbf{q}_{n+1}) \\ &= \sum_{n=1}^{N-1} \frac{h_n}{2} \mathcal{F}^\top(t_n, q_n, \mathbf{v}_{n+1/2}) \cdot \delta \mathbf{q}_n + \sum_{n=1}^{N-1} \frac{h_{n-1}}{2} \mathcal{F}^\top(t_n, q_n, \mathbf{v}_{n-1/2}) \cdot \delta \mathbf{q}_n \\ &= \sum_{n=1}^{N-1} \frac{h_n}{2} \mathcal{F}^\top(t_n, q_n, \mathbf{v}_{n+1/2}) \cdot \delta \mathbf{q}_n + \sum_{n=1}^{N-1} \frac{h_{n-1}}{2} \mathcal{F}^\top(t_n, q_n, \mathbf{v}_{n-1/2}) \cdot \delta \mathbf{q}_n, \end{aligned}$$

keeping the boundary conditions (3.8b) in mind.

We then arrive, since the variational principle has to hold for all variations, at (3.9), but with (3.9a) differing slightly and reading instead:

$$\left. \begin{aligned} & \mathbf{D}_1 \mathcal{L}^d(q_n, q_{n+1}, \boldsymbol{\lambda}_n^+, \boldsymbol{\lambda}_{n+1}^-) + \frac{h_n}{2} \mathcal{F}^\top(t_n, q_n, \mathbf{v}_{n+1/2}) \\ & + \mathbf{D}_2 \mathcal{L}^d(q_{n-1}, q_n, \boldsymbol{\lambda}_{n-1}^+, \boldsymbol{\lambda}_n^-) + \frac{h_{n-1}}{2} \mathcal{F}^\top(t_n, q_n, \mathbf{v}_{n-1/2}) = \mathbf{0} \end{aligned} \right\} \quad (3.15)$$

for $n = 1, \dots, N-1$, where \mathcal{L}^d is defined by (3.7), as before. Just like in section 3.1.1, we now apply the forced version of the discrete Legendre transformation [63], writing the impulses $(\mathbf{M} \cdot \mathbf{v}_n)^\top$ in terms of velocities \mathbf{v}_n , replace one of the identical equations (3.9b)

and (3.9c) by the hidden constraint (3.11), as well as extend the index ranges. We end up with (3.1), where

$$\mathbf{f}(t_n, q_n, \mathbf{v}_n) = -\mathbf{D}\mathcal{U}^\top(q_n) + \mathcal{F}(t_n, q_n, \mathbf{v}_n), \quad n = 0, \dots, N.$$

3.1.3. SHAKELie

In the previous sections, we have always used a discrete Legendre transformation. If, however, we proceed directly with (3.9), we end up with a Lie group generalization of SHAKE:

$$q_{n+1} = q_n \circ \widetilde{\exp}(h\mathbf{v}_{n+1/2}), \quad (3.16a)$$

$$h\mathbf{f}(t_n, q_n, \mathbf{v}_n) - h\mathbf{D}\Phi^\top(q_n) \cdot \boldsymbol{\lambda}_n^\pm = \mathbf{T}^{-\top}(-h\mathbf{v}_{n+1/2}) \cdot \mathbf{M} \cdot \mathbf{v}_{n+1/2} \\ - \mathbf{T}^{-\top}(h\mathbf{v}_{n-1/2}) \cdot \mathbf{M} \cdot \mathbf{v}_{n-1/2}, \quad (3.16b)$$

$$\mathbf{0} = \Phi(q_{n+1}) \quad (3.16c)$$

for constant step sizes $h_n \equiv h$ and the Lagrange multiplier $\boldsymbol{\lambda}_n^\pm = (\boldsymbol{\lambda}_n^+ + \boldsymbol{\lambda}_n^-)/2$. We can see that SHAKELie is a two-step method that discretizes the index-3 formulation (2.31) directly and that there are no approximations to $\mathbf{v}(t_n)$. In order to start the method from consistent initial configuration q_0 and velocity \mathbf{v}_0 , we need to calculate a $\mathbf{v}_{1/2}$, e. g. by computing q_1 by a first order method like the explicit Euler on Lie groups and then set $\mathbf{v}_{1/2} = \widetilde{\log}(q_0^{-1} \circ q_1)/h$. The method does not include velocities $\mathbf{v}_n \approx \mathbf{v}(t_n)$, but they could be approximated by interpolating the $\mathbf{v}_{n+1/2}$:

$$\mathbf{v}_n = \frac{\mathbf{v}_{n+1/2} + \mathbf{v}_{n-1/2}}{2}.$$

We will later see in section 5.3, that SHAKELie is usable for coarse step sizes, but suffers from the typical problems of index-3 integrators, see [6]. Not only the approximations to the Lagrange multipliers become less precise for very small step sizes, but also the approximations to the velocities. Therefore RATTLie is superior to SHAKELie in all respects, which is why SHAKELie will not be analyzed further in this thesis.

3.1.4. Extension to Nonholonomic Constraints

Now, we consider a conservative mechanical system with holonomic constraints $\Phi(q) = \mathbf{0}$ and, in addition, linear nonholonomic constraints $\mathbf{B}(q) \cdot \mathbf{v} = \mathbf{0}$ with a matrix-valued function \mathbf{B} , such that the total number of constraints does not exceed the dimension of G . We can use the variational principle (2.42) in order to derive the equations of motion of the system. As before, we restrict the set of admissible functions to continuous functions with piecewise constant derivative vectors and admit the Lagrange multipliers for the holonomic constraints to be discontinuous at the times where the derivative vectors are discontinuous, just as in section 3.1.1. We then arrive at a discrete variational principle (3.8), but with the additional condition

$$\mathbf{0} = \mathbf{B}(q_n) \cdot \delta \mathbf{q}_n, \quad n = 0, \dots, N. \quad (3.17)$$

Since the variational principle (3.8) has to hold for all variations $\delta \mathbf{q}_n \in \ker \mathbf{B}(q_n)$, the left-hand side of (3.9a) does not have to vanish, but still has to lie in $\text{im } \mathbf{B}^\top(q_n)$. This is true since the coefficient of $\delta \mathbf{q}_n$ must be orthogonal to the elements of $\ker \mathbf{B}(q_n)$ and its orthogonal complement is $(\ker \mathbf{B}(q_n))^\perp = \text{im } \mathbf{B}^\top(q_n)$. We choose vectors $\boldsymbol{\mu}_n \in \mathbb{R}^k$ for $n = 1, \dots, N-1$ such that the discrete equations of motion take the form

$$\mathbf{D}_1 \mathcal{L}^d(q_n, q_{n+1}, \boldsymbol{\lambda}_n^+, \boldsymbol{\lambda}_{n+1}^-) + \mathbf{D}_2 \mathcal{L}^d(q_{n-1}, q_n, \boldsymbol{\lambda}_{n-1}^+, \boldsymbol{\lambda}_n^-) = \frac{h_{n-1} + h_n}{2} \mathbf{B}^\top(q_n) \cdot \boldsymbol{\mu}_n \quad (3.18)$$

for $n = 1, \dots, N-1$ together with (3.9b) and (3.9c). Note that the factor $\frac{h_{n-1} + h_n}{2}$ in (3.18) is a scaling factor, which could be omitted, but ensures that the $\boldsymbol{\mu}_n$ do not scale with the step sizes.

As before, we use the forced discrete Legendre transformation [63], writing the impulses $(\mathbf{M} \cdot \mathbf{v}_n)^\top$ in terms of velocities \mathbf{v}_n . Again, we replace one of the identical equations (3.9b) and (3.9c) by the hidden constraint (3.11) and extend the index ranges just like in section 3.1.1. Eventually, we end up with

$$q_{n+1} = q_n \circ \widetilde{\text{exp}}(h_n \mathbf{v}_{n+1/2}) \quad (3.19a)$$

$$\mathbf{M} \cdot \mathbf{v}_n = \mathbf{T}^{-\top}(-h_n \mathbf{v}_{n+1/2}) \cdot \mathbf{M} \cdot \mathbf{v}_{n+1/2} - \frac{h_n}{2} \mathbf{f}(t_n, q_n, \mathbf{v}_n) \quad (3.19b)$$

$$+ \frac{h_n}{2} \mathbf{D}\boldsymbol{\Phi}^\top(q_n) \cdot \boldsymbol{\lambda}_n^+ + \frac{h_n}{2} \mathbf{B}^\top(q_n) \cdot \boldsymbol{\mu}_n, \quad (3.19c)$$

$$\mathbf{0} = \boldsymbol{\Phi}(q_{n+1}) \quad (3.19d)$$

$$\mathbf{M} \cdot \mathbf{v}_{n+1} = \mathbf{T}^{-\top}(h_n \mathbf{v}_{n+1/2}) \cdot \mathbf{M} \cdot \mathbf{v}_{n+1/2} + \frac{h_n}{2} \mathbf{f}(t_{n+1}, q_{n+1}, \mathbf{v}_{n+1}) \quad (3.19e)$$

$$- \frac{h_n}{2} \mathbf{D}\boldsymbol{\Phi}^\top(q_{n+1}) \cdot \boldsymbol{\lambda}_{n+1}^- - \frac{h_n}{2} \mathbf{B}^\top(q_{n+1}) \cdot \boldsymbol{\mu}_{n+1}, \quad (3.19f)$$

$$\mathbf{0} = \mathbf{D}\boldsymbol{\Phi}(q_{n+1}) \cdot \mathbf{v}_{n+1}, \quad (3.19g)$$

$$\mathbf{0} = \mathbf{B}(q_{n+1}) \cdot \mathbf{v}_{n+1}, \quad (3.19h)$$

for $n = 0, \dots, N$ with internal forces

$$\mathbf{f}(t_n, q_n, \mathbf{v}_n) = -\mathbf{D}\mathcal{U}^\top(q_n), \quad n = 0, \dots, N.$$

Of course, we can follow along the lines of section 3.1.2 and take \mathbf{f} to be the sum of internal and external forces:

$$\mathbf{f}(t_n, q_n, \mathbf{v}_n) = -\mathbf{D}\mathcal{U}^\top(q_n) + \mathcal{F}(t_n, q_n, \mathbf{v}_n), \quad n = 0, \dots, N.$$

3.2. Convergence Analysis

In this section, we will show that the RATTLie integration scheme is convergent of second order if \mathbf{f} and $\boldsymbol{\Phi}$ are smooth enough and some technical presumptions are fulfilled. This convergence analysis is not based on symplecticity, which is used in the convergence results in [35, 63] for RATTLE. Our approach views RATTLie as a one-step method of an

ODE in q and \mathbf{v} , which is equivalent to (2.31) and then applies techniques from one-step methods [36, 78] generalized to Lie groups. This means that this proof of convergence is not only valid for constant time step sizes, but also holds for any series of time steps. The calculation of approximations to the Lagrange multipliers is discussed in detail in section 3.2.3. Their convergence follows from the convergence of RATTLie in q and \mathbf{v} .

3.2.1. The Local Error

We will consider one time step from t_0 to $t_1 = t_0 + h_0$ with the RATTLie scheme. The consistent initial data $q_0 = q(t_0)$ and $\mathbf{v}_0 = \mathbf{v}(t_0)$, see (3.1f), is supposed to be the exact solution of the continuous system (2.31).

We assume that the functions \mathbf{f} and Φ are smooth enough (C^3 and C^4 respectively), the mass matrix \mathbf{M} is invertible and that $\mathbf{D}\Phi(q)$ always has full rank. Additionally, we use the technical assumptions

$$\mathbf{v}_{1/2}, \mathbf{v}_1, \boldsymbol{\lambda}_0^+, \boldsymbol{\lambda}_1^- \in \mathcal{O}(1), \quad \text{for } h_0 \rightarrow 0. \quad (3.20)$$

From (2.21) and [64] we know that for $h > 0$ and $\mathbf{w} \in \mathbb{R}^n$ it holds

$$\mathbf{T}^{-1}(h\mathbf{w}) = \sum_{i=0}^{\infty} \frac{(-1)^i h^i B_i}{i!} \widehat{\mathbf{w}}^i = \mathbf{I} + \frac{h}{2} \widehat{\mathbf{w}} + \frac{h^2}{12} \widehat{\mathbf{w}}^2 + \mathcal{O}(h^4), \quad (3.21)$$

where $(B_i)_{i \in \mathbb{N}_0}$ are the Bernoulli numbers.

From (3.1b) and (3.21) truncated to first order we get

$$\mathbf{v}_{1/2} = \mathbf{v}_0 + \mathcal{O}(h_0) \quad (3.22)$$

and by inserting (3.22) and (3.21) into (3.1b)

$$\begin{aligned} \mathbf{v}_{1/2} &= \mathbf{v}_0 + \frac{h_0}{2} \mathbf{M}^{-1} \cdot (\widehat{\mathbf{v}}_0^\top \cdot \mathbf{M} \cdot \mathbf{v}_0 + \mathbf{f}_0 - \mathbf{D}\Phi^\top(q_0) \cdot \boldsymbol{\lambda}_0^+) + \mathcal{O}(h_0^2) \\ &\stackrel{(2.31b)}{=} \mathbf{v}_0 + \frac{h_0}{2} \dot{\mathbf{v}}_0 + \frac{h_0}{2} \mathbf{M}^{-1} \cdot \mathbf{D}\Phi^\top(q_0)(\boldsymbol{\lambda}(t_0) - \boldsymbol{\lambda}_0^+) + \mathcal{O}(h_0^2), \end{aligned} \quad (3.23)$$

where $\dot{\mathbf{v}}_0 = \dot{\mathbf{v}}(t_0)$, see (2.31b) and $\mathbf{f}_0 = \mathbf{f}(t_0, q_0, \mathbf{v}_0)$. Now, we plug (3.1a) into (3.1c), use Taylor expansion of $h \mapsto \Phi(q_0 \circ \widehat{\exp}(h\mathbf{v}_{1/2}))$ around $h = 0$ up to third order, and subsequently use (3.23):

$$\begin{aligned} \boldsymbol{\theta} &= \Phi(q_0) + h_0 \mathbf{D}\Phi(q_0) \cdot \mathbf{T}(\boldsymbol{\theta}) \cdot \mathbf{v}_{1/2} + \frac{h_0^2}{2} \mathbf{D}^2\Phi(q_0)(\mathbf{T}(\boldsymbol{\theta}) \cdot \mathbf{v}_{1/2}, \mathbf{T}(\boldsymbol{\theta}) \cdot \mathbf{v}_{1/2}) + \mathcal{O}(h_0^3) \\ &\stackrel{(3.22)}{=} h_0 \mathbf{D}\Phi(q_0) \cdot \mathbf{v}_{1/2} + \frac{h_0^2}{2} \mathbf{D}^2\Phi(q_0)(\mathbf{v}_0, \mathbf{v}_0) + \mathcal{O}(h_0^3) \\ &\stackrel{(3.23)}{=} h_0 \mathbf{D}\Phi(q_0) \cdot \left(\mathbf{v}_0 + \frac{h_0}{2} \dot{\mathbf{v}}_0 + \frac{h_0}{2} \mathbf{M}^{-1} \cdot \mathbf{D}\Phi^\top(q_0)(\boldsymbol{\lambda}(t_0) - \boldsymbol{\lambda}_0^+) \right) \\ &\quad + \frac{h_0^2}{2} \mathbf{D}^2\Phi(q_0)(\mathbf{v}_0, \mathbf{v}_0) + \mathcal{O}(h_0^3). \end{aligned} \quad (3.24)$$

Here we have used the abbreviation (2.33). Since $\mathbf{D}\Phi(q_0) \cdot \mathbf{v}_0 = \mathbf{0}$ and $\mathbf{D}^2\Phi(q_0)(\mathbf{v}_0, \mathbf{v}_0) = -\mathbf{D}\Phi(q_0) \cdot \dot{\mathbf{v}}_0$, see (2.32), equation (3.24) implies

$$\boldsymbol{\lambda}_0^+ = \boldsymbol{\lambda}(t_0) + \mathcal{O}(h_0), \quad (3.25)$$

because $\mathbf{D}\Phi(q_0) \cdot \mathbf{M}^{-1} \cdot \mathbf{D}\Phi^\top(q_0)$ is invertible. Now, it follows from (3.23) and (3.25)

$$\mathbf{v}_{1/2} = \mathbf{v}_0 + \frac{h_0}{2} \dot{\mathbf{v}}_0 + \mathcal{O}(h_0^2). \quad (3.26)$$

By using a generalization of the qualitative Taylor theorem on Lie group valued functions, see lemma 2.22 and also [64], as well as the Baker-Campbell-Hausdorff formula, see lemma 2.13 and also [46], we obtain

$$\begin{aligned} & q_1^{-1} \circ q(t_1) \\ &= \widetilde{\exp}\left(h_0 \mathbf{v}_0 + \frac{h_0^2}{2} \dot{\mathbf{v}}_0 + \mathcal{O}(h_0^3)\right)^{-1} \circ q_0^{-1} \circ q(t_0) \circ \widetilde{\exp}\left(h_0 \mathbf{v}(t_0) + \frac{h_0^2}{2} \dot{\mathbf{v}}(t_0) + \mathcal{O}(h_0^3)\right) \\ &= \widetilde{\exp}\left(-h_0 \mathbf{v}_0 - \frac{h_0^2}{2} \dot{\mathbf{v}}_0 + h_0 \mathbf{v}(t_0) + \frac{h_0^2}{2} \dot{\mathbf{v}}(t_0) + \mathcal{O}(h_0^3)\right) \\ &= \widetilde{\exp}(\mathcal{O}(h_0^3)) \end{aligned} \quad (3.27)$$

with (3.1a) and (3.26).

Now, we subtract (3.1b) from (3.1d) and get

$$\begin{aligned} \mathbf{M} \cdot (\mathbf{v}_1 - \mathbf{v}_0) &= h_0 \widehat{\mathbf{v}}_{1/2}^\top \cdot \mathbf{M} \cdot \mathbf{v}_{1/2} + \frac{h_0}{2} (\mathbf{f}_0 + \mathbf{f}(t_1, q_1, \mathbf{v}_1)) \\ &\quad - \frac{h_0}{2} (\mathbf{D}\Phi^\top(q_0) \cdot \boldsymbol{\lambda}_0^+ + \mathbf{D}\Phi^\top(q_1) \cdot \boldsymbol{\lambda}_1^-), \end{aligned} \quad (3.28)$$

since all odd Bernoulli numbers in (3.21) vanish, except for B_1 . Considering $t_1 = t_0 + h_0$, (3.27) and the technical assumptions (3.20), we can see that it holds

$$\mathbf{f}(t_1, q_1, \mathbf{v}_1) = \mathbf{f}(t_0, q_0, \mathbf{v}_0) + \mathcal{O}(1) = \mathbf{f}_0 + \mathcal{O}(1). \quad (3.29)$$

From (3.28) it is clear that

$$\mathbf{v}_1 = \mathbf{v}_0 + \mathcal{O}(h_0) \quad (3.30a)$$

and therefore it follows from (3.27) and (3.30a):

$$\mathbf{f}(t_1, q_1, \mathbf{v}_1) = \mathbf{f}_0 + \mathcal{O}(h_0) \quad (3.30b)$$

and furthermore, by using (3.1a) and (3.26) it holds

$$\mathbf{D}\Phi(q_1) = \mathbf{D}\Phi(q_0) \cdot \mathbf{T}(\mathbf{0}) + \mathcal{O}(h_0) = \mathbf{D}\Phi(q_0) + \mathcal{O}(h_0) \quad (3.30c)$$

Now, we can apply the above equations in (3.1d) and obtain

$$\begin{aligned}
\mathbf{M} \cdot \mathbf{v}_1 &\stackrel{(3.30)}{=} \mathbf{T}^{-\top}(h_0 \mathbf{v}_{1/2}) \cdot \mathbf{M} \cdot \mathbf{v}_{1/2} + \frac{h_0}{2} \mathbf{f}(t_0, q_0, \mathbf{v}_0) - \frac{h_0}{2} \mathbf{D}\Phi^\top(q_0) \cdot \boldsymbol{\lambda}_1^- + \mathcal{O}(h_0^2) \\
&\stackrel{(3.21)}{=} \mathbf{M} \cdot \mathbf{v}_{1/2} + \frac{h_0}{2} \widehat{\mathbf{v}}_{1/2}^\top \cdot \mathbf{M} \cdot \mathbf{v}_{1/2} + \frac{h_0}{2} \mathbf{f}(t_0, q_0, \mathbf{v}_0) - \frac{h_0}{2} \mathbf{D}\Phi^\top(q_0) \cdot \boldsymbol{\lambda}_1^- + \mathcal{O}(h_0^2) \\
&\stackrel{(3.26)}{=} \mathbf{M} \cdot (\mathbf{v}_0 + \frac{h_0}{2} \dot{\mathbf{v}}_0) + \frac{h_0}{2} \widehat{\mathbf{v}}_0^\top \cdot \mathbf{M} \cdot \mathbf{v}_0 + \frac{h_0}{2} \mathbf{f}(t_0, q_0, \mathbf{v}_0) \\
&\quad - \frac{h_0}{2} \mathbf{D}\Phi^\top(q_0) \cdot \boldsymbol{\lambda}_1^- + \mathcal{O}(h_0^2)
\end{aligned} \tag{3.31}$$

$$\stackrel{(2.31b)}{=} \mathbf{M} \cdot (\mathbf{v}_0 + h_0 \dot{\mathbf{v}}_0) - \frac{h_0}{2} \mathbf{D}\Phi^\top(q_0) \cdot (\boldsymbol{\lambda}_1^- - \boldsymbol{\lambda}(t_0)) + \mathcal{O}(h_0^2). \tag{3.32}$$

Subsequently, we expand $h \mapsto \mathbf{D}\Phi(q_0 \circ \widehat{\exp}(h\mathbf{v}_{1/2})) \cdot \mathbf{w}$ for $\mathbf{w} \in \mathbb{R}^n$:

$$\mathbf{D}\Phi(q_1) \cdot \mathbf{w} = \mathbf{D}\Phi(q_0) \cdot \mathbf{w} + h_0 \mathbf{Z}(q_0, \mathbf{v}_{1/2}) \cdot \mathbf{w} + \mathcal{O}(h_0^2), \tag{3.33}$$

where $\mathbf{Z}(q_0, \mathbf{v}_{1/2})$ is the matrix that is given for the linear map $\mathbf{w} \mapsto \mathbf{D}^2\Phi(q_0)(\mathbf{w}, \mathbf{v}_{1/2})$, i. e. it holds

$$\mathbf{Z}(p, \mathbf{a}) \cdot \mathbf{b} = \mathbf{D}^2\Phi(p)(\mathbf{b}, \mathbf{a}) \tag{3.34}$$

for $p \in G$ and $\mathbf{a}, \mathbf{b} \in \mathbb{R}^n$. Now we consider (3.1e) and apply the above equations:

$$\begin{aligned}
\mathbf{0} &\stackrel{(3.33)}{=} (\mathbf{D}\Phi(q_0) + h_0 \mathbf{Z}(q_0, \mathbf{v}_{1/2})) \cdot \mathbf{v}_1 + \mathcal{O}(h_0^2) \\
&\stackrel{(3.32)}{=} (\mathbf{D}\Phi(q_0) + h_0 \mathbf{Z}(q_0, \mathbf{v}_{1/2}) \cdot (\mathbf{v}_0 + h_0 \dot{\mathbf{v}}_0 - \frac{h_0}{2} \mathbf{M}^{-1} \cdot \mathbf{D}\Phi^\top(q_0) \cdot (\boldsymbol{\lambda}_1^- - \boldsymbol{\lambda}(t_1)))) + \mathcal{O}(h_0^2) \\
&\stackrel{(3.22)}{=} \mathbf{D}\Phi(q_0) \cdot (\mathbf{v}_0 + h_0 \dot{\mathbf{v}}_0 - \frac{h_0}{2} \mathbf{M}^{-1} \cdot \mathbf{D}\Phi^\top(q_0) \cdot (\boldsymbol{\lambda}_1^- - \boldsymbol{\lambda}(t_1))) \\
&\quad + h_0 \mathbf{D}^2(q_0)(\mathbf{v}_0, \mathbf{v}_0) + \mathcal{O}(h_0^2) \\
&\stackrel{(2.32)}{=} \frac{-h_0}{2} \mathbf{D}\Phi(q_0) \cdot \mathbf{M}^{-1} \cdot \mathbf{D}\Phi^\top(q_0) \cdot (\boldsymbol{\lambda}_1^- - \boldsymbol{\lambda}(t_1)) + \mathcal{O}(h_0^2),
\end{aligned}$$

which in turn implies

$$\boldsymbol{\lambda}_1^- = \boldsymbol{\lambda}(t_0) + \mathcal{O}(h_0), \tag{3.35}$$

since $\mathbf{D}\Phi(q_0) \cdot \mathbf{M}^{-1} \cdot \mathbf{D}\Phi^\top(q_0)$ is invertible. Applying this result in (3.32) yields

$$\mathbf{v}_1 = \mathbf{v}_0 + h_0 \dot{\mathbf{v}}_0 + \mathcal{O}(h_0^2). \tag{3.36}$$

Let us now consider the time derivative of the dynamic equation (2.31b) at $t = t_0$:

$$\begin{aligned}
\mathbf{M} \cdot \ddot{\mathbf{v}}_0 &= \overbrace{\widehat{\mathbf{v}}_0^\top \cdot \mathbf{M} \cdot \dot{\mathbf{v}}_0 + \widehat{\mathbf{v}}_0^\top \cdot \mathbf{M} \cdot \mathbf{v}_0}^{=:A} + \overbrace{\mathrm{d}_t \mathbf{f}_0 + \mathbf{D}_q \mathbf{f}_0 \cdot \mathbf{v}_0 + \mathrm{d}_v \mathbf{f}_0 \cdot \dot{\mathbf{v}}_0}^{=:B} \\
&\quad - \mathbf{D}\Phi^\top(q_0) \cdot \dot{\boldsymbol{\lambda}}(t_0) - \mathbf{Z}(q_0, \mathbf{v}_0)^\top \cdot \boldsymbol{\lambda}(t_0),
\end{aligned} \tag{3.37}$$

where $\ddot{\mathbf{v}}_0 = \ddot{\mathbf{v}}(t_0)$. By applying a Taylor expansion, we get

$$\begin{aligned} & \mathbf{f}(t_0 + h, q_0 \circ \widehat{\text{exp}}(h\mathbf{v}_{1/2}), \mathbf{v}_0 + h\dot{\mathbf{v}}_0) \\ &= \mathbf{f}_0 + h(\text{d}_t \mathbf{f}_0 + \mathbf{D}_q \mathbf{f}_0 \cdot \mathbf{T}(\boldsymbol{\theta}) \cdot \mathbf{v}_{1/2} + \text{d}_v \mathbf{f}_0 \cdot \dot{\mathbf{v}}_0) + \mathcal{O}(h^2) \end{aligned}$$

and with $h = h_0$ as well as (3.26) it follows

$$\mathbf{f}(t_1, q_1, \mathbf{v}_1) = \mathbf{f}_0 + h_0 B + \mathcal{O}(h_0^2). \quad (3.38)$$

Furthermore, Taylor expansion of $h_0 \mapsto \mathbf{v}(t_0 + h_0)$ yields

$$\mathbf{v}(t_1) = \mathbf{v}_0 + h_0 \dot{\mathbf{v}}_0 + \frac{h_0^2}{2} \ddot{\mathbf{v}}_0 + \mathcal{O}(h_0^3). \quad (3.39)$$

Now we can consider (3.28):

$$\begin{aligned} \mathbf{M} \cdot \mathbf{v}_1 &\stackrel{(3.26)}{=} \mathbf{M} \cdot \mathbf{v}_0 + h_0 \widehat{\mathbf{v}}_0^\top \cdot \mathbf{M} \cdot \mathbf{v}_0 + \frac{h_0}{2} (h_0 A + \mathbf{f}_0 + \mathbf{f}(t_1, q_1, \mathbf{v}_1) - \mathbf{D}\boldsymbol{\Phi}^\top(q_0) \cdot \boldsymbol{\lambda}_0^+ \\ &\quad - \mathbf{D}\boldsymbol{\Phi}^\top(q_1) \cdot \boldsymbol{\lambda}_1^-) + \mathcal{O}(h_0^3) \\ &\stackrel{(3.38)}{=} \mathbf{M} \cdot \mathbf{v}_0 + h_0 \widehat{\mathbf{v}}_0^\top \cdot \mathbf{M} \cdot \mathbf{v}_0 + \frac{h_0}{2} (h_0(A + B) + 2\mathbf{f}_0 - \mathbf{D}\boldsymbol{\Phi}^\top(q_0) \cdot \boldsymbol{\lambda}_0^+ \\ &\quad - \mathbf{D}\boldsymbol{\Phi}^\top(q_1) \cdot \boldsymbol{\lambda}_1^-) + \mathcal{O}(h_0^3) \\ &\stackrel{(2.31b)}{=} \mathbf{M} \cdot (\mathbf{v}_0 + h_0 \dot{\mathbf{v}}_0) + \frac{h_0}{2} (h_0(A + B) + \mathbf{D}\boldsymbol{\Phi}^\top(q_0) \cdot (2\boldsymbol{\lambda}(t_0) - \boldsymbol{\lambda}_0^+) \\ &\quad - \mathbf{D}\boldsymbol{\Phi}^\top(q_1) \cdot \boldsymbol{\lambda}_1^-) + \mathcal{O}(h_0^3) \\ &\stackrel{(3.33)}{=} \mathbf{M} \cdot (\mathbf{v}_0 + h_0 \dot{\mathbf{v}}_0) + \frac{h_0}{2} \left(h_0(A + B) + \mathbf{D}\boldsymbol{\Phi}^\top(q_0) \cdot (2\boldsymbol{\lambda}(t_0) - \boldsymbol{\lambda}_0^+) \right. \\ &\quad \left. - (\mathbf{D}\boldsymbol{\Phi}(q_0) + h_0 \mathbf{Z}(q_0, \mathbf{v}_{1/2}))^\top \cdot \boldsymbol{\lambda}_1^- \right) + \mathcal{O}(h_0^3) \\ &\stackrel{(3.22)}{=} \mathbf{M} \cdot (\mathbf{v}_0 + h_0 \dot{\mathbf{v}}_0) + \frac{h_0}{2} (h_0(A + B) + \mathbf{D}\boldsymbol{\Phi}^\top(q_0) \cdot (2\boldsymbol{\lambda}(t_0) - \boldsymbol{\lambda}_0^+ - \boldsymbol{\lambda}_1^-) \\ &\quad - h_0 \mathbf{Z}^\top(q_0, \mathbf{v}_0) \cdot \boldsymbol{\lambda}_1^-) + \mathcal{O}(h_0^3) \\ &\stackrel{(3.35)}{=} \mathbf{M} \cdot (\mathbf{v}_0 + h_0 \dot{\mathbf{v}}_0) + \frac{h_0}{2} \left(h_0(A + B) + \mathbf{D}\boldsymbol{\Phi}^\top(q_0) \cdot (2\boldsymbol{\lambda}(t_0) - \boldsymbol{\lambda}_0^+ - \boldsymbol{\lambda}_1^-) \right. \\ &\quad \left. - h_0 \mathbf{Z}^\top(q_0, \mathbf{v}_0) \cdot \boldsymbol{\lambda}(t_0) \right) + \mathcal{O}(h_0^3) \\ &\stackrel{(3.37)}{=} \mathbf{M} \cdot \left(\mathbf{v}_0 + h_0 \dot{\mathbf{v}}_0 + \frac{h_0^2}{2} \ddot{\mathbf{v}}_0 \right) + \frac{h_0}{2} \mathbf{D}\boldsymbol{\Phi}^\top(q_0) \cdot (2\boldsymbol{\lambda}(t_0) + h_0 \dot{\boldsymbol{\lambda}}(t_0) \\ &\quad - \boldsymbol{\lambda}_0^+ - \boldsymbol{\lambda}_1^-) + \mathcal{O}(h_0^3) \\ &\stackrel{(3.39)}{=} \mathbf{M} \cdot \mathbf{v}(t_1) + \frac{h_0}{2} \mathbf{D}\boldsymbol{\Phi}^\top(q_0) \cdot (2\boldsymbol{\lambda}(t_0) + h_0 \dot{\boldsymbol{\lambda}}(t_0) - \boldsymbol{\lambda}_0^+ - \boldsymbol{\lambda}_1^-) + \mathcal{O}(h_0^3). \quad (3.40) \end{aligned}$$

Expanding $\mathbf{D}\boldsymbol{\Phi}(q_1)$ – similar to (3.33) – but this time around $q(t_1)$ yields

$$\mathbf{D}\boldsymbol{\Phi}(q_1) \stackrel{(3.27)}{=} \mathbf{D}\boldsymbol{\Phi}(q(t_1)) + \mathcal{O}(h_0^3). \quad (3.41)$$

Now we can use (3.40), (3.41), and (2.32a) for $t = t_1$ in (3.1e) and obtain

$$\mathbf{o} = \mathbf{D}\Phi(q(t_1)) \cdot \left(h_0 \mathbf{M}^{-1} \cdot \mathbf{D}\Phi^\top(q_0) \cdot \left(\frac{\lambda_0^+ + \lambda_1^-}{2} - \lambda(t_0) - \frac{h_0}{2} \dot{\lambda}(t_0) \right) \right) + \mathcal{O}(h_0^3),$$

which implies

$$\frac{\lambda_0^+ + \lambda_1^-}{2} = \lambda(t_0) + \frac{h_0}{2} \dot{\lambda}(t_0) + \mathcal{O}(h_0^2) = \lambda\left(\frac{t_0 + t_1}{2}\right) + \mathcal{O}(h_0^2), \quad (3.42)$$

since $\mathbf{D}\Phi$ is assumed to have full rank on the solution. Finally it follows

$$\mathbf{v}_1 - \mathbf{v}(t_1) = \mathcal{O}(h_0^3) \quad (3.43)$$

by using (3.42) in (3.40).

3.2.2. The Global Error

We will analyze the global error of the RATTLie scheme on the direct product Lie group $G \times \mathbb{R}^n$, where the elements in G represent the configuration and the elements of \mathbb{R}^n represent the velocity. This direct product structure is in contrast to the Lie group structure $G \times_{\text{Ad}} T_e G$ that is induced by G on the tangent bundle TG , see e. g. [27], which – as a manifold – is isomorphic to $G \times \mathbb{R}^n$.

We will adapt the proof of convergence for one-step methods [36, 78] to Lie groups. In order to do so, we will consider RATTLie as a mapping $(t_n, q_n, \mathbf{v}_n) \mapsto (t_{n+1}, q_{n+1}, \mathbf{v}_{n+1})$. To be more specific, we can define functions φ^q and φ^v with

$$\begin{aligned} q_{n+1} &= q_n \circ \widetilde{\exp}\left(h_n \varphi^q(t_n, (q_n, \mathbf{v}_n); h_n)\right), \\ \mathbf{v}_{n+1} &= \mathbf{v}_n + h_n \varphi^v(t_n, (q_n, \mathbf{v}_n); h_n), \end{aligned}$$

which is similar to Henrici's notation [36]. Both φ^q and φ^v are differentiable by the inverse function theorem. This gives rise, using the direct product Lie group structure of $G \times \mathbb{R}^n$, see remark 2.30, to the following equation:

$$(q_{n+1}, \mathbf{v}_{n+1}) = (q_n, \mathbf{v}_n) \circ \widetilde{\exp}\left(h_n \varphi(t_n, (q_n, \mathbf{v}_n); h_n)\right),$$

where $\varphi = (\varphi^q, \varphi^v)$ and the exponential function as well as the Lie group operation are with respect to the direct product Lie group $G \times \mathbb{R}^n$.

We consider G to be a metric space with a right invariant and almost left invariant distance $d_G: G \times G \rightarrow [0, \infty)$. On every Lie group G , such a distance function exists, see remark 2.47. Furthermore, we also consider $G \times \mathbb{R}^n$ to be a metric space with a distance function

$$d: (G \times \mathbb{R}^n) \times (G \times \mathbb{R}^n) \rightarrow [0, \infty), \quad ((q_1, \mathbf{v}_1), (q_2, \mathbf{v}_2)) \mapsto d_G(q_1, q_2) + \|\mathbf{v}_2 - \mathbf{v}_1\|_2, \quad (3.44)$$

which is then right invariant and almost left invariant as well.

Now, we can measure the distance between the analytic solution $(q(t_n), \mathbf{v}(t_n))$ and the numeric approximation (q_n, \mathbf{v}_n) calculated by RATTLie. For brevity let $R_n = (q_n, \mathbf{v}_n) \in G \times \mathbb{R}^n$ be the numerical approximation and $Q_n = (q(t_n), \mathbf{v}(t_n)) \in G \times \mathbb{R}^n$ be the analytical solution. Now, consider

$$d(R_{n+1}, Q_{n+1}) \leq d\left(R_{n+1}, Q_n \circ \widetilde{\exp}(h_n \varphi(t_n, Q_n; h_n))\right) + le_n, \quad (3.45)$$

where le_n measures the local error:

$$le_n = d\left(Q_n \circ \widetilde{\exp}(h_n \varphi(t_n, Q_n; h_n)), Q_{n+1}\right). \quad (3.46)$$

We can continue to estimate (3.45) by using the error translation from remark 2.47, the almost right invariance of d and lemma 2.42.

$$\begin{aligned} d(R_{n+1}, Q_{n+1}) &\leq d(R_n, Q_n) + \rho(Q_n) d\left(\widetilde{\exp}(h_n \varphi(t_n, R_n; h_n)), \widetilde{\exp}(h_n \varphi(t_n, Q_n; h_n))\right) + le_n \\ &\leq \left(1 + \rho(Q_n) \sup_{Q \in K_n} \|d_Q \widetilde{\exp}(h_n \varphi(t_n, Q; h_n))\|_*\right) d(R_n, Q_n) + le_n, \end{aligned} \quad (3.47)$$

where $\|\bullet\|_* = \|\bullet\|_{\widetilde{\exp}(h_n \varphi(t_n, Q; h_n)), Q}$ and K_n is a compact set depending on Q_n and R_n . Under the technical assumptions

$$h_n \in (0, H], \quad d(R_n, Q_n) \in \mathcal{O}(1), \quad \text{for all } n = 0, \dots, N \quad (3.48)$$

with some $H > 0$ we can consider (3.47) only in a compact neighborhood S of $\{Q(t) : t \in [t_0, t_e]\}$. Since

$$d_Q \widetilde{\exp}(h_n \varphi(t_n, Q; h_n)) = h_n d \widetilde{\exp}(h_n \varphi(t_n, Q; h_n)) d_Q \varphi(t_n, Q; h_n)$$

and $\varphi, \widetilde{\exp}$ are continuously differentiable, we get from (3.47) restricted to S that for some constant $L > 0$ it holds

$$d(R_{n+1}, Q_{n+1}) \leq (1 + h_n L) d(R_n, Q_n) + le_n. \quad (3.49)$$

The local error le_n can be treated by using remark 2.47, lemma 2.41, (3.27), and (3.43):

$$\begin{aligned} le_n &\leq \left\| \widetilde{\log}\left(Q_{n+1}^{-1} \circ Q_n \circ \widetilde{\exp}(h_n \varphi(t_n, Q_n; h_n))\right) \right\|_2 \\ &= \left\| \left[\begin{array}{c} \widetilde{\log}\left(q(t_{n+1})^{-1} \circ q(t_n) \circ \widetilde{\exp}(h_n \varphi^q(t_n, Q_n; h_n))\right) \\ -\mathbf{v}(t_{n+1}) + \mathbf{v}(t_n) + h_n \varphi^v(t_n, Q_n; h_n) \end{array} \right] \right\|_2 \leq Ch_n^3. \end{aligned} \quad (3.50)$$

for some constant $C > 0$. This can be done since the calculations leading up to (3.27) and (3.43) only depend on the starting values and we can take the maximum of all constants over the exact solution on the compact interval $[t_0, t_e]$. Now, we can put everything together in order to formulate the following:

Theorem 3.1: *Second order convergence of RATTLie.*

The RATTLie method is convergent of second order in q and \mathbf{v} for step sizes $h_n \in (0, H]$ with $H > 0$ small enough and under the technical assumptions (3.20), (3.48) and if \mathbf{f} and Φ are smooth enough. More precisely, it holds:

$$d\left((q_n, \mathbf{v}_n), (q(t_n), \mathbf{v}(t_n))\right) \leq \frac{C}{L} (e^{L(t_n-t_0)} - 1) h_{\max}^2, \quad n = 0, \dots, N \quad (3.51)$$

with constants $L, C > 0$ and the maximal step size $h_{\max} = \max_{n=0, \dots, N-1} h_n$.

Proof. We can use a standard inductive argument found in [36, 78]. It holds

$$d\left((q_0, \mathbf{v}_0), (q(t_0), \mathbf{v}(t_0))\right) = 0 = \frac{C}{L} (e^{L(t_0-t_0)} - 1) h_{\max}^2$$

because of the choice of initial data (3.1f). Assume that (3.51) is true for $m < N$. Now, we use (3.50) and the induction hypothesis in (3.49) and get

$$\begin{aligned} d\left((q_{m+1}, \mathbf{v}_{m+1}), (q(t_{m+1}), \mathbf{v}(t_{m+1}))\right) &\leq (1 + Lh_{m+1}) \frac{C}{L} (e^{L(t_m-t_0)} - 1) h_{\max}^2 + Ch_{m+1}^3 \\ &= \frac{C}{L} \underbrace{\left((1 + Lh_{m+1}) e^{L(t_m-t_0)} - 1 \right)}_{\leq e^{Lh_{m+1}}} h_{\max}^2 + C \underbrace{(h_{m+1}^3 - h_{m+1} h_{\max}^2)}_{\leq 0} \\ &\leq \frac{C}{L} (e^{L(t_{m+1}-t_0)} - 1) h_{\max}^2. \quad \square \end{aligned}$$

The equation (3.51) also implies

$$d_G(q_n, q(t_n)) \in \mathcal{O}(h_{\max}^2), \quad \mathbf{v}_n - \mathbf{v}(t_n) \in \mathcal{O}(h_{\max}^2), \quad n = 0, \dots, N \quad (3.52)$$

due to the direct product structure of $G \times \mathbb{R}^n$ and the choice of the distance function (3.44).

3.2.3. The Lagrange Multipliers

Let $q(t)$, $\mathbf{v}(t)$ and $\boldsymbol{\lambda}(t)$ be the exact solution of (2.31), $t_0 < t_1 < \dots < t_N$ a time grid, as well as $(q_n)_{n=0}^N$, $(\mathbf{v}_n)_{n=0}^N$, $(\boldsymbol{\lambda}_n^+)_{n=0}^{N-1}$, and $(\boldsymbol{\lambda}_n^-)_{n=1}^N$ be calculated by the RATTLie scheme (3.1) with exact and consistent initial values $q_0 = q(t_0)$, $\mathbf{v}_0 = \mathbf{v}(t_0)$. Furthermore, let the prerequisites of theorem 3.1 be fulfilled. We define

$$t_{n+1/2} = \frac{t_n + t_{n+1}}{2}, \quad \boldsymbol{\lambda}_{n+1/2} = \frac{\boldsymbol{\lambda}_n^+ + \boldsymbol{\lambda}_{n+1}^-}{2}, \quad (3.53)$$

which we will later use to calculate approximations to $\boldsymbol{\lambda}(t_n)$.

First, from theorem 3.1, we know that $d_G(q_n, q(t_n)) \in \mathcal{O}(h_{\max}^2)$. With remark 2.47 and lemma 2.43 it follows

$$\mathbf{F}(q_n) - \mathbf{F}(q(t_n)) \in \mathcal{O}\left(d_G(q_n, q(t_n))\right)$$

for any continuously differentiable function F . Therefore, (3.42) implies

$$\boldsymbol{\lambda}_{n+1/2} = \boldsymbol{\lambda}(t_{n+1/2}) + \mathcal{O}(h_{\max}^2). \quad (3.54)$$

Now, we can apply linear interpolation of $(t_{n-1/2}, \boldsymbol{\lambda}_{n-1/2})$ and $(t_{n+1/2}, \boldsymbol{\lambda}_{n+1/2})$ at t_n in order to obtain an approximation of $\boldsymbol{\lambda}(t_n)$:

$$\boldsymbol{\lambda}_n = \frac{h_n \boldsymbol{\lambda}_{n-1/2} + h_{n-1} \boldsymbol{\lambda}_{n+1/2}}{h_{n-1} + h_n}. \quad (3.55)$$

We will call Lagrange multipliers that were calculated by (3.55) ‘‘interpolated Lagrange multipliers’’. The properties of polynomial interpolation and (3.54) yield

$$\boldsymbol{\lambda}_n = \boldsymbol{\lambda}(t_n) + \mathcal{O}(h_{\max}^2). \quad (3.56)$$

In numerical experiments, it can be seen that the $\boldsymbol{\lambda}_n^+$ and $\boldsymbol{\lambda}_n^-$ approximate $\boldsymbol{\lambda}(t_n)$ only with first order, see remark 5.10. For small step sizes the $\boldsymbol{\lambda}_n^\pm$ suffer spurious oscillations, which can be observed as an increasing error. Since $\boldsymbol{\lambda}_n$ is directly calculated from $\boldsymbol{\lambda}_{n-1}^+$, $\boldsymbol{\lambda}_n^\pm$ and $\boldsymbol{\lambda}_{n+1}^-$, we have to suspect that $\boldsymbol{\lambda}_n$ may contain spurious oscillations as well. Therefore, we show an alternative way to calculate approximations $\boldsymbol{\lambda}_n^{\text{sep}}$ to $\boldsymbol{\lambda}(t_n)$ by using the index-1 formulation (2.34):

$$\begin{bmatrix} \mathbf{M} & \mathbf{D}\boldsymbol{\Phi}^\top(q_n) \\ \mathbf{D}\boldsymbol{\Phi}(q_n) & \mathbf{0} \end{bmatrix} \cdot \begin{bmatrix} \dot{\boldsymbol{v}}_n^{\text{sep}} \\ \boldsymbol{\lambda}_n^{\text{sep}} \end{bmatrix} = \begin{bmatrix} \hat{\boldsymbol{v}}_n^\top \cdot \mathbf{M} \cdot \boldsymbol{v}_n + \boldsymbol{f}(t_n, q_n, \boldsymbol{v}_n) \\ (\hat{c}_{n,-}^{\text{sep}} \mathbf{D}\boldsymbol{\Phi}(q_{n-1}) + \hat{c}_{n,0}^{\text{sep}} \mathbf{D}\boldsymbol{\Phi}(q_n) + \hat{c}_{n,+}^{\text{sep}} \mathbf{D}\boldsymbol{\Phi}(q_{n+1})) \cdot \boldsymbol{v}_n \end{bmatrix} \quad (3.57)$$

with

$$\hat{c}_{n,-}^{\text{sep}} = \frac{h_n}{h_{n-1}(h_{n-1} + h_n)}, \quad \hat{c}_{n,0}^{\text{sep}} = \frac{1}{h_n} - \frac{1}{h_{n-1}}, \quad \hat{c}_{n,+}^{\text{sep}} = \frac{-h_{n-1}}{h_n(h_{n-1} + h_n)}.$$

We will call Lagrange multipliers that were calculated by (3.57) ‘‘separately calculated Lagrange multipliers’’. It can be easily shown that

$$\hat{c}_{n,-}^{\text{sep}} \boldsymbol{\chi}(t_{n-1}) + \hat{c}_{n,0}^{\text{sep}} \boldsymbol{\chi}(t_n) + \hat{c}_{n,+}^{\text{sep}} \boldsymbol{\chi}(t_{n+1}) = -\boldsymbol{\chi}'(t_n) + \mathcal{O}(h_{n-1}^2) + \mathcal{O}(h_n^2) \quad (3.58)$$

for three times differentiable functions $\boldsymbol{\chi}: \mathbb{R} \rightarrow \mathbb{R}^n$ by Taylor’s theorem. Using (3.52), applying (3.58) with $\boldsymbol{\chi}(t) = \mathbf{D}\boldsymbol{\Phi}(q(t)) \cdot \boldsymbol{v}(t_n)$ in (3.57), and finally taking the difference of (2.34) at $t = t_n$ we end up with

$$\begin{bmatrix} \mathbf{M} & \mathbf{D}\boldsymbol{\Phi}^\top(q(t_n)) \\ \mathbf{D}\boldsymbol{\Phi}^\top(q(t_n)) & \mathbf{0} \end{bmatrix} \cdot \begin{bmatrix} \dot{\boldsymbol{v}}(t_n) - \dot{\boldsymbol{v}}_n^{\text{sep}} \\ \boldsymbol{\lambda}(t_n) - \boldsymbol{\lambda}_n^{\text{sep}} \end{bmatrix} = \begin{bmatrix} \mathcal{O}(h_{\max}^2) \\ \mathcal{O}(h_{\max}^2) \end{bmatrix}$$

Since the matrix on the left is invertible, see (2.35), we get the convergence result for the separately calculated approximations $\boldsymbol{\lambda}_n^{\text{sep}}$ and $\dot{\boldsymbol{v}}_n^{\text{sep}}$:

$$\boldsymbol{\lambda}_n^{\text{sep}} = \boldsymbol{\lambda}(t_n) + \mathcal{O}(h_{\max}^2), \quad \dot{\boldsymbol{v}}_n^{\text{sep}} = \dot{\boldsymbol{v}}(t_n) + \mathcal{O}(h_{\max}^2). \quad (3.59)$$

3.3. Implementation Details

Now we consider a time step of RATTLie from t_n to t_{n+1} with step size h_n , configuration q_n and derivative vector \mathbf{v}_n . First, we can solve (3.1a), (3.1b), (3.1c) with respect to $\boldsymbol{\lambda}_n^+$ and $\mathbf{v}_{n+1/2}$. This can be done by inserting (3.1a) into (3.1c) and solving the equivalent nonlinear system

$$\mathbf{0} = \boldsymbol{\Psi}_1(\boldsymbol{\xi}_1),$$

where

$$\boldsymbol{\xi}_1 = \begin{bmatrix} \mathbf{v}_{n+1/2} \\ h_n \boldsymbol{\lambda}_n^+ \end{bmatrix},$$

$$\boldsymbol{\Psi}_1(\boldsymbol{\xi}_1) = \begin{bmatrix} \mathbf{T}^{-\top}(-h_n \mathbf{v}_{n+1/2}) \cdot \mathbf{M} \cdot \mathbf{v}_{n+1/2} + \left(-\frac{h_n}{2} \mathbf{f}(t_n, q_n, \mathbf{v}_n) + \frac{1}{2} \mathbf{D}\boldsymbol{\Phi}^\top(q_n) \cdot (h_n \boldsymbol{\lambda}_n^+) - \mathbf{M} \cdot \mathbf{v}_n\right) \\ \boldsymbol{\Phi}(q_n \circ \widehat{\text{exp}}(h_n \mathbf{v}_{n+1/2})) / (2h_n) \end{bmatrix}$$

via the Newton-Raphson algorithm. Notice that the Lagrange multiplier $\boldsymbol{\lambda}_n^+$ is scaled with h_n and the constraints with $1/(2h_n)$, see e. g. [14, 61], such that the condition number of the Jacobian

$$\boldsymbol{\Psi}'_1(\boldsymbol{\xi}_1) = \frac{\text{d}}{\text{d}\boldsymbol{\xi}_1} \boldsymbol{\Psi}_1(\boldsymbol{\xi}_1) = \begin{bmatrix} \mathbf{M} + \mathcal{O}(h_n) & \frac{1}{2} \mathbf{D}\boldsymbol{\Phi}^\top(q_n) \\ \frac{1}{2} \mathbf{D}\boldsymbol{\Phi}(q_n \circ \widehat{\text{exp}}(h_n \mathbf{v}_{n+1/2})) \cdot \mathbf{T}(h_n \mathbf{v}_{n+1/2}) & \mathbf{0} \end{bmatrix}$$

of $\boldsymbol{\Psi}_1$ remains bounded for $h_n \rightarrow 0$:

$$\lim_{h_n \rightarrow 0} \boldsymbol{\Psi}'_1(\boldsymbol{\xi}_1) = \begin{bmatrix} \mathbf{M} & \frac{1}{2} \mathbf{D}\boldsymbol{\Phi}^\top(q_n) \\ \frac{1}{2} \mathbf{D}\boldsymbol{\Phi}(q_n) & \mathbf{0} \end{bmatrix}$$

has full rank, see (2.35), and therefore

$$\lim_{h_n \rightarrow 0} \kappa(\boldsymbol{\Psi}'_1(\boldsymbol{\xi}_1)) = \lim_{h_n \rightarrow 0} \left(\|\boldsymbol{\Psi}'_1(\boldsymbol{\xi}_1)\| \left\| (\boldsymbol{\Psi}'_1(\boldsymbol{\xi}_1))^{-1} \right\| \right) < \infty.$$

The Newton-Raphson iteration can be started with the initial guess $\boldsymbol{\xi}_1^{(0)} = [\mathbf{v}_n^\top, h_n (\boldsymbol{\lambda}_n^-)^\top]^\top$, if $\boldsymbol{\lambda}_n^-$ is available. If no approximation to the Lagrange multiplier is available, $\boldsymbol{\xi}_1^{(0)} = [\mathbf{v}_n^\top, \mathbf{0}^\top]^\top$ has to be used. Often, it is sufficient to use a simplified inexact Newton-Raphson method with an approximation to the Jacobian

$$\mathbf{J} = \begin{bmatrix} \mathbf{M} & \frac{1}{2} \mathbf{D}\boldsymbol{\Phi}^\top(q_n) \\ \frac{1}{2} \mathbf{D}\boldsymbol{\Phi}(q_n \circ \widehat{\text{exp}}(h_n \mathbf{v}_n)) \cdot \mathbf{T}(h_n \mathbf{v}_n) & \mathbf{0} \end{bmatrix} \approx \boldsymbol{\Psi}'_1(\boldsymbol{\xi}_1^{(0)}).$$

In order to check for convergence in an affinely invariant manner, we check the size of the increments in $\boldsymbol{\xi}_1$ rather than the size of the residuals $\boldsymbol{\Psi}_1(\mathbf{x}_1)$, see [25].

In the next step, we can calculate q_{n+1} by inserting $\mathbf{v}_{n+1/2}$ into (3.1a).

Now, we will solve (3.1d), (3.1e) with respect to \mathbf{v}_{n+1} and $\boldsymbol{\lambda}_{n+1}^-$ by applying the Newton-Raphson algorithm to the equivalent system

$$\mathbf{0} = \boldsymbol{\Psi}_2(\boldsymbol{\xi}_2),$$

where

$$\boldsymbol{\xi}_2 = \begin{bmatrix} \mathbf{v}_{n+1} \\ h_n \boldsymbol{\lambda}_{n+1}^- \end{bmatrix},$$

$$\boldsymbol{\Psi}_2(\boldsymbol{\xi}_2) = \begin{bmatrix} \mathbf{T}^{-\top} (h_n \mathbf{v}_{n+1/2}) \cdot \mathbf{M} \cdot \mathbf{v}_{n+1/2} + \left(\frac{h_n}{2} \mathbf{f}(t_{n+1}, q_{n+1}, \mathbf{v}_{n+1}) \right. \\ \left. - \frac{1}{2} \mathbf{D}\boldsymbol{\Phi}^\top(q_{n+1}) \cdot (h_n \boldsymbol{\lambda}_{n+1}^-) - \mathbf{M} \cdot \mathbf{v}_{n+1} \right) \\ \left. - \frac{1}{2} \mathbf{D}\boldsymbol{\Phi}(q_{n+1}) \cdot \mathbf{v}_{n+1} \right].$$

We have scaled the Lagrange multiplier with h_n and the hidden constraint with $-1/2$ such that the Jacobian

$$\boldsymbol{\Psi}'_2(\boldsymbol{\xi}_2) = \frac{d}{d\boldsymbol{\xi}_2} \boldsymbol{\Psi}_2(\boldsymbol{\xi}_2) = \begin{bmatrix} \frac{h_n}{2} d\mathbf{v}_{n+1} \mathbf{f}(t_{n+1}, q_{n+1}, \mathbf{v}_{n+1}) - \mathbf{M} & -\frac{1}{2} \mathbf{D}\boldsymbol{\Phi}^\top(q_{n+1}) \\ -\frac{1}{2} \mathbf{D}\boldsymbol{\Phi}(q_{n+1}) & \mathbf{0} \end{bmatrix}$$

of $\boldsymbol{\Psi}_2$ is symmetric and has bounded condition number for $h_n \rightarrow 0$:

$$\lim_{h_n \rightarrow 0} \boldsymbol{\Psi}'_2(\boldsymbol{\xi}_2) = - \begin{bmatrix} \mathbf{M} & \frac{1}{2} \mathbf{D}\boldsymbol{\Phi}^\top(q_{n+1}) \\ \frac{1}{2} \mathbf{D}\boldsymbol{\Phi}(q_{n+1}) & \mathbf{0} \end{bmatrix},$$

$$\lim_{h_n \rightarrow 0} \kappa(\boldsymbol{\Psi}'_2(\boldsymbol{\xi}_2)) = \lim_{h_n \rightarrow 0} \left(\|\boldsymbol{\Psi}'_2(\boldsymbol{\xi}_2)\| \|(\boldsymbol{\Psi}'_2(\boldsymbol{\xi}_2))^{-1}\| \right) < \infty.$$

The starting values can be selected to be $\boldsymbol{\xi}_2^{(0)} = [\mathbf{v}_{n+1/2}^\top, h_n (\boldsymbol{\lambda}_n^+)^\top]^\top$. Note that if the forces \mathbf{f} do not depend on the derivative vectors \mathbf{v} , this system is linear and can be solved by exactly one step of the Newton-Raphson algorithm. Otherwise, using a simplified (inexact) Newton-Raphson method is easy to implement and computationally efficient.

We have summarized the implementation of RATTLie in algorithm 1.

In order to calculate approximations to the Lagrange multipliers $\boldsymbol{\lambda}(t_n)$, we need at least two steps of RATTLie; $t_{n-1} \rightarrow t_n$ and $t_n \rightarrow t_{n+1}$. To calculate the interpolated Lagrange multipliers from the $\boldsymbol{\lambda}_m^+$ and $\boldsymbol{\lambda}_{m+1}^-$ with $m = n-1, n$, we can use (3.53) and (3.55). We could also discard all the Lagrange multipliers calculated by RATTLie and use (3.57) in order to separately calculate $\boldsymbol{\lambda}_n^{\text{sep}}$ purely on the basis of $q_{n-1}, q_n, q_{n+1}, \mathbf{v}_n$. The benefit is a better behavior for small time steps, see section 5.3, at the additional cost of the solution of one linear system. We have summarized the calculation of both variants in the algorithms 2 and 3.

The implementation of the nonholonomic version of RATTLie is very similar and can be found in compact version in algorithm 5 as well as algorithms 2 and 3 concerning the Lagrange multipliers.

Algorithm 1 One time step of RATTLie $t_0 \rightarrow t_1$

Require: mass matrix \mathbf{M} , generalized force function \mathbf{f} , its derivative with respect to the velocity $d_v \mathbf{f}$, constraint function Φ , its Lie group derivative $\mathbf{D}\Phi$, Lie group multiplication \circ , Lie group exponential $\widetilde{\text{exp}}$, tangent operator function \mathbf{T} , the function of the transposed and inversed tangent operator $\mathbf{T}^{-\top}$, maximum number of Newton-Raphson iterations maxit , absolute and relative tolerances for the Newton-Raphson method atol and rtol

```
1: procedure RATTLIE_STEP( $t_0, q_0, \mathbf{v}_0, t_1$ ; optional:  $\lambda_0^-$ )
2:    $h_0 \leftarrow t_1 - t_0$  ▷ Calculate step size
3:    $\mathbf{v}_{1/2} \leftarrow \mathbf{v}_0, q_1 \leftarrow q_0 \circ \widetilde{\text{exp}}(h_0 \mathbf{v}_{1/2})$  ▷ Initial guesses
4:    $\lambda_0^+ \leftarrow \lambda_0^-$  or  $\lambda_0^+ \leftarrow \mathbf{0}$  depending on whether  $\lambda_0^-$  was given
5:    $E \leftarrow \infty, i \leftarrow 0, \mathbf{J} \leftarrow \begin{bmatrix} \mathbf{M} & \frac{1}{2} \mathbf{D}\Phi^\top(q_0) \\ \frac{1}{2} \mathbf{D}\Phi(q_1) \cdot \mathbf{T}(h_0 \mathbf{v}_0) & \mathbf{0} \end{bmatrix}$ 
6:   while  $E > 1$  do ▷ Start first Newton-Raphson iteration
7:     if  $i \geq \text{maxit}$  then error: Newton iteration did not converge end if
8:      $\Psi \leftarrow \begin{bmatrix} \mathbf{T}^{-\top}(-h_0 \mathbf{v}_{1/2}) \cdot \mathbf{M} \cdot \mathbf{v}_{1/2} - \frac{h_0}{2} (\mathbf{f}(t_0, q_0, \mathbf{v}_0) - \mathbf{D}\Phi^\top(q_0) \cdot \lambda_0^+) - \mathbf{M} \cdot \mathbf{v}_0 \\ \Phi(q_1)/(2h_0) \end{bmatrix}$ 
9:     solve linear system  $\mathbf{J} \cdot \begin{bmatrix} \Delta \mathbf{v} \\ \Delta \lambda \end{bmatrix} = -\Psi$ 
10:     $E \leftarrow \left\| \begin{bmatrix} \Delta \mathbf{v} \\ \Delta \lambda \end{bmatrix} \right\| / \left( \text{atol} + \text{rtol} \text{abs} \begin{bmatrix} \mathbf{v}_{1/2} \\ h_0 \lambda_0^+ \end{bmatrix} \right)$  ▷ To be read element-wise
11:     $\mathbf{v}_{1/2} \leftarrow \mathbf{v}_{1/2} + \Delta \mathbf{v}, \lambda_0^+ \leftarrow \lambda_0^+ + \Delta \lambda / h_0, q_1 \leftarrow q_0 \circ \widetilde{\text{exp}}(h_0 \mathbf{v}_{1/2})$ 
12:  end while
13:   $\mathbf{v}_1 \leftarrow \mathbf{v}_{1/2}, \lambda_1^- \leftarrow \lambda_0^+$  ▷ Initial guesses
14:   $E \leftarrow \infty, i \leftarrow 0, \mathbf{J} \leftarrow \begin{bmatrix} \frac{h_0}{2} d_v \mathbf{f}(t_1, q_1, \mathbf{v}_1) - \mathbf{M} & -\frac{1}{2} \mathbf{D}\Phi^\top(q_1) \\ -\frac{1}{2} \mathbf{D}\Phi(q_1) & \mathbf{0} \end{bmatrix}$ 
15:  while  $E > 1$  do ▷ Start second Newton-Raphson iteration
16:    if  $i \geq \text{maxit}$  then error: Newton iteration did not converge end if
17:     $\Psi \leftarrow \begin{bmatrix} \mathbf{T}^{-\top}(h_0 \mathbf{v}_{1/2}) \cdot \mathbf{M} \cdot \mathbf{v}_{1/2} + \frac{h_0}{2} (\mathbf{f}(t_1, q_1, \mathbf{v}_1) - \mathbf{D}\Phi^\top(q_1) \cdot \lambda_1^-) - \mathbf{M} \cdot \mathbf{v}_1 \\ -\mathbf{D}\Phi(q_1) \cdot \mathbf{v}_1 / 2 \end{bmatrix}$ 
18:    solve linear system  $\mathbf{J} \cdot \begin{bmatrix} \Delta \mathbf{v} \\ \Delta \lambda \end{bmatrix} = -\Psi$ 
19:     $E \leftarrow \left\| \begin{bmatrix} \Delta \mathbf{v} \\ \Delta \lambda \end{bmatrix} \right\| / \left( \text{atol} + \text{rtol} \text{abs} \begin{bmatrix} \mathbf{v}_1 \\ h_0 \lambda_1^- \end{bmatrix} \right)$  ▷ To be read element-wise
20:     $\mathbf{v}_1 \leftarrow \mathbf{v}_1 + \Delta \mathbf{v}, \lambda_1^- \leftarrow \lambda_1^- + \Delta \lambda / h_0$ 
21:  end while
22:  return  $q_1, \mathbf{v}_1, \lambda_0^+, \lambda_1^-$ 
23: end procedure
```

Algorithm 2 Calculation of Lagrange multipliers for the (nonholonomic) RATTLie by using the λ^\pm quantities obtained by two subsequent steps of the (nonholonomic) RATTLie

```

1: procedure RATTLIE_LAGRANGE( $t_0, t_1, t_2, \lambda_0^+, \lambda_1^-, \lambda_1^+, \lambda_2^-$ )
2:    $h_0 \leftarrow t_1 - t_0, h_1 \leftarrow t_2 - t_1$  ▷ Calculate step sizes
3:    $\lambda_{1/2} \leftarrow \frac{1}{2}(\lambda_0^+ + \lambda_1^-)$  ▷ Calculate Lagrange multipliers at midpoints
4:    $\lambda_{3/2} \leftarrow \frac{1}{2}(\lambda_1^+ + \lambda_2^-)$ 
5:    $\lambda_1 \leftarrow \frac{h_1 \lambda_{1/2} + h_0 \lambda_{3/2}}{h_0 + h_1}$  ▷ Interpolate
6:   return  $\lambda_1$ 
7: end procedure

```

Algorithm 3 Separately calculated Lagrange multipliers and acceleration using two subsequent time steps

```

1: procedure RATTLIE_LAGRANGE_SEP( $t_0, t_1, t_2, q_0, q_1, q_2, \mathbf{v}_1$ )
2:    $h_0 \leftarrow t_1 - t_0, h_1 \leftarrow t_2 - t_1$  ▷ Calculate step sizes
3:    $c_- \leftarrow \frac{h_1}{h_0(h_0 + h_1)}, c_0 \leftarrow \frac{1}{h_1} - \frac{1}{h_0}, c_+ \leftarrow \frac{-h_0}{h_1(h_0 + h_1)}$ 
4:   solve  $\begin{bmatrix} \mathbf{M} & \mathbf{D}\Phi^\top(q_1) \\ \mathbf{D}\Phi(q_1) & \mathbf{0} \end{bmatrix} \cdot \begin{bmatrix} \dot{\mathbf{v}}_1 \\ \lambda_1 \end{bmatrix} = \begin{bmatrix} \hat{\mathbf{v}}_1^\top \cdot \mathbf{M} \cdot \mathbf{v}_1 + \mathbf{f}(t_1, q_1, \mathbf{v}_1) \\ (c_- \mathbf{D}\Phi(q_0) + c_0 \mathbf{D}\Phi(q_1) + c_+ \mathbf{D}\Phi(q_2)) \cdot \mathbf{v}_1 \end{bmatrix}$ 
5:   return  $\lambda_1, \dot{\mathbf{v}}_1$ 
6: end procedure

```

Algorithm 4 Separately calculated Lagrange multipliers and acceleration for nonholonomic systems using two subsequent time steps

```

1: procedure RATTLIE_NONHOL_LAGRANGE_SEP( $t_0, t_1, t_2, q_0, q_1, q_2, \mathbf{v}_1$ )
2:    $h_0 \leftarrow t_1 - t_0, h_1 \leftarrow t_2 - t_1$  ▷ Calculate step sizes
3:    $c_- \leftarrow \frac{h_1}{h_0(h_0 + h_1)}, c_0 \leftarrow \frac{1}{h_1} - \frac{1}{h_0}, c_+ \leftarrow \frac{-h_0}{h_1(h_0 + h_1)}$ 
4:   solve the linear system

```

$$\begin{bmatrix} \mathbf{M} & \mathbf{D}\Phi^\top(q_1) & \mathbf{B}^\top(q_1) \\ \mathbf{D}\Phi(q_1) & \mathbf{0} & \mathbf{0} \\ \mathbf{B}(q_1) & \mathbf{0} & \mathbf{0} \end{bmatrix} \cdot \begin{bmatrix} \dot{\mathbf{v}}_1 \\ \lambda_1 \\ \mu_1 \end{bmatrix} = \begin{bmatrix} \hat{\mathbf{v}}_1^\top \cdot \mathbf{M} \cdot \mathbf{v}_1 + \mathbf{f}(t_1, q_1, \mathbf{v}_1) \\ (c_- \mathbf{D}\Phi(q_0) + c_0 \mathbf{D}\Phi(q_1) + c_+ \mathbf{D}\Phi(q_2)) \cdot \mathbf{v}_1 \\ (c_- \mathbf{B}(q_0) + c_0 \mathbf{B}(q_1) + c_+ \mathbf{B}(q_2)) \cdot \mathbf{v}_1 \end{bmatrix}$$

```

5:   return  $\lambda_1, \mu_1, \dot{\mathbf{v}}_1$ 
6: end procedure

```

Algorithm 5 One time step of nonholonomic RATTLie $t_0 \rightarrow t_1$

Require: Requirements of algorithm 1 as well as the matrix function of the linear nonholonomic constraints \mathbf{B}

```

1: procedure RATTLIE_NONHOL_STEP( $t_0, q_0, \mathbf{v}_0, \boldsymbol{\mu}_0, t_1$ ; optional:  $\boldsymbol{\lambda}_0^-$ )
2:    $h_0 \leftarrow t_1 - t_0$  ▷ Calculate step size
3:    $\mathbf{v}_{1/2} \leftarrow \mathbf{v}_0, q_1 \leftarrow q_0 \circ \widetilde{\text{exp}}(h_0 \mathbf{v}_{1/2})$  ▷ Initial guesses
4:    $\boldsymbol{\lambda}_0^+ \leftarrow \boldsymbol{\lambda}_0^-$  or  $\boldsymbol{\lambda}_0^+ \leftarrow \mathbf{0}$  depending on whether  $\boldsymbol{\lambda}_0^-$  was given
5:    $E \leftarrow \infty, i \leftarrow 0, \mathbf{J} \leftarrow \begin{bmatrix} \mathbf{M} & \frac{1}{2} \mathbf{D}\boldsymbol{\Phi}^\top(q_0) \\ \frac{1}{2} \mathbf{D}\boldsymbol{\Phi}(q_1) \cdot \mathbf{T}(h_0 \mathbf{v}_0) & \mathbf{0} \end{bmatrix}$ 
6:   while  $E > 1$  do ▷ Start first Newton-Raphson iteration
7:     if  $i \geq \text{maxit}$  then error: Newton iteration did not converge end if
8:      $\boldsymbol{\Psi} \leftarrow \begin{bmatrix} \mathbf{T}^{-\top}(-h_0 \mathbf{v}_{1/2}) \cdot \mathbf{M} \cdot \mathbf{v}_{1/2} - \frac{h_0}{2} (\mathbf{f}(t_0, q_0, \mathbf{v}_0) - \mathbf{D}\boldsymbol{\Phi}^\top(q_0) \cdot \boldsymbol{\lambda}_0^+ \\ - \mathbf{B}^\top(q_0) \cdot \boldsymbol{\mu}_0) - \mathbf{M} \cdot \mathbf{v}_0 \\ \boldsymbol{\Phi}(q_1)/(2h_0) \end{bmatrix}$ 
9:     solve linear system  $\mathbf{J} \cdot \begin{bmatrix} \Delta \mathbf{v} \\ \Delta \boldsymbol{\lambda} \end{bmatrix} = -\boldsymbol{\Psi}$ 
10:     $E \leftarrow \left\| \begin{bmatrix} \Delta \mathbf{v} \\ \Delta \boldsymbol{\lambda} \end{bmatrix} \right\| / \left( \text{atol} + \text{rtol} \text{abs} \begin{bmatrix} \mathbf{v}_{1/2} \\ h_0 \boldsymbol{\lambda}_0^+ \end{bmatrix} \right)$  ▷ To be read element-wise
11:     $\mathbf{v}_{1/2} \leftarrow \mathbf{v}_{1/2} + \Delta \mathbf{v}, \boldsymbol{\lambda}_0^+ \leftarrow \boldsymbol{\lambda}_0^+ + \Delta \boldsymbol{\lambda}/h_0, q_1 \leftarrow q_0 \circ \widetilde{\text{exp}}(h_0 \mathbf{v}_{1/2})$ 
12:  end while
13:   $\mathbf{v}_1 \leftarrow \mathbf{v}_{1/2}, \boldsymbol{\lambda}_1^- \leftarrow \boldsymbol{\lambda}_0^+, \boldsymbol{\mu}_1 \leftarrow \boldsymbol{\mu}_0$  ▷ Initial guesses
14:   $E \leftarrow \infty, i \leftarrow 0, \mathbf{J} \leftarrow \begin{bmatrix} \frac{h_0}{2} \text{d}_v \mathbf{f}(t_1, q_1, \mathbf{v}_1) - \mathbf{M} & -\frac{1}{2} \mathbf{D}\boldsymbol{\Phi}^\top(q_1) & -\frac{1}{2} \mathbf{B}^\top(q_1) \\ -\frac{1}{2} \mathbf{D}\boldsymbol{\Phi}(q_1) & \mathbf{0} & \mathbf{0} \\ -\frac{1}{2} \mathbf{B}(q_1) & \mathbf{0} & \mathbf{0} \end{bmatrix}$ 
15:  while  $E > 1$  do ▷ Start second Newton-Raphson iteration
16:    if  $i \geq \text{maxit}$  then error: Newton iteration did not converge end if
17:     $\boldsymbol{\Psi} \leftarrow \begin{bmatrix} \mathbf{T}^{-\top}(h_0 \mathbf{v}_{1/2}) \cdot \mathbf{M} \cdot \mathbf{v}_{1/2} + \frac{h_0}{2} (\mathbf{f}(t_1, q_1, \mathbf{v}_1) - \mathbf{D}\boldsymbol{\Phi}^\top(q_1) \cdot \boldsymbol{\lambda}_1^- \\ - \mathbf{B}^\top(q_1) \cdot \boldsymbol{\mu}_1) - \mathbf{M} \cdot \mathbf{v}_1 \\ - \mathbf{D}\boldsymbol{\Phi}(q_1) \cdot \mathbf{v}_{1/2} \\ - \mathbf{B}(q_1) \cdot \mathbf{v}_{1/2} \end{bmatrix}$ 
18:    solve linear system  $\mathbf{J} \cdot \begin{bmatrix} \Delta \mathbf{v} \\ \Delta \boldsymbol{\lambda} \\ \Delta \boldsymbol{\mu} \end{bmatrix} = -\boldsymbol{\Psi}$ 
19:     $E \leftarrow \left\| \begin{bmatrix} \Delta \mathbf{v} \\ \Delta \boldsymbol{\lambda} \\ \Delta \boldsymbol{\mu} \end{bmatrix} \right\| / \left( \text{atol} + \text{rtol} \text{abs} \begin{bmatrix} \mathbf{v}_1 \\ h_0 \boldsymbol{\lambda}_1^- \\ h_0 \boldsymbol{\mu}_1 \end{bmatrix} \right)$  ▷ To be read element-wise
20:     $\mathbf{v}_1 \leftarrow \mathbf{v}_1 + \Delta \mathbf{v}, \boldsymbol{\lambda}_1^- \leftarrow \boldsymbol{\lambda}_1^- + \Delta \boldsymbol{\lambda}/h_0, \boldsymbol{\mu}_1 \leftarrow \boldsymbol{\mu}_1 + \Delta \boldsymbol{\mu}/h_0$ 
21:  end while
22:  return  $q_1, \mathbf{v}_1, \boldsymbol{\lambda}_0^+, \boldsymbol{\lambda}_1^-, \boldsymbol{\mu}_1$ 
23: end procedure

```

4. A Flexible Cosserat Beam Model and Its Discretization in Space

In this section, the main focus lies on the dynamics of a geometrically exact Cosserat beam model. Beam models can be used to simulate slender real-world objects that are significantly larger in one dimension than in the other two dimensions. The dynamics of Cosserat beam models has been an active field of research in recent times, see e. g. [11, 44, 55, 59, 74]. A Cosserat beam model does not consider the beam an arbitrary flexible body but rather considers it to consist of infinitesimal cross sections that are assumed to stay rigid.

Most of the research concerning Cosserat beams that we are going to consider here is based on the work of Simo and Vu-Quoc [71–73], see also the papers of G eradin and Cardona [32, 33] as well as [47]. These earlier studies had relied on finite element discretization of the beam model. In contrast, Leyendecker, Leitz, Demoures and others have focused on spatial discretization using the toolbox of variational integrators [23, 24, 55, 57, 58]. Simultaneously, research by Lang and Linn [51, 53, 59, 60] has considered a spatial discretization using finite differences. The spatial discretization we will present is inspired by the latter, although it will additionally employ the ansatz of variational integration [63]. We will also make use of the Lie group structure of rotation and rigid body motion similar to the research of Sonnevile and Br uls on geometrically exact beams [18, 74–76]. According to their research, locking can occur [76] if the model is formulated in such a way that position and orientation of the rigid cross sections are considered separately. Locking is a phenomenon where the bending stiffness of the discretized beam is much higher than the stiffness of the continuous beam. To avoid this problem, a semi-direct product structure of orientation and position can be used either in the form of $SE(3)$, see e. g. [23, 75, 76], or in the more computationally efficient form of $S^3 \times \mathbb{R}^3$, see [42, 44, 55], which will be used in this thesis.

The name ‘‘Cosserat’’ beam model refers to Eug ene and Fran ois Cosserat, who published their seminal book *Th eorie des corps d eformables* [22] as early as 1909. They had used a new approach in continuum mechanics where each material point has an orientation in addition to a position. The latter had already been used in classical continuum mechanics. In the Cosserat beam model, this is applied to the cross sections of the beam by essentially averaging over the material points of the cross sections [71].

This section is structured in the following way: Firstly, in section 4.1, we will consider rigid bodies since they constitute the foundation to treat the rigid cross sections of the Cosserat beam model. Secondly, in section 4.2, the beam model will be considered. Here, we introduce the continuous model in section 4.2.1 and subsequently show the spatial discretization in section 4.2.2.

Additionally, in appendix D, we will show a way to generalize the one-dimensional Cosserat beam model to two dimensions in order to obtain a micropolar Cosserat shell model.

4.1. Rigid Bodies

In this section we will consider a rigid body $Q \subseteq \mathbb{R}^3$. The theory of the dynamics of rigid bodies is well-known, see e. g. the textbook by Schiehlen and Eberhard [69]. We will use unit quaternions (Euler parameters) to describe orientation, a method that is also well-established, see e. g. [12] and the references therein. However, we will not only apply the concept of derivative vectors, see section 2.2, but also use the semi-direct product $\mathbb{S}^3 \ltimes \mathbb{R}^3$ as the configuration space. A semi-direct product in the form of $SE(3)$ has been used before, see e. g. [17] and in the form of dual quaternions it has been employed in e. g. [48].

Throughout this section, the configuration of the rigid body Q is described by the state variable $q(t) = (p(t), \mathbf{x}(t))$ with $p(t) \in \mathbb{S}^3$ and $\mathbf{x}(t) \in \mathbb{R}^3$ at each time instance t . The vector $\mathbf{x}(t) \in \mathbb{R}^3$ represents the position of the center of mass with respect to the inertial frame and the canonical basis vectors $\mathbf{e}_1, \mathbf{e}_2, \mathbf{e}_3$ with respect to the body-fixed frame, described by $p(t) \in \mathbb{S}^3$, point along the principal axes of the rigid body. This means that $p(t) \in \mathbb{S}^3$ is always given in such a way that the vectors

$$p(t)^{-1} \triangleright \mathbf{e}_1, p(t)^{-1} \triangleright \mathbf{e}_2, p(t)^{-1} \triangleright \mathbf{e}_3$$

with respect to the inertial frame point along the principal axes of the rigid body. We will use the Lie group structure $\mathbb{S}^3 \ltimes \mathbb{R}^3$, see section 2.3, for the configuration space of the rigid body. This will allow us to apply a Lie group time integrator, such as RATTLie from section 3, the Lie group generalized- α method, see e. g. [18], or the BLieDF method [84]. Like in section 2.2, we will use the derivative vectors in order to describe derivatives with respect to time: With the derivative vector $\mathbf{v}(t) = [\boldsymbol{\Omega}^\top(t), \mathbf{U}^\top(t)]^\top$ we get the kinematic equation (2.17), which reads in components

$$(\dot{p}(t), \dot{\mathbf{x}}(t)) = \text{d}L_{(p(t), \mathbf{x}(t))} \left[\widetilde{\begin{matrix} \boldsymbol{\Omega}(t) \\ \mathbf{U}(t) \end{matrix}} \right] = \left(\frac{1}{2} p(t) * \begin{bmatrix} 0 \\ \boldsymbol{\Omega}(t) \end{bmatrix}, p(t) \triangleright \mathbf{U}(t) \right). \quad (4.1)$$

Here, for $i = 1, 2, 3$, the i -th component of $\boldsymbol{\Omega}(t)$ describes the angular velocity of the rigid body around its i -th principal axis and the i -th component of $\mathbf{U}(t)$ describes the velocity of the rigid body along its i -th principal axis.

Let us now consider $Q \subseteq \mathbb{R}^3$ to be the set of points of the rigid body for the configuration $([1, 0, 0, 0]^\top, \mathbf{0})$, i. e. its center of mass is in the origin and the canonical unit vectors point along the principal axes of the body. Let $\rho: Q \rightarrow [0, \infty)$ be the density of the body at each point. Then the mass $m > 0$ of the rigid body and its inertia tensor $\mathbf{J} \in \mathbb{R}^{3 \times 3}$ are given by

$$\begin{aligned} m &= \int_Q \rho(\boldsymbol{\xi}) \, \text{d}\boldsymbol{\xi}, \\ \mathbf{J} &= \int_Q \rho(\boldsymbol{\xi}) (\mathbf{I}_3 \boldsymbol{\xi}^\top \cdot \boldsymbol{\xi} - \boldsymbol{\xi} \cdot \boldsymbol{\xi}^\top) \, \text{d}\boldsymbol{\xi} \\ &= \text{diag} \left(\int_Q \rho(\boldsymbol{\xi}) (\xi_2^2 + \xi_3^2) \, \text{d}\boldsymbol{\xi}, \int_Q \rho(\boldsymbol{\xi}) (\xi_1^2 + \xi_3^2) \, \text{d}\boldsymbol{\xi}, \int_Q \rho(\boldsymbol{\xi}) (\xi_1^2 + \xi_2^2) \, \text{d}\boldsymbol{\xi} \right), \end{aligned} \quad (4.2)$$

where $\boldsymbol{\xi} = [\xi_1, \xi_2, \xi_3]^\top$, see [69, Section 3.2.2]. The kinetic energy is given by the sum of the translational and rotational kinetic energies

$$\mathcal{T}(\mathbf{v}(t)) = \frac{1}{2} \boldsymbol{\Omega}^\top(t) \cdot \mathbf{J} \cdot \boldsymbol{\Omega}(t) + \frac{m}{2} \mathbf{U}^\top(t) \cdot \mathbf{U}(t) = \frac{1}{2} \mathbf{v}^\top(t) \cdot \mathbf{M} \cdot \mathbf{v}(t),$$

since it does not depend on the frame in which it is considered. Here

$$\mathbf{M} = \text{blkdiag}(\mathbf{J}, m\mathbf{I}_3) \in \mathbb{R}^{6 \times 6}$$

denotes the mass matrix, see section 2.5. We can see that the mass matrix is constant and does not depend on the configuration $q(t)$.

Let the rigid body have a potential energy $\mathcal{U}(q(t))$ and be subject to holonomic constraints $\boldsymbol{o} = \boldsymbol{\Phi}(q(t))$. Then the equations of motion take the form (2.31), see remark 2.35. If there are some additional external moments and forces applied, refer to remark 2.36. More specifically, we have

$$\mathcal{F}^\top(t, q(t), \mathbf{v}(t)) = \begin{bmatrix} \mathbf{M}^{\text{ex}}(t, q(t), \mathbf{v}(t)) \\ \mathbf{F}^{\text{ex}}(t, q(t), \mathbf{v}(t)) \end{bmatrix},$$

where $\mathbf{M}^{\text{ex}}(t, q(t), \mathbf{v}(t)) \in \mathbb{R}^3$ and $\mathbf{F}^{\text{ex}}(t, q(t), \mathbf{v}(t)) \in \mathbb{R}^3$ are external moments and forces with respect to the body-fixed frame applied to the center of mass of the rigid body. If we want to apply moments of force and forces $\mathbf{m}^{\text{ex}}(t, q(t), \mathbf{v}(t)) \in \mathbb{R}^3$ and $\mathbf{f}^{\text{ex}}(t, q(t), \mathbf{v}(t)) \in \mathbb{R}^3$ that are given with respect to the inertial frame, we can use

$$\begin{aligned} \mathbf{M}^{\text{ex}}(t, q(t), \mathbf{v}(t)) &= (p(t))^{-1} \triangleright \mathbf{m}^{\text{ex}}(t, q(t), \mathbf{v}(t)), \\ \mathbf{F}^{\text{ex}}(t, q(t), \mathbf{v}(t)) &= (p(t))^{-1} \triangleright \mathbf{f}^{\text{ex}}(t, q(t), \mathbf{v}(t)). \end{aligned}$$

Since we use the Lie group $\mathbb{S}^3 \times \mathbb{R}^3$, the Coriolis force term $\widehat{\mathbf{v}(t)}^\top \cdot \mathbf{M} \cdot \mathbf{v}(t)$ is given by [17]

$$\widehat{\mathbf{v}(t)} \cdot \mathbf{M} \cdot \mathbf{v}(t) = \begin{bmatrix} -\boldsymbol{\Omega}(t) \times (\mathbf{J} \cdot \boldsymbol{\Omega}(t)) \\ -m\boldsymbol{\Omega}(t) \times \mathbf{U}(t) \end{bmatrix},$$

see section 2.3.

Remark 4.1: *Gravitational field.*

If a rigid body is subject to a constant gravitational field $\boldsymbol{\gamma} \in \mathbb{R}^3$, the potential energy is given by

$$\mathcal{U}(q(t)) = \mathcal{U}(p(t), \mathbf{x}(t)) = -m\boldsymbol{\gamma}^\top \cdot \mathbf{x}(t)$$

and its derivative is

$$\mathbf{D}\mathcal{U}(q(t)) = \left[\mathbf{D}_{p(t)}\mathcal{U}(p(t), \mathbf{x}(t)), d_{\mathbf{x}(t)}\mathcal{U}(p(t), \mathbf{x}(t)) \right] = \left[\mathbf{0}_{1 \times 3}, -m(p^{-1}(t) \triangleright \boldsymbol{\gamma})^\top \right].$$

Therefore, the term $-\mathbf{D}\mathcal{U}^\top(q(t))$ is given by

$$-\mathbf{D}\mathcal{U}^\top(q(t)) = \begin{bmatrix} \mathbf{0} \\ mp^{-1}(t) \triangleright \boldsymbol{\gamma} \end{bmatrix}$$

see remarks 2.35 and 2.36. The gravitational field results in forces $mp^{-1}(t) \triangleright \boldsymbol{\gamma} \in \mathbb{R}^3$ with respect to the body-fixed frame without any moments.

4.2. The Cosserat Beam

A Cosserat beam model can be used to model a thin structure $Q^* \subseteq \mathbb{R}^3$ which is a lot larger in one dimension than in the two other dimensions. The model we are using is based on the work of Lang, Linn and Arnold [53], see also the technical reports [50, 52] as well as [51, 59]. The continuous model of the aforementioned research was itself based on the work of Simo [71, 72]. We will add internal constraints to the model in order to reduce the full Cosserat beam model to an (extensible or inextensible) Kirchhoff beam model [51].

The spatial discretization of the Cosserat beam with internal constraints follows a method of lines approach [81] and will be performed with the toolbox of variational integrators, similar to the derivation of RATTLie in section 3.1. The approach was heavily inspired by the staggered grid finite difference discretization employed in [53], which was geared towards the direct product configuration space $\mathbb{S}^3 \times \mathbb{R}^3$. We altered the approach to match the semi-direct configuration space $\mathbb{S}^3 \ltimes \mathbb{R}^3$ and end up with a scheme that was similar to the derivation of variational integrators [63], see also [55].

First, in section 4.2.1 we will introduce the continuous Cosserat beam model and subsequently, in section 4.2.2, we will discretize the constrained beam model in space.

4.2.1. The Continuous Cosserat Beam Model

We assume that for each time instant t , the line of mass centroids is given by the curve $s \mapsto \mathbf{x}(s, t) \in \mathbb{R}^3$ for $s \in [0, L]$ with an $L > 0$. The underlying assumption of Cosserat beams is that the cross sections of beams stay rigid at all times. That means we neglect any changes like bending or changes in size of the cross sections. Therefore, we can consider each of these cross sections at $s \in [0, L]$ to be an infinitesimally thin rigid body with configuration $q(s, t) = (p(s, t), \mathbf{x}(s, t)) \in \mathbb{S}^3 \ltimes \mathbb{R}^3$ as described in section 4.1. This means that the orientation of the rigid cross section that is attached to the center line at $\mathbf{x}(s, t)$ is described by a quaternion $p(s, t) \in \mathbb{S}^3$. Then the set of material points of the deformed beam $Q(t) \subset \mathbb{R}^3$ can be described as

$$Q(t) = \{\mathbf{x}(s, t) + p(s, t) \triangleright [\xi_1, \xi_2, 0]^\top \in \mathbb{R}^3 : s \in [0, L], [\xi_1, \xi_2]^\top \in A(s)\},$$

where $A(s) \subseteq \mathbb{R}^2$ is the cross section of the beam at $\mathbf{x}(s, t)$ such that the center of $A(s)$ is the origin and the canonical unit vectors $\mathbf{e}_1, \mathbf{e}_2 \in \mathbb{R}^2$ point along the principal axes of $A(s)$. In formulae this can be written as $\mathbf{0} = \int_{A(s)} \boldsymbol{\xi} \, d\boldsymbol{\xi}$ and $0 = \int_{A(s)} \xi_1 \xi_2 \, d[\xi_1, \xi_2]^\top$ assuming that the density is constant throughout the cross section. In this thesis, we additionally assume that the shape of the cross section is constant along the beam: $A(s) \equiv A$. To facilitate describing the material properties, we assume that in the undeformed state, the line of mass centroids $\mathbf{x}(\bullet, t)$ is parametrized by arc-length. Therefore, $L > 0$ is the length of the undeformed beam.

In summary, at each time t , the configuration of the beam can be described as a curve $s \mapsto q(s, t) \in \mathbb{S}^3 \ltimes \mathbb{R}^3$. Thus, the configuration space for the Cosserat beam model is $C([0, L]; \mathbb{S}^3 \ltimes \mathbb{R}^3)$, the space of all continuous functions that map from $[0, L]$ to $\mathbb{S}^3 \ltimes \mathbb{R}^3$. We can also interpret this model as a line of rigid bodies. As in section 4.1, we choose

the semidirect product Lie group structure $(\mathbb{S}^3 \times \mathbb{R}^3, \circ)$. We will denote time derivatives with a dot $(\partial \bullet / \partial t = \dot{\bullet})$ and derivatives with respect to the arc-length s with a prime $(\partial \bullet / \partial s = \bullet')$. Furthermore, we will define for each $(s, t) \in [0, L] \times [t_0, t_c]$ the derivative vector $\mathbf{v}(s, t) \in \mathbb{R}^6$ with respect to time in the same way as in (2.17) and a vector $\mathbf{w}(s, t) \in \mathbb{R}^6$ analogously to (2.17):

$$\begin{aligned}\dot{q}(s, t) &= \mathrm{d}L_{q(s,t)}(e) \widetilde{\mathbf{v}(s, t)}, \\ q'(s, t) &= \mathrm{d}L_{q(s,t)}(e) \widetilde{\mathbf{w}(s, t)}.\end{aligned}$$

The derivative vector $\mathbf{v}(s, t)$ contains, as before, the angular velocity $\boldsymbol{\Omega}(s, t)$ and the velocity $\mathbf{U}(s, t)$ of the cross section at $s \in [0, L]$, measured in the body-fixed frame:

$$\mathbf{v}(s, t) = [\boldsymbol{\Omega}^\top(s, t), \mathbf{U}^\top(s, t)]^\top.$$

The vector $\mathbf{w}(s, t)$ is the derivative vector with respect to the arc-length s of $q(s, t)$. It therefore corresponds to the spatial derivative of $q(s, t)$ and contains the material curvature vector $\mathbf{K}(s, t) \in \mathbb{R}^3$ and the material strain vector $\boldsymbol{\Gamma}(s, t)$, see e. g. [53]:

$$\mathbf{w}(s, t) = [\mathbf{K}^\top(s, t) + \mathbf{K}^{*\top}(s), \boldsymbol{\Gamma}^\top(s, t) + \boldsymbol{\Gamma}^{*\top}(s)]^\top, \quad (4.3)$$

where $\mathbf{K}^*(s) \in \mathbb{R}^3$ and $\boldsymbol{\Gamma}^*(s) \in \mathbb{R}^3$ are the precurvature and prestrain vectors of the undeformed beam, respectively. Note that angular velocity, velocity, material curvature, and material strain are measured with respect to the body-fixed frame.

We first want to develop the kinetic energy $\mathcal{T}(q(\bullet, t))$ of the beam. For this, we consider the kinetic energy density $T(q(s, t))$ along the center line of the beam:

$$T(q(s, t)) = \underbrace{\frac{1}{2} \boldsymbol{\Omega}^\top(s, t) \cdot \mathbf{J}(s) \cdot \boldsymbol{\Omega}(s, t)}_{\text{rotatory part}} + \underbrace{|A(s)| \rho(s) \frac{1}{2} \mathbf{U}^\top(s, t) \cdot \mathbf{U}(s, t)}_{\text{translatory part}},$$

where $\rho(s) > 0$ is the volumetric mass density, $|A(s)| > 0$ the area, and $\mathbf{J}(s) \in \mathbb{R}^{3 \times 3}$ the inertia tensor density of the cross section of the beam at s . Note that we assume that the density $\rho(s)$ is constant on all points of the cross section at arc-length s . The calculation for $\mathbf{J}(s)$ is similar to (4.2):

$$\mathbf{J}(s) = \rho(s) \operatorname{diag} \left(\int_{A(s)} \xi_2^2 \, \mathrm{d}\boldsymbol{\xi}, \int_{A(s)} \xi_1^2 \, \mathrm{d}\boldsymbol{\xi}, \int_{A(s)} (\xi_1^2 + \xi_2^2) \, \mathrm{d}\boldsymbol{\xi} \right),$$

where this time the integration variable is $\boldsymbol{\xi} = [\xi_1, \xi_2]^\top \in \mathbb{R}^2$. This can be obtained by considering a thin three-dimensional rigid body $A(s) \times [-\varepsilon, \varepsilon]$, calculating its inertia tensor, dividing it by the thickness 2ε and letting $\varepsilon \rightarrow 0$. Since we considered $A(s)$ to be aligned with its principal axes, the resulting inertia tensor is a diagonal matrix.

In this thesis, we will restrict ourselves to the case that not only the shape of the cross section, but also the volumetric mass density is constant along s : $A(s) \equiv A$ and $\rho(s) \equiv \rho$,

which imply $\mathbf{J}(s) \equiv \mathbf{J}$. The kinetic energy of the whole beam is then given by the integral over its energy density:

$$\mathcal{T}(q(\bullet, t)) = \int_0^L T(q(s, t)) ds = \int_0^L \frac{1}{2} \mathbf{v}^\top(s, t) \cdot \mathbf{N} \cdot \mathbf{v}(s, t) ds, \quad (4.4)$$

where $\mathbf{N} = \text{blkdiag}(\mathbf{J}, |A|\rho\mathbf{I}_3)$.

Now we focus on the potential energy $\mathcal{U}(q(\bullet, t))$ of the beam. Like for the kinetic energy, we consider a potential energy density $U(q(s, t))$. We want to apply linear (visco-)elastic material behavior of a homogeneous beam, thus $U(q(s, t))$ is quadratic in $\mathbf{K}(s, t)$ and $\mathbf{\Gamma}(s, t)$, see [53], where

$$U(q(s, t)) = \underbrace{\frac{1}{2} \mathbf{K}^\top(s, t) \cdot \mathbf{C}^{\mathbf{K}} \cdot \mathbf{K}(s, t)}_{\text{bending and torsion}} + \underbrace{\frac{1}{2} \mathbf{\Gamma}^\top(s, t) \cdot \mathbf{C}^{\mathbf{\Gamma}} \cdot \mathbf{\Gamma}(s, t)}_{\text{shearing and extension}},$$

with diagonal matrices $\mathbf{C}^{\mathbf{K}}, \mathbf{C}^{\mathbf{\Gamma}} \in \mathbb{R}^{3 \times 3}$, which contain material parameters [53]:

$$\mathbf{C}^{\mathbf{K}} = \text{diag}(EI_1, EI_2, GI_3), \quad \mathbf{C}^{\mathbf{\Gamma}} = \text{diag}(G|A|\kappa_1, G|A|\kappa_2, E|A|),$$

where E and G are Young's modulus and the shear modulus, respectively, κ_1 and κ_2 are Timoshenko shear correction factors, and $\text{diag}(I_1, I_2, I_3) = \mathbf{J}$. In practice, however, the products $EI_1, EI_2, GI_3, G|A|\kappa_1, G|A|\kappa_2, E|A|$ are measured individually, rather than calculated from the cross section, the moduli, and the shear correction factors, see e. g. [59]. The kinetic energy of the whole beam is then given by

$$\mathcal{U}(q(\bullet, t)) = \int_0^L U(q(s, t)) ds = \int_0^L \frac{1}{2} (\mathbf{w}(s, t) - \mathbf{w}^*(s))^\top \cdot \mathbf{C} \cdot (\mathbf{w}(s, t) - \mathbf{w}^*(s)) ds, \quad (4.5)$$

where $\mathbf{C} = \text{blkdiag}(\mathbf{C}^{\mathbf{K}}, \mathbf{C}^{\mathbf{\Gamma}})$ and $\mathbf{w}^* = [\mathbf{K}^{*\top}(s), \mathbf{\Gamma}^{*\top}(s)]^\top$.

Now we can derive the equations of motion of the unconstrained Cosserat beam by applying Hamilton's principle

$$0 = \delta \int_{t_0}^{t_e} \mathcal{T}(\mathbf{v}(\bullet, t)) - \mathcal{U}(q(\bullet, t)) dt \quad (4.6)$$

similar to remark 2.35 but without the constraints and hence without the augmentation of the Lagrangian. We will use the derivative vectors $\delta \mathbf{q}(s, t) \in \mathbb{R}^6$ of $q(s, t)$ with respect to variation, see (2.36). As additional boundary conditions to (2.39c), we assume that there are no inner forces and moments due to curvature and strains at the ends of the beam, such that $\mathbf{w}(0, t) - \mathbf{w}^*(0) = \mathbf{w}(L, t) - \mathbf{w}^*(L) = \mathbf{0}$. They describe that the beam is completely free at both ends [72]. The derivation of the equations of motion reads

$$\begin{aligned} 0 &= \delta \int_{t_0}^{t_e} \mathcal{T}(\mathbf{v}(\bullet, t)) - \mathcal{U}(q(\bullet, t)) dt \\ &= \delta \int_{t_0}^{t_e} \int_0^L T(\mathbf{v}(s, t)) - U(q(s, t)) ds dt \end{aligned}$$

$$\begin{aligned}
&= \int_{t_0}^{t_e} \int_0^L \mathbf{v}^\top(s, t) \cdot \mathbf{N} \cdot \delta \mathbf{v}(s, t) - (\mathbf{w}(s, t) - \mathbf{w}^*(s))^\top \cdot \mathbf{C} \cdot \delta \mathbf{w}(s, t) \, ds \, dt \\
&= \int_0^L [\mathbf{v}^\top(s, t) \cdot \mathbf{N} \cdot \delta q(s, t)]_{t=t_0}^{t_e} \\
&\quad + \int_{t_0}^{t_e} (\mathbf{v}^\top(s, t) \cdot \mathbf{N} \cdot \widehat{\mathbf{v}}(s, t) - \dot{\mathbf{v}}^\top(s, t) \cdot \mathbf{N}) \cdot \delta \mathbf{q}(s, t) \, dt \, ds \\
&\quad - \int_{t_0}^{t_e} [(\mathbf{w}(s, t) - \mathbf{w}^*(s))^\top \cdot \mathbf{C} \cdot \delta q(s, t)]_{s=0}^L \\
&\quad + \int_0^L ((\mathbf{w}(s, t) - \mathbf{w}^*(s))^\top \cdot \mathbf{C} \cdot \widehat{\mathbf{w}}(s, t) - \mathbf{w}'^\top(s, t) \cdot \mathbf{C}) \cdot \delta \mathbf{q}(s, t) \, ds \, dt \\
&= \int_{t_0}^{t_e} \int_0^L (\mathbf{v}^\top(s, t) \cdot \mathbf{N} \cdot \widehat{\mathbf{v}}(s, t) - \dot{\mathbf{v}}^\top(s, t) \cdot \mathbf{N} - (\mathbf{w}(s, t) - \mathbf{w}^*(s))^\top \cdot \mathbf{C} \cdot \widehat{\mathbf{w}}(s, t) \\
&\quad + \mathbf{w}'^\top(s, t) \cdot \mathbf{C}) \cdot \delta \mathbf{q}(s, t) \, ds \, dt.
\end{aligned}$$

In [52], this has been called a two-dimensional variational principle. Since the above equation has to hold for all variations, we can deduct that the equations of motion read

$$\dot{q}(s, t) = dL_{q(s,t)}(e) \widehat{\mathbf{v}}(s, t), \quad (4.7a)$$

$$q'(s, t) = dL_{q(s,t)}(e) \widehat{\mathbf{w}}(s, t), \quad (4.7b)$$

$$\mathbf{N} \cdot \dot{\mathbf{v}}(s, t) = \widehat{\mathbf{v}}(s, t)^\top \cdot \mathbf{N} \cdot \mathbf{v}(s, t) - \widehat{\mathbf{w}}(s, t)^\top \cdot \mathbf{g}(s, t) + \mathbf{g}'(s, t), \quad (4.7c)$$

where $\mathbf{g}(s, t) \in \mathbb{R}^6$ is the vector of generalized internal forces given by

$$\mathbf{g}(s, t) = \mathbf{C} \cdot (\mathbf{w}(s, t) - \mathbf{w}^*(s)). \quad (4.8)$$

The dynamic equation (4.7c) reads in components

$$\mathbf{J} \cdot \dot{\boldsymbol{\Omega}} = -\boldsymbol{\Omega} \times (\mathbf{J} \cdot \boldsymbol{\Omega}) + (\mathbf{K} + \mathbf{K}^*) \times \mathbf{M} + (\boldsymbol{\Gamma} + \boldsymbol{\Gamma}^*) \times \mathbf{F} + \mathbf{M}', \quad (4.9a)$$

$$\rho|A|\dot{\mathbf{U}} = -\boldsymbol{\Omega} \times (\rho|A|\mathbf{U}) + (\mathbf{K} + \mathbf{K}^*) \times \mathbf{F} + \mathbf{F}', \quad (4.9b)$$

where we omitted the arguments s and t and introduced the internal moment $\mathbf{M}(s, t) = \mathbf{C}^{\mathbf{K}} \cdot \mathbf{K}(s, t)$ and internal force $\mathbf{F}(s, t) = \mathbf{C}^{\boldsymbol{\Gamma}} \cdot \boldsymbol{\Gamma}(s, t)$, both measured with respect to the body-fixed frame.

Remark 4.2: *Equations of motion with respect to the inertial frame.*

If we choose to rewrite these equations in such a way that we use the spatial description

$$\begin{aligned}
\boldsymbol{\omega}(s, t) &= p(s, t) \triangleright \boldsymbol{\Omega}(s, t), & \mathbf{u}(s, t) &= p(s, t) \triangleright \mathbf{U}(s, t) = \dot{\mathbf{x}}(s, t), \\
\mathbf{m}(s, t) &= p(s, t) \triangleright \mathbf{M}(s, t), & \mathbf{f}(s, t) &= p(s, t) \triangleright \mathbf{F}(s, t), \\
\mathbf{j}(s, t) &= \mathbf{R}(p(s, t)) \cdot \mathbf{J} \cdot \mathbf{R}^\top(p(s, t)),
\end{aligned}$$

we end up with the equations

$$\begin{aligned}\mathbf{j}(s, t) \cdot \dot{\boldsymbol{\omega}}(s, t) + \boldsymbol{\omega}(s, t) \times (\mathbf{j}(s, t) \cdot \boldsymbol{\omega}(s, t)) &= \mathbf{m}'(s, t) + \boldsymbol{x}'(s, t) \times \mathbf{f}(s, t), \\ \rho|A|\dot{\mathbf{u}}(s, t) &= \mathbf{f}'(s, t),\end{aligned}$$

after applying the rotation $p(s, t)$ to both sides, see the papers of Simo [71, 72].

Remark 4.3: *Visco-elastic material behavior.*

We can include internal damping in this Cosserat beam model by assuming visco-elastic material behavior, see e. g. [53]. We introduce the dissipative generalized force density

$$D(\dot{\mathbf{w}}(s, t)) = -2\mathbf{V} \cdot \dot{\mathbf{w}}(s, t),$$

with visco-elastic material parameters $\mathbf{V} = \text{diag}(c_1^{\dot{\mathbf{K}}}, c_2^{\dot{\mathbf{K}}}, c_3^{\dot{\mathbf{K}}}, c_1^{\dot{\mathbf{I}}}, c_2^{\dot{\mathbf{I}}}, c_3^{\dot{\mathbf{I}}})$. We can then add the term

$$\int_{t_0}^{t_e} \int_0^L D^\top(\dot{\mathbf{w}}(s, t)) \cdot \delta \mathbf{w}(s, t) \, ds \, dt \quad (4.10)$$

on the right-hand side of the variational principle (4.6), similar to the external generalized forces in remark 2.36. The equations (4.7) remain valid, but with internal generalized forces

$$\mathbf{g}(s, t) = \mathbf{C} \cdot (\mathbf{w}(s, t) - \mathbf{w}^*(s)) + 2\mathbf{V} \cdot \dot{\mathbf{w}}(s, t). \quad (4.11)$$

In components, equations (4.9) also remain valid, but with inner moments and forces

$$\begin{aligned}\mathbf{M}(s, t) &= \mathbf{C}^{\mathbf{K}} \cdot \mathbf{K}(s, t) + 2 \text{diag}(c_1^{\dot{\mathbf{K}}}, c_2^{\dot{\mathbf{K}}}, c_3^{\dot{\mathbf{K}}}) \cdot \dot{\mathbf{K}}(s, t), \\ \mathbf{F}(s, t) &= \mathbf{C}^{\mathbf{I}} \cdot \mathbf{I}(s, t) + 2 \text{diag}(c_1^{\dot{\mathbf{I}}}, c_2^{\dot{\mathbf{I}}}, c_3^{\dot{\mathbf{I}}}) \cdot \dot{\mathbf{I}}(s, t),\end{aligned}$$

respectively.

Remark 4.4: *External moments and forces.*

External moments and forces can be incorporated similar to remark 2.36. We introduce a generalized force density

$$\mathbf{g}^{\text{ex}}(q, s, t) = \begin{bmatrix} \mathbf{M}^{\text{ex}}(q, s, t) \\ \mathbf{F}^{\text{ex}}(q, s, t) \end{bmatrix} \in \mathbb{R}^6$$

with external moments $\mathbf{M}^{\text{ex}}(q, s, t) \in \mathbb{R}^3$ and external forces $\mathbf{F}^{\text{ex}}(q, s, t) \in \mathbb{R}^3$ measured with respect to the body-fixed frame. By adding the term

$$\int_{t_0}^{t_e} \int_0^L (\mathbf{g}^{\text{ex}}(q, s, t))^\top \cdot \delta \mathbf{q}(s, t) \, ds \, dt \quad (4.12)$$

on the right-hand side of the variational principle (4.6), we get the additional term $\mathbf{g}^{\text{ex}}(q, s, t)$ on the right-hand side of (4.7). In components, we get the terms $\mathbf{M}^{\text{ex}}(q, s, t)$

and $\mathbf{F}^{\text{ex}}(q, s, t)$ on the right-hand sides of (4.9a) and (4.9b), respectively. Note that since the external moments and forces depend on the function q , they may not only depend on the values $q(s, t)$, but also on derivative vectors like $\mathbf{v}(s, t)$ and $\mathbf{w}(s, t)$. In case that we want to apply external moments $\mathbf{m}^{\text{ex}}(s, t)$ and forces $\mathbf{f}^{\text{ex}}(s, t)$ which are given with respect to the inertial frame, we have to use

$$\mathbf{M}^{\text{ex}}(q, s, t) = p^{-1}(s, t) \triangleright \mathbf{m}^{\text{ex}}(q, s, t), \quad \mathbf{F}^{\text{ex}}(q, s, t) = p^{-1}(s, t) \triangleright \mathbf{f}^{\text{ex}}(q, s, t).$$

A Cosserat beam model with a very high (shearing) stiffness or with very large cross sections leads to a very stiff differential equation [53]. On the other end of the spectrum, in very slender beams the shearing of the beam can be of no interest. In those cases, it might be appropriate to use a Kirchhoff beam model in which the cross sections are assumed to stay perpendicular to the center line, see e. g. [71]. We could go even further and also neglect the extension of the beam, leading to an inextensible Kirchhoff beam, see e. g. [51]. Instead of deriving a new model, we can reduce the already existing and more general model by introducing internal constraints [45]. With the internal constraints in place, the corresponding stiffness coefficients (for shearing or additionally extension) can be neglected and the result is a differential equation with reduced stiffness whose solution is more computationally efficient.

Remark 4.5: *Reduction of the model by internal constraints.*

In order to reduce the Cosserat beam model to a Kirchhoff beam model, we introduce a constraint density function $\Psi(\mathbf{w}(s, t)) \in \mathbb{R}^m$ which we assume to vanish. We will introduce this constraint by augmenting the Lagrangian in (4.6) with

$$\mathcal{C}(\mathbf{w}(\bullet, t), \boldsymbol{\lambda}(\bullet, t)) = \int_0^L \Psi^\top(\mathbf{w}(s, t)) \cdot \boldsymbol{\lambda}(s, t) \, ds, \quad (4.13)$$

where $\boldsymbol{\lambda}(s, t) \in \mathbb{R}^m$ are Lagrange multipliers. This means, we introduce the additional term

$$- \int_{t_0}^{t_e} \mathcal{C}(\mathbf{w}(\bullet, t), \boldsymbol{\lambda}(\bullet, t)) \, dt$$

on the right-hand side of (4.6), similar to (2.39). This adds the constraint equation

$$\mathbf{0} = \Psi(\mathbf{w}(s, t))$$

to the equations of motion (4.7), which remain valid with the sum of internal forces

$$\mathbf{g}(s, t) = \mathbf{C} \cdot (\mathbf{w}(s, t) - \mathbf{w}^*(s)) + d\Psi^\top(\mathbf{w}(s, t)) \cdot \boldsymbol{\lambda}(s, t). \quad (4.14)$$

In combination with added viscosity to the model, the generalized internal forces read

$$\mathbf{g}(s, t) = \mathbf{C} \cdot (\mathbf{w}(s, t) - \mathbf{w}^*(s)) + 2\mathbf{V} \cdot \dot{\mathbf{w}}(s, t) + d\Psi^\top(\mathbf{w}(s, t)) \cdot \boldsymbol{\lambda}(s, t), \quad (4.15)$$

see [45]. External moments and forces can still be applied like in remark 4.4.

Remark 4.6: *Internal constraints for a Kirchhoff beam model.*

In order to reduce the full Cosserat beam model to a Kirchhoff beam model, we introduce the constraint that no shearing from the undeformed state is possible, see e. g. [53]. This means that the first two components of the material strain vector $\boldsymbol{\Gamma}(s, t)$, see (4.3), have to vanish. We can formulate this by the constraint density

$$\mathbf{0} = \boldsymbol{\Psi}(\mathbf{w}(s, t)) = \begin{bmatrix} \mathbf{e}_1^\top \\ \mathbf{e}_2^\top \end{bmatrix} \cdot \boldsymbol{\Gamma}(s, t) = \begin{bmatrix} \mathbf{e}_4^\top \\ \mathbf{e}_5^\top \end{bmatrix} \cdot (\mathbf{w}(s, t) - \mathbf{w}^*(s)),$$

From the linear structure we can immediately see the derivatives

$$d\boldsymbol{\Psi}(\mathbf{w}(s, t)) = \begin{bmatrix} \mathbf{e}_4^\top \\ \mathbf{e}_5^\top \end{bmatrix}.$$

Remark 4.7: *Internal constraints for an inextensible Kirchhoff beam.*

In order to reduce the full Cosserat beam model to an inextensible Kirchhoff beam model, we need to make sure that additionally the length of the center line does not change, see e. g. [53]. This means that the third component of $\boldsymbol{\Gamma}(s, t)$ has to vanish as well. The corresponding constraint density is given by

$$\mathbf{0} = \boldsymbol{\Psi}(\mathbf{w}(s, t)) = \begin{bmatrix} \mathbf{e}_1^\top \\ \mathbf{e}_2^\top \\ \mathbf{e}_3^\top \end{bmatrix} \cdot \boldsymbol{\Gamma}(s, t) = \begin{bmatrix} \mathbf{e}_4^\top \\ \mathbf{e}_5^\top \\ \mathbf{e}_6^\top \end{bmatrix} \cdot (\mathbf{w}(s, t) - \mathbf{w}^*(s)).$$

Again, the derivatives are straightforward:

$$d\boldsymbol{\Psi}(\mathbf{w}(s, t)) = \begin{bmatrix} \mathbf{e}_4^\top \\ \mathbf{e}_5^\top \\ \mathbf{e}_6^\top \end{bmatrix}.$$

4.2.2. Discretizing the Cosserat Beam Model in Space

In this section, we will discretize the continuous Cosserat beam model from section 4.2.1 in space. In order to do so, we follow the framework of variational integrators: In the variational principle we only consider a finite-dimensional set of admissible configurations for each time instance and approximate the spatial integrals by second-order quadrature rules. In the end we obtain a spatially discrete Cosserat beam model.

In the following, we will consider the linearly elastic case and later also cover the case of visco-elastic material behavior. The internal constraints will be considered right away, but they could be dropped very easily in order to obtain a semi-discrete Cosserat beam model without internal constraints.

First, we will approximate the function $q(\bullet, t)$ by a piece-wise interpolation from remark 2.27:

$$q^d(s, t) = \text{pIp}\left(s, (s_m)_{m=0, \dots, M}, (q_m(t))_{m=0, \dots, M}\right),$$

with a spatial grid $s_0 < s_1 < \dots < s_M$ with step sizes $\Delta s_{m-1/2} = s_m - s_{m-1}$ for $m = 1, \dots, M$ and with interpolation points $q_m(t) \in \mathbb{S}^3 \times \mathbb{R}^3$ for $m = 0, \dots, M$. This approach is similar to the derivation of RATTLie in section 3.1. Let $\mathbf{v}^d(s, t)$ and $\mathbf{w}^d(s, t)$ be the derivative vectors of $q^d(s, t)$ with respect to time and space where they are well-defined:

$$\dot{q}^d(s, t) = dL_{q^d(s, t)}(e) \widetilde{\mathbf{v}^d(s, t)}, \quad (q^d)'(s, t) = dL_{q^d(s, t)}(e) \widetilde{\mathbf{w}^d(s, t)}.$$

Now we consider $s \in (s_{m-1}, s_m)$ for some $m \in \{1, \dots, M\}$. Then it holds

$$q^d(s, t) = q_{m-1}(t) \circ \widetilde{\exp}((s - s_{m-1})\mathbf{w}_{m-1/2}(t))$$

with

$$\mathbf{w}_{m-1/2}(t) = \frac{1}{\Delta s_{m-1/2}} \widetilde{\log}(q_{m-1}^{-1}(t) \circ q_m(t)), \quad m = 1, \dots, M. \quad (4.16)$$

For the derivative vector with respect to space it holds for $s \in (s_{m-1}, s_m)$, see (3.4),

$$\mathbf{w}^d(s, t) = \mathbf{w}_{m-1/2}(t).$$

We will furthermore define $\mathbf{v}_m(t)$ to be the derivative vector of $q_m(t)$ for $m = 0, \dots, M$. Then we can collect the configuration variables $q_m(t)$ in

$$q(t) = (q_0(t), \dots, q_M(t)) \in (\mathbb{S}^3 \times \mathbb{R}^3)^{M+1}$$

as well as the derivative vectors

$$\mathbf{v}(t) = [\mathbf{v}_0^\top(t), \dots, \mathbf{v}_M^\top(t)] \in \mathbb{R}^{6(M+1)}.$$

It is clear that $\mathbf{v}(t)$ is the derivative vector for $q(t)$ in the Lie group $(\mathbb{S}^3 \times \mathbb{R}^3)^{M+1}$ since this is the $(M+1)$ -fold direct product of $\mathbb{S}^3 \times \mathbb{R}^3$.

Now we can describe this discretized Cosserat beam model. This discretization is designed similar to the staggered grid discretization of Lang and Linn [53]. First, we approximate the kinetic energy $\mathcal{T}(q^d(\bullet, t))$ from (4.4) by the chained trapezoidal rule leading to a discretized kinetic energy

$$\begin{aligned} \mathcal{T}^d(\mathbf{v}(t)) &= \sum_{m=1}^M \frac{\Delta s_{m-1/2}}{2} \left(T(\mathbf{v}_{m-1}(t)) + T(\mathbf{v}_m(t)) \right) \\ &= \frac{\Delta s_0}{4} \mathbf{v}_0^\top(t) \cdot \mathbf{N} \cdot \mathbf{v}_0(t) + \sum_{m=1}^{M-1} \frac{\Delta s_{m-1/2} + \Delta s_{m+1/2}}{4} \mathbf{v}_m^\top(t) \cdot \mathbf{N} \cdot \mathbf{v}_m(t) \\ &\quad + \frac{\Delta s_{M-1/2}}{4} \mathbf{v}_M^\top(t) \cdot \mathbf{N} \cdot \mathbf{v}_M(t). \end{aligned}$$

The approximation $\mathcal{T}(q^d(\bullet, t)) \approx \mathcal{T}^d(\mathbf{v}(t))$ is of second order. We can see that $\mathcal{T}^d(\mathbf{v}(t))$ is actually quadratic in $\mathbf{v}(t)$:

$$\mathcal{T}^d(\mathbf{v}(t)) = \frac{1}{2} \mathbf{v}^\top(t) \cdot \mathbf{M} \cdot \mathbf{v}(t)$$

with

$$\mathbf{M} = \text{blkdiag}\left(\frac{\Delta s_{1/2}}{2}\mathbf{N}, \frac{\Delta s_{1/2} + \Delta s_{3/2}}{2}\mathbf{N}, \dots, \frac{\Delta s_{M-3/2} + \Delta s_{M-1/2}}{2}\mathbf{N}, \frac{\Delta s_{M-1/2}}{2}\mathbf{N}\right).$$

and thus, differentiation with respect to $\mathbf{v}(t)$ is straightforward.

Next, we approximate the potential energy $\mathcal{U}(q^{\text{d}}(\bullet, t))$ from (4.5) by the chained midpoint rule leading to a discrete potential energy

$$\begin{aligned}\mathcal{U}^{\text{d}}(q(t)) &= \sum_{m=1}^M \Delta s_{m-1/2} U(\mathbf{w}_{m-1/2}(t)) \\ &= \sum_{m=1}^M \frac{\Delta s_{m-1/2}}{2} (\mathbf{w}_{m-1/2}(t) - \mathbf{w}_{m-1/2}^*)^{\top} \cdot \mathbf{C} \cdot (\mathbf{w}_{m-1/2}(t) - \mathbf{w}_{m-1/2}^*),\end{aligned}$$

with $\mathbf{w}_{m-1/2}^* = \mathbf{w}^*(s_{m-1/2})$ for $m = 1, \dots, M$. Here we used the definition of $\mathbf{w}_{m-1/2}$ in terms of $q_{m-1}(t)$ and $q_m(t)$ according to (4.16). Again, the discrete potential energy $\mathcal{U}^{\text{d}}(q(t))$ is a second-order approximation to $\mathcal{U}(q^{\text{d}}(\bullet, t))$. In order to differentiate $\mathcal{U}^{\text{d}}(q(t))$ with respect to $q(t)$, we have to know $\mathbf{D}_{q_i(t)} \mathbf{w}_{j-1/2}(t)$ for $i = 0, \dots, M$ and $j = 1, \dots, M$. From lemma 2.25 applied to (4.16) we know that

$$\mathbf{D}_{q_i(t)} \mathbf{w}_{j-1/2}(t) = \mathbf{0}, \quad \frac{1}{2} < |i - (j - 1/2)|, \quad (4.17\text{a})$$

$$\mathbf{D}_{q_{m-1}(t)} \mathbf{w}_{m-1/2}(t) = -\frac{1}{\Delta s_{m-1/2}} \mathbf{T}^{-1}(-\Delta s_{m-1/2} \mathbf{w}_{m-1/2}(t)), \quad m = 0, \dots, M-1, \quad (4.17\text{b})$$

$$\mathbf{D}_{q_m(t)} \mathbf{w}_{m-1/2}(t) = \frac{1}{\Delta s_{m-1/2}} \mathbf{T}^{-1}(\Delta s_{m-1/2} \mathbf{w}_{m-1/2}(t)), \quad m = 1, \dots, M, \quad (4.17\text{c})$$

with \mathbf{T}^{-1} being the inverse matrix of the tangent operator of $\mathbb{S}^3 \times \mathbb{R}^3$, see definition 2.20 and appendix A. This result is similar to (3.12) in the derivation of RATTLie. It follows

$$\begin{aligned}\mathbf{D}_{q_0} \mathcal{U}^{\text{d}}(q(t)) &= -(\mathbf{w}_{1/2}(t) - \mathbf{w}_{1/2}^*)^{\top} \cdot \mathbf{C} \cdot \mathbf{T}^{-1}(-\Delta s_{1/2} \mathbf{w}_{1/2}(t)), \\ \mathbf{D}_{q_m} \mathcal{U}^{\text{d}}(q(t)) &= (\mathbf{w}_{m-1/2}(t) - \mathbf{w}_{m-1/2}^*)^{\top} \cdot \mathbf{C} \cdot \mathbf{T}^{-1}(\Delta s_{m-1/2} \mathbf{w}_{m-1/2}(t)) \\ &\quad - (\mathbf{w}_{m+1/2}(t) - \mathbf{w}_{m+1/2}^*)^{\top} \cdot \mathbf{C} \cdot \mathbf{T}^{-1}(-\Delta s_{m+1/2} \mathbf{w}_{m+1/2}(t)), \\ \mathbf{D}_{q_M} \mathcal{U}^{\text{d}}(q(t)) &= (\mathbf{w}_{M-1/2}(t) - \mathbf{w}_{M-1/2}^*)^{\top} \cdot \mathbf{C} \cdot \mathbf{T}^{-1}(\Delta s_{M-1/2} \mathbf{w}_{M-1/2}(t))\end{aligned}$$

and furthermore we know

$$\mathbf{D}\mathcal{U}^{\text{d}}(q(t)) = \begin{bmatrix} \left(\mathbf{D}_{q_0} \mathcal{U}^{\text{d}}(q(t))\right)^{\top} \\ \vdots \\ \left(\mathbf{D}_{q_M} \mathcal{U}^{\text{d}}(q(t))\right)^{\top} \end{bmatrix}^{\top}.$$

Now we consider the internal constraints. In remark 4.5, we augmented the Lagrangian with the term $\mathcal{C}(\mathbf{w}(\bullet, t), \boldsymbol{\lambda}(\bullet, t))$. Like for the potential energy, we will approximate the integral in $\mathcal{C}(\mathbf{w}^d(\bullet, t), \boldsymbol{\lambda}^d(\bullet, t))$ with the chained midpoint rule, which is of second order:

$$\mathcal{C}^d(q(t), \boldsymbol{\lambda}(t)) = \sum_{m=1}^M \Delta s_{m-1/2} \boldsymbol{\Psi}^\top(\mathbf{w}_{m-1/2}(t)) \cdot \boldsymbol{\lambda}_{m-1/2}(t),$$

where $\boldsymbol{\lambda}_{m-1/2}(t)$ are Lagrange multipliers for $m = 1, \dots, M$ and the definition

$$\boldsymbol{\lambda}(t) = [\boldsymbol{\lambda}_{1/2}^\top, \boldsymbol{\lambda}_{3/2}^\top, \dots, \boldsymbol{\lambda}_{M-1/2}^\top]^\top.$$

We define

$$\boldsymbol{\Phi}(q(t)) = \begin{bmatrix} \Delta s_{1/2} \boldsymbol{\Psi}(\mathbf{w}_{1/2}(t)) \\ \vdots \\ \Delta s_{M-1/2} \boldsymbol{\Psi}(\mathbf{w}_{M-1/2}(t)) \end{bmatrix}$$

and reformulate the constraint-related term by

$$\mathcal{C}^d(q(t), \boldsymbol{\lambda}(t)) = \boldsymbol{\Phi}^\top(q(t)) \cdot \boldsymbol{\lambda}(t).$$

The derivative of $\boldsymbol{\Phi}$ is given by the block matrix

$$\mathbf{D}\boldsymbol{\Phi}(q(t)) = \begin{bmatrix} \mathbf{Z}_{1/2}^- & \mathbf{Z}_{1/2}^+ & & & \\ & \ddots & & & \\ & & \ddots & & \\ & & & \mathbf{Z}_{M-1/2}^- & \mathbf{Z}_{M-1/2}^+ \end{bmatrix},$$

with

$$\mathbf{Z}_{m-1/2}^\pm = \pm d\boldsymbol{\Psi}(\mathbf{w}_{m-1/2}(t)) \cdot \mathbf{T}^{-1}(\pm \Delta s_{m-1/2} \mathbf{w}_{m-1/2}(t)),$$

where we have used the chain rule and (4.17). In the case of internal constraints which reduce the full Cosserat beam model to a Kirchhoff beam model or an inextensible Kirchhoff beam model, the derivative $d\boldsymbol{\Psi}$ is given explicitly, since $\boldsymbol{\Psi}$ is a linear function, see remarks 4.6 and 4.7.

In this discretized model with constraint function $\boldsymbol{\Phi}$ and Lagrange multipliers $\boldsymbol{\lambda}$, the potential and kinetic energy are given by $\mathcal{U}^d(q(t))$ and $\mathcal{T}^d(\mathbf{v}(t))$ respectively, and the equations of motion may be obtained as in remark 2.35 resulting in the form (2.31) in the Lie group $(\mathbb{S}^3 \times \mathbb{R}^3)^{M+1}$, where

$$\mathbf{f}(t, q(t), \mathbf{v}(t)) = -\left(\mathbf{D}\mathcal{U}^d(q(t))\right)^\top.$$

If we consider the components of this $(M + 1)$ -fold direct product, the equations of

motion take the following form:

$$\dot{q}_m = dL_{q_m}(e) \widehat{\mathbf{v}}_m, \quad (4.18a)$$

$$\frac{\Delta s_{1/2}}{2} \mathbf{N} \cdot \dot{\mathbf{v}}_0 = \frac{\Delta s_{1/2}}{2} \widehat{\mathbf{v}}_0^\top \cdot \mathbf{N} \cdot \mathbf{v}_0 + \mathbf{T}^{-\top}(-\Delta s_{1/2} \mathbf{w}_{1/2}) \cdot \mathbf{g}_{1/2}, \quad (4.18b)$$

$$\left. \begin{aligned} \frac{\Delta s_{m-1/2} + \Delta s_{m+1/2}}{2} \mathbf{N} \cdot \dot{\mathbf{v}}_m &= \frac{\Delta s_{m-1/2} + \Delta s_{m+1/2}}{2} \widehat{\mathbf{v}}_m^\top \cdot \mathbf{N} \cdot \mathbf{v}_m \\ &\quad + \mathbf{T}^{-\top}(-\Delta s_{m+1/2} \mathbf{w}_{m+1/2}) \cdot \mathbf{g}_{m+1/2} \\ &\quad - \mathbf{T}^{-\top}(\Delta s_{m-1/2} \mathbf{w}_{m-1/2}) \cdot \mathbf{g}_{m-1/2}, \end{aligned} \right\} m \neq 0, M, \quad (4.18c)$$

$$\frac{\Delta s_{M-1/2}}{2} \mathbf{N} \cdot \dot{\mathbf{v}}_M = \frac{\Delta s_{M-1/2}}{2} \widehat{\mathbf{v}}_M^\top \cdot \mathbf{N} \cdot \mathbf{v}_M \quad (4.18d)$$

$$- \mathbf{T}^{-\top}(\Delta s_{M-1/2} \mathbf{w}_{M-1/2}) \cdot \mathbf{g}_{M-1/2}, \quad (4.18e)$$

$$\mathbf{0} = \Delta s_{m-1/2} \Psi(\mathbf{w}_{m-1/2}), \quad m \neq 0, \quad (4.18f)$$

with the generalized internal forces

$$\mathbf{g}_{m-1/2} = \mathbf{C} \cdot (\mathbf{w}_{m-1/2} - \mathbf{w}_{m-1/2}^*) + d\Psi^\top(\mathbf{w}_{m-1/2}) \cdot \boldsymbol{\lambda}_{m-1/2}, \quad m \neq 0 \quad (4.18g)$$

for $m = 0, \dots, M$ where we have omitted the argument t .

Remark 4.8: *Visco-elastic material behavior.*

To include dissipation into the discretized Cosserat beam model, we follow along the lines of remark 4.3. First, we consider the time derivative of $\mathbf{w}_{m-1/2}(t)$ for $m = 1, \dots, M$:

$$\begin{aligned} \dot{\mathbf{w}}_{m-1/2}(t) &= \frac{d}{dt} \mathbf{w}_{m-1/2}(t) = \mathbf{D}_{q_m} \mathbf{w}_{m-1/2}(t) \cdot \mathbf{v}_m(t) + \mathbf{D}_{q_{m-1}} \mathbf{w}_{m-1/2}(t) \cdot \mathbf{v}_{m-1}(t) \\ &= \frac{1}{\Delta s_{m-1/2}} \left(\mathbf{T}^{-1}(\Delta s_{m-1/2} \mathbf{w}_{m-1/2}(t)) \cdot \mathbf{v}_m(t) \right. \\ &\quad \left. - \mathbf{T}^{-1}(-\Delta s_{m-1/2} \mathbf{w}_{m-1/2}(t)) \cdot \mathbf{v}_{m-1}(t) \right) \end{aligned}$$

using (4.17). If we plug the derivative vector with respect to space of the discretized curve $q^d(s, t)$ into the term (4.10) and approximate the integral over s by the chained midpoint rule, we end up with

$$\int_{t_0}^{t_e} \sum_{m=1}^M -2\Delta s_{m-1/2} \dot{\mathbf{w}}_{m-1/2}^\top \cdot \mathbf{V} \cdot \delta \mathbf{w}_{m-1/2}(t) dt$$

in the right-hand side of the variational principle (4.6), leading to the same equations of motion (4.18), but with generalized internal forces

$$\left. \begin{aligned} \mathbf{g}_{m-1/2}(t) &= \mathbf{C} \cdot (\mathbf{w}_{m-1/2}(t) - \mathbf{w}_{m-1/2}^*) + 2\mathbf{V} \cdot \dot{\mathbf{w}}_{m-1/2}(t) \\ &\quad + d\Psi^\top(\mathbf{w}_{m-1/2}(t)) \cdot \boldsymbol{\lambda}_{m-1/2}(t), \end{aligned} \right\} m = 1, \dots, M$$

instead of (4.18g).

Remark 4.9: *External forces and moments.*

External forces can, along the lines of remark 4.4, be included in the discretized Cosserat beam model. We consider the generalized force density

$$\mathbf{g}^{\text{ex}}(q^{\text{d}}, s, t) = \begin{bmatrix} \mathbf{M}^{\text{ex}}(q^{\text{d}}, s, t) \\ \mathbf{F}^{\text{ex}}(q^{\text{d}}, s, t) \end{bmatrix} \in \mathbb{R}^6$$

consisting of given external moments $\mathbf{M}^{\text{ex}}(q^{\text{d}}, s, t) \in \mathbb{R}^3$ and external forces $\mathbf{F}^{\text{ex}}(q^{\text{d}}, s, t) \in \mathbb{R}^3$ measured with respect to the body-fixed frame. We plug the discretized configuration curve $q^{\text{d}}(s, t)$ into (4.12) and approximate the inner integral by the chained trapezoidal rule:

$$\int_0^L (\mathbf{g}^{\text{ex}})^{\top}(q^{\text{d}}, s, t) \cdot \delta \mathbf{q}^{\text{d}}(s, t) \, ds \approx \sum_{m=0}^M (\mathbf{g}_m^{\text{ex}})^{\top}(q, t) \cdot \delta \mathbf{q}_m(t), \quad (4.19)$$

where

$$\begin{aligned} \mathbf{g}_0^{\text{ex}}(q, t) &= \frac{\Delta s_{1/2}}{2} \mathbf{g}^{\text{ex}}(q^{\text{d}}, 0, t), \\ \mathbf{g}_m^{\text{ex}}(q, t) &= \frac{\Delta s_{m-1/2} + \Delta s_{m+1/2}}{2} \mathbf{g}^{\text{ex}}(q^{\text{d}}, s_m, t), \quad m = 1, \dots, M-1, \\ \mathbf{g}_M^{\text{ex}}(q, t) &= \frac{\Delta s_{M-1/2}}{2} \mathbf{g}^{\text{ex}}(q^{\text{d}}, L, t). \end{aligned}$$

Now we can use

$$\mathcal{F}(t) = \begin{bmatrix} \mathbf{g}_0^{\text{ex}}(q, t) \\ \vdots \\ \mathbf{g}_M^{\text{ex}}(q, t) \end{bmatrix}$$

in remark 2.36. If we consider the resulting equations of motion in components, we end up with the same equations of motion (4.18), but with additional terms $+\mathbf{g}_m^{\text{ex}}(q, t)$ on the right-hand sides of (4.18b-d).

Note however, that this approach will neglect any narrow spikes of the external forces and moments, which might be crucial for the overall behavior of the beam. As an alternative we could use the total external generalized forces that act on a certain segment of the beam:

$$\begin{aligned} \mathbf{g}_0^{\text{ex}}(q, t) &= \int_0^{(s_0+s_1)/2} \mathbf{g}^{\text{ex}}(q^{\text{d}}, s, t) \, ds, \\ \mathbf{g}_m^{\text{ex}}(q, t) &= \int_{(s_{m-1}+s_m)/2}^{(s_m+s_{m+1})/2} \mathbf{g}^{\text{ex}}(q^{\text{d}}, s, t) \, ds, \quad m = 1, \dots, M-1, \\ \mathbf{g}_M^{\text{ex}}(q, t) &= \int_{(s_{M-1}+s_M)/2}^{s_M} \mathbf{g}^{\text{ex}}(q^{\text{d}}, s, t) \, ds. \end{aligned}$$

Moreover, we can model generalized forces $\mathbf{h}(q^{\text{d}}, t)$ that are applied at a specific point $s^* = s_m$ by setting:

$$\mathbf{g}_m^{\text{ex}}(q^{\text{d}}, t) = \mathbf{h}(q^{\text{d}}, t).$$

In case the generalized force is applied to a cross section at $s^* \in (s_{m-1}, s_m)$, we distribute the generalized force linearly to the neighboring nodes:

$$\mathbf{g}_{m-1}^{\text{ex}}(q^d, t) = \frac{s^* - s_m}{s_{m-1} - s_m} \mathbf{h}(q^d, t), \quad \mathbf{g}_m^{\text{ex}}(q^d, t) = \frac{s^* - s_{m-1}}{s_m - s_{m-1}} \mathbf{h}(q^d, t).$$

Remark 4.10: *Band structure.*

If we apply an integration method to solve the equations of motion of the spatially discretized Cosserat beam model with internal constraints, often a linear system with coefficient matrix

$$\begin{bmatrix} \mathbf{M} & \mathbf{D}\Phi^\top(q) \\ \mathbf{D}\Phi(q) & \mathbf{0} \end{bmatrix}$$

or similar structure has to be solved, see e.g. algorithms 1 and 3 for the RATTLie integration scheme and the algorithm of the Lie group generalized- α method [8, 9, 16]. The dimension M of the space grid might be large, such that the coefficient matrix is large as well. In order to solve such a system efficiently, we rearrange the unknowns and right-hand sides resulting in a coefficient matrix with band structure, see [9, 51].

The unknowns are related to derivative vectors and Lagrange multipliers at and in between the spatial nodes. Similarly, the right-hand sides are related to forces and geometric curvature terms at and in between the spatial nodes. Let us write

$$\begin{bmatrix} \mathbf{M} & \mathbf{D}\Phi^\top(q) \\ \mathbf{D}\Phi(q) & \mathbf{0} \end{bmatrix} \cdot \begin{bmatrix} \mathbf{V}_0 \\ \vdots \\ \mathbf{V}_M \\ \Lambda_{1/2} \\ \vdots \\ \Lambda_{M-1/2} \end{bmatrix} = \begin{bmatrix} \mathbf{G}_0 \\ \vdots \\ \mathbf{G}_M \\ \mathbf{C}_{1/2} \\ \vdots \\ \mathbf{C}_{M-1/2} \end{bmatrix}$$

and rearrange the unknowns and the components of the right-hand side with increasing index:

$$\mathbf{A} \cdot \begin{bmatrix} \mathbf{V}_0 \\ \Lambda_{1/2} \\ \mathbf{V}_1 \\ \Lambda_{3/2} \\ \vdots \\ \mathbf{V}_{M-1} \\ \Lambda_{M-1/2} \\ \mathbf{V}_M \end{bmatrix} = \begin{bmatrix} \mathbf{G}_0 \\ \mathbf{C}_{1/2} \\ \mathbf{G}_1 \\ \mathbf{C}_{3/2} \\ \vdots \\ \mathbf{G}_{M-1} \\ \mathbf{C}_{M-1/2} \\ \mathbf{G}_M \end{bmatrix},$$

then the resulting coefficient matrix \mathbf{A} has band structure.

5. Numerical Experiments

In this section, we will put the numerical algorithms developed in section 3 as well as the spatial discretization of the constrained Cosserat beam model from section 4 to the test. In order to do so, we will first introduce some example problems in section 5.1, namely the heavy top example, the rolling disk example, the flying spaghetti benchmark and the roll-up benchmark. In section 5.2 we will talk about the implementation of the numerical algorithms and the example problems. Finally, in section 5.3 we will present the results of the numerical experiments and give an interpretation to each one. Note that we have omitted all units by assuming that all quantities are given in their respective SI base units.

5.1. Examples and Benchmarks

In this section, we present in detail the example problems and benchmarks that will be used in the numerical examples.

Remark 5.1: *The fast and slow heavy top.*

The so-called heavy top is a well-known academic example that is used to study Lie group DAE integration schemes, see e. g. [16, 33]. It consists of a three-dimensional spinning top that is attached to the point of origin by a massless spherical joint. The initial position of the top's center of gravity is $\mathbf{x}_0 = [0, 1, 0]^\top$ and we consider this configuration of the top as its reference orientation. The mass of the top is $m = 15$ and the inertia tensor is $\mathbf{J} = \text{diag}(0.234375, 0.46875, 0.234375)$ with respect to the center of gravity of the top. The top is subjected to a constant gravitational field $\boldsymbol{\gamma} = [0, 0, -9.81]^\top$.

If we choose the Lie group $\mathbb{S}^3 \times \mathbb{R}^3$ as the configuration space, we have the kinetic and potential energies

$$\mathcal{T}(\mathbf{v}(t)) = \frac{1}{2} \mathbf{v}^\top(t) \cdot \mathbf{M} \cdot \mathbf{v}(t), \quad \mathcal{U}(q(t)) = -m \boldsymbol{\gamma}^\top \cdot \mathbf{x}(t),$$

with the mass matrix $\mathbf{M} = \text{blkdiag}(\mathbf{J}, m\mathbf{I}_{3 \times 3})$, the configuration variable $q(t) \in \mathbb{S}^3 \times \mathbb{R}^3$ with $q(t) = (p(t), \mathbf{x}(t))$ and derivative vectors $\mathbf{v}(t) = [\boldsymbol{\Omega}^\top(t), \mathbf{U}^\top(t)]^\top \in \mathbb{R}^6$, see section 2.2. Since the top is attached to the origin, we additionally need to consider the constraint $\mathbf{0} = \boldsymbol{\Phi}(q(t))$ with the constraint function

$$\boldsymbol{\Phi}(q(t)) = p^{-1}(t) \triangleright \mathbf{x}(t) - \mathbf{X},$$

where $\mathbf{X} = p_0^{-1} \triangleright \mathbf{x}_0$ is the reference position of the top and $p_0 \in \mathbb{S}^3$ is the initial orientation of the top. The equations of motion of the top then take the form (2.31), see remark 2.35, with

$$\begin{aligned} \mathbf{D}\mathcal{U}^\top(q(t)) &= \begin{bmatrix} \mathbf{0} \\ -mp^{-1}(t) \triangleright \boldsymbol{\gamma} \end{bmatrix}, \\ \mathbf{D}\boldsymbol{\Phi}(q(t)) &= [\text{skw}(\mathbf{X}), \mathbf{I}], \end{aligned}$$

where the latter equation holds for configurations $q(t)$ that fulfill the constraint equation $\mathbf{0} = \boldsymbol{\Phi}(q(t))$.

We distinguish between the scenario of the fast heavy top with initial angular velocity $\boldsymbol{\Omega}_0 = [0, 150, -4.61538]^\top$, see e. g. [16], and the scenario of the slow heavy top with lower initial angular velocity $\boldsymbol{\Omega}_0 = [0, 1.5, -0.0461538]^\top$, see [83]. We have considered the heavy top example in numerous different formulations including the ODE formulation in $SO(3)$, DAE formulations in the direct products $SO(3) \times \mathbb{R}^3$ and $\mathbb{S}^3 \times \mathbb{R}^3$, as well as DAE formulations in the semi-direct products $SE(3)$, $\mathbb{S}^3 \ltimes \mathbb{R}^3$ and UDQ , see section 2. The equations of motion for the different Lie group formulations can be found in appendix C.

The heavy top problem was implemented in the project `heavy_top`, see section 5.2.

Remark 5.2: *The rolling disk.*

This example consists of an infinitely thin disk of radius $r = 1$ that rolls without slip on the plane $H = \{[x, y, z]^\top \in \mathbb{R}^3 : z = 0\}$. The mass of the disk is $m = 15$ and the inertia tensor is $\mathbf{J} = mr^2 \text{diag}(1/4, 1/4, 1/2)$, calculated for the reference configuration of the disk $D^* = \{[x, y, z]^\top \in \mathbb{R}^3 : z = 0, x^2 + y^2 \leq r^2\}$ with respect to rotation around its center of mass. The disk is subjected to a constant gravitational field $\boldsymbol{\gamma} = [0, 0, -9.81]^\top$.

Similar to the heavy top in remark 5.1, we choose to represent the configuration of the disk by $q(t) = (p(t), \mathbf{x}(t)) \in \mathbb{S}^3 \ltimes \mathbb{R}^3$, where $p(t) \in \mathbb{S}^3$ is a unit quaternion representing the disk's orientation and $\mathbf{x}(t) \in \mathbb{R}^3$ is the position of the center of mass of the disk. The kinetic and potential energy are thus given by

$$\mathcal{T}(\mathbf{v}(t)) = \frac{1}{2} \mathbf{v}^\top(t) \cdot \text{blkdiag}(\mathbf{J}, m\mathbf{I}_3) \cdot \mathbf{v}(t), \quad \mathcal{U}(q(t)) = -m\boldsymbol{\gamma}^\top \cdot \mathbf{x}(t),$$

Here, $\mathbf{v}(t) = [\boldsymbol{\Omega}^\top(t), \mathbf{U}^\top(t)]^\top \in \mathbb{R}^6$ are the derivative vectors of $q(t)$, see section 2.2. It can easily be seen that

$$\mathbf{D}\mathcal{U}^\top(q(t)) = \begin{bmatrix} \mathbf{0} \\ -m(p(t))^{-1} \triangleright \boldsymbol{\gamma} \end{bmatrix}.$$

Since the disk is supposed to roll without slip on the plane H , the velocity of the point of the disk closest to H must vanish, see e. g. [69]. We assume the disk to be above H and not lying flat, so the point closest to H is the point of the disk's rim with the smallest z -coordinate. This velocity of the point on the disk closest to H expressed with respect to the body-fixed frame can be calculated by

$$\mathbf{U}_{\text{low}}(t) = \mathbf{U}(t) + \boldsymbol{\Omega}(t) \times \mathbf{X}_{\text{low}}(t),$$

where $\mathbf{X}_{\text{low}}(t)$ is the vector from the center of mass of the disk to the lowest point of the disk expressed with respect to the body-fixed frame. It holds

$$\mathbf{X}_{\text{low}}(t) = \begin{bmatrix} \frac{p_0 p_2 - p_1 p_3}{\sqrt{(p_0^2 + p_3^2)(p_1^2 + p_2^2)}} \\ \frac{p_0 p_1 + p_2 p_3}{\sqrt{(p_0^2 + p_3^2)(p_1^2 + p_2^2)}} \\ 0 \end{bmatrix},$$

where $p = [p_0, p_1, p_2, p_3]^\top \in \mathbb{S}^3$, omitting the argument t for readability. This can be worked out by applying the method of Lagrange multipliers and finding the stationary points of

$$(X_1, X_2, \lambda) \mapsto [0, 0, 1] \cdot (p(t) \triangleright [X_1, X_2, 0]^\top) - (X_1^2 + X_2^2 - 1^2)\lambda,$$

which gives two antipodal points; one corresponds to the point on the rim with maximal z -coordinate and one with minimal z -coordinate. Now we will consider the lowest point and its velocity with respect to the inertial frame:

$$\mathbf{x}_{\text{low}}(t) = p(t) \triangleright \mathbf{X}_{\text{low}}(t), \quad \mathbf{u}_{\text{low}}(t) = p(t) \triangleright \mathbf{U}_{\text{low}}(t).$$

Furthermore, we introduce the Cartesian coordinates

$$\mathbf{x}_{\text{low}}(t) = \begin{bmatrix} x_{\text{low},1}(t) \\ x_{\text{low},2}(t) \\ x_{\text{low},3}(t) \end{bmatrix}, \quad \mathbf{u}_{\text{low}}(t) = \begin{bmatrix} u_{\text{low},1}(t) \\ u_{\text{low},2}(t) \\ u_{\text{low},3}(t) \end{bmatrix}, \quad \mathbf{x}(t) = \begin{bmatrix} x_1(t) \\ x_2(t) \\ x_3(t) \end{bmatrix}.$$

The no-slip condition gives us that $\mathbf{u}_{\text{low}}(t) \equiv \mathbf{0}$. The third condition $u_{\text{low},3}(t) \equiv 0$ is actually integrable, since for

$$\phi(t) = x_3(t) + x_{\text{low},3}(t)$$

it holds

$$\frac{d}{dt}\phi(t) = u_{\text{low},3}(t).$$

The condition $x_3(t) = -x_{\text{low},3}(t)$ corresponds to the fact that the disk must touch the plane H . In order to simplify the equations and possibly increase efficiency of the implementation, we use $(x_3(t))^2/2 = (x_{\text{low},3}(t))^2/2$ as an equivalent condition and use the constraint function

$$\Phi(q) = \frac{1}{2}x_3^2 - \frac{1}{2}x_{\text{low},3}^2 = \frac{1}{2}x_3^2 - 2(p_1^2 + p_2^2)(p_0^2 + p_3^2),$$

omitting the argument t . Of course, this assumes that the initial values fulfill the original condition $x_3(t) = -x_{\text{low},3}(t)$. The derivative $\mathbf{D}\Phi(q)$ is given by

$$\mathbf{D}\Phi(q) = \begin{bmatrix} 2(p_0p_1 + p_2p_3)(p_1^2 + p_2^2 - p_0^2 - p_3^2) \\ 2(p_1p_3 - p_0p_2)(p_0^2 + p_3^2 - p_1^2 - p_2^2) \\ 0 \\ 2(p_1p_3 - p_0p_2)x_3 \\ 2(p_0p_1 + p_2p_3)x_3 \\ (p_0^2 + p_3^2 - p_1^2 - p_2^2)x_3 \end{bmatrix}^\top.$$

The other conditions $0 = u_{\text{low},2}(t)$ and $0 = u_{\text{low},1}(t)$ are not integrable, but they are linear in the derivative vector $\mathbf{v}(t)$. For easier notation and more efficient evaluation, we

scale these conditions with $x_3(t)$ and use that $x_3(t) = -x_{\text{low},3}(t)$. This means that the system is subject to linear nonholonomic constraints (2.41) with

$$\mathbf{B}(q) = \begin{bmatrix} -4(p_0p_2 + p_1p_3)(p_0p_1 + p_2p_3) & 4(p_0p_1 - p_2p_3)(p_0p_1 + p_2p_3) \\ -4(p_0^2p_2^2 + p_1^2p_3^2) & 4(p_0p_2 - p_1p_3)(p_0p_1 - p_2p_3) \\ 2(p_0p_1 - p_2p_3) & 2(p_0p_2 + p_1p_3) \\ (p_0^2 + p_1^2 - p_2^2 - p_3^2)x_3 & 2(p_1p_2 + p_0p_3)x_3 \\ 2(p_1p_2 - p_0p_3)x_3 & (p_0^2 - p_1^2 + p_2^2 - p_3^2)x_3 \\ 2(p_0p_2 + p_1p_3)x_3 & 2(p_2p_3 - p_0p_1)x_3 \end{bmatrix}^\top.$$

The equations of motion of the rolling disk now take the form (2.43). A plot of the trajectory of the disks center of mass can be found in figure 1 on page 97.

The rolling disk example was implemented in the project `rolling_disk`, see section 5.2. The project also contains a Mathematica script for the derivation of the holonomic and nonholonomic constraints.

Remark 5.3: *The flying spaghetti benchmark.*

The flying spaghetti benchmark is a benchmark problem featuring a soft, slender beam that first appeared in a paper of Simo and Vu-Quoc [73]. At one end of the initially straight beam of length $L = 10$, moments and forces are applied, first ramping up and subsequently ramping down until they vanish. The initial and undeformed configuration is given by

$$\mathbf{x}_0(s) = \begin{bmatrix} 6 \\ 0 \\ 0 \end{bmatrix} + \frac{s}{L} \mathbf{d}, \quad p_0(s) \equiv \begin{bmatrix} \cos(\pi/4) \\ \sin(\pi/4) \mathbf{e}_3 \times \mathbf{d} / \|\mathbf{d}\|_2 \end{bmatrix}$$

with

$$\mathbf{d} = \begin{bmatrix} -6 \\ 8 \\ 0 \end{bmatrix}$$

and vanishing initial angular velocities and velocities. The moments and forces

$$\mathbf{M}^{\text{ex}}(t) = \begin{bmatrix} 0 \\ -1/2 \\ -1 \end{bmatrix} g(t), \quad \mathbf{F}^{\text{ex}}(t) = \begin{bmatrix} 1/10 \\ 0 \\ 0 \end{bmatrix} g(t),$$

are applied at the right end of the beam ($s = L$) with

$$g(t) = \begin{cases} 200t/2.5, & t \in [0, 2.5] \\ 200(5 - t)/2.5, & t \in [2.5, 5] \\ 0, & t > 5 \end{cases}.$$

Initial conditions as well as applied moments and forces are depicted in figure 2 on page 97. The product of density and area of cross section is assumed to be

$$\rho|A| = 1$$

and the product of density and the inertia tensor density

$$\rho\mathbf{J} = \text{diag}(10, 10, 10).$$

Moreover, elastic material behavior is assumed and the material parameters are chosen to be

$$\mathbf{C}^{\mathbf{K}} = \text{diag}(5 \times 10^2, 5 \times 10^2, 5 \times 10^2), \quad \mathbf{C}^{\mathbf{I}} = \text{diag}(10^4, 10^4, 10^4).$$

In order to describe the beam, we use the Cosserat beam model constrained to an (extensible) Kirchhoff beam model as described in section 4.2 and discretize it with $M \in \mathbb{N}$ discretization intervals, see section 4.2.2. Snapshots of the solution of the flying spaghetti problem can be found in figure 3 on page 98.

This benchmark problem can be realized using the project `crmS3R3`, see section 5.2.

Remark 5.4: *Roll-up of a clamped beam.*

This benchmark problem features a heavily damped beam that is clamped at one end and on the other end a constant moment is applied. From a static analysis, see e. g. [32], it is known that if the moment is chosen in a special way, a configuration where both ends touch is an equilibrium point.

In this example, a Cosserat beam model, see section 4.2, of length $L = 10$ is used. The initial configuration is chosen to be

$$\mathbf{x}_0(s) = s\mathbf{e}_1, \quad p_0(s) \equiv \begin{bmatrix} \cos(\pi/4) \\ \sin(\pi/4)\mathbf{e}_3 \times \mathbf{e}_1 \end{bmatrix}$$

with vanishing initial angular velocity and velocity. As in the flying spaghetti benchmark, we assume the product of density and area of cross section to be

$$\rho|A| = 1$$

and the product of density and the inertia tensor density

$$\rho\mathbf{J} = \text{diag}(10, 10, 10).$$

In this benchmark, however, we assume viscoelastic material behavior with material parameters

$$\begin{aligned} \mathbf{C}^{\mathbf{K}} &= \text{diag}(5 \times 10^2, 5 \times 10^2, 5 \times 10^2), & \mathbf{C}^{\mathbf{I}} &= \text{diag}(10^4, 10^4, 10^4) \\ \mathbf{C}^{\dot{\mathbf{K}}} &= \text{diag}(10^2, 10^2, 10^2), & \mathbf{C}^{\dot{\mathbf{I}}} &= \text{diag}(10^2, 10^2, 10^2), \end{aligned}$$

where $\mathbf{V} = \text{blkdiag}(\mathbf{C}^{\dot{\mathbf{K}}}, \mathbf{C}^{\dot{\mathbf{I}}})$.

Similar to the flying spaghetti benchmark, the beam model was discretized in space as described in section 4.2.2 and a depiction of snapshots of the beam can be found in figure 4 on page 98.

This benchmark problem can be realized, just as the previous example, using the project `crmS3R3`, see section 5.2.

5.2. Implementation

In order to run numerical examples, we have implemented the integrators from section 3 and the discretized Cosserat beam model from section 4.2.2 as well as the examples from the previous section 5.1. For the implementation of the integrator and the problems, object-oriented Fortran 2003 was used. Everything was compiled under Linux using GNU make. In order to parametrize the problems, the script language Lua was used to write configuration files. These Lua configuration files can be read by the problem files as well as by Matlab, which was used to analyze the results and generate plots. For version control, Git was used and all implementations are now publicly available on GitHub under an MIT license.

In the following, we will present a list of Git projects that were implemented for this thesis:

- **RATTLie**: <https://github.com/StHante/RATTLie>
In this project, the Lie group time integration algorithm RATTLie, see section 3 was implemented. The project defines a Fortran module `RATTLie`, which contains the declaration of an abstract type `RATTLie_problem` with procedures for integration as well as deferred procedures for the problem-dependent subroutines and functions. These deferred procedures define e. g. the mass matrix, the applied generalized forces, generalized Coriolis forces, constraints and their derivatives, Lie group product, Lie group exponential map, tangential operator and its inverse, as well as initialization and output routines. The deferred procedures are specified by an abstract interface which defines the signature, i. e. input, output and result declarations. The abstract type `RATTLie_problem` has to be extended by the problem files, which also has to implement all deferred procedures.
- **RATTLie_nonhol**: https://github.com/StHante/RATTLie_nonhol
This project implements the nonholonomic version of the Lie group time integration method, see section 3.1.4. It is very similar to the project `RATTLie` in its structure, but additionally has deferred procedures in the problem type for the matrix of linear nonholonomic constraints and its derivative.
- **SHAKELie**: <https://github.com/StHante/SHAKELie>
In this project, the SHAKELie time integration method, see section 3.1.3, was implemented. It is likewise very similar to `RATTLie` in its structure. Note that the implementation is done with a constant extrapolation of the initial velocity \mathbf{v}_0 in order to determine the first $\mathbf{v}_{-1/2}$, which is needed in order to compute the first step.
- **heavy_top**: https://github.com/StHante/heavy_top
This project implements the heavy top problem, see remark 5.1, in different configuration spaces, see section 2.5 and appendix C. It can be used as a problem implementation for `RATTLie` and `SHAKELie` as well as for the projects `gena` and `BLieDF` that implement the Lie group generalized- α integration scheme [8] and the `BLieDF` scheme [85], see below.

The supported configuration spaces are $SO(3)$ and S^3 (as an ODE) as well as $SO(3) \times \mathbb{R}^3$, $S^3 \times \mathbb{R}^3$, $SE(3) = SO(3) \times \mathbb{R}^3$, $S^3 \times \mathbb{R}^3$ and UDQ (as a DAE). The Lie group, initial values, problem parameters such as mass, inertia tensor or gravity, as well as integrator options including the time step size can be specified. The fast and slow heavy top are described in the configuration files `diss_config_test_slow.lua` and `diss_config_test_fast.lua`, respectively, which are found in the `test` directory.

Furthermore, in the `test/als` subdirectory, there are Matlab functions that can be used to analyze the results of the computations easily. All tests with the heavy top example that are considered in this thesis can be run by executing the Matlab script `test/als/diss_test.m`.

- **rolling_disk**: https://github.com/StHante/rolling_disk
In this project, the rolling disk example, see remark 5.2, is implemented. It can be used as a test problem for the nonholonomic RATTLie integrator `RATTLie_nonhol`. The project has a similar structure to the `heavy_top` project, with configuration files controlling the parameters of the problem and the integrator. The configuration that was used in this thesis can be found in `test/diss_conf.lua`. All tests with the rolling disk example can be run by executing the Matlab script `test/als/diss_test.m`.
- **crmS3R3**: <https://github.com/StHante/crmS3R3>
This project implements the spatial discretization of the Cosserat beam model described in section 4.2. It supports the full Cosserat beam model as well as constraining it to an extensible Kirchhoff beam model, see remark 4.6. It can be used, just as `heavy_top`, as a test problem for the integrator projects `RATTLie`, `SHAKELie`, `gena` and `BLieDF`.

It likewise features a similar structure to the `heavy_top` project with configuration files controlling the parameters of the beam and the integrator. The configuration for the flying spaghetti, see remark 5.3, can be found in the `test/diss_test_fs_*.lua` configuration files and the configuration for the roll-up example, see remark 5.4, can be found in the file `test/diss_test_rollup.lua`. All tests with the Cosserat beam model that are considered in this thesis can be run by executing the Matlab scripts `test/als/diss_test.m` and `test/als/diss_test_rollup.m`. Note that the tests have a rather high computation time and produce a lot of data. Therefore, the scripts should be executed cell by cell.

For more information on the different projects, refer to the corresponding readme files. All of the above projects possess a Git tag `Dissertation_StHante`, which can be checked out in order to mark the version of the projects that were used to perform the numerical experiments in this thesis.

Furthermore, we have used the following projects that were written by the author of this thesis, including implementations of the Lie group generalized- α and `BLieDF` integrators:

- **gena**: <https://github.com/StHante/gena>
This project implements the Lie group generalized- α scheme [16], see also [7, 8, 18, 21], in Fortran. It is structured very similar to the RATTLie project with a module that contains an abstract type with deferred procedures. Note that here the applied generalized forces have to include the Coriolis terms, whereas they are treated separately by RATTLie.
- **BLieDF**: <https://github.com/StHante/BLieDF>
In this project, the BLieDF method [61, 84, 85] up to $k = 2$ is implemented. It is likewise structured similarly to the RATTLie and gena projects.
- **liegroup**: <https://github.com/StHante/liegroup>
This Fortran project provides several modules that implement functions relating to cross product, quaternions, the Lie groups \mathbb{S}^3 and $\mathbb{S}^3 \times \mathbb{R}^3$, see appendix A, as well as functions with a removable singularity, see appendix B, that appear in coefficients of Lie group exponential functions and their various derivatives.
- **expandconfig**: <https://github.com/StHante/expandconfig>
This program written in plain C is used to pre-process the configuration files of the implementations of the test problems for describing a whole test series in just one configuration file.
- **readLua**: <https://github.com/StHante/readLua-for-Matlab-and-Octave>
This project implements a Matlab and Octave function `readLua` which can be used to read the Lua configuration files in Matlab and Octave. The function is realized as a MEX function written in C.

In addition, we will mention a few tools and libraries that were used in the implementation:

- **Gfortran** from the GNU Compiler Collection:
This compiler (version 8.3.0) has been used to compile all the Fortran code.
- **Aotus**: <https://geb.sts.nt.uni-siegen.de/doxy/aotus/>
This library allows to read Lua files in Fortran. It works by providing a Fortran wrapper to the C-API of Lua.
- **GNU Parallel**: [79]
This tool allows for parallel execution of code. It has been used to run several tests in parallel on separate CPUs.

5.3. Results and Interpretation

In this section, we will discuss the results of numerical experiments with the examples from section 5.1, which were implemented according to the previous section 5.2. All figures can be found starting from page 97.

A lot of the following experiments involve the absolute error of some variable \mathbf{y} . This means that the numerical algorithm has calculated a sequence

$$\mathbf{y}_n \approx \mathbf{y}(t_n), \quad n = 0, \dots, N,$$

where N is the number of time steps and $t_0 < t_1 < \dots < t_N$ is the time grid on which the algorithm has calculated an approximation to the exact solution $\mathbf{y}(t_n)$ for all $n = 1, \dots, N$. Most of the experiments use a fixed time step size of the form $h = 2^{-\ell}$ with $\ell \geq 7$ or $\ell \geq 8$. In order to calculate the absolute error in \mathbf{y} in these cases, we have used the following formula:

$$\max_{n=n^*, 2n^*, \dots, N} \|\mathbf{y}_n - \mathbf{y}(t_n)\|_{L^2},$$

where we have used the discrete L^2 norm defined by

$$\left\| \begin{bmatrix} y_1 \\ \vdots \\ y_N \end{bmatrix} \right\|_{L^2} = \sqrt{\frac{1}{N} \sum_{a=1}^N y_a^2}$$

and $n^* = 2^{-\ell^*} / h$ with $\ell^* = 7$ or $\ell^* = 8$. Of course, instead of using the exact solution, which is usually not available, we compare to the results of a numerical solution $y_{n^{\text{ref}}} \approx y(t_{n^{\text{ref}}}^{\text{ref}})$ for $n^{\text{ref}} = 0, \dots, N^{\text{ref}}$ with much smaller time step size $h^{\text{ref}} = t_1^{\text{ref}} - t_0^{\text{ref}} \ll h$.

Note also that we have considered Lie group elements as elements of the surrounding vector space in order to calculate errors. This is possible since Lie groups locally resemble Euclidean space and therefore these errors calculated in the surrounding vector space are a good measure for the distances of the elements in question, assuming they are sufficiently close to each other. The alternative, using a notion of distance independent of the surrounding space, is a lot more difficult to implement. Except for the calculation of errors, Lie group elements are never treated as elements of the surrounding space in this thesis.

Remark 5.5: *RATTLie.*

We want to investigate if the convergence of the RATTLie method can be observed numerically. First, we can have a look at the results of the fast and slow heavy top examples, see remark 5.1. In figures 5 and 6, the absolute error in the configuration q against the step size of the RATTLie scheme is depicted. We can clearly see the slope of 2 for any Lie group, indicating a second order convergence of RATTLie in q . In figure 5, the error begins to saturate at the level of the absolute tolerance `atol` of the Newton-Raphson method which was chosen to be 10^{-8} .

Similarly, we can observe second order convergence of RATTLie in q in figure 7, where the absolute errors of the flying spaghetti benchmark, see remark 5.3, are depicted over the time step sizes. We can also see second order convergence of RATTLie in the derivative vectors \mathbf{v} in figure 8. Concerning the Lagrange multipliers, we can observe second order convergence of RATTLie in figure 9, at least of the separately calculated Lagrange multipliers, see algorithm 3. Note that for very fine time step sizes, we can

observe an error saturation of the separately calculated Lagrange multipliers in the realm of, again, the absolute tolerance `atol` of the Newton-Raphson method. For the discussion of the interpolated Lagrange multipliers, see remark 5.10.

In summary, numerical convergence of second order, which was analytically shown in section 3.2, can indeed be observed.

Remark 5.6: *Comparison of RATTLie with competing Lie group integration schemes.*

In figures 7, 8 and 9, we have shown the absolute errors of different Lie group integration methods such as the generalized- α scheme [16], see also [7, 8, 18, 21], the BLieDF method of second order, see [61, 84, 85], as well as SHAKELie, see section 3.1.3. In this remark, we will compare RATTLie to the former two; SHAKELie will be discussed later in remark 5.9. Note that both the generalized- α method as well as the BLieDF method were applied in their stabilized index-2 formulation, avoiding error amplification for small time step sizes, see [6, 8, 31]. We can observe that both methods converge in q , \mathbf{v} , and $\boldsymbol{\lambda}$ with second order. For the generalized- α method, the convergence was proved in [7] and for BLieDF with $k = 2$ in [85]. In the absolute errors in the configuration q , it can be seen that the RATTLie method is more accurate by a factor between 10 and 100. Concerning the errors in the derivative vectors \mathbf{v} , RATTLie is still overall the most accurate of the three methods, but here the factor is only between 1 and 10. Roughly the same holds true for the Lagrange multipliers $\boldsymbol{\lambda}$, considering the separately calculated Lagrange multipliers of RATTLie. We can observe error saturation in the Lagrange multipliers of all three methods for very small time step sizes.

It can be seen that the behavior of BLieDF and the generalized- α scheme changes slightly between $h = 2^{-14} \approx 6 \times 10^{-5}$ and $h = 2^{-15} \approx 3 \times 10^{-5}$. Interestingly, this is exactly the range where SHAKELie's errors start to increase. We have seen in other tests whose results are not shown here that the errors of the Lagrange multipliers start to increase for the index-3 formulations of the generalized- α and the BLieDF method. This points to the presumption that this change in convergence behavior is due to the stabilization of the generalized- α and BLieDF schemes becoming necessary. Note that RATTLie needs no stabilization since it automatically fulfills the hidden constraints on the velocity level.

Overall, it can be seen that, at least for the example of the flying spaghetti benchmark, RATTLie outperforms both the generalized- α method as well as the BLieDF method of second order when it comes to accuracy.

Remark 5.7: *The choice of the Lie group.*

Let us consider the fast heavy top once more. Figure 5 shows the absolute error over the various step sizes using different Lie groups as the configuration space. The errors were calculated by first transforming all configurations to $SO(3) \times \mathbb{R}^3$ in order to have a better comparison of the magnitude of the errors independent of the representation of the configuration. It can be seen that the errors are not influenced by the choice of parametrization of rotations, but the errors in this example are generally smaller by

a factor between 10 and 100 if a direct product Lie group is chosen, compared to a semi-direct product structure. In [17], it was shown for the generalized- α scheme that this relationship inverts when the slow heavy top is considered. We have confirmed this in our own numerical tests with the generalized- α method, but we can observe something different for RATTLie: Figure 6 shows the absolute errors for the slow heavy top and we can see that here the direct products are still more accurate. This difference might be due to the fact that RATTLie directly incorporates the Coriolis forces in its algorithm, whereas the generalized- α and the BLieDF scheme consider them together with the external forces.

Let us now talk about computing times: In figure 10, the average computing times for the various Lie groups relative to $SE(3)$ over the time step sizes are depicted. Naturally, the computing times of the direct products are generally lower than those of the semi-direct products, since the algebraic expressions for exponential map, tangential operator, and their derivatives are more involved for semi-direct products. It can be seen that the Lie group formulations with quaternions are generally a little faster than those with rotation matrices, since there are less parameters and less floating-point operations per Lie group operation and exponential map, see [42]. The computing times for $S^3 \times \mathbb{R}^3$ are smaller than those for the unit dual quaternions UDQ , see remark 2.33, since unit dual quaternions require more parameters and more floating-point operations, see [42]. Additionally, they provide less insight since the translation vector is not directly available. Note that for coarse time step sizes, the computing times are very small and cannot be sensibly compared.

Summarizing, we can say that using quaternions is faster than using rotation matrices and using direct products is faster and – in this example – produces more accurate results than using semi-direct products.

Remark 5.8: *The nonholonomic RATTLie scheme.*

In this remark, we want to examine the numerical convergence behavior of the nonholonomic RATTLie scheme, see section 3.1.4. In order to do so, we consider the rolling disk example, see remark 5.2. We have depicted the absolute errors in the configuration variables q , the derivative vectors \mathbf{v} , the Lagrange multipliers corresponding to the holonomic constraints $\boldsymbol{\lambda}$, as well as the Lagrange multipliers corresponding to the nonholonomic constraints $\boldsymbol{\eta}$ over the step size in figure 11. Note that the Lagrange multipliers were separately calculated, see algorithm 3. We can clearly see that the errors decrease with decreasing time step size with second order. This suggests that the nonholonomic RATTLie scheme might be second order convergent, although an analytic proof has not been given for this particular integration method and remains an open problem.

Remark 5.9: *SHAKELie.*

Let us again consider the flying spaghetti benchmark problem. The absolute errors in the configuration variables, the derivative vectors and the Lagrange multipliers are shown in

figures 7, 8, and 9. This time, we will concentrate on the SHAKELie method. It can be seen that SHAKELie produces very similar results to RATTLie for time step sizes larger than 10^{-4} . For smaller time step sizes, however, the errors start to increase. This increase can be seen most clearly in the Lagrange multipliers, where we see an increase with second order. This behavior is known from the SHAKE method [35]. It appears to be similar to the problems of integration methods that directly discretize the index-3 formulation of the equations of motion [6]. Since the erroneous Lagrange multipliers that are calculated in one step are directly used in the next step, the error bleeds through to the configuration and derivative vectors.

It is obvious that the SHAKELie method is inferior to the RATTLie method since the latter does not show such problems and respects the hidden constraints on the velocity level.

Remark 5.10: *RATTLie and Lagrange multipliers.*

We have already seen in figure 9 that the two ways of calculating the Lagrange multipliers for the RATTLie scheme differ in their accuracy, especially for small time step sizes. Let us now consider figure 12, where we have additionally shown the absolute errors in the Lagrange multipliers λ^+ and λ^- of RATTLie over the time step size. It can be seen that the errors in both λ^+ and λ^- decrease with first order, as shown in section 3.2.3, for coarse time step sizes. Unfortunately, they increase for step sizes smaller than 10^{-4} with second order, similarly to Lagrange multipliers for schemes that directly discretize the index-3 formulation of the equations of motion. Since the interpolated Lagrange multipliers are calculated from λ^+ and λ^- they surely have to inherit this error increase. The error in the interpolated Lagrange multipliers decreases with second order for coarse time step sizes, as shown in section 3.2.3, but – surely enough – the order drops to one for smaller time step sizes, similar to the error increase of λ^\pm . An in-depth analysis of this problem, which is not reproduced in this thesis, has shown that the expression for λ^+ involves a term that approximates $\dot{\mathbf{v}}$ as it appears on the right-hand side of (3.16) from SHAKELie, which is subject to a similar loss of significance, see remark 5.9. All our attempts of correcting this error by techniques using insights from [6] have failed, even in the case of a linear Lie group as the configuration space.

In summary, the separately calculated Lagrange multipliers should be used for fine time step sizes, while the interpolated Lagrange multipliers are slightly less computationally costly and are acceptable for coarse step sizes.

Remark 5.11: *RATTLie and irregular time grids.*

Up to now, we have considered the RATTLie integration scheme only with constant time step sizes. In this remark, we investigate RATTLie with varying time step sizes. In figure 13, we have depicted the absolute errors of the flying spaghetti benchmark, see remark 5.3, that were calculated with RATTLie and varying time step sizes with the maximal step size h_{\max} . The step sizes were chosen pseudo-randomly in $[h_{\max}/4, h_{\max}]$. We can clearly see second order convergence in the configuration variables q , the derivative

vectors \mathbf{v} as well as the separately calculated Lagrange multipliers, as we have predicted in section 3.2.3. For the interpolated Lagrange multipliers, we can see that the order seems to drop to one, similar to the constant time step size scenario, see remark 5.10.

This shows that variable time step sizes can be easily implemented in RATTLie without any changes to the algorithm. Similar results have been shown for RATTLE in [10] but with the need of introducing a time transformation. Together with a suitable error estimator, RATTLie could be extended to an integration scheme with adaptive step size sequences.

Remark 5.12: *RATTLie energy behavior.*

RATTLie was constructed using the framework of variational integrators. Since variational integrators are known to preserve a perturbed energy for conservative systems [63], we expect that if we use RATTLie to simulate a conservative system like the fast heavy top, see remark 5.1, there should be no systematic drift in the mechanical energy of the system. In figure 14 we have shown the mechanical energy of the fast heavy top over time computed with RATTLie, BLieDF of second order and the Lie group generalized- α scheme with $\rho_\infty = 0.9$. For the generalized- α scheme and BLieDF, we can see a systematic loss of energy of the actually conservative heavy top example. This was to be expected, since one of the strengths of the generalized- α scheme is to damp high oscillations effectively, while conserving a lot of the low frequencies; the BLieDF on the other hand is the generalization of the A-stable two-step BDF method. Note that the initial energy jump for BLieDF is likely due to the starting method, which is the implicit Lie group Euler method; a generalization of the implicit Euler method or the one-step BDF method. For RATTLie, however, the energy stays almost constant, only showing a slight oscillation around the initial energy.

This means that RATTLie is especially useful in scenarios with little to no damping or if energy conservation is a concern.

Remark 5.13: *Convergence in space of the discrete constrained Cosserat beam model.*

Let us now consider the spatial discretization of the Cosserat beam model. We have again considered the flying spaghetti benchmark problem with Kirchhoff constraints, see remark 5.3, and simulated it using RATTLie with $h = 2^{-15} \approx 3.05 \times 10^{-5}$ and a varying number of spatial discretization intervals. The absolute errors are shown in figure 15.

Note that the errors were calculated interpolating the beam at $s/L = 0, 1/16, \dots, 1$ and comparing the errors at $t = 15$ in these 17 interpolated points. The interpolation in the configuration variables q was done using remark 2.27, while \mathbf{v} and $\boldsymbol{\lambda}$ were interpolated piecewise linearly.

We can see that the absolute errors in q clearly decrease with second order, the errors in \mathbf{v} decrease with second order, but show a saturation for large M . This saturation could be due to the fact that we had to use finite time steps or that the piecewise linear interpolation in \mathbf{v} is not compatible with the semi-direct product structure of the configuration space $\mathbb{S}^3 \times \mathbb{R}^3$. The errors in the Lagrange multipliers decrease with at

least first order, while the order seems to increase for larger M . This first order could be a similar effect to the one-sided Lagrange multipliers in RATTLie, see remark 5.10, or even to the Lagrange multipliers in SHAKELie, since we have not split up the Lagrange multipliers in two one-sided limits in the spatial discretization of the Cosserat beam like we have done in the derivation of RATTLie. Here, additional analysis is required.

These results show that the spatial discretization converges numerically and indicate that the convergence order might be 2 for q and v and 1 or 2 for λ , although this has not been proved analytically.

Remark 5.14: *Locking.*

In this remark, we will consider the roll-up example, see remark 5.4, and simulate it using the generalized- α method ($\rho_\infty = 0.9$) with $h = 2^{-10} \approx 9.7 \times 10^{-4}$ and $h = 2^{-16} \approx 1.5 \times 10^{-5}$. In figure 4, we have shown snapshots of the heavily damped and clamped Cosserat beam model, where we can see how applying the correct amount of moments results in the beam forming a perfect circle. In figures 16 and 17 we have depicted the distance between both ends as well as the velocities of the end points. We can observe that at $t = 30$, both ends have the same position and orientation up to 10^{-3} and are barely moving.

This shows that the spatial discretization of the Cosserat beam model does not suffer from shear locking. Shear locking manifests itself in an artificial increase of the bending stiffness of the beam in configurations where the beam undergoes large spatial deformations. It is known that the lack of shear locking is connected to the semi-direct product structure of the configuration space, see e. g. [55, 76].

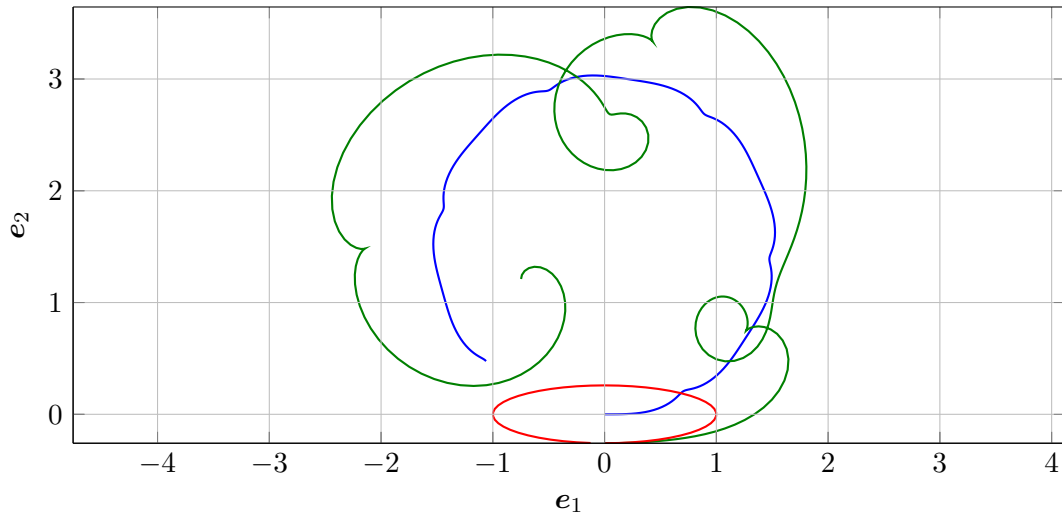


Figure 1: Rolling disk: Top view: Trajectory of the midpoint of the disk (blue), trajectory of a point on the edge of the disk (green) as well as the initial configuration of the disk (red).

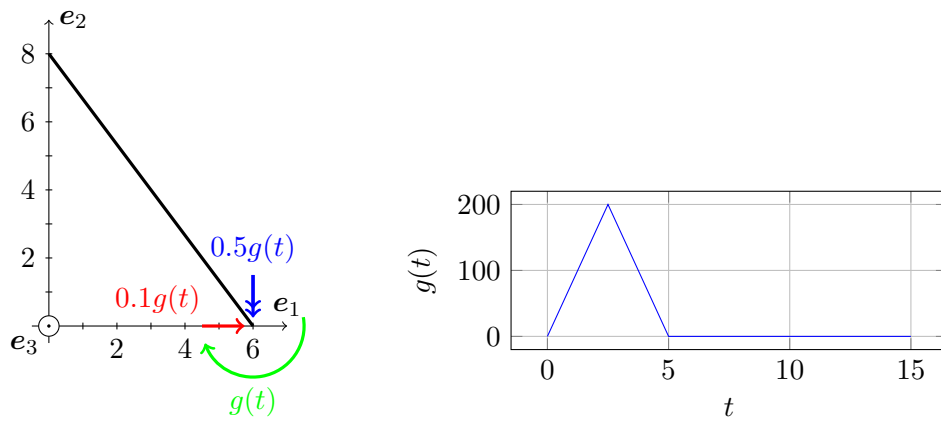


Figure 2: Description of the flying spaghetti benchmark [73]: Initial position as well as applied forces and moments on the left and the magnitude of the forces and moments on the right.

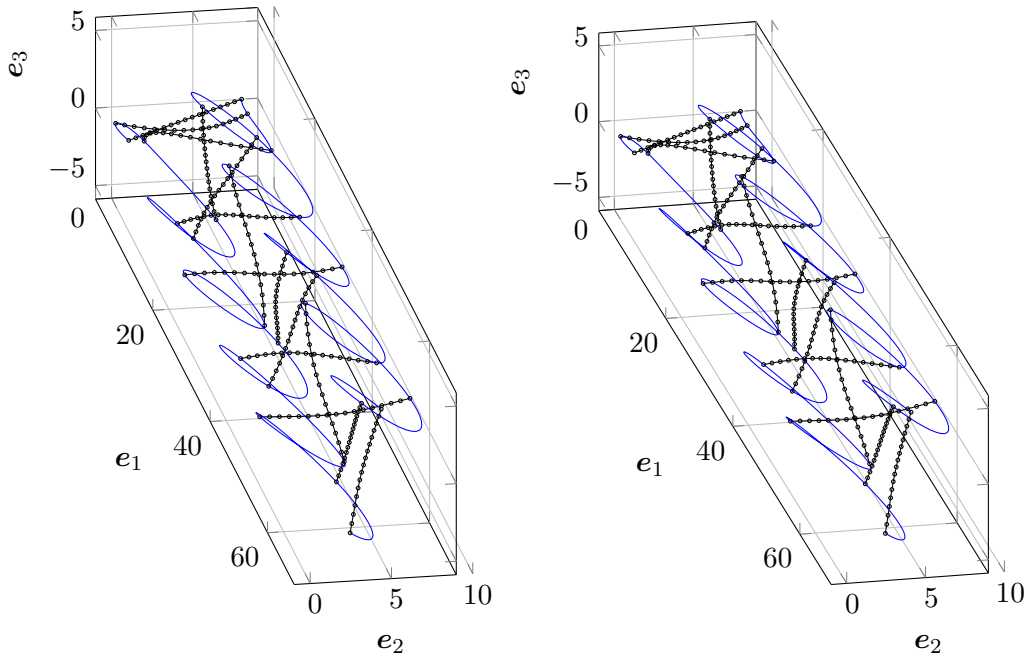


Figure 3: Flying spaghetti: Snapshots of the configuration with $M = 16$ beam segments at $t = 0, 2, 3, 4, \dots, 15$ and the trajectory of the end points in blue. The reader should cross their eyes in order to perceive a three-dimensional image.

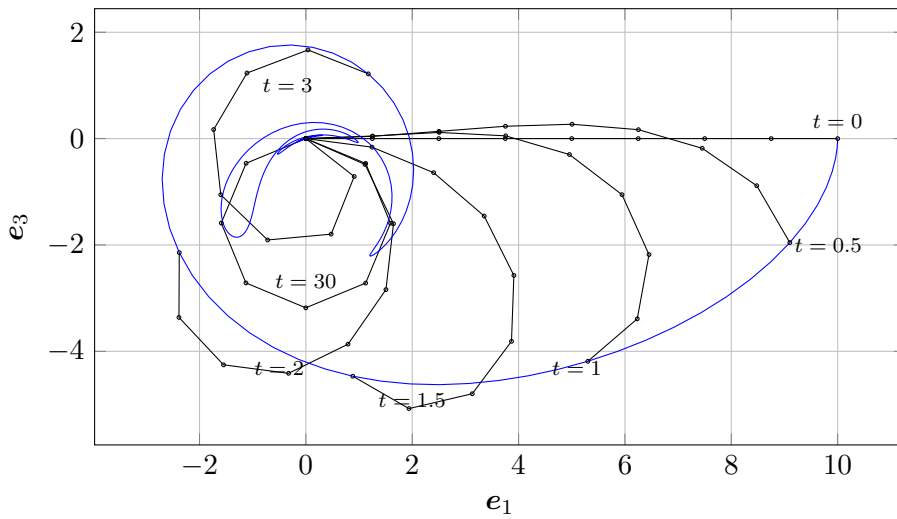


Figure 4: Roll-up: Snapshots of the configuration with $M = 8$ beam segments at $t = 0, 0.5, 1, 1.5, 2, 3, 30$ and the trajectory of the right end point in blue.

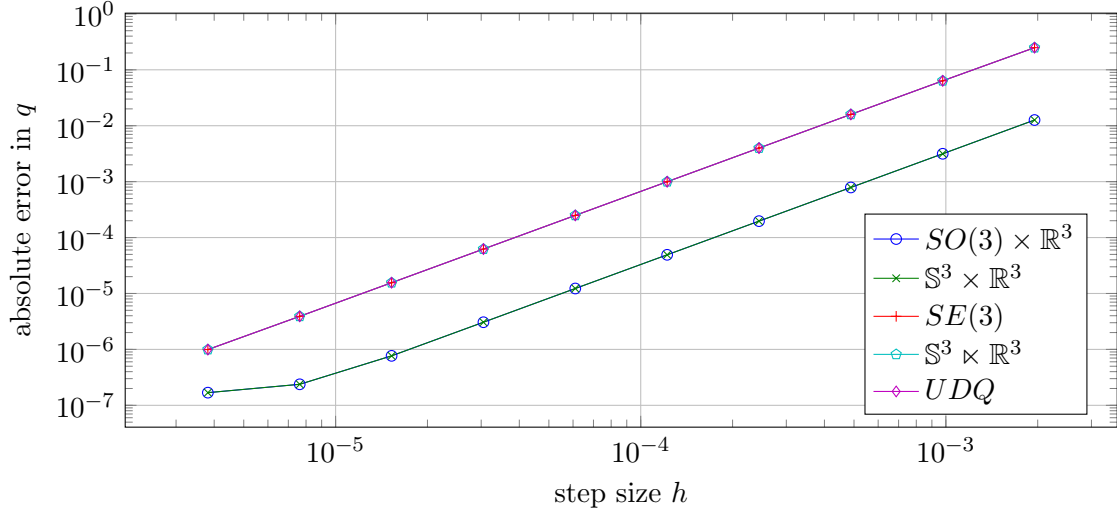


Figure 5: Fast heavy top: Maximum of the absolute discretized L^2 error in the configuration variable q expressed in $SO(3) \times \mathbb{R}^3$. Results were calculated with RATTLie, the reference solution with the generalized- α method ($\rho_\infty = 0.9$) in the Lie group $SO(3)$ and $h = 2^{-21} \approx 4.8 \times 10^{-7}$. The data for $SO(3) \times \mathbb{R}^3$ and $\mathbb{S}^3 \times \mathbb{R}^3$ closely coincide as well as the data for $SE(3)$, $\mathbb{S}^3 \times \mathbb{R}^3$, and UDQ .

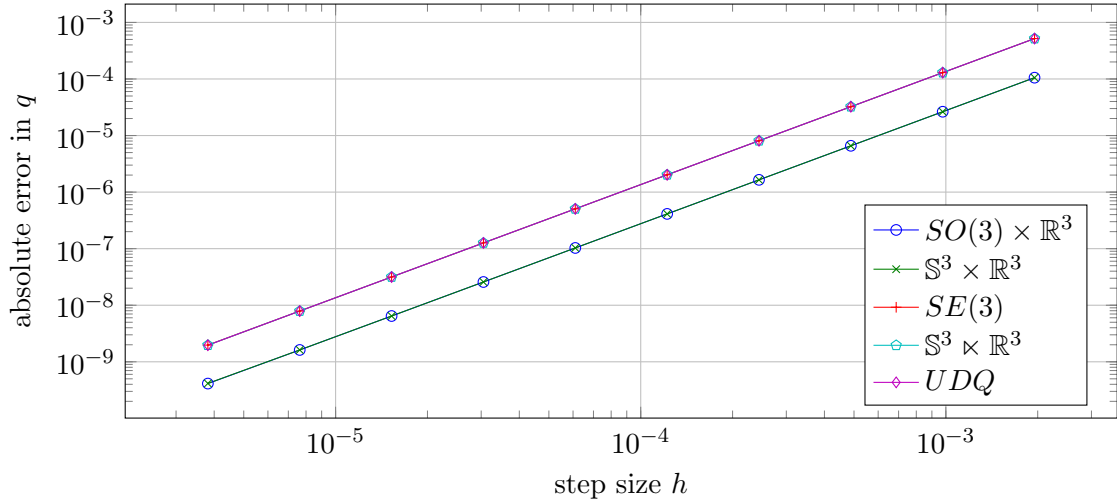


Figure 6: Slow heavy top: Maximum of the absolute discretized L^2 error in the configuration variable q expressed in $SO(3) \times \mathbb{R}^3$. Results were calculated with RATTLie, the reference solution with the generalized- α method ($\rho_\infty = 0.9$) in the Lie group $SO(3)$ and $h = 2^{-21} \approx 4.8 \times 10^{-7}$. The data for $SO(3) \times \mathbb{R}^3$ and $\mathbb{S}^3 \times \mathbb{R}^3$ closely coincide as well as the data for $SE(3)$, $\mathbb{S}^3 \times \mathbb{R}^3$, and UDQ .

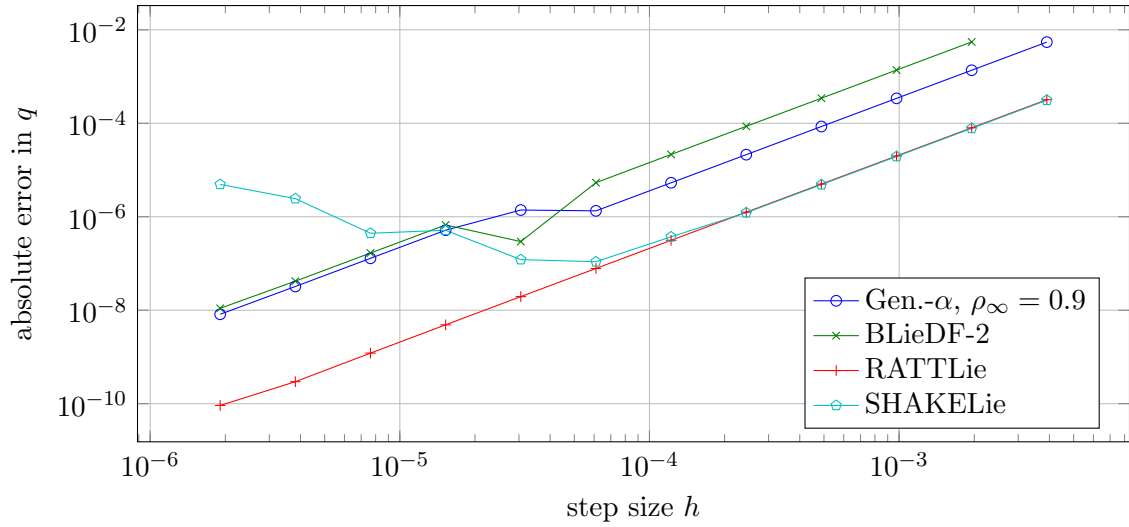


Figure 7: Kirchhoff beam model: Flying spaghetti: Maximum of the absolute discretized L^2 error in the configuration variables q with different integration schemes. The reference solution was calculated with RATTLie and $h = 2^{-20} \approx 9.5 \times 10^{-7}$.

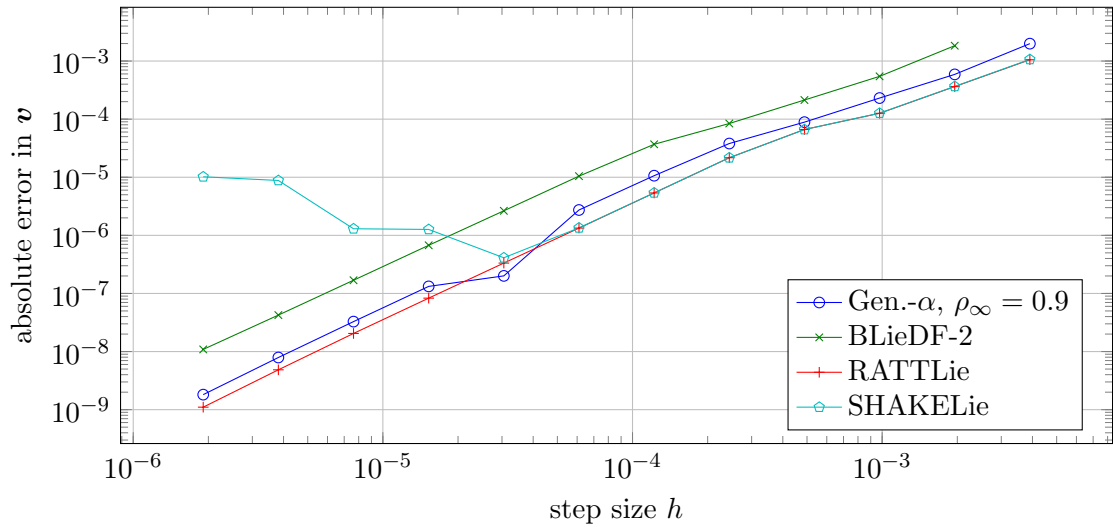


Figure 8: Kirchhoff beam model: Flying spaghetti: Maximum of the absolute discretized L^2 error in the derivative vectors v with different integration schemes. The reference solution was calculated with RATTLie and $h = 2^{-20} \approx 9.5 \times 10^{-7}$.

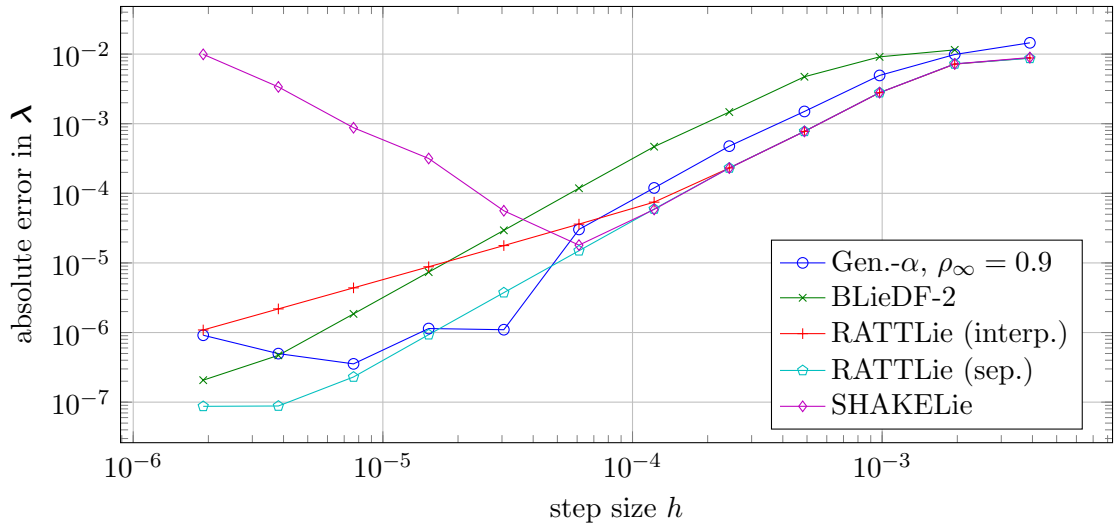


Figure 9: Kirchhoff beam model: Flying spaghetti: Maximum of the absolute discretized L^2 error in the Lagrange multiplier λ with different integration schemes. The reference solution was calculated with RATTLie (separately calculated λ) and $h = 2^{-20} \approx 9.5 \times 10^{-7}$.

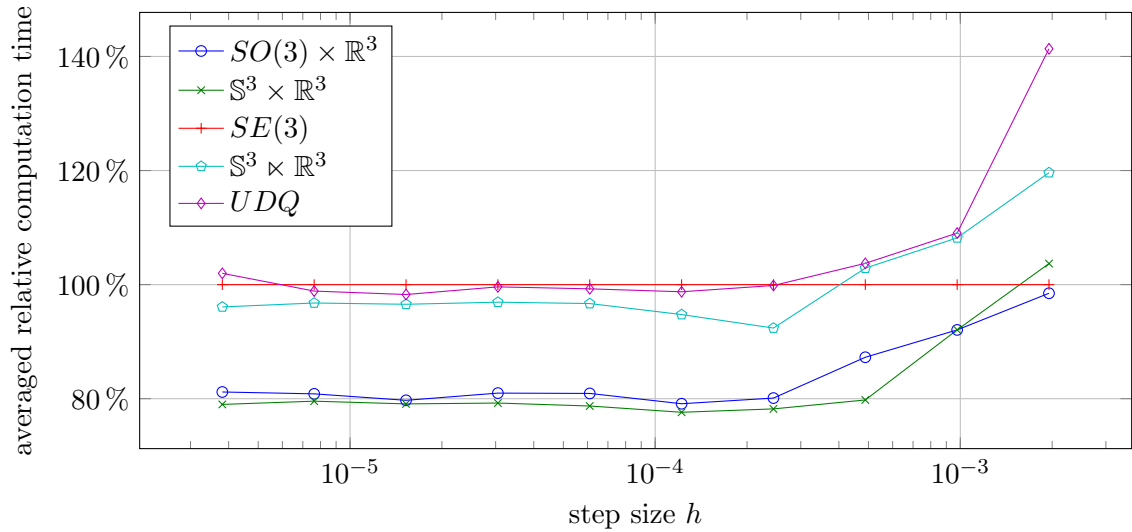


Figure 10: Fast heavy top: Average computation time compared to the computation time with Lie group $SE(3)$. Results were calculated with RATTLie. The relative computation times have been averaged over 100 runs.

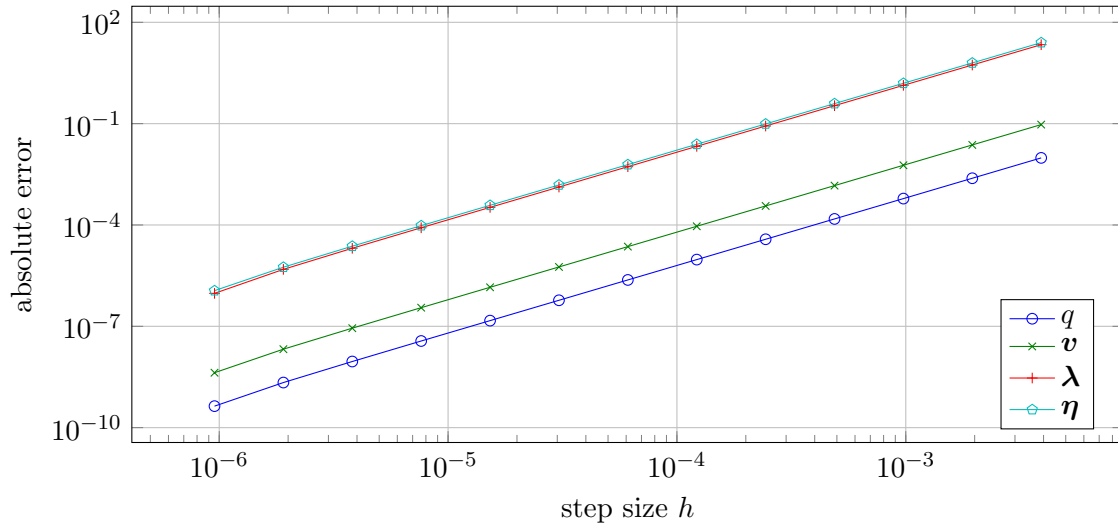


Figure 11: Rolling disk: Maximum of the absolute discretized L^2 error in the configuration variables q , the derivative vectors \mathbf{v} , the Lagrange multipliers corresponding to the holonomic constraints $\boldsymbol{\lambda}$ and the Lagrange multipliers corresponding to the nonholonomic constraints $\boldsymbol{\eta}$. Results were calculated with the nonholonomic RATTLie; the reference solution with $h = 2^{-21} \approx 4.7684 \times 10^{-7}$.

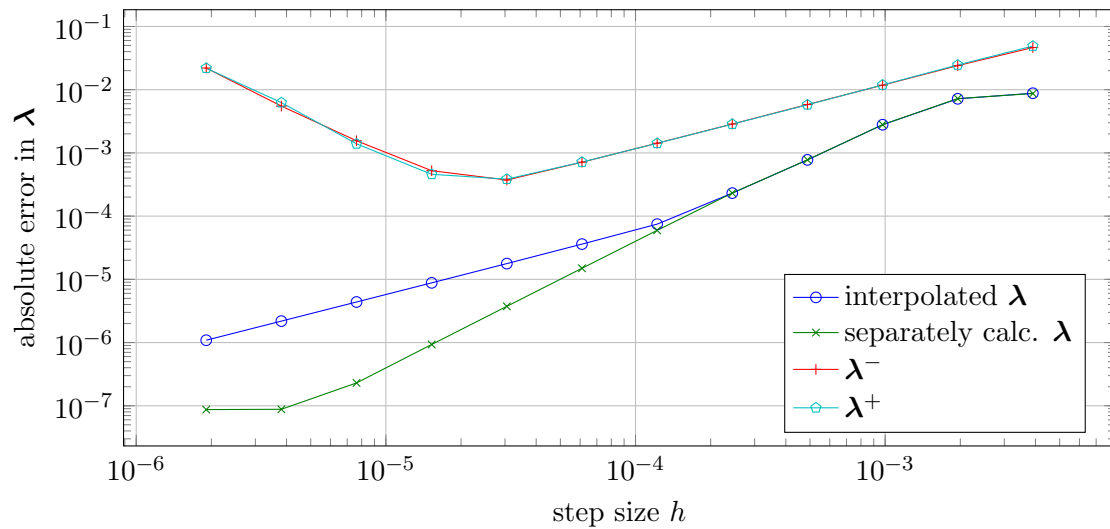


Figure 12: Kirchhoff beam model: Flying spaghetti: Maximum of the absolute discretized L^2 error in the different approximations to the Lagrange multiplier $\boldsymbol{\lambda}$. The reference solution was calculated with RATTLie (separately calculated $\boldsymbol{\lambda}$) and $h = 2^{-20} \approx 9.5 \times 10^{-7}$.

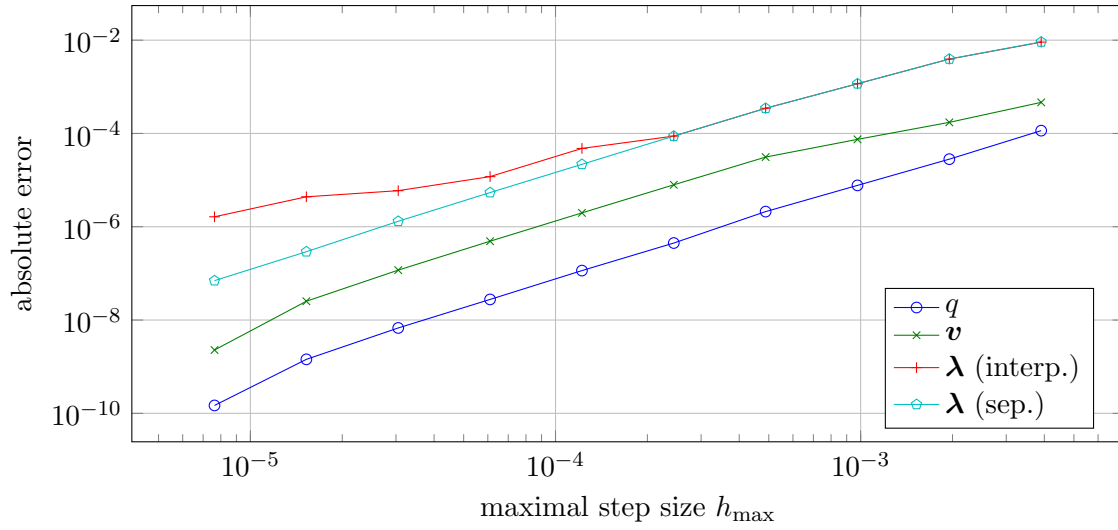


Figure 13: Kirchhoff beam model: Flying spaghetti: Maximum of the absolute discretized L^2 error in q , v and λ with RATTLie and variable step sizes that were chosen pseudo-randomly between h_{\max} and $h_{\max}/4$. The reference solution was calculated with RATTLie and $h = 2^{-18} \approx 3.8 \times 10^{-6}$.

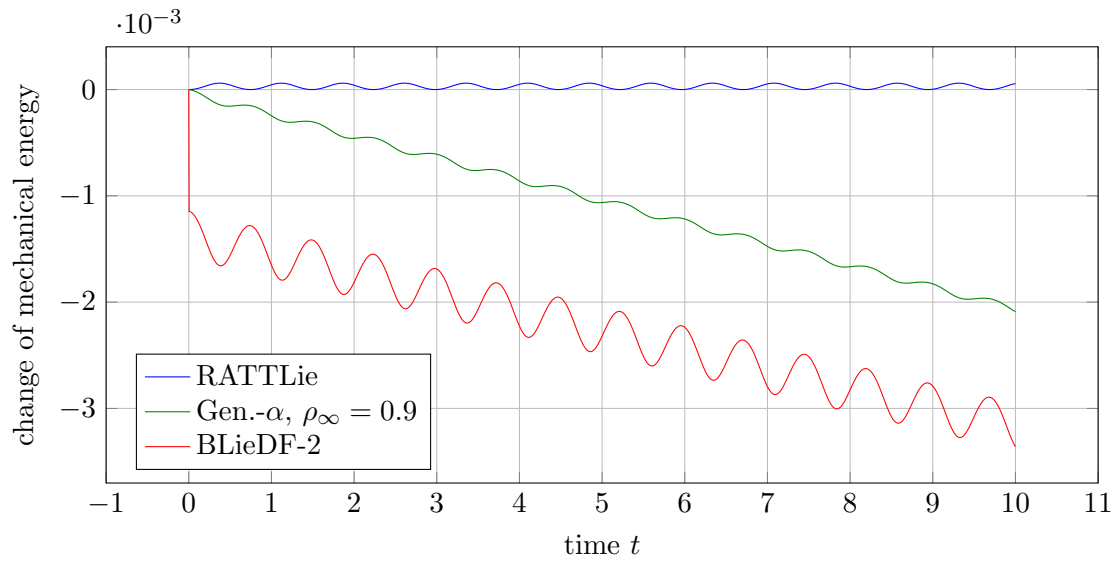


Figure 14: Fast heavy top: Change of mechanical energy over time. Results were calculated in the Lie group $\mathbb{S}^3 \times \mathbb{R}^3$, with step size $h = 2^{-16} \approx 1.5 \times 10^{-5}$ with different integration schemes.

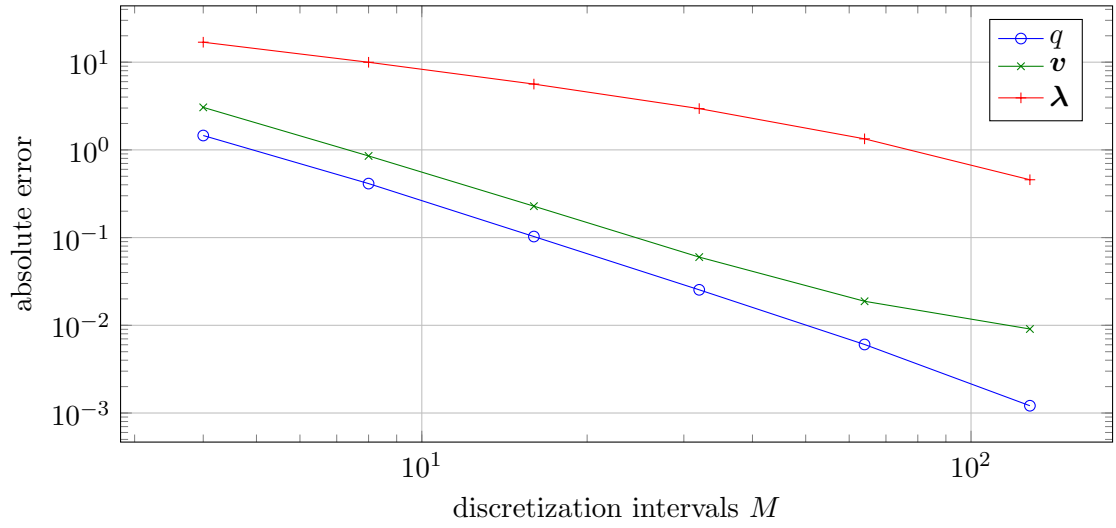


Figure 15: Kirchhoff beam model: Flying spaghetti: Maximum of the absolute discretized L^2 error in the configuration variables q , the derivative vectors v and the Lagrange multipliers λ . Results were calculated with RATTLie with time step size $h = 2^{-15} \approx 3.05 \times 10^{-5}$ and the reference solution used $M = 256$ spatial discretization intervals.

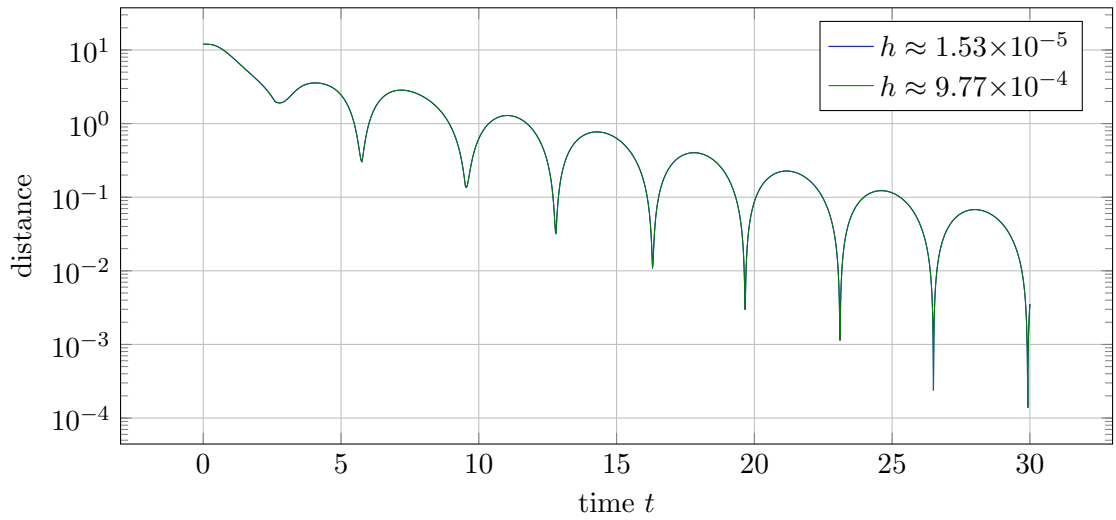


Figure 16: Cosserat beam model: Roll-up: Distance $\|\mathbf{x}_0(t) - \mathbf{x}_M(t)\|_2 + \|-p_0(t) - p_M(t)\|_2$ between the end points of the beam over time t . Note that due to the 360° rotation of the right end, the orientation $p_M(t)$ approaches the antipode $-p_0(t)$. Both curves closely coincide.

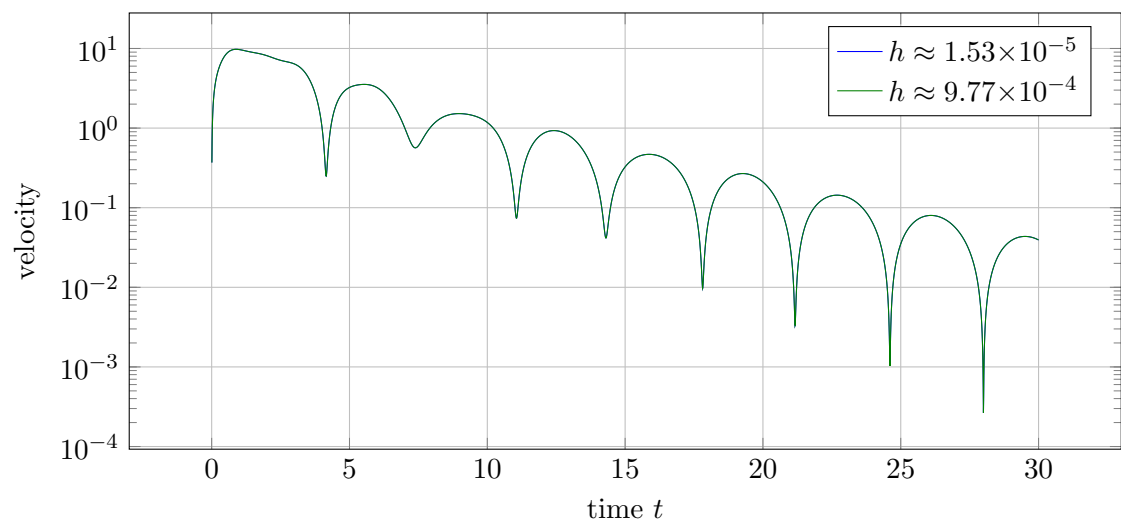


Figure 17: Cosserat beam model: Roll-up: Velocity $\|[\boldsymbol{\Omega}_M^\top(t), \boldsymbol{U}_M^\top(t)]^\top\|_2$ of the right end of the beam over time t . Both curves closely coincide.

6. Conclusion

Section 2 introduces the well-known elements of Lie group theory, where we have laid the focus on eventually formulating everything in the language of derivative vectors. The Lie group $\mathbb{S}^3 \times \mathbb{R}^3$, which is a relatively unknown semi-direct product Lie group, is given special attention since it was used as the configuration space for rigid bodies as well as the Cosserat beam model. Furthermore, we have shown the connections and isomorphies between $\mathbb{S}^3 \times \mathbb{R}^3$, $SE(3)$, dual unit quaternions and matrix Lie groups. This also gives a justification that Lie groups, whose elements are not given as matrices can under some conditions be used in time integration algorithms designed for ODEs and DAEs with matrix Lie group structured configuration spaces. Additionally, we collected definitions and theorems about Lie groups as Riemann surfaces and metric spaces, which are relatively unknown in mechanics and numerical analysis but constitute an essential building block in the proof of convergence of RATTLie.

Section 3 introduces RATTLie: a novel integration scheme for constrained mechanical systems. It can be thought of as a generalization of the well-known RATTLE method to mechanical systems on Lie group structured configuration spaces. RATTLie can be compared to stabilized index-2 integration methods, because it respects the hidden constraints on velocity level. It can be derived using the tools of variational integrators, see section 3.1. Additionally, we have introduced a novel nonholonomic version of RATTLie as well as the related SHAKELie scheme, which turns out to be uncompetitive. In section 3.2 we give a proof of second order convergence of the RATTLie method. The analysis tool used is a generalization of the well-known proof for one-step methods injected with the notion of Lie groups as metric spaces. This tool has not been used before in order to prove convergence of a DAE Lie group time integration method for mechanical systems. We also do not rely on constant time step sizes nor assume that the system in question has to be conservative. This also proves that RATTLE is convergent for variable time step sizes and gives an interpretation and a proof of convergence for the two distinct Lagrange multipliers that appear in RATTLE and RATTLie. Finally, section 3.3 gives some details on the implementation of the presented integration schemes, which are rather similar to the implementation of the Lie group generalized- α method. We also show pseudocode that should make it easy to implement RATTLie and its nonholonomic version.

The main part of section 4 consists of describing the Cosserat beam model which was constrained to a Kirchhoff beam model as well as the spatial discretization of the model. The model itself is well-known, but the discretization using $\mathbb{S}^3 \times \mathbb{R}^3$ is rather new, while other works, e. g. [23, 55, 75], have used similar techniques, only with similar Lie groups.

Section 5 was dedicated to numerical experiments. First, in section 5.1 we have proposed four common test problems, namely the heavy top example, the rolling disk, the flying spaghetti benchmark, as well as the roll-up of a clamped beam. These test problems have, together with the integrators from section 3 as well as two other integration schemes, been efficiently implemented in object-oriented Fortran, as presented in section 5.2. Finally, section 5.3 shows and interprets the numerical experiments. We can observe,

that the RATTLie method converges numerically with second order, as predicted by the analytical investigations in section 3.2. The two ways of calculating the Lagrange multipliers in RATTLie have been compared, yielding that the separate calculation is more reliable for fine time steps, while matching the slightly computationally cheaper interpolated calculation for coarser time steps. We have also numerically confirmed that RATTLie really does not only work for equidistant time grids, but also for varying time step sizes. Furthermore, we can see that for our test problems, RATTLie even mostly outperforms the competitors, namely the well-known generalized- α method, the BLieDF method, as well as SHAKELie, which produces wrong results for fine time step sizes. Additionally, RATTLie does not show a systematic drift in energy for a conservative system, whereas the competitors tend to dissipate energy for the sake of stability. We have shown that the formulation in the Lie group $\mathbb{S}^3 \ltimes \mathbb{R}^3$ can compete with other semi-direct product Lie groups such as $SE(3)$ and unit dual quaternions, while being slightly more efficient. Note that for time integration of the equations of motion of rigid bodies, the formulation in direct products seem to be computationally superior, as they produce lower errors and faster computation times due to measuring the velocities with respect to the inertial frame. For discretizing flexible Cosserat beams in space however, the semi-direct product approach seems to be superior since we can observe no shear locking of the beam discretized in a semi-direct product Lie group. Furthermore, we have observed second-order convergence of the nonholonomic RATTLie method; an analytic proof of this, however, has not yet been given. Lastly, we have shown that the coupled space/time discretization of the Cosserat beam model converges with second order numerically, which was to be expected by the variational discretization method, which used only second-order approximations.

7. References

- [1] Alexandrino, M., Bettiol, R. (eds.): Lie groups and geometric aspects of isometric actions. Springer, Cham (2015)
- [2] Alexandrino, M., Bettiol, R.: Lie groups with bi-invariant metrics. In: M. Alexandrino, R. Bettiol (eds.) Lie groups and geometric aspects of isometric actions, pp. 27–47. Springer, Cham (2015)
- [3] Altenbach, H., Eremeyev, V. (eds.): Shell-like structures. CISM International Centre for Mechanical Sciences. Springer, Cham (2017)
- [4] Altenbach, J., Altenbach, H., Eremeyev, V.: On generalized Cosserat-type theories of plates and shells: a short review and bibliography. *Archive of Applied Mechanics* **80**(1), 73–92 (2010)
- [5] Andersen, H.: Rattle: A “velocity” version of the shake algorithm for molecular dynamics calculations. *Journal of Computational Physics* **52**(1), 24–34 (1983)
- [6] Arnold, M.: A perturbation analysis for the dynamical simulation of mechanical multibody systems. *Applied Numerical Mathematics* **18**(1-3), 37–56 (1995)
- [7] Arnold, M., Brüls, O., Cardona, A.: Error analysis of generalized- α Lie group time integration methods for constrained mechanical systems. *Numerische Mathematik* **129**(1), 149–179 (2015)
- [8] Arnold, M., Cardona, A., Brüls, O.: A Lie algebra approach to Lie group time integration of constrained systems. In: P. Betsch (ed.) *Structure-preserving integrators in nonlinear structural dynamics and flexible multibody dynamics, CISM courses and lectures*, vol. 565, pp. 91–158. Springer, Cham (2016)
- [9] Arnold, M., Hante, S.: Implementation details of a generalized- α differential-algebraic equation Lie group method. *Journal of Computational and Nonlinear Dynamics* **12**(2), 021002 (2017)
- [10] Barth, E., Leimkuhler, B., Reich, S.: A time-reversible variable-stepsize integrator for constrained dynamics. *SIAM Journal on Scientific Computing* **21**(3), 1027–1044 (1999)
- [11] Bauchau, O., Betsch, P., Cardona, A., Gerstmayr, J., Jonker, B., Masarati, P., Sonneville, V.: Validation of flexible multibody dynamics beam formulations using benchmark problems. *Multibody System Dynamics* **37**(1), 29–48 (2016)
- [12] Betsch, P., Siebert, R.: Rigid body dynamics in terms of quaternions: Hamiltonian formulation and conserving numerical integration. *International Journal for Numerical Methods in Engineering* **79**(4), 444–473 (2009)

- [13] Bîrsan, M., Neff, P.: Analysis of the deformation of Cosserat elastic shells using the dislocation density tensor. In: F. dell’Isola, M. Sofonea, D. Steigmann (eds.) *Mathematical modelling in solid mechanics, Advanced Structured Materials*, vol. 69, pp. 13–30. Springer, Singapore (2017)
- [14] Botasso, C., Bauchau, O., Cardona, A.: Time-step-size-independent conditioning and sensitivity to perturbations in the numerical solution of index three differential algebraic equations. *SIAM Journal on Scientific Computing* **29**(1), 397–414 (2007)
- [15] Botasso, C., Borri, M.: Integrating finite rotations. *Computer Methods in Applied Mechanics and Engineering* **164**(3-4), 307–331 (1998)
- [16] Brüls, O., Cardona, A.: On the use of Lie group time integrators in multibody dynamics. *Journal of Computational and Nonlinear Dynamics* **5**(3) (2010)
- [17] Brüls, O., Cardona, A., Arnold, M.: Two Lie group formulations for dynamic multibody systems with large rotations. In: *Proceedings of the ASME 2011 International Design Engineering Technical Conferences and Computers and Information in Engineering Conference*, pp. 85–94. ASME (2011)
- [18] Brüls, O., Cardona, A., Arnold, M.: Lie group generalized- α time integration of constrained flexible multibody systems. *Mechanism and Machine Theory* **48**, 121–137 (2012)
- [19] do Carmo, M.: *Riemannian geometry. Mathematics.* Birkhäuser, Boston (1992)
- [20] Celledoni, E., Owren, B.: Lie group methods for rigid body dynamics and time integration on manifolds. *Computer Methods in Applied Mechanics and Engineering* **192**(3), 421–438 (2003)
- [21] Chung, J., Hulbert, G.: A time integration algorithm for structural dynamics with improved numerical dissipation: the generalized- α method. *ASME Journal of Applied Mechanics* **60**, 371–375 (1993)
- [22] Cosserat, E., Cosserat, F.: *Théorie des corps déformables.* Hermann (1909)
- [23] Demoures, F., Gay-Balmaz, F., Leitz, T., Leyendecker, S., Ober-Blöbaum, S., Ratiu, T.: Asynchronous variational Lie group integration for geometrically exact beam dynamics. *PAMM* **13**(1), 45–46 (2013)
- [24] Demoures, F., Gay-Balmaz, F., Leyendecker, S., Ober-Blöbaum, S., Ratiu, T., Weinand, Y.: Discrete variational Lie group formulation of geometrically exact beam dynamics. *Numerische Mathematik* **130**(1), 73–123 (2015)
- [25] Deuffhard, P.: Newton methods for nonlinear problems: affine invariance and adaptive algorithms, *Springer Series in Computational Mathematics*, vol. 35. Springer, Berlin (2004)

- [26] Ebbinghaus, H.D., Hermes, H., Hirzebruch, F., Koecher, M., Mainzer, K., Neukirch, J., Prestel, A., Remmert, R.: Numbers, *Graduate Texts in Mathematics*, vol. 123. Springer, New York, NY (1991)
- [27] Engø, K.: Partitioned Runge-Kutta methods in Lie-group setting. *BIT Numerical Mathematics* **43**(1), 21–39 (2003)
- [28] Eremeyev, V., Altenbach, H.: Basics of mechanics of micropolar shells. In: H. Altenbach, V. Eremeyev (eds.) *Shell-like structures, CISM International Centre for Mechanical Sciences*, vol. 572, pp. 63–111. Springer, Cham (2017)
- [29] Faltinsen, S.: Backward error analysis for Lie-group methods. *BIT Numerical Mathematics* **40**(4), 652–670 (2000)
- [30] Ferraro, S., Iglesias-Ponte, D., de Diego, D.: Numerical and geometric aspects of the nonholonomic SHAKE and RATTLE methods. In: *Conference Publications*, vol. 2009, p. 220. American Institute of Mathematical Sciences (2009)
- [31] Gear, C., Gupta, G., Leimkuhler, B.: Automatic integration of Euler-Lagrange equations with constraints. *Journal of Computational and Applied Mathematics* **12-13**, 77–90 (1985)
- [32] Géradin, M., Cardona, A.: Kinematics and dynamics of rigid and flexible mechanisms using finite elements and quaternion algebra. *Computational Mechanics* **4**(2), 115–135 (1988)
- [33] Géradin, M., Cardona, A.: *Flexible multibody dynamics: a finite element approach*. Wiley, Chichester (2001)
- [34] Gladwell, G., Angeles, J., Hommel, G., Kovács, P.: *Computational kinematics, Solid Mechanics and Its Applications*, vol. 28. Springer, Dordrecht (1993)
- [35] Hairer, E., Lubich, C., Wanner, G.: *Geometric numerical integration: structure-preserving algorithms for ordinary differential equations, Springer Series in Computational Mathematics*, vol. 31, first softcover print of 2nd edn. Springer, Berlin, Heidelberg (2010)
- [36] Hairer, E., Nørsett, S., Wanner, G.: *Solving Ordinary Differential Equations I: Nonstiff problems, Springer Series in Computational Mathematics*, vol. 8, rev. 2nd edn. Springer, Berlin, Heidelberg (1993)
- [37] Hairer, E., Wanner, G.: *Solving Ordinary Differential Equations II: Stiff and Differential-Algebraic Problems*, 2nd edn. Springer, Berlin, Heidelberg (2002)
- [38] Hall, B.: *Lie groups, Lie algebras, and representations, Graduate Texts in Mathematics*, vol. 222. Springer, Cham (2015)
- [39] Hall, J., Leok, M.: Spectral variational integrators. *Numerische Mathematik* **130**(4), 681–740 (2015)

- [40] Hanson, A.: Visualizing quaternions. Morgan Kaufmann series in interactive 3D technology. Elsevier professional (2005)
- [41] Hante, S.: A Lie group generalization of the RATTLE scheme applied to non-holonomic constraints. In: T. Gleim, S. Lange (eds.) Proceedings of 8th GACM Colloquium on Computational Mechanics, pp. 207–210. Kassel University Press, Kassel (2019)
- [42] Hante, S., Arnold, M.: A novel approach to Lie group structured configuration spaces of rigid bodies. PAMM **17**(1), 151–152 (2017)
- [43] Hante, S., Arnold, M.: Staggered grid discretizations on Lie groups with applications in beam and shell theory. PAMM **18**, e201800277 (2018)
- [44] Hante, S., Arnold, M.: RATTLie: a variational Lie group integration scheme for constrained mechanical systems. Journal of Computational and Applied Mathematics **387**, 112492 (2021)
- [45] Hante, S., Tumiotto, D., Arnold, M.: A Lie group variational integration approach to the full discretization of a constrained geometrically exact Cosserat beam model. Multibody System Dynamics **54**, 97–123 (2022)
- [46] Iserles, A., Munthe-Kaas, H., Nørset, S., Zanna, A.: Lie-group methods. Acta Numerica **9**, 215–365 (2000)
- [47] Jelenić, G., Crisfield, M.: Geometrically exact 3D beam theory: implementation of a strain-invariant finite element for statics and dynamics. Computer methods in applied mechanics and engineering **171**(1-2), 141–171 (1999)
- [48] Jüttler, B.: Visualization of moving objects using dual quaternion curves. Computers & Graphics **18**(3), 315–326 (1994)
- [49] Kenwright, B.: A beginners guide to dual-quaternions. WSCG Communication proceedings pp. 1–10 (2012)
- [50] Lang, H., Arnold, M.: Numerical aspects in the dynamic simulation of geometrically exact rods. Tech. Rep. 179, Fraunhofer ITWM, Kaiserslautern (2009)
- [51] Lang, H., Arnold, M.: Numerical aspects in the dynamic simulation of geometrically exact rods. Applied Numerical Mathematics **62**(10), 1411–1427 (2012)
- [52] Lang, H., Linn, J.: Lagrangian field theory in space-time for geometrically exact Cosserat rods. Tech. Rep. 150, Fraunhofer ITWM, Kaiserslautern (2009)
- [53] Lang, H., Linn, J., Arnold, M.: Multi-body dynamics simulation of geometrically exact Cosserat rods. Multibody System Dynamics **25**(3), 285–312 (2011)

- [54] Lee, T., Leok, M., McClamroch, N.: Lie group variational integrators for the full body problem. *Computer Methods in Applied Mechanics and Engineering* **196**(29-30), 2907–2924 (2007)
- [55] Leitz, T., de Almagro, R., Leyendecker, S.: Multisymplectic Galerkin Lie group variational integrators for geometrically exact beam dynamics based on unit dual quaternion interpolation – no shear locking. *Computer Methods in Applied Mechanics and Engineering* **374**, 113475 (2021)
- [56] Leitz, T., Leyendecker, S.: Galerkin Lie-group variational integrators based on unit quaternion interpolation. *Computer Methods in Applied Mechanics and Engineering* **338**, 333–361 (2018)
- [57] Leyendecker, S., Betsch, P., Steinmann, P.: The discrete null space method for the energy-consistent integration of constrained mechanical systems: part III: flexible multibody dynamics. *Multibody System Dynamics* **19**(1-2), 45–72 (2008)
- [58] Leyendecker, S., Marsden, J., Ortiz, M.: Variational integrators for constrained dynamical systems. *ZAMM* **88**(9), 677–708 (2008)
- [59] Linn, J., Hermansson, T., Andersson, F., Schneider, F.: Kinetic aspects of discrete Cosserat rods based on the difference geometry of framed curves. In: M. Valáček (ed.) *ECCOMAS thematic conference on multibody dynamics* (2017)
- [60] Linn, J., Stephan, T.: Simulation of quasistatic deformations using discrete rod models. Tech. Rep. 144, Fraunhofer ITWM, Kaiserslautern (2008)
- [61] Lötstedt, P., Petzold, L.: Numerical solution of nonlinear differential equations with algebraic constraints I: convergence results for backward differentiation formulas. *Math. of Comp.* **46**(174), 491–516 (1986)
- [62] Magnus, W.: On the exponential solution of differential equations for a linear operator. *Communications on Pure and Applied Mathematics* **7**(4), 649–673 (1954)
- [63] Marsden, J., West, M.: Discrete mechanics and variational integrators. *Acta Numerica* **10**, 357–514 (2001)
- [64] Müller, A.: Approximation of finite rigid body motions from velocity fields. *ZAMM* **90**(6), 514–521 (2010)
- [65] Müller, A., Maißer, P.: A Lie-group formulation of kinematics and dynamics of constrained MBS and its application to analytical mechanics. *Multibody System Dynamics* **9**, 311–352 (2003)
- [66] Müller, A., Terze, Z.: Modelling and integration concepts of multibody systems on Lie groups. In: Z. Terze (ed.) *Multibody dynamics*, pp. 123–144. Springer, Cham (2014)

- [67] Neff, P.: A geometrically exact planar Cosserat shell-model with microstructure: existence of minimizers for zero Cosserat couple modulus. *Mathematical Models and Methods in Applied Sciences* **17**(03), 363–392 (2007)
- [68] Roller, M., Betsch, P., Gallrein, A., Linn, J.: On the use of geometrically exact shells for dynamic tire simulation. In: Z. Terze (ed.) *Multibody dynamics*, pp. 205–236. Springer, Cham (2014)
- [69] Schiehlen, W., Eberhard, P.: *Applied Dynamics*. Springer, Cham (2014)
- [70] Schiff, J., Shnider, S.: Lie groups and error analysis. *Journal of Lie Theory* **11**(1), 231–254 (2001)
- [71] Simo, J.: A finite strain beam formulation: the three-dimensional dynamic problem: part I. *Computer Methods in Applied Mechanics and Engineering* **49**(1), 55–70 (1985)
- [72] Simo, J., Vu-Quoc, L.: A three-dimensional finite-strain rod model: part II: computational aspects. *Computer Methods in Applied Mechanics and Engineering* **58**(1), 79–116 (1986)
- [73] Simo, J., Vu-Quoc, L.: On the dynamics in space of rods undergoing large motions: a geometrically exact approach. *Computer Methods in Applied Mechanics and Engineering* **66**(2), 125–161 (1988)
- [74] Sonnevile, V., Brüls, O., Bauchau, O.: Interpolation schemes for geometrically exact beams: a motion approach. *International Journal for Numerical Methods in Engineering* **112**(9), 1129–1153 (2017)
- [75] Sonnevile, V., Cardona, A., Brüls, O.: Geometric interpretation of a non-linear beam finite element on the Lie group $SE(3)$. *Archive of Mechanical Engineering* **61**(2), 305–329 (2014)
- [76] Sonnevile, V., Cardona, A., Brüls, O.: Geometrically exact beam finite element formulated on the special Euclidean group $SE(3)$. *Computer Methods in Applied Mechanics and Engineering* **268**, 451–474 (2014)
- [77] Stillwell, J.: *Naive Lie theory*. Undergraduate Texts in Mathematics. Springer, New York, NY (2008)
- [78] Strehmel, K., Weiner, R., Podhaisky, H.: *Numerik gewöhnlicher Differentialgleichungen: Nichtsteife, steife und differential-algebraische Gleichungen*, 2nd edn. Vieweg & Teubner, Wiesbaden (2012)
- [79] Tange, O.: GNU Parallel 2018. *Zenodo* (2018)
- [80] Varadarajan, V.: *Lie groups, Lie algebras, and their representations*, *Graduate Texts in Mathematics*, vol. 102. Springer, New York, Berlin, Heidelberg (1984)

- [81] Verwer, J., Sanz-Serna, J.: Convergence of method of lines approximations to partial differential equations. *Computing* **33**(3-4), 297–313 (1984)
- [82] Weber, S.: Singulär gestörte Differentialgleichungssysteme und quasistatische Lösungsverfahren in der Mehrkörperdynamik. Ph.D. thesis, Martin-Luther-Universität Halle-Wittenberg, Halle (2013)
- [83] Wieloch, V.: Analytisch äquivalente Lie-Gruppen-Beschreibungen des Starrkörpers: Ein numerischer Vergleich. Ph.D. thesis, Martin Luther University Halle-Wittenberg, Institute of Mathematics (2013)
- [84] Wieloch, V., Arnold, M.: BLieDF2nd: a k-step BDF integrator for constrained mechanical systems on Lie groups. In: Proc. 5th Joint International Conference on Multibody System Dynamics (2018)
- [85] Wieloch, V., Arnold, M.: BDF integrators for constrained mechanical systems on Lie groups. *Journal of Computational and Applied Mathematics* **387**, 112517 (2021)
- [86] Zhang, F.: The Schur complement and its applications, vol. 4. Springer, New York, NY (2005)

A. Lie Group Functions

In this section we will present the most important Lie group functions related to the linear Lie group $(\mathbb{R}^n, +)$, the Lie group of rotation matrices $(SO(3), \cdot)$, the Lie group of unit quaternions $(\mathbb{S}^3, *)$, the special Euclidean Lie group $(SE(3), \cdot)$, the semi-direct product $(\mathbb{S}^3 \times \mathbb{R}^3, \circ)$, as well as the Lie group of unit dual quaternions $(UDQ, *)$. A lot of these functions can be found in the project `liegroup` or `heavytop`, see section 5.2. Especially the Mathematica script that comes with `liegroup` might be helpful in verifying these statements.

A.1. Linear Lie Groups \mathbb{R}^n

Let $n \in \mathbb{N}$. We consider the linear Lie group $(\mathbb{R}^n, +)$, where the group operation is the vector addition, inversion is negation, and the identity element is $\mathbf{0} \in \mathbb{R}^n$. Let $\mathbf{x}, \mathbf{y}, \mathbf{v}, \mathbf{w} \in \mathbb{R}^n$:

$$\begin{aligned} T_{\mathbf{0}}\mathbb{R}^n &= \mathbb{R}^n, & \tilde{\mathbf{v}} &= \mathbf{v}, \\ dL_{\mathbf{x}}(\mathbf{0})\tilde{\mathbf{v}} &= \mathbf{v}, & \widetilde{\exp}(\mathbf{v}) &= \mathbf{v}, \\ \widetilde{\log}(\mathbf{x}) &= \mathbf{x}, & \hat{\mathbf{v}} &= \mathbf{I}, \\ \mathbf{T}(\mathbf{v}) &= \mathbf{I}, & \mathbf{T}^{-1}(\mathbf{v}) &= \mathbf{I}, \\ \frac{\partial}{\partial \mathbf{v}}(\mathbf{T}^{-\top}(\mathbf{v}) \cdot \mathbf{w}) &= \mathbf{0}. \end{aligned}$$

A.2. Lie Group of Rotation Matrices $SO(3)$

We consider the Lie group of rotation matrices $(SO(3), \cdot)$ that is called the special orthogonal group in three dimensions. It is defined as

$$SO(3) = \{\mathbf{R} \in \mathbb{R}^{3 \times 3} : \mathbf{R} \cdot \mathbf{R}^{\top} = \mathbf{I}, \det \mathbf{R} = 1\}$$

and its dimension is $\dim SO(3) = 3$. The group operation is matrix multiplication, inversion is matrix transposition since $\mathbf{R}^{\top} = \mathbf{R}^{-1}$ for $\mathbf{R} \in SO(3)$, and the identity element is the identity matrix $\mathbf{I} \in SO(3)$. Let $\mathbf{R} \in SO(3)$ and $\mathbf{v}, \mathbf{w} \in \mathbb{R}^3$:

$$\begin{aligned} T_{\mathbf{I}}SO(3) &= \mathfrak{so}(3) = \{\mathbf{A} \in \mathbb{R}^{3 \times 3} : \mathbf{A} + \mathbf{A}^{\top} = \mathbf{0}\}, \\ \tilde{\mathbf{v}} &= \text{skw}(\mathbf{v}), \\ dL_{\mathbf{R}}(\mathbf{I})\tilde{\mathbf{v}} &= \mathbf{R} \cdot \text{skw}(\mathbf{v}), \\ \widetilde{\exp}(\mathbf{v}) &= \mathbf{I} + f_1(\|\mathbf{v}\|) \text{skw}(\mathbf{v}) - f_2(\|\mathbf{v}\|) (\text{skw}(\mathbf{v}))^2, \\ \hat{\mathbf{v}} &= \text{skw}(\mathbf{v}), \\ \mathbf{T}(\mathbf{v}) &= \mathbf{I} + f_2(\|\mathbf{v}\|) \text{skw}(\mathbf{v}) + f_3(\|\mathbf{v}\|) (\text{skw}(\mathbf{v}))^2, \\ \mathbf{T}^{-1}(\mathbf{v}) &= \mathbf{I} + \frac{1}{2} \text{skw}(\mathbf{v}) + f_6(\|\mathbf{v}\|) (\text{skw}(\mathbf{v}))^2, \end{aligned}$$

$$\begin{aligned} \mathbf{S}(\mathbf{v}, \mathbf{w}) &= \frac{\partial}{\partial \mathbf{v}} (\mathbf{T}^{-\top}(\mathbf{v}) \cdot \mathbf{w}) \frac{1}{2} \text{skw}(\mathbf{w}) - f_8(\|\mathbf{v}\|) (\text{skw}(\mathbf{w}))^2 \cdot \mathbf{v} \cdot \mathbf{v}^\top \\ &\quad - f_6(\|\mathbf{v}\|) (\text{skw}(\mathbf{v}) \cdot \text{skw}(\mathbf{w}) + \text{skw}(\mathbf{v} \times \mathbf{w})). \end{aligned}$$

Here, we have used the skew-symmetric matrix $\text{skw}(\bullet)$ defined in (2.29) as well as the singular functions defined in appendix B.

A.3. The Special Euclidean Group $SE(3)$

We consider the special Euclidean Lie group in three dimensions ($SE(3), \cdot$). It is often defined as

$$SE(3) = \left\{ \begin{bmatrix} \mathbf{R} & \mathbf{x} \\ \mathbf{0} & 1 \end{bmatrix} \in \mathbb{R}^{4 \times 4} : \mathbf{R} \in SO(3), \mathbf{x} \in \mathbb{R}^3 \right\}$$

and its dimension is $\dim SE(3) = 6$. The group operation is matrix multiplication, inversion is matrix inversion, and the identity element is $e = \mathbf{I}_4 \in SE(3)$. Note that when using this Lie group in an implementation, one should only store the rotation matrix $\mathbf{R} \in SO(3)$ and the vector $\mathbf{x} \in \mathbb{R}^3$, dropping the last row, which is constant. In order to make this visible in the formulae and to simplify notation, we will write the elements as pairs:

$$(\mathbf{R}, \mathbf{x}) = \begin{bmatrix} \mathbf{R} & \mathbf{x} \\ \mathbf{0} & 1 \end{bmatrix}.$$

Let $(\mathbf{R}, \mathbf{x}), (\mathbf{Q}, \mathbf{y}) \in SE(3)$, $\boldsymbol{\Omega}, \mathbf{U}, \mathbf{A}, \mathbf{W} \in \mathbb{R}^3$ and $\mathbf{v} = [\boldsymbol{\Omega}^\top, \mathbf{U}^\top]^\top$:

$$(\mathbf{R}, \mathbf{x}) \cdot (\mathbf{Q}, \mathbf{y}) = (\mathbf{R} \cdot \mathbf{Q}, \mathbf{x} + \mathbf{R} \cdot \mathbf{y}),$$

$$(\mathbf{R}, \mathbf{x})^{-1} = (\mathbf{R}^\top, -\mathbf{R}^\top \cdot \mathbf{x}),$$

$$e = (\mathbf{I}, \mathbf{0}),$$

$$T_e SE(3) = \mathfrak{se}(3) = \left\{ \begin{bmatrix} \mathbf{A} & \mathbf{a} \\ \mathbf{0} & 0 \end{bmatrix} \in \mathbb{R}^{4 \times 4} : \mathbf{A} \in \mathfrak{so}(3), \mathbf{a} \in \mathbb{R}^3 \right\},$$

$$\tilde{\mathbf{v}} = \begin{bmatrix} \text{skw}(\boldsymbol{\Omega}) & \mathbf{U} \\ \mathbf{0} & 0 \end{bmatrix},$$

$$dL_{(\mathbf{R}, \mathbf{x})}(e) \tilde{\mathbf{v}} = \begin{bmatrix} \mathbf{R} \cdot \text{skw}(\boldsymbol{\Omega}) & \mathbf{R} \cdot \mathbf{U} \\ \mathbf{0} & 0 \end{bmatrix},$$

$$\widetilde{\exp}(\mathbf{v}) = (\widetilde{\exp}_{SO(3)}(\boldsymbol{\Omega}), \mathbf{T}_{SO(3)}^\top(\boldsymbol{\Omega}) \cdot \mathbf{U}),$$

$$\hat{\mathbf{v}} = \begin{bmatrix} \text{skw}(\boldsymbol{\Omega}) & \mathbf{0} \\ \text{skw}(\mathbf{U}) & \text{skw}(\boldsymbol{\Omega}) \end{bmatrix},$$

$$\begin{aligned} \mathbf{C}_1(\boldsymbol{\Omega}, \mathbf{U}) &= f_2(\|\boldsymbol{\Omega}\|) \text{skw}(\mathbf{U}) + f_3(\|\boldsymbol{\Omega}\|) (\text{skw}(\mathbf{U}) \cdot \text{skw}(\boldsymbol{\Omega}) + \text{skw}(\boldsymbol{\Omega}) \cdot \text{skw}(\mathbf{U})) \\ &\quad + f_4(\|\boldsymbol{\Omega}\|) (\boldsymbol{\Omega}^\top \cdot \mathbf{U}) \text{skw}(\boldsymbol{\Omega}) - f_5(\|\boldsymbol{\Omega}\|) (\boldsymbol{\Omega}^\top \cdot \mathbf{U}) (\text{skw}(\boldsymbol{\Omega}))^2, \end{aligned}$$

$$\mathbf{T}(\mathbf{v}) = \begin{bmatrix} \mathbf{T}_{SO(3)}(\boldsymbol{\Omega}) & \mathbf{0} \\ \mathbf{C}_1(\boldsymbol{\Omega}, \mathbf{U}) & \mathbf{T}_{SO(3)}(\boldsymbol{\Omega}) \end{bmatrix},$$

$$\begin{aligned} \mathbf{C}_2(\boldsymbol{\Omega}, \mathbf{U}) &= \frac{1}{2} \text{skw}(\mathbf{U}) + f_6(\|\boldsymbol{\Omega}\|) (\text{skw}(\mathbf{U}) \cdot \text{skw}(\boldsymbol{\Omega}) + \text{skw}(\boldsymbol{\Omega}) \cdot \text{skw}(\mathbf{U})) \\ &\quad + f_8(\|\boldsymbol{\Omega}\|) (\boldsymbol{\Omega}^\top \cdot \mathbf{U}) (\text{skw}(\boldsymbol{\Omega}))^2, \end{aligned}$$

$$\mathbf{T}^{-1}(\mathbf{v}) = \begin{bmatrix} \mathbf{T}_{SO(3)}^{-1}(\boldsymbol{\Omega}) & \mathbf{0} \\ \mathbf{C}_2(\boldsymbol{\Omega}, \mathbf{U}) & \mathbf{T}_{SO(3)}^{-1}(\boldsymbol{\Omega}) \end{bmatrix},$$

$$\begin{aligned} \mathbf{C}_3(\boldsymbol{\Omega}, \mathbf{U}, \mathbf{W}) &= -f_6(\|\boldsymbol{\Omega}\|) (\text{skw}(\mathbf{U}) \cdot \text{skw}(\mathbf{W}) - \text{skw}(\mathbf{W} \times \mathbf{U})) \\ &\quad - f_8(\|\boldsymbol{\Omega}\|) (\mathbf{U}^\top \cdot \boldsymbol{\Omega}) (\text{skw}(\boldsymbol{\Omega}) \cdot \text{skw}(\mathbf{W}) + \text{skw}(\boldsymbol{\Omega} \times \mathbf{W})) \\ &\quad + f_8(\|\boldsymbol{\Omega}\|) \left((\boldsymbol{\Omega} \times (\boldsymbol{\Omega} \times \mathbf{W})) \cdot \mathbf{U}^\top + (\mathbf{U} \times (\boldsymbol{\Omega} \times \mathbf{W}) + \boldsymbol{\Omega} \times (\mathbf{U} \times \mathbf{W})) \cdot \boldsymbol{\Omega}^\top \right) \\ &\quad + f_9(\|\boldsymbol{\Omega}\|) (\boldsymbol{\Omega}^\top \cdot \mathbf{U}) (\boldsymbol{\Omega} \times (\boldsymbol{\Omega} \times \mathbf{W})) \cdot \boldsymbol{\Omega}^\top, \end{aligned}$$

$$\begin{aligned} \mathbf{S}\left(\mathbf{v}, \begin{bmatrix} \mathbf{A} \\ \mathbf{W} \end{bmatrix}\right) &= \frac{\partial}{\partial \mathbf{v}} \left(\mathbf{T}^{-\top}(\mathbf{v}) \cdot \begin{bmatrix} \mathbf{A} \\ \mathbf{W} \end{bmatrix} \right) \\ &= \begin{bmatrix} \mathbf{S}_{SO(3)}(\boldsymbol{\Omega}, \mathbf{A}) + \mathbf{C}_3(\boldsymbol{\Omega}, \mathbf{U}, \mathbf{W}) & \mathbf{S}_{SO(3)}(\boldsymbol{\Omega}, \mathbf{W}) \\ \mathbf{S}_{SO(3)}(\boldsymbol{\Omega}, \mathbf{W}) & \mathbf{0} \end{bmatrix}. \end{aligned}$$

We have used references to functions from the Lie group $SO(3)$ that are marked by the index $\bullet_{SO(3)}$ as well as singular functions defined in appendix A.

A.4. The Lie Group of Unit Quaternions \mathbb{S}^3

We consider the Lie group of unit quaternions $(\mathbb{S}^3, *)$. It holds, see section 2.3,

$$\mathbb{S}^3 = \{p \in \mathbb{R}^4 : \|p\| = 1\}$$

and the dimension is $\dim \mathbb{S}^3 = 3$. The group operation is quaternion multiplication $*$, inversion is quaternion conjugation, and the identity element is $e = [1, 0, 0, 0]^\top \in \mathbb{S}^3$, see section 2.3. Let $p, p_1, p_2 \in \mathbb{S}^3$ and $\mathbf{v}, \mathbf{w} \in \mathbb{R}^3$:

$$T_e \mathbb{S}^3 = \mathfrak{s}^3 = \left\{ \begin{bmatrix} 0 \\ \mathbf{a} \end{bmatrix} \in \mathbb{R}^{4 \times 4} : \mathbf{a} \in \mathbb{R}^3 \right\},$$

$$\tilde{\mathbf{v}} = \begin{bmatrix} 0 \\ \frac{1}{2} \mathbf{v} \end{bmatrix},$$

$$dL_p(e) \tilde{\mathbf{v}} = p * \tilde{\mathbf{v}} = \frac{1}{2} p * \begin{bmatrix} 0 \\ \mathbf{v} \end{bmatrix},$$

$$\widetilde{\text{exp}}(\mathbf{v}) = \begin{bmatrix} \cos(\|\mathbf{v}\|/2) \\ \frac{1}{2} f_1(\|\mathbf{v}\|/2) \mathbf{v} \end{bmatrix},$$

$$\widetilde{\text{log}}(p) = f_7(\text{Re } p) \text{Im } p,$$

$$\hat{\mathbf{v}} = \text{skw}(\mathbf{v}),$$

$$\mathbf{T}(\mathbf{v}) = \mathbf{T}_{SO(3)}(\mathbf{v}),$$

$$\begin{aligned}\mathbf{T}^{-1}(\mathbf{v}) &= \mathbf{T}_{SO(3)}(\mathbf{v}), \\ \mathbf{S}(\mathbf{v}, \mathbf{w}) &= \frac{\partial}{\partial \mathbf{v}} (\mathbf{T}^{-\top}(\mathbf{v}) \cdot \mathbf{w}) = \mathbf{S}_{SO(3)}(\mathbf{v}, \mathbf{w}).\end{aligned}$$

Again, we have used references to functions from the Lie group $SO(3)$ that are marked by the index $\bullet_{SO(3)}$, the real and imaginary part Re and Im from section 2.3, as well as singular functions defined in appendix B. Note that the Lie algebras of \mathbb{S}^3 and $SO(3)$ are isomorphic and by choosing the appropriate tilde operator, all functions related to only the Lie algebra coincide.

A.5. The Semi-Direct Product $\mathbb{S}^3 \ltimes \mathbb{R}^3$

We consider the semi-direct product Lie group $(\mathbb{S}^3 \ltimes \mathbb{R}^3, \circ)$. It is (as a set) defined by

$$\mathbb{S}^3 \ltimes \mathbb{R}^3 = \{(p, \mathbf{x}) : p \in \mathbb{S}^3, \mathbf{x} \in \mathbb{R}^3\}$$

and its dimension is $\dim(\mathbb{S}^3 \ltimes \mathbb{R}^3) = 6$. Let $(p, \mathbf{x}), (q, \mathbf{y}) \in \mathbb{S}^3 \ltimes \mathbb{R}^3$, $\boldsymbol{\Omega}, \mathbf{U}, \mathbf{A}, \mathbf{W} \in \mathbb{R}^3$ and $\mathbf{v} = [\boldsymbol{\Omega}^\top, \mathbf{U}^\top]^\top$:

$$\begin{aligned}(p, \mathbf{x}) \circ (q, \mathbf{y}) &= (p * q, \mathbf{x} + p \triangleright \mathbf{y}), \\ (p, \mathbf{x})^{-1} &= (p^{-1}, -p^{-1} \triangleright \mathbf{x}), \\ e &= ([1, 0, 0, 0]^\top, \mathbf{0}), \\ T_e(\mathbb{S}^3 \ltimes \mathbb{R}^3) &= \left\{ \left(\begin{bmatrix} 0 \\ \mathbf{a} \end{bmatrix}, \mathbf{b} \right) : \mathbf{a}, \mathbf{b} \in \mathbb{R}^3 \right\}, \\ \tilde{\mathbf{v}} &= \left(\begin{bmatrix} 0 \\ \frac{1}{2}\boldsymbol{\Omega} \end{bmatrix}, \mathbf{U} \right), \\ dL_{(p, \mathbf{x})}(e)\tilde{\mathbf{v}} &= \left(p * \begin{bmatrix} 0 \\ \frac{1}{2}\boldsymbol{\Omega} \end{bmatrix}, p \triangleright \mathbf{U} \right), \\ \widetilde{\exp}(\mathbf{v}) &= (\widetilde{\exp}_{\mathbb{S}^3}(\boldsymbol{\Omega}), \mathbf{T}_{\mathbb{S}^3}^\top(\boldsymbol{\Omega}) \cdot \mathbf{U}), \\ \widetilde{\log}((p, \mathbf{x})) &= \begin{bmatrix} \widetilde{\log}_{\mathbb{S}^3}(p) \\ \mathbf{T}_{\mathbb{S}^3}^{-\top}(\widetilde{\log}_{\mathbb{S}^3}(p)) \cdot \mathbf{x} \end{bmatrix}, \\ \hat{\mathbf{v}} &= \begin{bmatrix} \text{skw}(\boldsymbol{\Omega}) & \mathbf{0} \\ \text{skw}(\mathbf{U}) & \text{skw}(\boldsymbol{\Omega}) \end{bmatrix}, \\ \mathbf{T}(\mathbf{v}) &= \mathbf{T}_{SE(3)}(\mathbf{v}), \\ \mathbf{T}^{-1}(\mathbf{v}) &= \mathbf{T}_{SE(3)}^{-1}(\mathbf{v}), \\ \mathbf{S}\left(\mathbf{v}, \begin{bmatrix} \mathbf{A} \\ \mathbf{W} \end{bmatrix}\right) &= \frac{\partial}{\partial \mathbf{v}} \left(\mathbf{T}^{-\top}(\mathbf{v}) \cdot \begin{bmatrix} \mathbf{A} \\ \mathbf{W} \end{bmatrix} \right) = \mathbf{S}_{SE(3)}\left(\mathbf{v}, \begin{bmatrix} \mathbf{A} \\ \mathbf{W} \end{bmatrix}\right).\end{aligned}$$

We have used the action \triangleright as defined in section 2.3 and references to functions from the Lie groups \mathbb{S}^3 and $SE(3)$ that are marked by an appropriate index. Note that the Lie

algebras of $\mathbb{S}^3 \times \mathbb{R}^3$ and $SE(3)$ are isomorphic and by choosing the appropriate tilde operator, all functions related to only the Lie algebra coincide.

A.6. The Lie Group of Unit Dual Quaternions UDQ

We consider the Lie group $(UDQ, *)$ of unit dual quaternions. It is defined by

$$UDQ = \{\mathbf{p} + \epsilon \mathbf{r} : \mathbf{p}, \mathbf{r} \in \mathbb{R}^4, \|\mathbf{p}\| = 1, \mathbf{p}^\top \cdot \mathbf{r} = 0\},$$

see remark 2.33, with an imaginary unit $\epsilon \neq 0$ that fulfills $\epsilon^2 = 0$. The dimension is $\dim UDQ = 6$. Note that when using this Lie group in an implementation, one should store the real part \mathbf{p} and the imaginary part \mathbf{r} as a pair or an 8-dimensional vector. In order to simplify notation, we will write the elements as pairs:

$$(\mathbf{p}, \mathbf{r}) = \mathbf{p} + \epsilon \mathbf{r}.$$

Let $(\mathbf{p}, \mathbf{r}), (\mathbf{q}, \mathbf{s}) \in UDQ$, $\boldsymbol{\Omega}, \mathbf{U}, \mathbf{A}, \mathbf{W} \in \mathbb{R}^3$ and $\mathbf{v} = [\boldsymbol{\Omega}^\top, \mathbf{U}^\top]^\top$:

$$\begin{aligned} (\mathbf{p}, \mathbf{r}) * (\mathbf{q}, \mathbf{s}) &= (\mathbf{p} * \mathbf{q}, \mathbf{r} * \mathbf{q} + \mathbf{p} * \mathbf{s}), \\ (\mathbf{p}, \mathbf{r})^{-1} &= (\mathbf{p}^{-1}, -\mathbf{p}^{-1} * \mathbf{r} * \mathbf{p}^{-1}), \\ e &= ([1, 0, 0, 0]^\top, \mathbf{0}), \\ T_e UDQ &= \left\{ \left(\begin{bmatrix} 0 \\ \mathbf{a} \end{bmatrix}, \begin{bmatrix} 0 \\ \mathbf{b} \end{bmatrix} \right) : \mathbf{a}, \mathbf{b} \in \mathbb{R}^3 \right\}, \\ \tilde{\mathbf{v}} &= \left(\begin{bmatrix} 0 \\ \frac{1}{2} \boldsymbol{\Omega} \end{bmatrix}, \begin{bmatrix} 0 \\ \frac{1}{2} \mathbf{U} \end{bmatrix} \right), \\ dL_{(\mathbf{p}, \mathbf{r})}(e) \tilde{\mathbf{v}} &= \left(\mathbf{p} * \begin{bmatrix} 0 \\ \frac{1}{2} \boldsymbol{\Omega} \end{bmatrix}, \mathbf{r} * \begin{bmatrix} 0 \\ \frac{1}{2} \boldsymbol{\Omega} \end{bmatrix} + \mathbf{p} * \begin{bmatrix} 0 \\ \frac{1}{2} \mathbf{U} \end{bmatrix} \right), \\ \widetilde{\exp}(\mathbf{v}) &= \left(\widetilde{\exp}_{\mathbb{S}^3}(\boldsymbol{\Omega}), \left[\frac{1}{2} \mathbf{T}_{\mathbb{S}^3}^\top(\boldsymbol{\Omega}) \cdot \mathbf{U} \right] * \widetilde{\exp}_{\mathbb{S}^3}(\boldsymbol{\Omega}) \right), \\ \hat{\mathbf{v}} &= \begin{bmatrix} \text{skw}(\boldsymbol{\Omega}) & \mathbf{0} \\ \text{skw}(\mathbf{U}) & \text{skw}(\boldsymbol{\Omega}) \end{bmatrix}, \\ \mathbf{T}(\mathbf{v}) &= \mathbf{T}_{SE(3)}(\mathbf{v}), \\ \mathbf{T}^{-1}(\mathbf{v}) &= \mathbf{T}_{SE(3)}^{-1}(\mathbf{v}), \\ \mathbf{S}\left(\mathbf{v}, \begin{bmatrix} \mathbf{A} \\ \mathbf{W} \end{bmatrix}\right) &= \frac{\partial}{\partial \mathbf{v}} \left(\mathbf{T}^{-\top}(\mathbf{v}) \cdot \begin{bmatrix} \mathbf{A} \\ \mathbf{W} \end{bmatrix} \right) = \mathbf{S}_{SE(3)}\left(\mathbf{v}, \begin{bmatrix} \mathbf{A} \\ \mathbf{W} \end{bmatrix}\right). \end{aligned}$$

We have used references to functions from the Lie groups \mathbb{S}^3 and $SE(3)$ that are marked by an appropriate index. Note that the Lie algebras of UDQ and $SE(3)$ are isomorphic and by choosing the appropriate tilde operator, all functions related to only the Lie algebra coincide. If an element $(\mathbf{p}, \mathbf{r}) \in UDQ$ describes a rigid body configuration, $\mathbf{p} \in \mathbb{S}^3$ is the orientation as a unit quaternion and the position can be calculated as $\mathbf{x} = 2 \text{Im}(\mathbf{r} * \mathbf{p}^{-1})$.

B. Functions with Isolated Singularity

We consider the following functions with removable singularities:

$$\begin{aligned}
 f_1(x) &= \begin{cases} \frac{\sin x}{x}, & x > 0, \\ 1, & x = 0, \end{cases} \\
 f_2(x) &= \begin{cases} \frac{\cos x - 1}{x^2}, & x > 0, \\ -\frac{1}{2}, & x = 0, \end{cases} \\
 f_3(x) &= \begin{cases} \frac{x - \sin x}{x^3}, & x > 0, \\ \frac{1}{6}, & x = 0, \end{cases} \\
 f_4(x) &= \begin{cases} \frac{2 - 2 \cos x - x \sin x}{x^4}, & x > 0, \\ \frac{1}{12}, & x = 0, \end{cases} \\
 f_5(x) &= \begin{cases} \frac{x(2 + \cos x) - 3 \sin x}{x^5}, & x > 0, \\ \frac{1}{60}, & x = 0, \end{cases} \\
 f_6(x) &= \begin{cases} \frac{2 - x \cot(x/2)}{2x^2}, & x > 0, \\ \frac{1}{12}, & x = 0, \end{cases} \\
 f_7(x) &= \begin{cases} \frac{2 \arccos x}{\sqrt{1-x^2}}, & -1 < x < 1, \\ 2, & x = 1, \end{cases} \\
 f_8(x) &= \begin{cases} \frac{x \sin x + 4 \cos x + x^2 - 4}{4 \sin^2(x/2)x^4}, & x > 0, \\ \frac{1}{360}, & x = 0, \end{cases} \\
 f_9(x) &= \begin{cases} \frac{64 - 12x \cot(x/2) + \frac{4x^2(3+x \cot(x/2))}{\cos x - 1}}{8x^6}, & x > 0, \\ \frac{1}{3780}, & x = 0. \end{cases}
 \end{aligned}$$

All of them are continuous for $x > 0$ and right-continuous in $x = 0$, except for f_7 , which is continuous for $-1 < x < 1$ and left-continuous for $x = 1$. When these functions are evaluated on a computer near $x = 0$ (or $x = 1$ in the case of f_7), there is a large loss of significance. Therefore, these functions must be approximated, e. g., by Taylor polynomials in these cases in order to obtain an accurate and precise function value. The intervals where to calculate the function value by its actual function or by its Taylor approximation has to be chosen in a way that there is only negligible loss of significance and the Taylor approximation is of sufficient order. Of course, the order is chosen as low as possible at the same time. The limits that we used in the project `liegroup`, which

Table 1: Limits for when to evaluate the singular functions by their function definition and when by their Taylor polynomial

Function	Taylor polynomial for	Function definition for	Order of Taylor poly.
f_1	$x < 10^{-4}$	$x \geq 10^{-4}$	2
f_2	$x < 10^{-2}$	$x \geq 10^{-2}$	4
f_3	$x < 10^{-4}$	$x \geq 10^{-4}$	4
f_4	$x < 10^{-1}$	$x \geq 10^{-1}$	6
f_5	$x < 10^{-1}$	$x \geq 10^{-1}$	6
f_6	$x < 10^{-2}$	$x \geq 10^{-2}$	4
f_7	$x > 1 - 5 \times 10^{-3}$	$-1 < x \leq 1 - 5 \times 10^{-3}$	5
f_8	$x < 2 \times 10^{-1}$	$x \geq 2 \times 10^{-1}$	4
f_9	$x < 4 \times 10^{-1}$	$x \geq 4 \times 10^{-1}$	6

implements these nine functions, are chosen by hand using the Mathematica script in the project and are displayed in table 1. We aimed for an absolute error in the Taylor approximation of about 10^{-16} and a relative error in the actual function of about 10^{-10} . The implemented Taylor polynomials are:

$$T_{f_1}(x) = 1 - \frac{x^2}{6},$$

$$T_{f_2}(x) = -\frac{1}{2} + \frac{x^2}{24} - \frac{x^4}{720},$$

$$T_{f_3}(x) = \frac{1}{6} - \frac{x^2}{120} + \frac{x^4}{5040},$$

$$T_{f_4}(x) = \frac{1}{12} - \frac{x^2}{180} + \frac{x^4}{6720} - \frac{x^6}{453600},$$

$$T_{f_5}(x) = \frac{1}{60} - \frac{x^2}{1260} + \frac{x^4}{60480} - \frac{x^6}{4989600},$$

$$T_{f_6}(x) = \frac{1}{12} + \frac{x^2}{720} + \frac{x^4}{30240},$$

$$T_{f_7}(x) = 2 - \frac{2(x-1)}{3} + \frac{4(x-1)^2}{15} - \frac{4(x-1)^3}{35} + \frac{16(x-1)^4}{315} - \frac{16(x-1)^5}{693},$$

$$T_{f_8}(x) = \frac{1}{360} + \frac{x^2}{7560} + \frac{x^4}{201600} + \frac{x^6}{5987520} + \frac{691x^8}{130767436800},$$

$$T_{f_9}(x) = \frac{1}{3780} + \frac{x^2}{50400} + \frac{x^4}{997920} + \frac{691x^6}{16345929600}.$$

C. The Heavy Top in Several Lie Group Formulations

The equations of motion of the heavy top example, see e. g. [16] as well as remark 5.1, take the form (2.31). In this section, we will list the explicit form of mass matrix, generalized

forces, constraint function as well as its derivative. We will use the mass $m > 0$, the inertia tensor $\mathbf{J} \in \mathbb{R}^{3 \times 3}$, the gravity vector $\boldsymbol{\gamma} \in \mathbb{R}^3$ and the reference position $\mathbf{X} \in \mathbb{R}^3$ as defined in remark 5.1. Note that we do not give explicit formula for the Coriolis force $\widehat{\mathbf{v}(t)}^\top \cdot \mathbf{M} \cdot \mathbf{v}(t)$ as it can be easily calculated by the hat operator found in appendix A. Furthermore, we will show how to calculate the initial conditions from given initial rotation $p_0 \in \mathbb{S}^3$, initial position $\mathbf{x}_0 \in \mathbb{R}^3$ and initial angular velocity $\boldsymbol{\Omega}_0 \in \mathbb{R}^3$. Of course we assume that $p_0^{-1} \triangleright \mathbf{x}_0 = \mathbf{X}$. We will use the Euler map $\mathbf{R}_{\text{Euler}}: \mathbb{S}^3 \rightarrow SO(3)$ that maps a unit quaternion to the corresponding rotation matrix with

$$\mathbf{R}_{\text{Euler}}(p) = [p \triangleright \mathbf{e}_1, p \triangleright \mathbf{e}_2, p \triangleright \mathbf{e}_3],$$

see remark 2.31.

C.1. Unconstrained in $SO(3)$

We can formulate the heavy top in $SO(3)$ by only considering the rotation matrix $q(t) = \mathbf{R}(t) \in SO(3)$, where we can calculate the position $\mathbf{x}(t) = \mathbf{R}(t) \cdot \mathbf{X}$. The derivative vector of $\mathbf{R}(t)$ is the angular velocity $\mathbf{v}(t) = \boldsymbol{\Omega}(t) \in \mathbb{R}^3$. Of course, in this case, we do not need the constraint function: We can formally omit all occurrences of the constraint function $\boldsymbol{\Phi}$, its derivatives, as well as the Lagrange multiplier $\boldsymbol{\lambda}$, see remark 2.38.

$$\begin{aligned} \mathbf{M} &= \mathbf{J} - m \operatorname{skw}(\mathbf{X}) \cdot \operatorname{skw}(\mathbf{X}), & \mathbf{f}(t, q(t), \mathbf{v}(t)) &= m\mathbf{X} \times (\mathbf{R}^\top(t) \cdot \boldsymbol{\gamma}), \\ q_0 &= \mathbf{R}_{\text{Euler}}(p_0), & \mathbf{v}_0 &= \boldsymbol{\Omega}_0. \end{aligned}$$

C.2. Unconstrained in \mathbb{S}^3

Similarly, we can formulate the heavy top in \mathbb{S}^3 by only considering the unit quaternion $q(t) = p(t) \in \mathbb{S}^3$. The position can be obtained by $\mathbf{x}(t) = p(t) \triangleright \mathbf{X}$ and the derivative vector of $p(t)$ is the angular velocity $\mathbf{v}(t) = \boldsymbol{\Omega}(t) \in \mathbb{R}^3$. Again, we do not need the constraint function.

$$\begin{aligned} \mathbf{M} &= \mathbf{J} - m \operatorname{skw}(\mathbf{X}) \cdot \operatorname{skw}(\mathbf{X}), & \mathbf{f}(t, q(t), \mathbf{v}(t)) &= m\mathbf{X} \times (p^{-1}(t) \triangleright \boldsymbol{\gamma}), \\ q_0 &= p_0, & \mathbf{v}_0 &= \boldsymbol{\Omega}_0. \end{aligned}$$

C.3. Constrained in the Direct Product $SO(3) \times \mathbb{R}^3$

We can use $SO(3) \times \mathbb{R}^3$ to formulate the equations of motion for the heavy top by using the tuple of rotation matrix $\mathbf{R}(t)$ and position $\mathbf{x}(t)$ as the configuration $q(t) = (\mathbf{R}(t), \mathbf{x}(t)) \in SO(3) \times \mathbb{R}^3$. The derivative vector is comprised of angular velocity $\boldsymbol{\Omega}(t)$ with respect to the body-fixed frame and the velocity $\mathbf{u}(t)$ with respect to the inertia

frame: $\mathbf{v}(t) = [\boldsymbol{\Omega}^\top(t), \mathbf{u}^\top(t)]^\top \in \mathbb{R}^6$.

$$\begin{aligned} \mathbf{M} &= \text{blkdiag}(\mathbf{J}, m\mathbf{I}), & \mathbf{f}(t, q(t), \mathbf{v}(t)) &= \begin{bmatrix} \mathbf{0} \\ m\mathbf{R}^\top(t) \cdot \boldsymbol{\gamma} \end{bmatrix}, \\ \boldsymbol{\Phi}(q(t)) &= \mathbf{R}^\top(t) \cdot \mathbf{x}(t) - \mathbf{X}, & \mathbf{D}\boldsymbol{\Phi}(q(t)) &= [\text{skw}(\mathbf{X}), \mathbf{R}^\top(t)], \\ q_0 &= (\mathbf{R}_{\text{Euler}}(p_0), \mathbf{x}_0), & \mathbf{v}_0 &= \begin{bmatrix} \boldsymbol{\Omega}_0 \\ \mathbf{R}_{\text{Euler}}^\top(p_0) \cdot (\boldsymbol{\Omega}_0 \times \mathbf{X}) \end{bmatrix}. \end{aligned}$$

C.4. Constrained in the Direct Product $\mathbb{S}^3 \times \mathbb{R}^3$

Similarly, we can use $\mathbb{S}^3 \times \mathbb{R}^3$ to formulate the equations of motion of the heavy top by using the tuple of unit quaternion $p(t)$ and position $\mathbf{x}(t)$ as the configuration $q(t) = (p(t), \mathbf{x}(t)) \in \mathbb{S}^3 \times \mathbb{R}^3$. Again, the derivative vector is comprised of angular velocity $\boldsymbol{\Omega}(t)$ with respect to the body-fixed frame and velocity $\mathbf{u}(t)$ with respect to the inertia frame: $\mathbf{v}(t) = [\boldsymbol{\Omega}^\top(t), \mathbf{u}^\top(t)]^\top \in \mathbb{R}^6$.

$$\begin{aligned} \mathbf{M} &= \text{blkdiag}(\mathbf{J}, m\mathbf{I}), & \mathbf{f}(t, q(t), \mathbf{v}(t)) &= \begin{bmatrix} \mathbf{0} \\ p^{-1}(t) \triangleright (m\boldsymbol{\gamma}) \end{bmatrix}, \\ \boldsymbol{\Phi}(q(t)) &= p^{-1}(t) \triangleright \mathbf{x}(t) - \mathbf{X}, & \mathbf{D}\boldsymbol{\Phi}(q(t)) &= [\text{skw}(\mathbf{X}), \mathbf{R}_{\text{Euler}}^\top(p(t))], \\ q_0 &= (p_0, \mathbf{x}_0), & \mathbf{v}_0 &= \begin{bmatrix} \boldsymbol{\Omega}_0 \\ p_0^{-1} \triangleright (\boldsymbol{\Omega}_0 \times \mathbf{X}) \end{bmatrix}. \end{aligned}$$

C.5. Constrained in $SE(3)$

The Lie group $SE(3)$ can be used to formulate the equations of motion of the heavy top. Here, $q(t) = (\mathbf{R}(t), \mathbf{x}(t)) \in SE(3)$ is the configuration, using the tuple notation from appendix A.3, with the rotation matrix $\mathbf{R}(t) \in SO(3)$ and the position $\mathbf{x}(t)$. The derivative vector is comprised of angular velocity $\boldsymbol{\Omega}(t)$ and velocity $\mathbf{U}(t)$ with respect to the body-fixed frame: $\mathbf{v}(t) = [\boldsymbol{\Omega}^\top(t), \mathbf{U}^\top(t)]^\top \in \mathbb{R}^6$.

$$\begin{aligned} \mathbf{M} &= \text{blkdiag}(\mathbf{J}, m\mathbf{I}), & \mathbf{f}(t, q(t), \mathbf{v}(t)) &= \begin{bmatrix} \mathbf{0} \\ m\mathbf{R}^\top(t) \cdot \boldsymbol{\gamma} \end{bmatrix}, \\ \boldsymbol{\Phi}(q(t)) &= \mathbf{R}^\top(t) \cdot \mathbf{x}(t) - \mathbf{X}, & \mathbf{D}\boldsymbol{\Phi}(q(t)) &= [\text{skw}(\mathbf{X}), \mathbf{I}], \\ q_0 &= (\mathbf{R}_{\text{Euler}}(p_0), \mathbf{x}_0), & \mathbf{v}_0 &= \begin{bmatrix} \boldsymbol{\Omega}_0 \\ \boldsymbol{\Omega}_0 \times \mathbf{X} \end{bmatrix}. \end{aligned}$$

C.6. Constrained in the Semi-Direct Product $\mathbb{S}^3 \times \mathbb{R}^3$

Similarly, the Lie group $\mathbb{S}^3 \times \mathbb{R}^3$ can be used to formulate the equations of motion for the heavy top. Here, $q(t) = (p(t), \mathbf{x}(t)) \in \mathbb{S}^3 \times \mathbb{R}^3$ is the configuration with the unit quaternion $p(t) \in \mathbb{S}^3$ and the position $\mathbf{x}(t)$. The derivative vector is again comprised of angular velocity $\boldsymbol{\Omega}(t)$ and velocity $\mathbf{U}(t)$ with respect to the body-fixed frame: $\mathbf{v}(t) =$

$$[\boldsymbol{\Omega}^\top(t), \mathbf{U}^\top(t)]^\top \in \mathbb{R}^6.$$

$$\begin{aligned} \mathbf{M} &= \text{blkdiag}(\mathbf{J}, m\mathbf{I}), & \mathbf{f}(t, q(t), \mathbf{v}(t)) &= \begin{bmatrix} \mathbf{0} \\ p^{-1}(t) \triangleright (m\boldsymbol{\gamma}) \end{bmatrix}, \\ \boldsymbol{\Phi}(q(t)) &= p^{-1}(t) \triangleright \mathbf{x}(t) - \mathbf{X}, & \mathbf{D}\boldsymbol{\Phi}(q(t)) &= [\text{skw}(\mathbf{X}), \mathbf{I}], \\ q_0 &= (p_0, \mathbf{x}_0), & \mathbf{v}_0 &= \begin{bmatrix} \boldsymbol{\Omega}_0 \\ \boldsymbol{\Omega}_0 \times \mathbf{X} \end{bmatrix}. \end{aligned}$$

C.7. Constrained in Unit Dual Quaternions UDQ

Lastly, the Lie group UDQ of unit dual quaternions can be used to formulate the equations of motion for the heavy top as well. Here, $q(t) = (\mathbf{p}(t), \mathbf{r}(t)) \in UDQ$ is the configuration, using the notation from appendix A.6, with the quaternions $\mathbf{p}(t), \mathbf{r}(t)$. Here, $\mathbf{p}(t) \in \mathbb{S}^3$ specifies the orientation as before and the position can be calculated as $\mathbf{x}(t) = 2 \text{Im}(\mathbf{r}(t) * \mathbf{p}^{-1}(t))$. The derivative vector is again comprised of angular velocity $\boldsymbol{\Omega}(t)$ and velocity $\mathbf{U}(t)$ with respect to the body-fixed frame: $\mathbf{v}(t) = [\boldsymbol{\Omega}^\top(t), \mathbf{U}^\top(t)]^\top \in \mathbb{R}^6$.

$$\begin{aligned} \mathbf{M} &= \text{blkdiag}(\mathbf{J}, m\mathbf{I}), & \mathbf{f}(t, q(t), \mathbf{v}(t)) &= \begin{bmatrix} \mathbf{0} \\ m\mathbf{p}^{-1}(t) \triangleright \boldsymbol{\gamma} \end{bmatrix}, \\ \boldsymbol{\Phi}(q(t)) &= 2 \text{Im}(\mathbf{p}^{-1}(t) * \mathbf{r}(t)) - \mathbf{X}, & \mathbf{D}\boldsymbol{\Phi}(q(t)) &= [\text{skw}(\mathbf{X}), \mathbf{I}], \\ q_0 &= \left(p_0, \begin{bmatrix} 0 \\ \frac{1}{2}\mathbf{x}_0 \end{bmatrix} * p_0 \right), & \mathbf{v}_0 &= \begin{bmatrix} \boldsymbol{\Omega}_0 \\ \boldsymbol{\Omega}_0 \times \mathbf{X} \end{bmatrix}. \end{aligned}$$

D. Generalizing the Cosserat Beam Model: A Micropolar Shell Model

A shell model is used to describe thin structures $Q^* \subseteq \mathbb{R}^3$ that are a lot larger in two dimensions than in the remaining third dimension, see e. g. [67]. In this appendix we will show a way to generalize the Cosserat beam model from section 4.2 to two spatial dimensions, which will lead us to a Cosserat shell model. While there has been a lot of research on Cosserat shells, see e. g. [3, 13], this exploratory approach had already been touched on in [43], but requires additional research and is in heavy need of validation from the perspective of continuum mechanics and shell theory.

Since the orientation of each one-dimensional cross-section is described by a unit quaternion, the resulting shell model belongs to the micropolar shell models [28]. These models are in contrast to director-based shell models where the rotation of the one-dimensional cross section around its longitudinal axis is not considered [68]. For an extensive review on the literature on Cosserat shell theories, see e. g. [4].

Like in section 4.2, we will first describe the continuous Cosserat shell model in section D.1 and in section D.2, the continuous shell model will be discretized for a shell with rectangular base area.

D.1. The Continuous Cosserat Shell

We assume that for each time $t \in [t_0, t_e]$ the mass centroids of the shell are given by a surface $\mathbf{s} \mapsto \mathbf{x}(\mathbf{s}, t) \in \mathbb{R}^3$ for $\mathbf{s} \in \Omega \subseteq \mathbb{R}^2$, where Ω is a compact set with piecewise smooth boundary. We assume that the one-dimensional cross section at each mass centroid stays rigid. We describe the orientation of the cross section attached to $\mathbf{x}(\mathbf{s}, t)$ by a quaternion $p(\mathbf{s}, t) \in \mathbb{S}^3$. Thus, we describe the deformed shell $Q(t)$ as follows:

$$Q(t) = \{\mathbf{x}(\mathbf{s}, t) + p(\mathbf{s}, t) \triangleright [0, 0, \xi]^\top \in \mathbb{R}^3 : \mathbf{s} \in \Omega, \xi \in [-\theta(\mathbf{s})/2, \theta(\mathbf{s})/2]\},$$

where $\theta(\mathbf{s})$ is the thickness of the shell. Again, we will assume that all cross sections of the shell are equal, so we have $\theta(\mathbf{s}) \equiv \theta$.

The configuration space of the shell is given by $C(\Omega; \mathbb{S}^3 \times \mathbb{R}^3)$ and again, we choose the semi-direct product Lie group structure $(\mathbb{S}^3 \times \mathbb{R}^3, \circ)$. We denote time derivatives with a dot ($\partial \bullet / \partial t = \dot{\bullet}$) as before and introduce the notation $\partial_\ell \bullet = \partial \bullet / \partial s^{(\ell)}$ for spatial derivatives for $\ell = 1, 2$. Additionally, we write $\mathbf{s} = [s^{(1)}, s^{(2)}]^\top$. Furthermore, we will use the concept of derivative vectors and introduce $\mathbf{v}(\mathbf{s}, t)$ and $\mathbf{w}^{(\ell)}(\mathbf{s}, t)$ for $\ell = 1, 2$ with

$$\begin{aligned} \dot{q}(\mathbf{s}, t) &= \mathrm{d}L_{q(\mathbf{s}, t)}(e) \widetilde{\mathbf{v}(\mathbf{s}, t)}, \\ \partial_\ell q(\mathbf{s}, t) &= \mathrm{d}L_{q(\mathbf{s}, t)}(e) \widetilde{\mathbf{w}^{(\ell)}(\mathbf{s}, t)}, \end{aligned} \quad \ell = 1, 2.$$

Similar to the case of the Cosserat beam model, we will now present the kinetic and potential energy of the shell by integrals over energy densities. The kinetic energy of the shell is given by

$$\mathcal{T}(\mathbf{v}(\bullet, t)) = \int_{\Omega} T(\mathbf{v}(\mathbf{s}, t)) \, \mathrm{d}\mathbf{s}$$

with a kinetic energy density

$$T(\mathbf{v}(\mathbf{s}, t)) = \frac{1}{2} \mathbf{v}^\top(\mathbf{s}, t) \cdot \mathbf{N} \cdot \mathbf{v}(\mathbf{s}, t),$$

where $\mathbf{N} = \mathrm{blkdiag}(\mathbf{J}, \theta \rho \mathbf{I}_3)$. Here, $\rho > 0$ is the density of the shell and $\mathbf{J} \in \mathbb{R}^{3 \times 3}$ is the inertia tensor of the one-dimensional cross section $\{[0, 0, \xi]^\top : \theta < \xi < \theta\}$ and is given by

$$\mathbf{J} = \mathrm{diag}\left(\frac{\theta^3}{12}, \frac{\theta^3}{12}, 0\right).$$

The result can be obtained by considering a thin three-dimensional rigid body $[-\varepsilon, \varepsilon] \times [-\varepsilon, \varepsilon] \times [-\theta/2, \theta/2]$, calculating its inertia tensor by (4.2), dividing it by $(2\varepsilon)^2$, the product of the thicknesses and letting $\varepsilon \rightarrow 0$. As before, $T(\mathbf{v}(\mathbf{s}, t))$ is essentially the sum of the rotatory and translatory energy density of the now one-dimensional cross section. Note that now \mathbf{J} is singular because the mass moment of inertia along one of the principal axes of the cross section – corresponding to drilling motions – vanishes.

Then we define the potential energy by

$$\mathcal{U}(q(\bullet, t)) = \int_{\Omega} U(q(\mathbf{s}, t)) \, \mathrm{d}\mathbf{s}$$

with a potential energy density

$$U(q(\mathbf{s}, t)) = \frac{1}{2} \begin{bmatrix} \mathbf{w}^{(1)}(\mathbf{s}, t) - \mathbf{w}^{*,(1)}(\mathbf{s}) \\ \mathbf{w}^{(2)}(\mathbf{s}, t) - \mathbf{w}^{*,(2)}(\mathbf{s}) \end{bmatrix}^\top \cdot \mathbf{C} \cdot \begin{bmatrix} \mathbf{w}^{(1)}(\mathbf{s}, t) - \mathbf{w}^{*,(1)}(\mathbf{s}) \\ \mathbf{w}^{(2)}(\mathbf{s}, t) - \mathbf{w}^{*,(2)}(\mathbf{s}) \end{bmatrix}$$

with a symmetric matrix $\mathbf{C} \in \mathbb{R}^{12 \times 12}$ containing material and geometric parameters and $\mathbf{w}^{*,(i)}(\mathbf{s}) \in \mathbb{R}^6$, which reflect the undeformed configuration of the shell. We have assumed that the potential energy of the shell is quadratic and indeed, a careful translation of the potential energy in [67] to the language of derivative vectors leads for curvature exponent $p = 1$ from [67] to such a quadratic term. Furthermore, we will decompose the matrix \mathbf{C} into four parts:

$$\mathbf{C} = \begin{bmatrix} \mathbf{C}^{(11)} & \mathbf{C}^{(12)} \\ \mathbf{C}^{(21)} & \mathbf{C}^{(22)} \end{bmatrix}.$$

Now, we want to derive the equations of motion of the shell by applying Hamilton's principle

$$0 = \delta \int_{t_0}^{t_e} \mathcal{T}(\mathbf{v}(\mathbf{s}, t)) - \mathcal{U}(q(\mathbf{s}, t)) dt \quad (\text{D.1})$$

with the usual boundary conditions $\delta \mathbf{q}(t_0, \mathbf{s}) = \delta \mathbf{q}(t_e, \mathbf{s}) = \mathbf{0}$. Considering both terms separately, we get

$$\begin{aligned} \delta \int_{t_0}^{t_e} \mathcal{T}(\mathbf{v}(\mathbf{s}, t)) dt &= \int_{\Omega} \int_{t_0}^{t_e} \delta T(\mathbf{v}(\mathbf{s}, t)) dt d\mathbf{s} = \int_{\Omega} \int_{t_0}^{t_e} \mathbf{v}^\top(\mathbf{s}, t) \cdot \mathbf{N} \cdot \delta \mathbf{v}(\mathbf{s}, t) dt d\mathbf{s} \\ &= \int_{\Omega} \int_{t_0}^{t_e} \mathbf{v}^\top(\mathbf{s}, t) \cdot \mathbf{N} \cdot \left(\widehat{\mathbf{v}(\mathbf{s}, t)} \cdot \delta \mathbf{q}(\mathbf{s}, t) + \frac{\partial}{\partial t} \delta \mathbf{q}(\mathbf{s}, t) \right) dt d\mathbf{s} \\ &= \int_{\Omega} \underbrace{\left[\mathbf{v}^\top(\mathbf{s}, t) \cdot \mathbf{N} \cdot \delta \mathbf{q}(\mathbf{s}, t) \right]_{t=t_0}^{t_e}}_{=0} + \int_{t_0}^{t_e} \left(\mathbf{v}^\top(\mathbf{s}, t) \cdot \mathbf{N} \cdot \widehat{\mathbf{v}(\mathbf{s}, t)} - \dot{\mathbf{v}}^\top(\mathbf{s}, t) \cdot \mathbf{N} \right) \cdot \delta \mathbf{q}(\mathbf{s}, t) dt d\mathbf{s}, \end{aligned}$$

where $\delta \mathbf{q}(\mathbf{s}, t)$ is the derivative vector associated with $\delta q(\mathbf{s}, t)$. We have applied partial integration, where the terms $\delta \mathbf{q}(\mathbf{s}, t_0)$ and $\delta \mathbf{q}(\mathbf{s}, t_e)$ vanish by Hamilton's principle. Now we treat the second integral, where, for readability, we drop the arguments \mathbf{s} and t :

$$\begin{aligned} \delta \int_{t_0}^{t_e} \mathcal{U}(q) dt &= \int_{t_0}^{t_e} \int_{\Omega} \delta U(q) d\mathbf{s} dt = \int_{t_0}^{t_e} \int_{\Omega} \begin{bmatrix} \mathbf{w}^{(1)} - \mathbf{w}^{*,(1)} \\ \mathbf{w}^{(2)} - \mathbf{w}^{*,(2)} \end{bmatrix}^\top \cdot \mathbf{C} \cdot \begin{bmatrix} \delta \mathbf{w}^{(1)} \\ \delta \mathbf{w}^{(2)} \end{bmatrix} d\mathbf{s} dt \\ &= \int_{t_0}^{t_e} \int_{\Omega} \begin{bmatrix} \mathbf{w}^{(1)} - \mathbf{w}^{*,(1)} \\ \mathbf{w}^{(2)} - \mathbf{w}^{*,(2)} \end{bmatrix}^\top \cdot \mathbf{C} \cdot \begin{bmatrix} \widehat{\mathbf{w}^{(1)}} \cdot \delta \mathbf{q} + \partial_1 \delta \mathbf{q} \\ \widehat{\mathbf{w}^{(2)}} \cdot \delta \mathbf{q} + \partial_2 \delta \mathbf{q} \end{bmatrix} d\mathbf{s} dt \\ &= \int_{t_0}^{t_e} \int_{\Omega} \begin{bmatrix} \mathbf{w}^{(1)} - \mathbf{w}^{*,(1)} \\ \mathbf{w}^{(2)} - \mathbf{w}^{*,(2)} \end{bmatrix}^\top \cdot \mathbf{C} \cdot \begin{bmatrix} \widehat{\mathbf{w}^{(1)}} \cdot \delta \mathbf{q} \\ \widehat{\mathbf{w}^{(2)}} \cdot \delta \mathbf{q} \end{bmatrix} - \sum_{i,j=1}^2 \partial_j (\mathbf{w}^{(i)})^\top \cdot \mathbf{C}^{(ij)} \cdot \delta \mathbf{q} d\mathbf{s} dt \\ &\quad + \int_{t_0}^{t_e} \int_{\partial \Omega} \sum_{\ell=1}^2 \left[\begin{bmatrix} \mathbf{w}^{(\ell)} - \mathbf{w}^{*,(\ell)} \\ \mathbf{w}^{(\ell)} - \mathbf{w}^{*,(\ell)} \end{bmatrix}^\top \cdot \mathbf{C}^{(\ell 1)} \cdot \delta \mathbf{q} \right]^\top \cdot \mathbf{n} d\sigma dt \\ &= \int_{t_0}^{t_e} \left(\sum_{i,j=1}^2 (\mathbf{w}^{(i)} - \mathbf{w}^{*,(i)})^\top \cdot \mathbf{C}^{(ij)} \cdot \widehat{\mathbf{w}^{(j)}} - \partial_j (\mathbf{w}^{(i)})^\top \cdot \mathbf{C}^{(ij)} \right) \cdot \delta \mathbf{q} d\mathbf{s} dt. \end{aligned}$$

We have applied the divergence theorem where an integral over $\partial\Omega$, the boundary of Ω , is introduced and where $\mathbf{n}(\mathbf{s})$ are the unit normal vectors of $\mathbf{s} \in \partial\Omega$. This integral vanishes, since we assume – as in the Cosserat beam model – that the internal moments and forces at the boundary of the shell vanish, thus it is free at its boundary.

Putting everything together, we get the equations of motion of the continuous Cosserat shell model:

$$\dot{q} = dL_q(e) \tilde{\mathbf{v}}, \quad (\text{D.2a})$$

$$\partial_\ell q = dL_q(e) \widetilde{\mathbf{w}}^{(\ell)}, \quad \ell = 1, 2, \quad (\text{D.2b})$$

$$\mathbf{N} \cdot \dot{\mathbf{v}} = \widehat{\mathbf{v}}^\top \cdot \mathbf{N} \cdot \mathbf{v} + \sum_{i,j=1}^2 \partial_i \mathbf{g}^{(ij)} - \widetilde{\mathbf{w}}^{(i)\top} \cdot \mathbf{g}^{(ij)}, \quad (\text{D.2c})$$

$$\mathbf{g}^{(ij)} = \mathbf{C}^{(ij)} \cdot (\mathbf{w}^{(j)} - \mathbf{w}^{*,(j)}), \quad i, j = 1, 2, \quad (\text{D.2d})$$

where we have omitted the arguments \mathbf{s} and t for readability as well as introduced the generalized forces $\mathbf{g}^{(ij)}(\mathbf{s}, t) \in \mathbb{R}^6$ for $i, j = 1, 2$.

D.2. Discretizing the Cosserat Shell Model in Space

We will apply a spatial discretization similarly to the way we have discretized the continuous beam model in section 4.2.2. For simplicity, we will restrict ourselves to a rectangular set $\Omega = [0, L^{(1)}] \times [0, L^{(2)}]$ and constant spatial step sizes. We introduce an $M^{(1)} \times M^{(2)}$ -sized grid $\{s_0^{(1)}, \dots, s_{M^{(1)}}^{(1)}\} \times \{s_0^{(2)}, \dots, s_{M^{(2)}}^{(2)}\}$, where

$$s_{m^{(\ell)}}^{(\ell)} = m^{(\ell)} \Delta s^{(\ell)}, \quad m^{(\ell)} = 0, \dots, M^{(\ell)}$$

with step sizes $\Delta s^{(\ell)} = L^{(\ell)}/M^{(\ell)}$ for $\ell = 1, 2$. Now, we consider configurations $q^d(\mathbf{s}, t)$ of the following form

$$q^d\left(\begin{bmatrix} s^{(1)} \\ s^{(2)} \end{bmatrix}, t\right) = \text{Ip}\left(\frac{s^{(1)} - s_{m^{(1)}}^{(1)}}{\Delta s^{(1)}}, \text{Ip}\left(\frac{s^{(2)} - s_{m^{(2)}}^{(2)}}{\Delta s^{(2)}}, q_{m^{(1)}, m^{(2)}}(t), q_{m^{(1)}, m^{(2)}+1}(t)\right), \right. \\ \left. \text{Ip}\left(\frac{s^{(2)} - s_{m^{(2)}}^{(2)}}{\Delta s^{(2)}}, q_{m^{(1)}+1, m^{(2)}}(t), q_{m^{(1)}+1, m^{(2)}+1}(t)\right)\right)$$

for $s^{(\ell)} \in [s_{m^{(\ell)}}^{(\ell)}, s_{m^{(\ell)}+1}^{(\ell)}]$ and $\ell = 1, 2$ with the interpolation operator (2.24). The interpolation is done in the $s^{(2)}$ direction first and subsequently in the $s^{(1)}$ direction. This is a generalization of bilinear interpolation. Note that the interpolating function is different, when we interpolate in the $s^{(1)}$ direction first. We will later see, however, that the order will not influence the resulting scheme.

Furthermore, we define the derivative vectors $\mathbf{w}^{d,(\ell)}$ for $\ell = 1, 2$ and \mathbf{v}^d of $q^d(\mathbf{s}, t)$ with respect to the two spatial directions and t , respectively, where

$$\dot{q}^d(\mathbf{s}, t) = dL_{q^d(\mathbf{s}, t)}(e) \widetilde{\mathbf{v}}^d(\mathbf{s}, t), \\ \partial_\ell q^d(\mathbf{s}, t) = dL_{q^d(\mathbf{s}, t)}(e) \widetilde{\mathbf{w}}^{d,(\ell)}(\mathbf{s}, t), \quad \ell = 1, 2$$

and where they are well-defined. It can be seen, similar to section 4.2.2, that it holds

$$\begin{aligned}\mathbf{w}^{\text{d},(1)}\left(\begin{bmatrix} s^{(1)} \\ s_{m^{(2)}}^{(2)} \end{bmatrix}, t\right) &\equiv \mathbf{w}_{m^{(1)}+1/2, m^{(2)}}^{(1)}, & s^{(1)} \in (s_{m^{(1)}}^{(1)}, s_{m^{(1)}+1}^{(1)}), \\ \mathbf{w}^{\text{d},(2)}\left(\begin{bmatrix} s_{m^{(1)}}^{(1)} \\ s^{(2)} \end{bmatrix}, t\right) &\equiv \mathbf{w}_{m^{(1)}, m^{(2)}+1/2}^{(2)}, & s^{(2)} \in (s_{m^{(2)}}^{(2)}, s_{m^{(2)}+1}^{(2)}),\end{aligned}$$

where

$$\begin{aligned}\mathbf{w}_{m^{(1)}+1/2, m^{(2)}}^{(1)}(t) &= \frac{1}{\Delta s^{(1)}} \widetilde{\log}(q_{m^{(1)}, m^{(2)}}^{-1}(t) \circ q_{m^{(1)}+1, m^{(2)}}(t)), \\ \mathbf{w}_{m^{(1)}, m^{(2)}+1/2}^{(2)}(t) &= \frac{1}{\Delta s^{(2)}} \widetilde{\log}(q_{m^{(1)}, m^{(2)}}^{-1}(t) \circ q_{m^{(1)}, m^{(2)}+1}(t))\end{aligned}$$

for all appropriate indices $m^{(1)}, m^{(2)}$. Furthermore, it holds

$$\mathbf{v}^{\text{d}}([s_{m^{(1)}}^{(1)}, s_{m^{(2)}}^{(2)}]^\top, t) = \mathbf{v}_{m^{(1)}, m^{(2)}}(t),$$

where $\mathbf{v}_{m^{(1)}, m^{(2)}}(t)$ is the derivative vector of $q_{m^{(1)}, m^{(2)}}(t)$.

We will only consider trajectories of this type in the variational principle (D.1) and approximate the spatial integrals by combinations of trapezoidal and midpoint rule in order to arrive at a discrete variational principle (2.39) with

$$q(t) = \begin{bmatrix} q_{1,1}(t) \\ \vdots \\ q_{M^{(1)},1}(t) \\ q_{1,2}(t) \\ \vdots \\ q_{M^{(1)},2}(t) \\ \vdots \\ q_{M^{(1)},M^{(2)}}(t) \end{bmatrix}, \quad \mathbf{v}(t) = \begin{bmatrix} \mathbf{v}_{1,1}(t) \\ \vdots \\ \mathbf{v}_{M^{(1)},1}(t) \\ \mathbf{v}_{1,2}(t) \\ \vdots \\ \mathbf{v}_{M^{(1)},2}(t) \\ \vdots \\ \mathbf{v}_{M^{(1)},M^{(2)}}(t) \end{bmatrix}, \quad (\text{D.3})$$

ultimately leading to equations of motion of the form (2.31). Note that since we are in an unconstrained setting, we omit all occurrences of the constraint function Φ and the Lagrange multipliers λ , see remark 2.38.

Let us now derive a discrete kinetic energy \mathcal{T}^{d} by considering $\mathcal{T}(\mathbf{v}^{\text{d}}(\bullet, t))$ and approxi-

mating the integrals using the trapezoidal rule:

$$\begin{aligned}
\mathcal{T}(\mathbf{v}^d) &= \sum_{m^{(1)}=1}^{M^{(1)}} \sum_{m^{(2)}=1}^{M^{(2)}} \int_{s_{m^{(1)}-1}^{(1)}}^{s_{m^{(1)}}^{(1)}} \int_{s_{m^{(2)}-1}^{(2)}}^{s_{m^{(2)}}^{(2)}} T(\mathbf{v}^d) \, ds^{(1)} \, ds^{(2)} \\
&\approx \sum_{m^{(1)}=1}^{M^{(1)}} \sum_{m^{(2)}=1}^{M^{(2)}} \frac{\Delta s^{(1)} \Delta s^{(2)}}{4} \left(T(\mathbf{v}_{s_{m^{(1)}-1}^{(1)}, s_{m^{(2)}-1}^{(2)}}) + T(\mathbf{v}_{s_{m^{(1)}}^{(1)}, s_{m^{(2)}-1}^{(2)}}) \right. \\
&\quad \left. + T(\mathbf{v}_{s_{m^{(1)}-1}^{(1)}, s_{m^{(2)}}^{(2)}}) + T(\mathbf{v}_{s_{m^{(1)}}^{(1)}, s_{m^{(2)}}^{(2)}}) \right) \\
&= \Delta s^{(1)} \Delta s^{(2)} \sum_{m^{(1)}=0}^{M^{(1)}} \sum_{m^{(2)}=0}^{M^{(2)}} \chi_{m^{(1)}, m^{(2)}} \mathbf{v}_{s_{m^{(1)}}, s_{m^{(2)}}}^\top \cdot \mathbf{N} \cdot \mathbf{v}_{s_{m^{(1)}}, s_{m^{(2)}}} \\
&= \mathbf{v}^\top \cdot \mathbf{M} \cdot \mathbf{v} =: \mathcal{T}^d(\mathbf{v}),
\end{aligned}$$

where we have omitted some of the arguments and with

$$\chi_{a^{(1)}, a^{(2)}} = \begin{cases} \frac{1}{4}, & (a^{(1)} = 0 \vee a^{(1)} = M^{(1)}) \wedge (a^{(2)} = 0 \vee a^{(2)} = M^{(2)}), \\ \frac{1}{2}, & (a^{(1)} = 0 \vee a^{(1)} = M^{(1)}) \wedge (0 < a^{(2)} < M^{(2)}), \\ \frac{1}{2}, & (0 < a^{(1)} < M^{(1)}) \wedge (a^{(2)} = 0 \vee a^{(2)} = M^{(2)}), \\ 1, & (0 < a^{(1)} < M^{(1)}) \wedge (0 < a^{(2)} < M^{(2)}) \\ 0, & \text{otherwise} \end{cases}$$

for $a^{(1)}, a^{(2)} \in \mathbb{R}$ and a mass matrix

$$\mathbf{M} = \Delta s^{(1)} \Delta s^{(2)} \text{blkdiag}(\chi_{1,1} \mathbf{N}, \dots, \chi_{M^{(1)},1} \mathbf{N}, \chi_{1,2} \mathbf{N}, \dots, \chi_{M^{(1)},2} \mathbf{N}, \dots, \chi_{M^{(1)},M^{(2)}} \mathbf{N}).$$

Since \mathbf{J} (and therefore \mathbf{N} and \mathbf{M}) are singular, we will use an approximation of the inertia tensor \mathbf{J} instead of \mathbf{J} itself in the definition of \mathbf{M} :

$$\mathbf{J} \approx \text{diag}\left(\frac{1}{12}\theta((\Delta s^{(2)})^2 + \theta^2), \frac{1}{12}\theta((\Delta s^{(1)})^2 + \theta^2), \frac{1}{12}\theta((\Delta s^{(1)})^2 + (\Delta s^{(2)})^2)\right). \quad (\text{D.4})$$

We have chosen this approximation by considering the inertia tensor of a rigid body

$$[-\Delta s^{(1)}/2, \Delta s^{(1)}/2] \times [-\Delta s^{(1)}/2, \Delta s^{(1)}/2] \times [-\theta/2, \theta/2],$$

see (4.2), and dividing it by $\Delta s^{(1)}$ and $\Delta s^{(2)}$, since \mathbf{J} actually measures an inertial density.

Now we want to derive the discrete potential energy \mathcal{U}^d by considering $\mathcal{U}(q^d(\bullet, t))$ and approximating the integrals. In order to do that, we split up $U(q^d(\mathbf{s}, t))$ in four parts with $i, j = 1, 2$:

$$\begin{aligned}
U^{(ij)}(\mathbf{w}^{d,(i)}(\mathbf{s}, t), \mathbf{w}^{d,(j)}(\mathbf{s}, t)) \\
= \frac{1}{2} (\mathbf{w}^{d,(i)}(\mathbf{s}, t) - \mathbf{w}^{*,(i)}(\mathbf{s}))^\top \cdot \mathbf{C}^{(ij)} \cdot (\mathbf{w}^{d,(j)}(\mathbf{s}, t) - \mathbf{w}^{*,(j)}(\mathbf{s}))
\end{aligned}$$

and it holds

$$U(q^d(\mathbf{s}, t)) = \sum_{i=1}^2 \sum_{j=1}^2 U^{(ij)}(\mathbf{w}^{d,(j)}(\mathbf{s}, t), \mathbf{w}^{d,(i)}(\mathbf{s}, t)).$$

Now, for $U^{(ii)}$ with $i = 1, 2$, we split up the integration range and apply the midpoint rule for one spatial direction and the trapezoidal rule for the other spatial direction:

$$\begin{aligned} & \int_{\Omega} U^{(11)}(\mathbf{w}^{d,(1)}, \mathbf{w}^{d,(1)}) d\mathbf{s} \\ &= \sum_{m^{(1)}=1}^{M^{(1)}} \sum_{m^{(2)}=1}^{M^{(2)}} \int_{s_{m^{(1)}-1}^{(1)}}^{s_{m^{(1)}}^{(1)}} \int_{s_{m^{(2)}-1}^{(2)}}^{s_{m^{(2)}}^{(2)}} U^{(11)}(\mathbf{w}^{d,(1)}, \mathbf{w}^{d,(1)}) ds^{(1)} ds^{(2)} \\ &\approx \frac{\Delta s^{(1)} \Delta s^{(2)}}{2} \sum_{m^{(1)}=1}^{M^{(1)}} \sum_{m^{(2)}=1}^{M^{(2)}} (U^{(11)}(\mathbf{w}_{m^{(1)}-1/2, m^{(2)}}^{(1)}, \mathbf{w}_{m^{(1)}-1/2, m^{(2)}}^{(1)}) \\ &\quad + U^{(11)}(\mathbf{w}_{m^{(1)}-1/2, m^{(2)}-1}^{(1)}, \mathbf{w}_{m^{(1)}-1/2, m^{(2)}-1}^{(1)})), \\ &= \Delta s^{(1)} \Delta s^{(2)} \sum_{m^{(1)}=0}^{M^{(1)}} \sum_{m^{(2)}=0}^{M^{(2)}} \chi_{m^{(1)}-1/2, m^{(2)}} U^{(11)}(\mathbf{w}_{m^{(1)}-1/2, m^{(2)}}^{(1)}, \mathbf{w}_{m^{(1)}-1/2, m^{(2)}}^{(1)}), \end{aligned}$$

where we have omitted some arguments. Note that this is well-defined even for $m^{(1)} = 0$ since all undefined quantities are multiplied with $\chi_{-1/2, m^{(2)}} = 0$. The case of $U^{(22)}$ can be treated analogously. We can consider $U^{(12)}$ in a similar way, but use the midpoint rule in both directions and approximate the value of $\mathbf{w}^{d,(\ell)}$ for $\ell = 1, 2$ at the midpoints $[s_{m^{(1)}}^{(1)} + \Delta s^{(1)}/2, s_{m^{(2)}}^{(2)} + \Delta s^{(2)}/2]^\top$ by their mean value:

$$\begin{aligned} & \int_{\Omega} U^{(12)}(\mathbf{w}^{d,(1)}, \mathbf{w}^{d,(2)}) d\mathbf{s} \\ &\approx \Delta s^{(1)} \Delta s^{(2)} \sum_{m^{(1)}=1}^{M^{(1)}} \sum_{m^{(2)}=1}^{M^{(2)}} U^{(12)}(\mathbf{w}_{m^{(1)}-1/2, m^{(2)}-1/2}^{(1)}, \mathbf{w}_{m^{(1)}-1/2, m^{(2)}-1/2}^{(2)}) \\ &= \Delta s^{(1)} \Delta s^{(2)} \sum_{m^{(1)}=0}^{M^{(1)}} \sum_{m^{(2)}=0}^{M^{(2)}} \chi_{m^{(1)}-1/2, m^{(2)}-1/2} U^{(12)}(\mathbf{w}_{m^{(1)}-1/2, m^{(2)}-1/2}^{(1)}, \mathbf{w}_{m^{(1)}-1/2, m^{(2)}-1/2}^{(2)}) \end{aligned}$$

and analogously for $U^{(21)}$. Note that in the definition of $U^{(ij)}$ with discretized arguments we have to use the corresponding discretized quantities defined by

$$\mathbf{w}_{a,b}^{*,(\ell)} = \mathbf{w}^{*,(\ell)}([s_a^{(1)}, s_b^{(2)}]^\top), \quad \ell = 1, 2$$

for appropriate indices a, b . Furthermore we have introduced the midpoints and mean

values

$$\begin{aligned}
s_{m^{(\ell)}-1/2}^{(\ell)} &= \frac{1}{2}(s_{m^{(\ell)}-1}^{(\ell)} + s_{m^{(\ell)}}^{(\ell)}), \\
\mathbf{w}_{m^{(1)}-1/2, m^{(2)}-1/2}^{(1)} &= \frac{1}{2}(\mathbf{w}_{m^{(1)}-1/2, m^{(2)}-1}^{(1)} + \mathbf{w}_{m^{(1)}-1/2, m^{(2)}}^{(1)}), \\
\mathbf{w}_{m^{(1)}-1/2, m^{(2)}-1/2}^{(2)} &= \frac{1}{2}(\mathbf{w}_{m^{(1)}-1, m^{(2)}-1/2}^{(2)} + \mathbf{w}_{m^{(1)}, m^{(2)}-1/2}^{(2)})
\end{aligned}$$

Plugging everything together, we define

$$\begin{aligned}
\mathcal{U}^d(q) &= \Delta s^{(1)} \Delta s^{(2)} \sum_{m^{(1)}=0}^{M^{(1)}} \sum_{m^{(2)}=0}^{M^{(2)}} \left(\chi_{m^{(1)}-1/2, m^{(2)}} U^{(11)}(\mathbf{w}_{m^{(1)}-1/2, m^{(2)}}^{(1)}, \mathbf{w}_{m^{(1)}-1/2, m^{(2)}}^{(1)}) \right. \\
&\quad + \chi_{m^{(1)}, m^{(2)}-1/2} U^{(22)}(\mathbf{w}_{m^{(1)}, m^{(2)}-1/2}^{(2)}, \mathbf{w}_{m^{(1)}, m^{(2)}-1/2}^{(2)}) \\
&\quad \left. + 2\chi_{m^{(1)}-1/2, m^{(2)}-1/2} U^{(12)}(\mathbf{w}_{m^{(1)}-1/2, m^{(2)}-1/2}^{(1)}, \mathbf{w}_{m^{(1)}-1/2, m^{(2)}-1/2}^{(2)}) \right).
\end{aligned}$$

Note that due to the symmetry of \mathbf{C} , we have $U^{(12)}(\mathbf{a}, \mathbf{b}) = U^{(21)}(\mathbf{b}, \mathbf{a})$.

In order to write the equations of motion of the spatially discretized shell, we apply remark 2.35. In order to do this, we also need to calculate the derivative of the potential energy. This can be done in components:

$$\begin{aligned}
\mathbf{D}_{q_{m^{(1)}, m^{(2)}}} \mathcal{U}^d &= \Delta s^{(1)} \Delta s^{(2)} \frac{1}{2} \sum_{a, b \in \{-1/2, 1/2\}} \left((\mathbf{g}_{m^{(1)}+a, m^{(2)}}^{(11)} + \mathbf{g}_{m^{(1)}+a, m^{(2)}+b}^{(12)})^\top \cdot \mathbf{D}_{q_{m^{(1)}, m^{(2)}}} \mathbf{w}_{m^{(1)}+a, m^{(2)}}^{(1)} \right. \\
&\quad \left. + (\mathbf{g}_{m^{(1)}, m^{(2)}+b}^{(22)} + \mathbf{g}_{m^{(1)}+a, m^{(2)}+b}^{(21)})^\top \cdot \mathbf{D}_{q_{m^{(1)}, m^{(2)}}} \mathbf{w}_{m^{(1)}, m^{(2)}+b}^{(2)} \right),
\end{aligned}$$

where

$$\begin{aligned}
\mathbf{g}_{m^{(1)}-1/2, m^{(2)}}^{(11)} &= \chi_{m^{(1)}-1/2, m^{(2)}} \mathbf{C}^{(11)} \cdot (\mathbf{w}_{m^{(1)}-1/2, m^{(2)}}^{(1)} - \mathbf{w}_{m^{(1)}-1/2, m^{(2)}}^{*,(1)}), \\
\mathbf{g}_{m^{(1)}, m^{(2)}-1/2}^{(22)} &= \chi_{m^{(1)}, m^{(2)}-1/2} \mathbf{C}^{(22)} \cdot (\mathbf{w}_{m^{(1)}, m^{(2)}-1/2}^{(2)} - \mathbf{w}_{m^{(1)}, m^{(2)}-1/2}^{*,(2)}), \\
\mathbf{g}_{m^{(1)}-1/2, m^{(2)}-1/2}^{(12)} &= \chi_{m^{(1)}-1/2, m^{(2)}-1/2} \mathbf{C}^{(12)} \cdot (\mathbf{w}_{m^{(1)}-1/2, m^{(2)}-1/2}^{(2)} - \mathbf{w}_{m^{(1)}-1/2, m^{(2)}-1/2}^{*,(2)}), \\
\mathbf{g}_{m^{(1)}-1/2, m^{(2)}-1/2}^{(21)} &= \chi_{m^{(1)}-1/2, m^{(2)}-1/2} \mathbf{C}^{(21)} \cdot (\mathbf{w}_{m^{(1)}-1/2, m^{(2)}-1/2}^{(1)} - \mathbf{w}_{m^{(1)}-1/2, m^{(2)}-1/2}^{*,(1)})
\end{aligned}$$

for all applicable indices, omitting some arguments.

All in all, we can formulate the equations of motion of the spatially discretized Cosserat

shell model in components

$$\begin{aligned}
\dot{q}_{m^{(1)},m^{(2)}} &= \mathbf{d}L_{q_{m^{(1)},m^{(2)}}}(e) \widetilde{\mathbf{v}}_{m^{(1)},m^{(2)}} \\
\Delta s^{(1)} \Delta s^{(2)} \chi_{m^{(1)},m^{(2)}} \mathbf{N} \cdot \dot{\mathbf{v}}_{m^{(1)},m^{(2)}} & \\
&= \Delta s^{(1)} \Delta s^{(2)} \chi_{m^{(1)},m^{(2)}} \widetilde{\mathbf{v}}_{m^{(1)},m^{(2)}} \mathbf{N} \cdot \mathbf{v}_{m^{(1)},m^{(2)}} \\
&+ \sum_{a,b \in \{-1/2, 1/2\}} \left(\Delta s^{(2)} a \mathbf{T}^{-\top} (-2a \Delta s^{(1)} \mathbf{w}_{m^{(1)+1/2,m^{(2)}}^{(1)}) (\mathbf{g}_{m^{(1)+a,m^{(2)}}}^{(11)} + \mathbf{g}_{m^{(1)+a,m^{(2)}+b}^{(12)}) \right. \\
&\quad \left. + \Delta s^{(1)} b \mathbf{T}^{-\top} (-2b \Delta s^{(2)} \mathbf{w}_{m^{(1),m^{(2)}+b}^{(2)}) (\mathbf{g}_{m^{(1),m^{(2)}+b}^{(22)}} + \mathbf{g}_{m^{(1)+a,m^{(2)}+b}^{(21)}) \right),
\end{aligned}$$

where we have used an analogue of (4.17) and where \mathbf{N} contains the non-singular approximation (D.4) of \mathbf{J} .

Publikationsliste

- Hante, S., Tumiotto, D., Arnold, M.: A Lie group variational integration approach to the full discretization of a constrained geometrically exact Cosserat beam model. *Multibody System Dynamics* **54**, 97–123 (2022)
- Hante, S.: A Lie group generalization of the RATTLE scheme applied to non-holonomic constraints. In: T. Gleim, S. Lange (eds.) *Proceedings of 8th GACM Colloquium on Computational Mechanics*, pp. 207–210. Kassel University Press, Kassel (2019)
- Hante, S., Arnold, M.: RATTLie: A variational Lie group integration scheme for constrained mechanical systems. *Journal of Computational and Applied Mathematics* **387**, 112492 (2021)
- Hante, S., Arnold, M., Köbis, M.: The SNiMoWrapper: An FMI-compatible testbed for numerical algorithms in co-simulation. In: B. Schweizer (ed.) *IUTAM Symposium on Solver-Coupling and Co-Simulation*, pp. 99–116. Springer, Cham (2019)
- Hante, S., Arnold, M.: Staggered grid discretizations on Lie groups with applications in beam and shell theory. *PAMM* **18**(1), e201800277 (2018)
- Arnold, M., Hante, S.: Implementation details of a generalized- α differential-algebraic equation Lie group method. *Journal of Computational and Nonlinear Dynamics* **12**(2), 021002 (2017)
- Hante, S., Arnold, M.: A novel approach to Lie group structured configuration spaces of rigid bodies. *Proceedings in Applied Mathematics and Mechanics* **17**(1), 151–152 (2017)
- Arnold, M., Hante, S., Köbis, M.: Error analysis for co-simulation with force-displacement coupling. *PAMM* **14**(1), 43–44 (2014)

Lebenslauf

	Stefan Hante, M.Sc., geboren am 26. März 1990 in Eisenach
seit 2021	Application Engineer bei dSPACE GmbH (Paderborn)
2016 – 2021	Wissenschaftlicher Mitarbeiter am Institut für Mathematik der Martin-Luther-Universität Halle-Wittenberg
2016	Wissenschaftlicher Mitarbeiter am Institut für Mathematik der Martin-Luther-Universität Halle-Wittenberg im BMBF-geförderten Projekt MusiKa
2012 – 2015	Master Mathematik mit Anwendungsfach Informatik an der Martin-Luther-Universität Halle-Wittenberg Masterarbeit: “A general purpose Lie group generalized- α time integrator applied to nonlinear flexible geometrically exact beam models” Gesamtprädikat: sehr gut (1,1)
2012 – 2013	Wissenschaftlicher Mitarbeiter am Institut für Mathematik der Martin-Luther-Universität Halle-Wittenberg im BMBF-geförderten Projekt SNiMoRed
2008 – 2012	Bachelor Mathematik mit Anwendungsfach Chemie an der Martin-Luther-Universität Halle-Wittenberg Bachelorarbeit: “Simulation of a Cosserat rod model and its discretisations in space and time” Gesamtprädikat: gut (1,6)
2000 – 2008	Tilesius-Gymnasium (Mühlhausen) Abitur (1,0)

Selbstständigkeitserklärung

Hiermit erkläre ich an Eides statt, dass ich die vorliegende Dissertation selbständig und ohne fremde Hilfe angefertigt habe, sowie keine anderen als die angegebenen Quellen und Hilfsmittel benutzt. Die den benutzten Werken wörtlich oder inhaltlich entnommenen Stellen habe ich als solche kenntlich gemacht.

Salzkotten, den 23. Februar 2022